



**Institute of
Genetic Medicine**

**Senescence as a potential therapeutic target
for ischaemia-reperfusion injury following
acute myocardial infarction**

Emily Dookun

**Thesis submitted in accordance with the requirement for the degree of
Doctor of Philosophy**

**Institute of Genetic Medicine
Newcastle University**

April 2020

Abstract

Myocardial infarction (MI) is the leading cause of morbidity and mortality worldwide. The gold-standard intervention is reperfusion via primary percutaneous coronary intervention, however, reperfusion can induce ischaemia-reperfusion injury (IRI). A key component of IRI is increased oxidative stress and MI patients often exhibit progressive remodelling resulting in heart failure. This lab has previously demonstrated that during ageing, oxidative stress drives senescence which contributes to myocardial remodeling via the senescence-associated secretory phenotype (SASP), including pro-hypertrophic and pro-fibrotic proteins. I therefore hypothesised following MI with IRI cellular stress induces senescence which contributes to adverse remodeling via similar mechanisms.

Three-month-old mice underwent 60-minute ligation of the left anterior descending coronary artery (LAD) followed by reperfusion, and were assessed for characteristics of senescence. To test the impact of senescence post-MI with IRI, I eliminated senescent cells pharmacologically using the senolytic drug navitoclax, or targeted deletion of *p16^{Ink4a}* in cardiomyocytes using a novel mouse model (p16-MerCreMer). Hearts were assessed using histological and qRT-PCR analysis. Cardiac function was assessed via magnetic resonance imaging.

As expected, LAD ligation resulted in a typical intramural infarct and reduction in cardiac function. A significant increase in senescence markers was observed in both cardiomyocytes and interstitial cells. Mice treated with Navitoclax demonstrated a significant reduction in senescence markers as well as a global reduction in SASP and remodelling gene expression. Functionally, treated mice improved at 5 weeks post-LAD compared to controls, which may be explained by their reduced scar size. In comparison, the p16-MerCreMer mouse was insufficient to attenuate remodelling and demonstrated no functional improvement. Analysis by cytokine array demonstrated a decline in several SASP factors during navitoclax treatment and *in vitro* studies suggest a fibrotic SASP may detrimentally impact cardiomyocytes and angiogenesis. These data suggest that eliminating senescent cells or attenuating the SASP are viable strategies to improve outcome following IRI.

Acknowledgements

Firstly, I wish to thank my supervisors Dr Gavin Richardson and Dr João Passos for their expertise in this field of research as well as their continued support and mentoring throughout my PhD. They have been fantastic supervisors and made the PhD a highly enjoyable process. I would also like to thank Dr Andrew Owens for his advice and insight that has helped structure my project along the way. Additionally, I wish to extend my thanks to others that have provided invaluable comments and technical support during my PhD including Professor Helen Arthur, Professor Ioakim Spyridopoulos, Dr Diana Jurk, Professor Michael Taggart, Dr Helen Phillips, Dr Simon Bamforth and Dr Gabriele Saretzki.

Within the cardiovascular and senescence groups there are many people who have been of great help and support with helping me learn new techniques and conduct specialised experiments. Particularly, Dr Rachael Redgrave for her expertise with the LAD ligations, Dr Anna Walaszczyk for all her help in the lab and with the MRIs, Dr Kate Bailey for her extensive technical knowledge, Dr Simon Tual-Chalot for teaching me surgical techniques, and Dr Anthony Lagando and Dr Stella Victorelli for their advice regarding senescence markers. As well as these, I would also like to thank all the undergraduate and postgraduate students that I have worked with over the years.

In particular, I am most grateful to the many friends I have made within the Institute of Genetic Medicine and Institute for Ageing for their kindness, entertainment and free therapy sessions. Special thanks to Catherine Stothard, Lauren Phillips, James Chapman and all those in the lunch club for keeping me sane and always being available for “refreshments” on a Friday evening. I also wish to acknowledge the amazing staff with the Institute of Genetic Medicine for all their help, no matter the problem, and to my work mothers Trish Dunham and Debra Jones.

Finally, I thank all my friends and family, especially my parents Roy and Alison, for their constant encouragement and feigning interest in my work to keep me motivated. Thanks to Lauren Roberts for her emotional support, but particular thanks to my partner Maciej Misiura. These years would have been impossible without him, and I am eternally grateful for his support, patience, proof reading and humour that has helped me tremendously throughout the course of my PhD.

Table of Contents

Abstract	i
Acknowledgements	iii
List of Abbreviations	xiii
List of Tables	xvii
List of Figures	xviii
Chapter 1. Introduction	1
1.1 Coronary heart disease and myocardial infarction	1
1.2 Myocardial infarction	1
<i>1.2.1 Classification and diagnosis of the acute coronary syndromes</i>	<i>1</i>
1.3 Ischaemia-reperfusion injury phenomenon	5
<i>1.3.1 Categories of ischaemia-reperfusion injury</i>	<i>6</i>
<i>1.3.2 Pathophysiology</i>	<i>8</i>
1.4 Myocardial repair and adverse remodelling	10
<i>1.4.1 Myocardial regeneration</i>	<i>12</i>
<i>1.4.2 Therapeutic strategies trialled for ischaemia-reperfusion injury</i>	<i>14</i>
1.5 Cellular senescence	16
<i>1.5.1 Replicative senescence</i>	<i>16</i>
<i>1.5.2 Stress-induced premature senescence</i>	<i>17</i>
<i>1.5.3 Oncogene-induced senescence</i>	<i>19</i>

1.5.4	<i>Common pathways controlling senescence</i>	19
1.5.5	<i>Classical senescence marker</i>	22
1.6	Senescence, age-related disease and the senescence-associated secretory phenotype	22
1.7	Senescence and the heart	26
1.7.1	<i>Senescence, ageing and regeneration</i>	29
1.7.2	<i>Role of senescence in cardiac remodelling</i>	30
1.7.3	<i>Targeting senescence therapeutically</i>	36
1.8	Aims	42
Chapter 2. Materials and Methods		45
2.1	Coronary artery ligation mouse model	45
2.2	Navitoclax treatment	46
2.2.1	<i>Cardiac magnetic resonance imaging</i>	46
2.2.2	<i>Magnetic resonance imaging analysis</i>	47
2.3	Novel transgenic mouse generation	49
2.3.1	<i>Genotyping polymerase chain reactions</i>	51
2.4	Tissue collection and processing	53
2.4.1	<i>Tissue embedding</i>	54
2.5	Histology and immunofluorescence	54
2.5.1	<i>p21^{Cip} and troponin C dual staining</i>	57
2.5.2	<i>p16^{Ink4a}, troponin C and vimentin triple staining</i>	57
2.5.3	<i>Senescence-associated β-galactosidase staining</i>	57
2.5.4	<i>Telomere-associated DNA damage foci staining</i>	58
2.5.5	<i>Masson's Trichrome staining</i>	59

2.5.6	<i>Wheat Germ Agglutinin staining</i>	60
2.5.7	<i>5-Ethynyl-2-deoxyuridine staining</i>	60
2.5.8	<i>RNAscope</i>	60
2.5.9	<i>4-Hydroxynonenal staining</i>	61
2.5.10	<i>TUNEL staining</i>	61
2.6	Microscopy and image analysis	62
2.7	Characterisation of a cardiomyoblast senescence-associated secretory phenotype <i>in vitro</i>	63
2.7.1	<i>Cell culture of H9C2 cells</i>	64
2.7.2	<i>Irradiation of H9C2 cells</i>	64
2.7.3	<i>H9C2 cells treatment with navitoclax</i>	64
2.8	Characterisation of fibroblast senescence <i>in vitro</i>	65
2.8.1	<i>Cell culture of MRC5 cells</i>	65
2.8.2	<i>MRC5 cell treatment with navitoclax</i>	66
2.8.3	<i>Isolation of primary adult mouse cardiac fibroblasts</i>	66
2.8.4	<i>Irradiation of MRC5 and primary adult mouse cardiac fibroblast cells to obtain conditioned media</i>	67
2.8.5	<i>Endothelial cell culture</i>	68
2.8.6	<i>Isolation of primary embryonic mouse cardiomyocytes</i>	68
2.8.7	<i>Analysis of irradiated primary fibroblast senescence-associated secretory phenotype</i>	71
2.9	Gene expression analysis	71
2.9.1	<i>RNA isolation</i>	72
2.9.2	<i>cDNA synthesis</i>	73
2.9.3	<i>Quantitative reverse transcriptase polymerase chain reaction</i>	73
2.10	Protein expression analysis	73

2.10.1 Serum isolation from whole blood	74
2.10.2 Protein isolation from tissue	74
2.10.3 Cytokine/Chemokine array	75
2.11 Statistical analysis.....	75

Chapter 3. Cardiomyocyte senescence post-myocardial infarction and subsequent reperfusion in a mouse model of ischaemia-reperfusion injury **79**

3.1 Introduction.....	79
3.2 Experimental model.....	81
3.3 Detection of senescence in a model of ischaemia-reperfusion injury	82
3.3.1 Oxidative stress markers are increased post-ischaemia-reperfusion injury	82
3.3.2 Presence of telomere-associated DNA damage is elevated after ischaemia-reperfusion injury.....	86
3.3.3 Cardiomyocytes are positive for senescence-associated β -galactosidase activity 1 week post-ischaemia-reperfusion injury	89
3.3.4 RNA levels for p21 ^{Cip} and p16 ^{Ink4a} are also increased following ischaemia-reperfusion injury.....	92
3.3.5 In the border zone proximal to the infarct, cardiomyocytes remain positive for p21 ^{Cip} and p16 ^{Ink4a}	93
3.4 Discussion.....	98

Chapter 4. Pharmacological clearance of senescence modulates ischaemia-reperfusion injury and cardiac remodelling **103**

4.1 Introduction.....	103
4.2 Navitoclax treatment reduces viability of senescent but not proliferative cardiomyoblasts <i>in vitro</i>	105

4.3	<i>In vivo</i> model to investigate the effect of navitoclax on recovery post-ischaemia-reperfusion injury	108
4.4	Navitoclax treatment reduces senescence markers expression in cardiomyocytes	109
	<i>4.4.1 Both p21^{Cip} and p16^{Ink4a} are significantly reduced following treatment with navitoclax.....</i>	<i>111</i>
4.5	Treatment with navitoclax improves functional outcome.....	115
	<i>4.5.1 Left ventricular mass is unchanged following ischaemia-reperfusion injury and is unaffected by navitoclax treatment.....</i>	<i>116</i>
	<i>4.5.2 Navitoclax treatment improves systolic but not diastolic function post-myocardial infarction</i>	<i>118</i>
	<i>4.5.3 Navitoclax significantly increased stroke volume.</i>	<i>121</i>
	<i>4.5.4 Navitoclax treatment after ischaemia-reperfusion injury significantly increased cardiac output.....</i>	<i>123</i>
	<i>4.5.5 Navitoclax treatment following ischaemia-reperfusion injury improves ejection fraction.....</i>	<i>125</i>
4.6	Navitoclax treatment post-ischaemia-reperfusion injury reduces infarct size but has no effect on cardiomyocyte hypertrophy	127
4.7	Discussion	130
	Chapter 5. Characterisation of a novel p16^{Ink4a} cardiomyocyte specific transgenic knockout model to investigate outcome to ischaemia-reperfusion injury.....	137
5.1	Introduction.....	137
5.2	Experimental Design and Model Validation.	140
5.3	Validation of exon 1α excision from p16^{Ink4a} in cardiomyocytes.....	141

5.3.1	<i>p16^{Ink4a} and p21^{Cip} are significantly reduced in the mouse cohort with cardiomyocytes not expressing p16^{Ink4a}</i>	142
5.4	Cardiac function remains unchanged in this model	148
5.4.1	<i>Left ventricular mass is unaltered with the removal of p16^{Ink4a} expression from cardiomyocytes</i>	148
5.4.2	<i>End diastolic volume and end systolic volume are not affected by floxing out p16^{Ink4a} from cardiomyocytes</i>	150
5.4.3	<i>Inhibition of p16^{Ink4a} expression in cardiomyocytes does not lead to any improvements in stroke volume</i>	153
5.4.5	<i>Preventing cardiomyocytes from expressing p16^{Ink4a} is insufficient to rescue ejection fraction post-myocardial infarction</i>	154
5.5	Transgenic model does not result in attenuated remodelling despite reduction of senescence markers	156
5.6	Alternative hypothesis: persistent senescence signalling from fibroblasts may be responsible for a decline in heart function	159
5.6.1	<i>p16^{Ink4a} expression in non-cardiomyocytes is affected by preventing p16^{Ink4a} expression in cardiomyocytes</i>	160
5.7	Discussion	162
Chapter 6. Interstitial cell senescence is postulated to exert a greater effect on the heart post-ischaemia-reperfusion injury		169
6.1	Introduction	169
6.2	<i>In vitro</i> irradiated fibroblasts are senescent and clearance by navitoclax is targeted to senescent cells	171
6.3	A fibroblast senescence-associated secretory phenotype influences the biology of different cardiac lineages <i>in vitro</i>	173
6.3.1	<i>Conditioned media from senescent MRC5 fibroblasts inhibits endothelial cell proliferation and leads to senescence marker expression</i>	173

6.3.2 Both irradiated MRC5 and primary cardiac fibroblast conditioned media constrains embryonic cardiomyocyte proliferation and triggers cardiomyocyte senescence.....	178
6.4 Navitoclax treatment following ischaemia-reperfusion injury significantly reduced the number of p16^{Ink4a} and p21^{Cip} expressing myocardial interstitial cells.....	182
6.5 Investigation of the short term effects of navitoclax post-ischaemia-reperfusion injury.....	184
6.5.1 Total p21 ^{Cip} expression is significantly decreased following four days of navitoclax treatment.....	185
6.5.2 TUNEL staining reveals navitoclax treatment increases apoptosis post-myocardial infarction, which primarily occurs in the interstitial cell population ..	186
6.5.3 Cytokine array demonstrates effects on a variety of cytokines within the protein samples from left ventricle but minimal effects observed on cytokines circulating in the serum.....	189
6.5.4 Proliferation of cardiomyocytes is not upregulated following navitoclax therapy, but total proliferation and proliferation in the endothelial cell population is increased.....	198
6.6 Discussion	202
Chapter 7. Discussion.....	211
Appendix A	223
Raw values from MD-44 and TGFB1-3 Arrays from Eve Technologies	223
Appendix B	227
Conferences and travel awards:	227
Publications:.....	228

Bibliography..... 229

List of Abbreviations

ABT199 = Venetoclax
ABT263 = Navitoclax
ACS = Acute Coronary Syndrome
ATP = Adenosine Triphosphate
 α MHC = Alpha Myosin Heavy Chain
BAK = BCL-2 Homologous Antagonist Killer
BAX = BCL-2 Associated X Protein
BCL = B-Cell Lymphoma
BID = BH3-Interacting Domain Death Agonist
BIM = BCL-2 Interacting Mediator of Cell Death
BSA = Bovine Serum Albumin
BW = Body Weight
BZ = Border Zone
 Ca^{2+} = Calcium Ion
CAD = Coronary Artery Disease
CBSB = Cardiomyocyte Balanced Salt Buffer
CCL = CC Chemokine Ligand
CDK = Cyclin-Dependent Kinase
CF = Cardiac Fibroblast
CHD = Coronary Heart Disease
CK = Creatine Kinase
CM = Cardiomyocyte
CM-GM = Cardiomyocyte Growth Media
CO = Cardiac Output
cTn = Cardiac Troponin
CVD = Cardiovascular Disease
CXCL = Chemokine Ligand
ddH₂O = Purified Water
DDR = DNA Damage Response
DHE = Dihydroethidium

DMEM = Dulbecco's Modified Eagle Medium
DMSO = Dimethyl Sulfoxide
DSB = Double Stranded Break
D&Q = Dastinib and Quercetin
ECG = Electrocardiogram
ECM = Extracellular Matrix
EdU = 5-Ethynyl-2-Deoxyuridine
EDV = End Diastolic Volume
EF = Ejection Fraction
EndMT = Endothelial-to-Mesenchymal Transition
ERG = ETS-Related Gene
ESV = End Systolic Volume
ETC = Electron Transport Chain
EtBr = Ethidium Bromide
EtOH = Ethanol
FBS = Foetal Bovine Serum
FCS = Foetal Calf Serum
GCP = Granulocyte Chemotactic Protein
G3 = Generation 3
H⁺ = Hydrogen Ion
HEPES = 4-(2-Hydroxyethyl)-1-Piperazineethanesulfonic Acid
HIF-1 α = Hypoxia Inducible Factor-1 α
HSV-TK = Herpes Simplex Virus 1 Thymidine Kinase
HUVEC = Human Umbilical Vein Endothelial Cells
H₂O₂ = Hydrogen Peroxide
H9C2 = Rat Cardiomyoblasts
IHD = Ischaemic Heart Disease
IL = Interleukin
IMR90 = Human Lung Fibroblasts
IP = Intraperitoneal Injection
IP-10 = Interferon γ -induced Protein-10

IPC = Ischaemic Preconditioning
IRI = Ischaemia-Reperfusion Injury
IRI + Nav = Ischaemia-Reperfusion Injury and Navitoclax
IRI + Veh = Ischaemia-Reperfusion Injury and Vehicle
LAD = Left Anterior Descending Coronary Artery
LV = Left Ventricle
MAO-A = Monoamine Oxidase-A
MCP = Monocyte Chemoattractant Protein
M-CSF = Macrophage Colony-Stimulating Factor
MDC = Macrophage-Derived Chemokine
MEF = Mouse Embryonic Fibroblasts
MI = Myocardial Infarction
MIP-3 β = Macrophage Inflammatory Protein-3 β
MMP = Matrix Metalloproteinases
MMVEC-C = Mouse Cardiac Endothelial Cells
MOMP = Mitochondrial Outer Membrane Permeabilisation
mPTP = Mitochondria Permeability Transition Pore
MRC5 = Human Foetal Lung-Derived Fibroblast Cell Line
mRFP = Renilla Luciferase
MRI = Magnetic Resonance Imaging
MVO = Microvascular Obstruction
Na⁺ = Sodium Ion
NAC = N-Acetyl Cysteine
NADPH = reduced Nicotinamide Adenine Dinucleotide Phosphate
NHEJ = Non-Homologous End Joining
Non-STEMI = Non-ST Elevated Myocardial Infarction
OCT = Optimal Cutting Temperature Compound
OIS = Oncogene Induced Senescence
OS = Oxidative Stress
PBS = Phosphate Buffered Saline
PCR = Polymerase Chain Reaction

PDGF = Platelet-Derived Growth Factor
PFA = Paraformaldehyde
PPCI = Primary Percutaneous Coronary Intervention
P/S = Penicillin-Streptomycin
 $p16^{ff}$ = Mice with $p16^{Ink4a}$ exon 1 α flanked by *loxP* sites
 $p16^{-/-}$ = Mice with $p16^{Ink4a}$ exon 1 α floxed
Rb = Retinoblastoma
ROS = Reactive Oxygen Species
RT = Room Temperature
RV = Right Ventricle
RZ = Remote Zone
SA- β -Gal = Senescence β -Galactosidase
SASP = Senescence-Associated Secretory Phenotype
SIPS = Stress-Induced Premature Senescence
SR = Sarcoplasmic Reticulum
SSC = Sodium Citrate Buffer
STEMI = ST-Elevated Myocardial Infarction
SV = Stroke Volume
TAC = Transverse Aortic Constriction
TAE = Tris-Acetate-EDTA
TAF = Telomere-Associated DNA Damage Foci
TARC = Thymus and Activation-Regulated Chemokine
TGF- β = Transforming Growth Factor- β
TIMP = Tissue Inhibitor of Metalloproteinases
TNF- α = Tumour Necrosis Factor- α
WGA = Wheat Germ Agglutinin
1 $^{\circ}$ Ab = Primary Antibody
2 $^{\circ}$ Ab = Secondary Antibody
4-HNE = 4-Hydroxynonenal
4-OHT = 4-Hydroxytamoxifen

List of Tables

Table 1.1 Table of senolytics, based on (Kirkland <i>et al.</i> , 2017; Kim and Kim, 2019) .	39
Table 2.1 Variables quantified from magnetic resonance imaging analysis.	49
Table 2.2 Sequences for primers used for genotyping polymerase chain reactions..	52
Table 2.3 Polymerase chain reaction master mix reagent volumes.	52
Table 2.4 Polymerase chain reaction product sizes.	53
Table 2.5 List of antibodies use for all analyses.	56
Table 2.6 Probe hybridisation mix reagent volumes.	59
Table 2.7 Solutions for isolation of primary embryonic cardiomyocytes.	70
Table 2.8 TaqMan probes, ThermoFisher Cat. Number 4331182.	73

List of Figures

Figure 1.1 Myocardial infarction - type 1.....	3
Figure 1.2 Primary percutaneous coronary intervention.	5
Figure 1.3 Contribution of ischaemia-reperfusion injury to final infarct size.	8
Figure 1.4 Replicative senescence vs stress-induced premature senescence.	18
Figure 1.5 Activation of senescence.	21
Figure 1.6 Cellular changes after induction of senescence.....	23
Figure 1.7 Age-related cellular disorders.	25
Figure 1.8 Turnover of human cardiomyocytes.....	29
Figure 1.9 Hypothesised association between myocardial infarction, ischaemia-reperfusion injury, oxidative stress and cellular senescence.	36
Figure 1.10 Navitoclax mechanism of action.	40
Figure 2.1 Position of suture around the left anterior descending coronary artery....	46
Figure 2.2 Measurements taken for magnetic resonance imaging analysis.....	48
Figure 2.3 Schematic of generation of $p16^{Ink4a}$ floxed mice from crossing the $p16^{Ink4a^{flox/flox}}$ line with the Myh6-MerCreMer line.....	51
Figure 2.4 Images of a transverse heart section.....	63
Figure 2.5 Experimental timeline of navitoclax study on H9C2s <i>in vitro</i>	65
Figure 2.6 Experimental timeline of irradiating the fibroblast cell lines MRC5 and primary cardiac fibroblasts to investigate a fibrotic senescence-associated secretory phenotype.	68
Figure 2.7 Flow chart to determine appropriate statistical test to perform according to the outcome from a Shapiro-Wilk test.	76
Figure 2.8 Example of a QQ Plot showing the distribution of the data residuals against a theoretical normally distributed population.	76
Figure 3.1 Graphical hypothesis.	81
Figure 3.2 Experimental timeline.	82
Figure 3.3 Fluorescence intensity of 4-hydroxynonenal as a marker of oxidative stress increases at 24 hours after surgery and elevated levels are maintained up to a week.	84
Figure 3.4 At 24 hours after ischaemia-reperfusion injury , 4-hydroxynonenal intensity was elevated in the region of the left ventricle predicted to become infarct.	85

Figure 3.5 Proximal to the infarct cardiomyocyte nuclei are positive for telomere-associated DNA damage foci.	88
Figure 3.6 Senescence-associated β -galactosidase expression is observed within the infarct and cardiomyocyte population post-ischaemia-reperfusion injury.	90
Figure 3.7 A sub-population of cardiomyocytes are positive for senescence-associated β -galactosidase 1 week after ischaemia-reperfusion injury.	91
Figure 3.8 mRNA expression of p21 ^{Cip} and p16 ^{Ink4a} from tissue samples collected from regions proximal and distal to the infarct.	93
Figure 3.9 Cardiomyocytes express p21 ^{Cip} post-ischaemia-reperfusion injury.	95
Figure 3.10 Cardiomyocytes express p16 ^{Ink4a} post-ischaemia-reperfusion injury.	97
Figure 4.1 Graphical hypothesis.	105
Figure 4.2 Treatment with navitoclax specifically reduces the viability of senescent (irradiated) H9C2 cultures that are positive for senescence-associated β -galactosidase. Navitoclax has no effect on the viability of healthy, proliferative (non-irradiated) H9C2s.	107
Figure 4.3 Experimental timeline.	109
Figure 4.4 Navitoclax reduces the percentage of cardiomyocytes positive for telomere-associated DNA damage foci and mean foci number.	110
Figure 4.5 Senescence-associated β -galactosidase staining in the ischaemia-reperfusion injury model with and without navitoclax treatment.	111
Figure 4.6 Navitoclax reduces percentage of cardiomyocytes positive for p21 ^{Cip} after ischaemia-reperfusion injury.	113
Figure 4.7 Cardiomyocytes positive for p16 ^{Ink4a} after ischaemia-reperfusion injury is reduced by navitoclax.	114
Figure 4.8 Example of measurements taken for each magnetic resonance imaging slice at diastole and systole from ischaemia-reperfusion injury (lipid control) and navitoclax treated mice.	115
Figure 4.9 Left ventricular mass remains unchanged after ischaemia-reperfusion injury and navitoclax treatment.	117
Figure 4.10 End diastolic volume increases after ischaemia-reperfusion injury but remains unchanged following navitoclax treatment.	119
Figure 4.11 End systolic volume increases after ischaemia-reperfusion injury and continually increases from weeks 3 to 5. Navitoclax treatment is able to stabilise or reduce end systolic volume over this time frame.	120

Figure 4.12 Stroke volume continuously declines after ischaemia-reperfusion injury, however, navitoclax treatment is able to partially recover stroke volume.	122
Figure 4.13 Cardiac output continuously declines after ischaemia-reperfusion injury, however, navitoclax treatment is able to maintain cardiac output and prevent this observed continuous decline.	124
Figure 4.14 Ejection fraction continuously declines after ischaemia-reperfusion injury, however, ejection fraction is stabilised or improved following navitoclax treatment.	126
Figure 4.15 Navitoclax significantly reduces scar size within the left ventricle.	128
Figure 4.16 Ischaemia-reperfusion injury leads to significant changes in hypertrophy of the cardiomyocytes. Navitoclax slightly reduces hypertrophy, but insignificantly, compared to the ischaemia-reperfusion injury cohort.	129
Figure 5.1 Graphical hypothesis.	140
Figure 5.2 Experimental timeline.	141
Figure 5.3 Genotyping polymerase chain reactions to confirm the presence of Cre and that it had been activated to flox <i>p16^{Ink4a}</i> exon 1 α	142
Figure 5.4 Cardiomyocytes have reduced expression of <i>p16^{Ink4a}</i> following floxing of <i>p16^{Ink4a}</i> after ischaemia-reperfusion injury.	143
Figure 5.5 <i>p16^{Ink4a}</i> expression by RNAscope is significantly decreased in knockout mice, and levels are comparable to those quantified by immunofluorescence when normalised to the negative control.	145
Figure 5.6 Floxing <i>p16^{Ink4a}</i> from cardiomyocytes reduces the percentage of cardiomyocytes positive for p21 ^{Cip} after ischaemia-reperfusion injury.	146
Figure 5.7 Floxing of <i>p16^{Ink4a}</i> has no effect on telomere-associated DNA damage foci in cardiomyocytes.	147
Figure 5.8 Example of measurements taken for each magnetic resonance imaging slice at diastole and systole after ischaemia-reperfusion injury.	148
Figure 5.9 Left ventricular mass is unchanged after ischaemia-reperfusion injury in both cohorts.	149
Figure 5.10 End diastolic volume increases after ischaemia-reperfusion injury but is not affected by <i>p16^{Ink4a}</i> expression in cardiomyocytes.	151
Figure 5.11 End systolic volume increases after ischaemia-reperfusion injury but is also not affected by <i>p16^{Ink4a}</i> expression in cardiomyocytes.	152
Figure 5.12 Ischaemia-reperfusion injury causes a reduction in stroke volume, however, altered <i>p16^{Ink4a}</i> expression in cardiomyocytes has no effect.	154

Figure 5.13 Ischaemia-reperfusion injury significantly reduces ejection fraction. Preventing <i>p16^{Ink4a}</i> expression to reduce senescence has no effect on ejection fraction.	155
Figure 5.14 Scar size is unchanged after removal of <i>p16^{Ink4a}</i> from cardiomyocytes.	157
Figure 5.15 Cardiomyocyte area after inhibition of <i>p16^{Ink4a}</i> activity in the cardiomyocytes is not altered.	158
Figure 5.16 Senescence-associated β -galactosidase expression is lost in knockout mice.	159
Figure 5.17 Preventing <i>p16^{Ink4a}</i> expression in the cardiomyocytes leads to significantly fewer interstitial cells also expressing <i>p16^{Ink4a}</i>	161
Figure 6.1 Graphical hypothesis.	171
Figure 6.2 Treatment with navitoclax specifically reduces the viability of senescent (irradiated) MRC5 cultures that are positive for senescence-associated β -galactosidase. Navitoclax has no effect on the viability of healthy, proliferative (non-irradiated) MRC5s.	172
Figure 6.3 Proliferation of MMVEC-Cs is significantly reduced when exposed to irradiated MRC5 conditioned media.	174
Figure 6.4 Expression of the senescence marker <i>p21^{Cip}</i> was significantly upregulated in MMVEC-C cells following exposure to conditioned media from irradiated senescent MRC5s.	175
Figure 6.5 Irradiation of MRC5 cells significantly increases generation of the oxidative stress marker dihydroethidium in a paracrine fashion in MMVEC-C cell cultures.	177
Figure 6.6 The senescence-associated secretory phenotype generated from cardiac fibroblasts is comparable to MRC5 fibroblasts, as both significantly reduce proliferation of isolated embryonic cardiomyocytes.	179
Figure 6.7 Levels of the senescence marker senescence-associated β -galactosidase were raised in cardiomyocytes cultured with irradiated media.	181
Figure 6.8 Navitoclax reduces the percentage of cardiac interstitial cells positive for <i>p16^{Ink4a}</i> after ischaemia-reperfusion injury to baseline levels.	183
Figure 6.9 Navitoclax reduces the percentage of cardiac interstitial cells positive for <i>p21^{Cip}</i> post-ischaemia-reperfusion injury to baseline levels.	184
Figure 6.10 Experimental timeline.	185

Figure 6.11 Expression of p21 ^{Cip} is significantly reduced following navitoclax after ischaemia-reperfusion injury.	186
Figure 6.12 After ischaemia-reperfusion injury cells are TUNEL positive, with the majority of cells being interstitial cells.	188
Figure 6.13 Heat map showing changes in expression of cytokines and chemokines from left ventricle protein samples run on the MD44 and TGFB1-3 arrays.	192
Figure 6.14 Graphs showing trends in the expression of left ventricle protein cytokines and chemokines relating to fibrosis and cardiovascular disease following ischaemia-reperfusion injury with and without navitoclax treatment.	194
Figure 6.15 Heat map showing changes in expression of cytokines and chemokines from serum samples run on the MD44 and TGFB1-3 arrays.	196
Figure 6.16 Circulating serum cytokines relating to fibrosis and cardiovascular disease following ischaemia-reperfusion injury with and without navitoclax treatment.	197
Figure 6.17 Navitoclax treatment increased proliferation of endothelial cells but not cardiomyocytes after ischaemia-reperfusion injury.	200
Figure 7.1 Chemical structure of navitoclax and venetoclax.	215
Figure 7.2 Isolated primary adult mouse cardiac fibroblasts are positive for the fibroblast marker vimentin.	219
Figure 7.3 Graphical summary.	221

Chapter 1. Introduction

1.1 Coronary heart disease and myocardial infarction

Cardiovascular diseases (CVDs) account for the highest proportion of deaths and disabilities globally, with an estimated 17.5 million deaths in 2012 (Hausenloy and Yellon, 2013; World Health Organisation, 2014; Bansilal *et al.*, 2015). The rate of coronary heart disease (CHD), one of the most common subsets of CVDs, has been declining over the past few decades. However, it still constitutes about a third of mortalities in middle aged individuals (Bansilal *et al.*, 2015; Sanchis-Gomar *et al.*, 2016). A major and severe manifestation of CHD is acute myocardial infarction (MI) (Hausenloy and Yellon, 2013).

1.2 Myocardial infarction

Myocardial infarction is characterised by a sustained period of myocardial ischaemia that leads to a disrupted balance between oxygen supply and demand, which results in cardiomyocyte (CM) death and necrosis of the myocardium, and potentially progressive myocardial remodelling all of which are detrimental to cardiac function. In most cases, a MI arises due to the rupture or breakdown of a coronary atherosclerotic plaque that generates a thrombus, leading to the coronary artery becoming occluded and cessation of blood flow distal to the occlusion (Thygesen *et al.*, 2012; Montecucco *et al.*, 2016). The myocardium affected during occlusion is outlined as the area at risk (Hausenloy and Yellon, 2013). Acute MI can, however, also be generated by coronary artery embolism or dissection, hypotension, anaemia and cocaine use (Boateng and Sanborn, 2013).

1.2.1 Classification and diagnosis of the acute coronary syndromes

Clinical CHD manifests as a spectrum of symptoms collectively termed acute coronary syndrome (ACS) which are classified based on severity and the degree and nature of the coronary artery blockage. Acute coronary syndrome progresses from unstable

angina in which a partial blockage of the artery results in reduced oxygen and patients present with chest pain (angina), either at rest or with marginal physical exertion, or with pain that is increasing in severity or duration (Boateng and Sanborn, 2013).

Next on the ACS spectrum is non-ST elevated myocardial infarction (non-STEMI). Non-ST elevated myocardial infarction has the same hallmark features as unstable angina but also results in MI as indicated by an elevation in biomarkers for myocardial trauma (Boateng and Sanborn, 2013). These biomarkers included cardiac troponin (cTn) I and T, which are both components of the myocyte contractile unit, and creatine kinase (CK) (Thygesen *et al.*, 2012; Aldous, 2013), as these are released into the bloodstream subsequent to myocardial damage. The increase in the biomarkers differentiates non-STEMI from unstable angina (Silva *et al.*, 2015). However, in this setting the occlusion leading to ischaemia still only partially blocks the coronary artery (Deckers, 2013) and critically there is no elevation of the ST-segment on an electrocardiogram (ECG) (Riezebos and Verheugt, 2013). Upon hospital admission the most appropriate therapy path for these patients is revascularisation via drug therapy with only patients in the higher risk categories being suitable to undergo high-risk surgical interventions (Roleder *et al.*, 2015; Silva *et al.*, 2015). Finally, and most relevant to this project is the ST-elevated myocardial infarction (STEMI) group.

ST-elevated myocardial infarction lies at the far end of the ACS spectrum and is diagnosed as per the clinical manifestations, seen in unstable angina and non-STEMI, but also by a ST-segment elevation as detected by ECG (Boateng and Sanborn, 2013). While STEMI patients can be further divided into a number of subgroups, a common feature is that in these cases the MI arises from a complete blockage of the artery leading to ischaemia and subsequent myocardial damage (Figure 1.1) (Thygesen *et al.*, 2012).

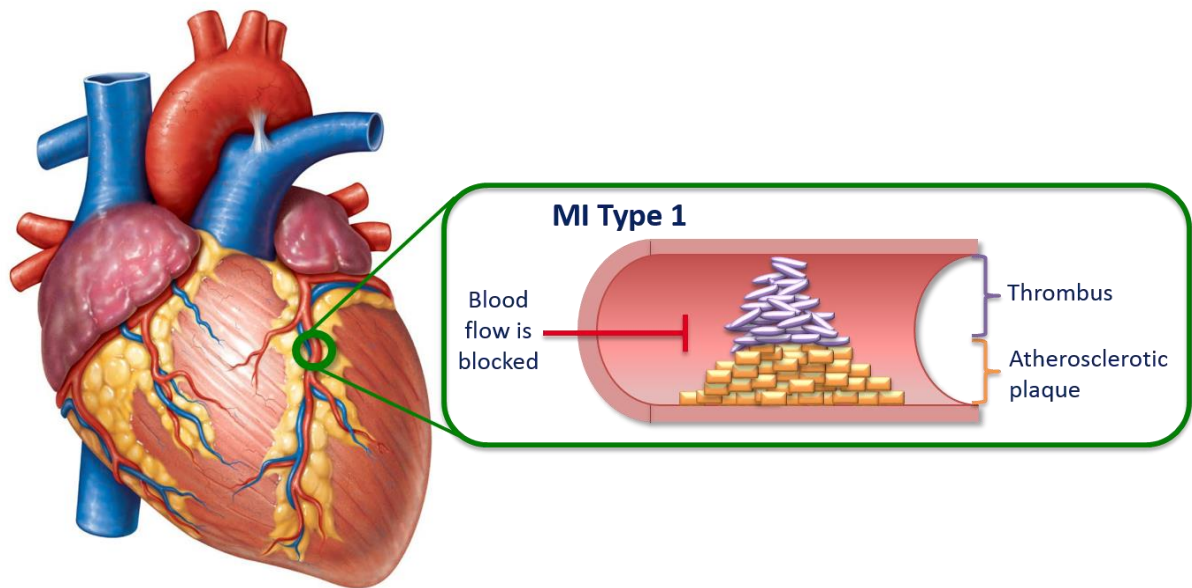


Figure 1.1 Myocardial infarction - type 1.

Type 1 MI showing atherosclerotic plaque and thrombus formation that blocks blood flow through coronary artery. This project will only be focusing on MI - type 1. Adapted from Thygesen et al (Thygesen *et al.*, 2012) and Pearson Education Inc. 2010.

Once STEMI has been diagnosed, it is essential to immediately reperfuse the heart (Boateng and Sanborn, 2013). The recommended treatment is either fibrinolysis therapy or primary percutaneous coronary intervention (PPCI) to improve patient outcomes (Hausenloy and Yellon, 2013). Fibrinolytic drugs, however, are not an ideal option as they do not achieve reperfusion in approximately 20-30% of cases, as they are unsuitable for certain patients or in a few instances cause further complications such as haemorrhagic stroke (National Clinical Guideline Centre (UK). 2013). Therefore, PPCI is the treatment of choice for STEMI and has been shown by many randomised control trials to be superior to fibrinolytics. Patients receive fibrinolytics if the time delay from the onset of symptoms has been too long to undergo PPCI, which in 2011/12 was about 5% of STEMI cases in the UK (Keeley *et al.*, 2003; Boersma and Primary Coronary Angioplasty vs. Thrombolysis, 2006; Terkelsen *et al.*, 2009; National Clinical Guideline Centre (UK). 2013).

Primary percutaneous coronary intervention has evolved from the first percutaneous transluminal coronary angioplasties performed by Grüntzig in 1979. This technique involved inserting a catheter to deliver a balloon, which once inflated, dilated the artery

allowing blood re-flow. It then progressed to the insertion of metal stents after this process to avoid restenosis (Figure 1.2), to the stents currently used that can act as a drug delivery system (Grüntzig *et al.*, 1979; Lei *et al.*, 2011; Nabel and Braunwald, 2012). Although globally accepted as the gold-standard treatment for STEMI, the acceptable time period to deliver PPCI that is of benefit is still debated. The main obstacle to deliver timely PPCI is physical proximity to an appropriate centre (National Clinical Guideline Centre (UK). 2013; Whittaker *et al.*, 2013; Jordan and Caesar, 2016). Guidelines state a 60-90 minute door-to-balloon time window, which is the time from arriving at a PPCI centre to undergoing surgery, and that reperfusion by PPCI ideally occurs within 2-3 hours of symptoms presenting (Terkelsen *et al.*, 2009; Windecker *et al.*, 2014). These time frames are vital. Within the first hour of occlusion nearly half the salvageable myocardium is irrecoverable, and after 3 hours this increases to two-thirds (National Clinical Guideline Centre (UK). 2013). However, in some studies and clinical settings PPCI is performed irrespective of these time periods being exceeded (Terkelsen *et al.*, 2009; Windecker *et al.*, 2014).

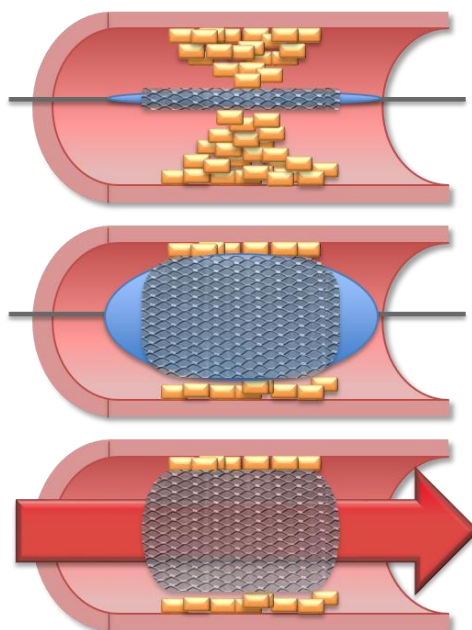


Figure 1.2 Primary percutaneous coronary intervention.

Diagram illustrating insertion of catheter into coronary artery to position balloon and stent at the site of blockage, then inflation of balloon, and finally removal of catheter and balloon leaving the stent open and reflow of blood through artery. Adapted from Healthwise incorporated.

Since PPCI has become routinely performed, mortality rates post-STEMI have declined over the last two decades. In those 20 years, use of PPCI has increased from about 12% to over 60% (Lønborg, 2015; Doost Hosseiny *et al.*, 2016) and as such mortality rates after 1 year are around 7-10%, which is more than half of what they were 20 years ago. The rationale behind the deceleration in mortality rates in the long-term, despite there being an increase in survival post-MI and PPCI, is the phenomenon called ischaemia-reperfusion injury (IRI) and the fact that even after successful PPCI many patients still demonstrate a progressive decline in cardiac function as a result of adverse remodelling ultimately leading to heart failure and even death (Lønborg, 2015).

1.3 Ischaemia-reperfusion injury phenomenon

Despite the advantageous effects of PPCI and other revascularisation methods, the resulting reperfusion after an ischaemic event can itself detrimentally impact and exacerbate myocardial dysfunction via IRI (Hausenloy and Yellon, 2013; Lønborg,

2015). Numerous clinical conditions besides MI have been linked to the occurrence of IRI. These include, but are not limited to, stroke, organ transplantation and peripheral vascular disease (Kalogeris *et al.*, 2012; Widgerow, 2014). Regardless of its systemic prevalence, the exact mechanisms behind IRI remain unclear so it cannot be exploited therapeutically. The current understanding of the underlying pathophysiology is highly complex and multifactorial (Hausenloy and Yellon, 2013; Halladin, 2015; Neri *et al.*, 2017).

1.3.1 Categories of ischaemia-reperfusion injury

Ischaemia-reperfusion injury has been categorized into 4 forms: reperfusion-induced arrhythmias, myocardial stunning, microvascular obstruction (MVO) and lethal myocardial reperfusion injury. The first two are reversible whereas the last two are irreversible (Hausenloy and Yellon, 2013).

Reperfusion-induced arrhythmias can arise at the onset of reperfusion from PPCI. They include idioventricular rhythm, ventricular tachycardia and fibrillation, which either naturally terminate or can be simply treated (Fröhlich *et al.*, 2013; Hausenloy and Yellon, 2013).

Myocardial stunning is the term for the temporary contractile dysfunction caused by the effects of reactive oxidative species (ROS) and calcium ion (Ca^{2+}) overload, as described above, and is associated with injury to the microvasculature (Fröhlich *et al.*, 2013; Hausenloy and Yellon, 2013; Pinto *et al.*, 2017). It can occur even if the ischaemic period was around 15 minutes, which is too short to bring about myocardial necrosis (Buja, 2005).

Microvascular obstruction was first reported by Krug *et al.* in 1966 as the “inability to reperfuse a previously ischemic region” (Krug *et al.*, 1966). Roughly 30-40% of patients that undergo reperfusion suffer from MVO, also known as the “no-reflow” phenomena. It is caused by microembolism of platelets, De Novo thrombosis, neutrophil plugging, capillary damage associated with compromised vasodilation, release of vasoconstricting and thrombogenic elements, or capillary compression via external CM or endothelial cell swelling (Moens *et al.*, 2005; Hausenloy and Yellon, 2013; Kidambi *et al.*, 2013). Together with endothelial dysfunction, oedema and oxidative stress (OS), MVO can be a key mediator in the pathogenesis of microvascular dysfunction. Blood

flow in MVO is retarded and there are distinctive areas of hypoperfusion (Moens *et al.*, 2005). Microvascular obstruction manifestation is associated with numerous adverse outcomes in STEMI patients that have been reperfused. They include a larger infarct size, poorer short and long term clinical outcomes, lower left ventricle (LV) ejection fraction (EF) and, independent of the final infarct size, adverse remodelling and function of the LV (Fröhlich *et al.*, 2013; Kidambi *et al.*, 2013).

Lethal myocardial reperfusion injury refers to the death of CMs during reperfusion, that after the ischaemic event were potentially still viable. Confirming the exact extent of lethal myocardial reperfusion injury is challenging, and has been indirectly verified using therapeutic interventions at the onset of MI both in experimental models and STEMI patients. These studies showed a reduction in final infarct size of 40-50%. This suggestion that IRI via lethal myocardial reperfusion injury can account for as much as 50% of the final infarct (Figure 1.3) makes it a hugely important target to potentially exploit therapeutically to improve STEMI patient outcomes (Fröhlich *et al.*, 2013; Hausenloy and Yellon, 2013; Lønborg, 2015). Factors instrumental in the development of lethal myocardial reperfusion injury includes Ca^{2+} overload, the mitochondria permeability transition pore (mPTP) opening, hypercontraction of myofibrils and the large burst of OS caused by excessive ROS generation (Hausenloy and Yellon, 2013).

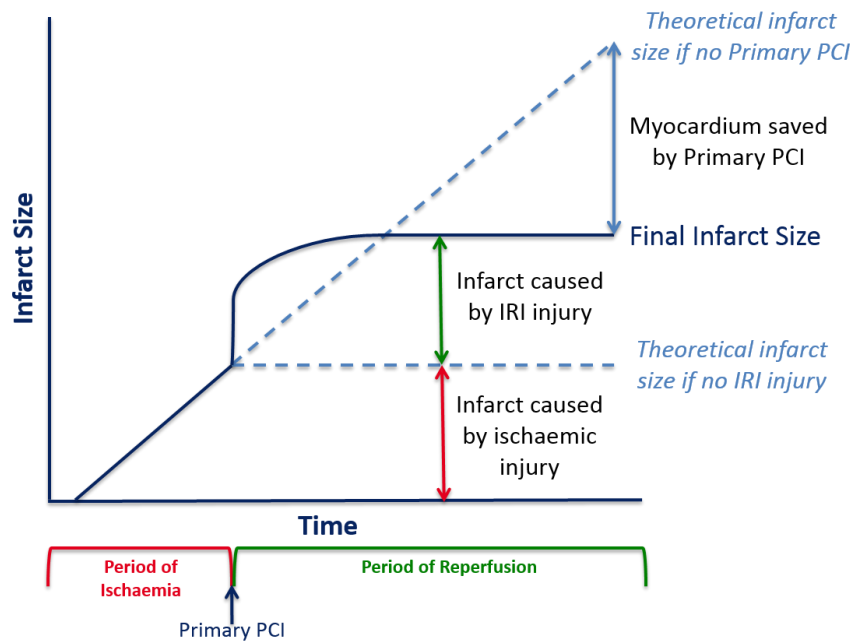


Figure 1.3 Contribution of ischaemia-reperfusion injury to final infarct size.

Graph illustrating the potential contribution of both myocardial ischaemia and IRI to the final infarct size. Adapted from Hausenloy et al (Hausenloy and Yellon, 2013).

It is clear that these processes are important in determining the severity of the patient's symptoms following IRI. From Figure 1.3 it is clear that the size of the infarct is smaller if the heart is reperfused, and by association will have improved CM viability and heart function. However, these patients still possess a high likelihood of progressing to heart failure, and therefore it is possible that other yet unknown cellular events may contribute (Konstam *et al.*, 2011; Hausenloy and Yellon, 2013) that may offer targets for novel therapeutics.

1.3.2 Pathophysiology

Ischaemia-reperfusion injury is composed of both the myocardial ischaemic and reperfusion phases (Hausenloy and Yellon, 2013; Widgerow, 2014).

At the onset of ischaemia, the rapid switch to an anaerobic metabolic state and the changes in biochemical demands negatively impact the myocardium. Oxidative phosphorylation is arrested due to lack of oxygen causing depolarisation of the mitochondrial membrane, loss of adenosine triphosphate (ATP) and suppression of the myocardium to contract as normal. Cellular metabolism rapidly shifts to anaerobic

glycolysis generating lactic acid and an accumulation of hydrogen ions (H^+) that reduces the intracellular pH levels, inhibiting myofibril contraction and closure of the mPTP. To counterbalance the H^+ increase membrane sodium-hydrogen (Na^+-H^+) ion exchangers are activated that expel H^+ for sodium ions (Na^+). The depletion of ATP through halted production and hydrolysis means that the sodium-potassium ($3Na^+-2K^+$) ATPase transporters cannot function to remove the build-up of Na^+ , creating an intracellular Na^+ overload. The cell responds by utilising the sodium-calcium ($2Na^+-Ca^{2+}$) exchangers, but by addressing the Na^+ overload this causes an intracellular Ca^{2+} overload. Calcium dependent proteases are subsequently activated causing tissue damage through disrupting cellular structures (de Groot and Rauen, 2007; Kalogeris *et al.*, 2012; Hausenloy and Yellon, 2013; Widgerow, 2014). Calpains are a family of proteases that activates sarcomeric apoptosis and degrade structural proteins leading to cell death, as well as proteolysis of myofibril proteins that alter CM contractility and contributes to heart failure (Kalogeris *et al.*, 2012; Neri *et al.*, 2017).

Reperfusion delivers oxygen and substrates essential for aerobic ATP generation, and also restores physiological pH levels by washing out lactic acid. However, reperfusion also initiates damaging mechanisms. The oxygen influx triggers the electron transport chain within the mitochondria to be reactivated generating high amounts of ROS. Reactive oxygen species levels are augmented by other sources including reduced nicotinamide adenine dinucleotide phosphate (NADPH) oxidase and xanthine oxidase brought in by neutrophil and endothelial cells in the restored blood flow. Ischaemia-reperfusion injury mediated by ROS occurs via attracting more neutrophils to the CM, opening of the mPTP and disrupting sarcoplasmic reticulum (SR) function. The SR exacerbates the intracellular Ca^{2+} overload by releasing more Ca^{2+} into the cytosol. ROS also denatures enzymes and directly damages DNA. The overall effect of an increase in ROS, overload of Ca^{2+} and opening of the mPTP in IRI is mediated through myofibril hypercontracture, endothelial dysfunction and inflammatory cascade activation (Kalogeris *et al.*, 2012; Hausenloy and Yellon, 2013; Neri *et al.*, 2017). Furthermore ROS can act as a potential contributor to mitochondrial Ca^{2+} overload, which can be a major contributor to increasing ROS levels, therefore creating a feedback loop to continually maintain a state of Ca^{2+} overload and increased ROS (Kaneko *et al.*, 1990; Murphy and Steenbergen, 2007; Penna *et al.*, 2009). In addition to these effects, ROS can have downstream consequences including stimulating an

extremely organised, acute inflammatory response characterised by increased expression of pro-inflammatory genes and cytokine release. Indeed it has been demonstrated in models of MI that the release of pro-inflammatory cytokines including tumour necrosis factor- α (TNF- α), interleukin-1 β (IL-1 β) and interleukin-6 (IL-6) are increased (Neri *et al.*, 2015). While these pathophysiological processes contribute directly to CM death, MI and IRI also impact on the biology of the surviving myocardium and may contribute to adverse myocardial remodelling although the exact mechanisms by which this occurs remains unclear (van der Laan *et al.*, 2012; Muhlestein, 2014; Vanezis *et al.*, 2016).

1.4 Myocardial repair and adverse remodelling

Shortly after MI, repair mechanisms are stimulated by the damaged myocardium and the heart undergoes remodelling that can have dramatic effects on the heart, both structurally and functionally. The process of repair in the myocardium following an MI can be divided into multiple stages. The first phase is composed of CM death either by apoptosis or necrosis, which is initiated within 6 hours of a coronary occlusion (Blankesteyn *et al.*, 2001). The timings and stimuli to trigger apoptosis and necrosis in the heart post-MI is still debated. It has been suggested that apoptosis occurs predominantly in the early acute stages after MI between 6 and 8 hours of the occlusion and necrosis is subsequently activated over the period between 12 hours and up to 4 days after MI (Blankesteyn *et al.*, 2001). Additionally, as necrosis is a passive process it has been postulated that activation of necrosis occurs if the cell ATP levels are diminished resulting from IRI, whereas the CM will undergo apoptosis if ATP is available (Krijnen *et al.*, 2002).

Apoptosis followed by necrosis would also fit as only necrosis is associated with an inflammatory response, which is the second phase of myocardial repair starting at around 12 hours and continuing for roughly 3 days (Blankesteyn *et al.*, 2001). This phase involves the activation of the complement cascade, release of cytokines and ROS. All three act in unison to recruit immune cells including neutrophils, monocytes and leukocytes as well as other cells such as fibroblast and endothelial cells. Neutrophils secrete components to augment cell recruitment to the injured myocardium as well as oxidative and protease factors (Nah and Rhee, 2009). Reduction of

neutrophil levels in animal models of MI and IRI resulted in smaller overall infarcts, suggesting that neutrophils are involved in cardiac injury (Romson *et al.*, 1983; Jordan *et al.*, 1999). Cytokines such as TNF- α not only act as chemoattractants but also upregulate fibroblast matrix metalloprotease (MMP) expression to regulate collagen deposition in the extracellular matrix (ECM) (Nah and Rhee, 2009; Lin *et al.*, 2015). Overall, the inflammatory phase acts to attract cells to remove cell debris released from dead CMs and that are required for the third phase; the proliferative phase to lead to granulation (Blankesteyn *et al.*, 2001; Nah and Rhee, 2009).

The granulation tissue generated after MI is primarily directed by the myofibroblast population (Blankesteyn *et al.*, 2001). Myofibroblasts produce collagens that are continuously synthesised to keep levels stable. They also are contractile within the ECM. This contractile function is not involved in cardiac contraction, but acts to close and strengthen the wound. Inefficient myofibroblast recruitment and organisation can weaken the infarct, however, excessive fibrosis is deleterious to cardiac function (Blankesteyn *et al.*, 2001; Baum and Duffy, 2011; Davis and Molkenin, 2014). Another important event during the granulation phase is angiogenesis, or formation of new blood vessels (Honnegowda *et al.*, 2015). Angiogenesis is vital for cardiac repair to supply the myocardium with adequate oxygen and nutrients to meet the elevated metabolic demand of the proliferating cells during this stage of wound repair (Darby *et al.*, 2014; DiPietro, 2016; Broughton *et al.*, 2018).

After several weeks of granulation, the infarct begins to stabilise over the fourth phase; the maturation phase, which continues for up to 2 months after MI. The scar is never fully resolved, and as such myofibroblasts remain resident within the region for numerous years (Blankesteyn *et al.*, 2001; Czubryt, 2012). This results in a stiffer heart with impaired contractility and relaxation, as well as interfering with cardiac electrical conduction increasing the risk of arrhythmias (Czubryt, 2012).

The morphological changes the heart undergoes during and after repair in response to injury are termed pathological remodelling events (Cohn *et al.*, 2000). These encapsulate all alterations to both the function and structure of the myocardium, such as CM hypertrophy, dilated ventricular wall and fibrosis (Azevedo *et al.*, 2016). Initially after MI the scar formation leads to the LV wall becoming thinner, longer and the internal volume increases. The heart starts to undergo remodelling where the CMs become hypertrophic to increase the wall mass. The amount of remodelling that occurs

is proportional to the level of injured myocardium, and if not resolved, the hypertrophy and dysfunctional contraction of the LV will continue to decline with time causing progression to heart failure (Konstam *et al.*, 2011). Cardiac dysfunction predisposing the patient to heart failure is the primary outcome of adverse remodelling (Azevedo *et al.*, 2016). This adverse remodelling is again linked to an inflated inflammatory response and elevated cytokine levels including interleukins, transforming growth factor- β (TGF- β) and TNF- α (Konstam *et al.*, 2011; van der Laan *et al.*, 2012). The presence of these inflammatory mediators is again central to the establishment of IRI, and patients with heart failure and IRI are associated with a more adverse prognosis (Kleinbongard *et al.*, 2011; Joost *et al.*, 2016).

1.4.1 Myocardial regeneration

Although the heart is a relatively quiescent organ and the majority of CMs are post-mitotic, it does have a limited but measurable potential to regenerate CMs. It is also evident that this regenerative potential contributes to recovery following MI and IRI in a meaningful way (Carvalho and de Carvalho, 2010; Bergmann *et al.*, 2015).

Some of the best evidence that CMs are replaced during normal myocardial homeostasis is provided by (Bergmann *et al.*, 2015). This study took advantage of the C^{14} released during the cold war nuclear bomb testing to retrospectively carbon date CM DNA in order to compare the turnover of an individual's CMs to their chronological age. Using this technique, it was demonstrated that in CMs the majority of postnatal DNA synthesis occurs during the first two decades of life, with the highest CM turnover observed during the first decade of life, and after the first decade around 80% of CMs will not be exchanged throughout the lifetime of the heart. It was also shown that CM turnover and exchange is at a much lower rate than other cardiac cell types such as endothelial and mesenchymal cells (Bergmann *et al.*, 2015).

Cardiomyocyte regeneration also contributes to recovery post-MI (Malliaras *et al.*, 2013). Cardiomyocytes possessing mitotic activity post-MI are located in both the border zone (BZ), adjoining the area of scar, and remote zone (RZ), areas further away from the scar. Post-infarct the number of mitotic CMs in the LV are more than three times higher than is normally expected, requiring further explanation as to why this replication is insufficient to repair the infarct (Beltrami *et al.*, 2001). Although other

studies report an increase in CM proliferation after MI, there are discrepancies regarding the source of these new CMs. Some studies name recruited endogenous stem cells as the primary source. Others state that due to the absence of stimulating cytokines and other signals, circulating stem cell numbers are too low to be the source and therefore new CMs arise from resident CMs. However, it has also been shown that CMs arise from both sources (Beltrami *et al.*, 2001; Carvalho and de Carvalho, 2010; Malliaras *et al.*, 2013; Nakada *et al.*, 2017).

In a healthy, un-infarcted heart, it has been proposed that the majority of CM turnover arises from a subpopulation of CMs that retain some degree of proliferative potential, as roughly 90% of resident stem cells have been reported to be in a state of quiescence (Hsieh *et al.*, 2007; Ellison *et al.*, 2013; Malliaras *et al.*, 2013; Senyo *et al.*, 2013; van Berlo *et al.*, 2014; Ellison-Hughes and Lewis, 2017). However, following injury, including hypoxia and MI, there is an increase in CM proliferation and also stimulation of quiescent stem and progenitor cells to contribute to CM replacement within the BZ (Hsieh *et al.*, 2007; Ellison *et al.*, 2013; Malliaras *et al.*, 2013). While a number of cardiac stem cell populations have been described (Cai *et al.*, 2008; Zhou *et al.*, 2008; Smart *et al.*, 2011), perhaps the most extensively studied is the c-kit positive population. However, approximately 1% of c-kit expressing cells are cardiac stem cells, and therefore identification of cardiac stem cells should be used in conjunction with the additional markers Sca-1 (positive expression), CD31 (negative expression), CD45 (negative expression) and tryptase (negative expression) (Ellison *et al.*, 2013; Vicinanza *et al.*, 2017).

During repair post-MI with IRI, proliferation and generation of endothelial cells is also essential for the process of angiogenesis. Angiogenesis is an essential recovery and remodelling mechanism after MI for the revascularisation of damaged myocardium (He *et al.*, 2017), by maintaining survival, function and stimulating growth of CMs (Cochain *et al.*, 2013). Preventing angiogenesis *in vivo* promoted progression to heart failure in a model of CM hypertrophy and dilated cardiomyopathy (Shiojima *et al.*, 2005), pressure overload via transverse aorta constriction (Sano *et al.*, 2007), and hypoxia and necrosis following transgenic removal of laminin- α 4 (an important ECM protein) from the myocardial blood vessels (Wang *et al.*, 2006). Additionally, models stimulating angiogenesis at the time of MI in a mouse led to improved cardiac function (Tirziu *et*

al., 2007) and reactivated CMs that entered a state of reversible contractile arrest, or hibernation, that evaded cell death (May *et al.*, 2008).

1.4.2 Therapeutic strategies trialled for ischaemia-reperfusion injury

Considering the impact PPCI has had on survival rates following MI, there has been a great effort to identify therapies to limit IRI so that the clinical progression of these patients is favourable (Hausenloy and Yellon, 2013).

Despite the capacity for CM regeneration, this mechanism is clearly insufficient to fully repair the extensive damage produced following MI and IRI (Bergmann *et al.*, 2009; Bergmann *et al.*, 2015; Foglia and Poss, 2016). Maintaining cardiac function following injury relies on remodelling presenting its own problems (Kehat and Molkentin, 2010), as detailed above. As such, there has been extensive research and clinical trials into the possibility of using stem or cellular therapies to enhance CM regeneration post-MI or in patients suffering from heart failure (Min *et al.*, 2002; Lalit *et al.*, 2014). Unfortunately, despite these promising pre-clinical studies, Phase I and II clinical trials transplanting stem cells with the aim to repair cardiac damage have shown variable outcomes, likely due to a combination of factors such as method of delivery and type of stem cell transplanted (Sheng *et al.*, 2013; Chen *et al.*, 2015; Lemcke *et al.*, 2018). Additionally, cardiosphere cardiac derived stem cells have been tested in clinical trials, demonstrating promising results from the pre-clinical CADUCEUS study (Makkar *et al.*, 2012) especially regarding the safety profile of this therapy (Marbán, 2014; Kapelios *et al.*, 2016; Chakravarty *et al.*, 2017). However, again subsequent trials (ALLSTAR and CAREMI trial) have failed to demonstrate improvements in heart function correlating with attenuating remodelling after MI following treatment with cardiosphere cardiac derived stem cells (Tyler *et al.*, 2018; Rikhtegar *et al.*, 2019).

Likewise, promising pre-clinical trials showing the benefit of promoting angiogenesis following MI to improve recovery led to a number of clinical trials. However, these also have resulted in varying outcomes with many not replicating the positive results from *in vivo* studies (Silvestre, 2012; Gaspar *et al.*, 2019). Mostly these have been based on the transplantation of bone-derived stem cells, with results varying from unsuccessful transplantation to a modest increase in LV EF (Tateishi-Yuyama *et al.*, 2002; Assmus *et al.*, 2006; Lunde *et al.*, 2006; Schächinger *et al.*, 2006), or testing

gene delivery of pro-angiogenic growth factors (Losordo *et al.*, 1999; Kastrup *et al.*, 2005; Stewart *et al.*, 2006; Stewart *et al.*, 2009). Transplantation of growth factors have also been trialled (Schumacher *et al.*, 1998; Unger *et al.*, 2000; Simons *et al.*, 2002), but neither strategy have developed any therapies with a clear benefit and further studies are necessary (Gaspar *et al.*, 2019).

An alternative therapy for myocardial IRI that has been trialled is the use of anti-inflammatory therapies, given the role inflammation plays in directing myocardial repair and remodelling (Huang and Frangogiannis, 2018). Again, studies have seemed encouraging, yet clinical trials are unable to consistently recapitulate the beneficial outcomes from murine models to patients (Roberts *et al.*, 1976; Peters *et al.*, 1978; Bush *et al.*, 1980; Gislason *et al.*, 2006; Brophy *et al.*, 2007). This is likely due to the heterogeneity of MI and repair processes between patients, therefore generating more targeted and tailored approaches may be more successful in the future (Huang and Frangogiannis, 2018).

Given the prominent role OS and ROS play in establishing IRI, antioxidants have also been suggested as a therapy (Hausenloy and Yellon, 2013). However, like the regeneration, angiogenic and anti-inflammatory therapies, the outcomes from clinical trials varies (Barta *et al.*, 1991; Westhuyzen *et al.*, 1997; Demirag *et al.*, 2001; Marczin *et al.*, 2003) and as such the National Institute for Health and Care Excellence no longer recommends administering antioxidant supplements to patients post-MI (National Institute for Health and Care Excellence (NICE), 2007).

Instead of using antioxidants to target OS generally, antioxidants have also been developed that specifically target mitochondrial OS. These antioxidants specific to mitochondria include MitoQ, which is able to enter and accumulate within the mitochondria where it is reduced to form an active antioxidant. The accumulation of MitoQ makes it a more potent antioxidant compared to normal antioxidants, and therefore an attractive potential therapy. MitoQ was tested in a model for IRI, where rats were orally administered MitoQ in their water supply, their hearts were then excised, perfused by a Langendorff system, and then subjected to ischaemia followed by reperfusion. The MitoQ regime correlated with improved cellular and tissue function, decreased cytochrome c release and limited mitochondrial dysfunction (Adlam *et al.*, 2005). However, this work needs to be continued to trial the effects of MitoQ and other

mitochondria-targeting antioxidants on heart function in humans before it can be accepted as a routine therapy to protect against the effects of IRI (Xia *et al.*, 2016).

Given the lack of promising therapies for IRI as a mechanism to limit adverse remodelling and improve cardiac function, alternative strategies and targets are desperately required. A number of studies from this lab have demonstrated that in the heart and other tissue systems, including the liver, lungs and brain, OS can induce cellular senescence (Hewitt *et al.*, 2012; Jurk *et al.*, 2014; Ogrodnik *et al.*, 2017; Birch *et al.*, 2018; Anderson *et al.*, 2019). Furthermore, in a number of animal models it has been shown that senescence could contribute to myocardial remodelling (Bujak *et al.*, 2008; Zhu *et al.*, 2013). The role of senescence in other CVDs associated with increased OS, such as MI with IRI, has not been investigated and is postulated to represent a potential therapeutic target in this study.

1.5 Cellular senescence

Cellular senescence was classically defined as a somatic cell irreversibly losing the potential to proliferate, and which has permanently exited the cell cycle (Passos *et al.*, 2009; Campisi, 2013; Childs *et al.*, 2015). As such, senescence is also considered to be a potent anti-cancer mechanism. Unfortunately senescence may contribute to tissue dysfunction, as an accumulation of senescent cells is associated with many age-related disorders (Campisi and d'Adda di Fagagna, 2007).

Senescence was first described in 1961 by Hayflick and Moorhead (Hayflick and Moorhead, 1961) and has been classified into the following groups; replicative, stress-induced premature senescence (SIPS), and oncogenic induced senescence (OIS) (Lowe *et al.*, 2016).

1.5.1 Replicative senescence

Replicative senescence was the first type of cellular senescence to be discovered and defined in 1961 (Hayflick and Moorhead, 1961). In this study they discovered that embryonic fibroblasts had a finite potential to replicate. In culture the fibroblasts were capable of 50 divisions \pm 10, however, past this point they were unable to continue proliferating and went into a state of permanent arrest (Passos *et al.*, 2009). Years

later it was reported that telomeres, the nucleotide tandem repeats capping chromosomes to keep chromosomes stable (Martínez and Blasco, 2015), were the stimulus for initiating senescence (Passos *et al.*, 2009). As a result of inefficiencies in DNA replication with each round of cellular division, the telomeric regions progressively shorten, until they can no longer protect the chromosome ends, termed uncapping, and are recognised as DNA double strand breaks (DSBs). This elicits a DNA damage response (DDR), and an upregulation of p53, and the cell therefore exits the cell cycle. If this damage is not repaired, cell replication is inhibited irreversibly. This event is called “Hayflick Limit”, which was first used in 1974 to describe this discovery (Burnett, 1975; Shay and Wright, 2000).

1.5.2 Stress-induced premature senescence

Another form of senescence is SIPS. Stress-induced premature senescence refers to senescent events stimulated by non-oncogenic stress stimuli and in somatic cells that have not yet reached their Hayflick limit. This type of senescence shares many molecular and cellular characteristics with replicative senescence and OIS (Suzuki *et al.*, 2013). In the case of SIPS sub-lethal stress stimuli, including OS, prompt senescence through accumulation of DNA damage that activates the DDR (Dumont *et al.*, 2000). Although this form of DDR and senescence activation does not require telomere shortening this lab has recently demonstrated that telomeres also play a role in SIPS. It was shown that not only are telomeres highly susceptible to stress-inducible DNA damage, from OS or irradiation, but also the DNA repair machinery is not able to efficiently repair DSBs. Therefore, unlike the majority of genomic DNA damage, which can be repaired, these telomere-associated foci of DNA damage, termed TAF, are persistent. This persistent presence of DSBs continuously activates the DDR and induces senescence, regardless of telomere length (Figure 1.4) (Victorelli and Passos, 2017; Anderson *et al.*, 2019). As such TAFs are not only an important mediator of senescence but also a robust marker of SIPS (Hewitt *et al.*, 2012).

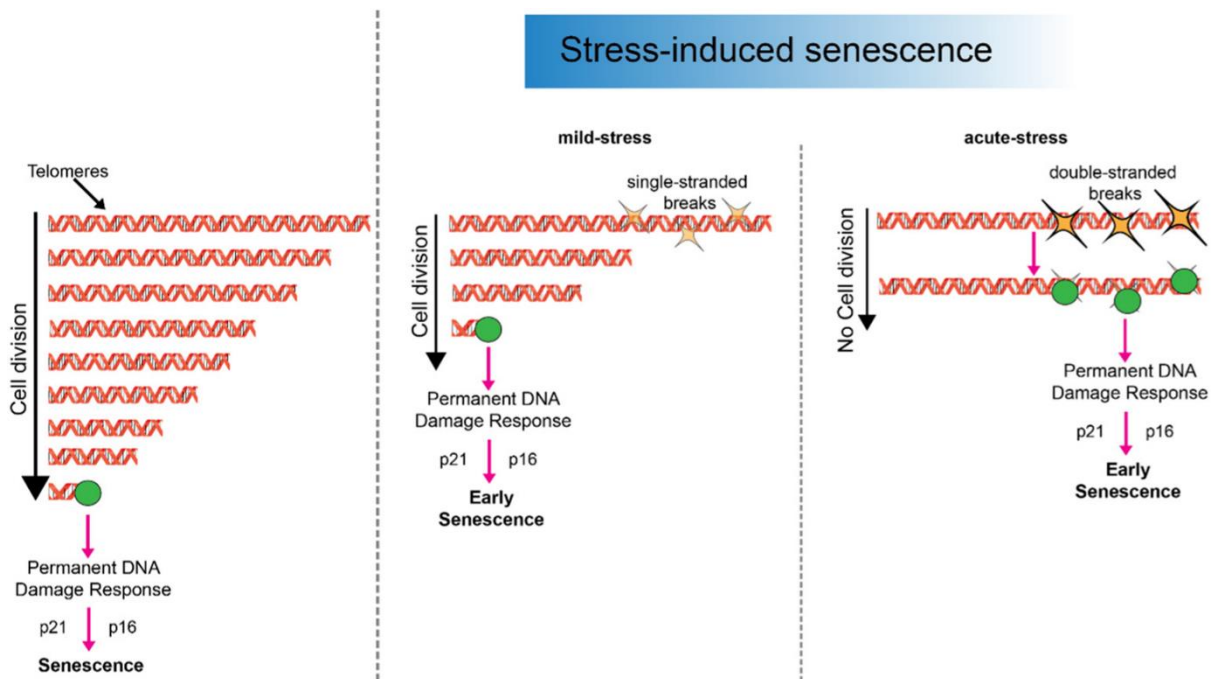


Figure 1.4 Replicative senescence vs stress-induced premature senescence.

Normal telomere shortening with each cell division leads to telomeres being uncapped and recognised as DNA damage leading to senescence, or replicative senescence, on left panel. The central panel illustrates how mild-stress causes single-stranded breaks that accelerate the rate at which a cell becomes senescent; a form of SIPS. DSBs on the other hand immediately activate the DDR and the cell is prematurely senescent. Taken from Victorelli and Passos (Victorelli and Passos, 2017).

Further demonstrating that continued replication is not required for senescence induction are the observations that post-mitotic cells can acquire a senescent phenotype. Neurons and adipocytes have been identified *in vivo*, both human and mice, to express markers and characteristics of senescent cells such as elevated p21^{CIP}, senescence-associated β -galactosidase (SA- β -Gal) activity and pro-inflammatory interleukin levels (Sedelnikova *et al.*, 2004; Minamino *et al.*, 2009; van Deursen, 2014; Ogrodnik *et al.*, 2019b). Non-dividing cells are not immune from mutations occurring, and there is increasing evidence demonstrating that post-mitotic cells such as CMs and neurons can become senescent. However, the role of senescence has not been fully characterised in all post-mitotic cells and diseases affecting them, and further investigations are essential to answer outstanding questions (Campisi and d'Adda di Fagagna, 2007; van Deursen, 2014; Sapielha and Mallette, 2018; Anderson *et al.*, 2019; Ogrodnik *et al.*, 2019b; Walaszczyk *et al.*, 2019).

1.5.3 Oncogene-induced senescence

Oncogene-induced senescence operates as a tumour suppressor mechanism that acts to prevent benign tumours developing into malignant tumours, which have an immortal phenotype and cannot become senescent. When activated, the oncogene Ras induces a short period of cellular proliferation that is then halted. Simultaneously, there is a rise in the levels of p53 and p16^{INK4a} proteins, both of which are tumour suppressors and play pivotal roles in the establishment of senescence (Campisi and d'Adda di Fagagna, 2007; Courtois-Cox *et al.*, 2008; Kilbey *et al.*, 2008).

1.5.4 Common pathways controlling senescence

While the mechanism driving the induction maybe different in these different classes, a common feature of senescence is that DNA damage and activation of the DDR are central events in senescence establishment. The DDR network exists to detect DNA damage, halt cell cycle progression and initiate DNA damage repair mechanisms (Hanawalt, 2015). The tumour suppressor and transcription factor p53 plays a vital role in regulating the DDR. Transcriptional activation of many specific downstream genes, including the cyclin-dependent kinases (CDK) inhibitor p21^{CIP}, initiates the DDR to halt cell cycle progression and repair DNA (Lieberman *et al.*, 2017). p21^{CIP} blocks CDK2 from inhibiting the retinoblastoma (Rb) protein family members (Figure 1.5). Activated Rb drives senescence by halting the cell progressing through the cell cycle. p53 and subsequently p21^{CIP} can be activated by numerous stimuli including the CDK inhibitor p14^{ARF}/19^{Arf} (in humans/mice) which are other suggested senescence biomarkers (Campisi and d'Adda di Fagagna, 2007; Capparelli *et al.*, 2012; Childs *et al.*, 2015). Persistent DDR activation due to a failure in repairing the DNA damage will lead to a cell to undergo apoptosis, autophagy or senescence (Lieberman *et al.*, 2017).

Another important CDK inhibitor that causes cell cycle arrest is p16^{INK4a}. In this case, activated p16^{INK4a} prevents CDK4/6 from exerting inhibitory effects on Rb family members (Figure 1.5). Together p21^{CIP} and p16^{INK4a} are both often upregulated in many types of senescent cells. Some studies report that majority of senescent cells express p16^{INK4a} (Baker *et al.*, 2011). p16^{INK4a} and p21^{CIP} appear to be the best CDK inhibitors as candidates or senescence biomarkers (Baker *et al.*, 2011; Capparelli *et al.*, 2012; Childs *et al.*, 2015; Watanabe *et al.*, 2017).

Many studies have highlighted the importance that p16^{INK4a} plays in senescence development and disease pathogenesis (Muñoz-Espín *et al.*, 2013; Munoz-Espin and Serrano, 2014; Da Silva-Álvarez *et al.*, 2019). With this in mind a mouse model with a drug inducible system of p16^{Ink4a} expressing cells was developed in 2011 (Baker *et al.*, 2011; Naylor *et al.*, 2013). The INK-ATTAC mouse model was designed to express caspase-8 under transcriptional control of p16^{Ink4a} expression. Upon administration of the drug AP20187, the caspase-8 proteins in the senescent cell membranes would dimerise to activate caspase-8 and initiate apoptosis of p16^{Ink4a} expressing senescent cells (Baker *et al.*, 2011). Improved outcomes were observed when AP20187 was administered including hindered tumour formation, delayed age-related organ dysfunction and improved life span (Baker *et al.*, 2011; Baker *et al.*, 2016).

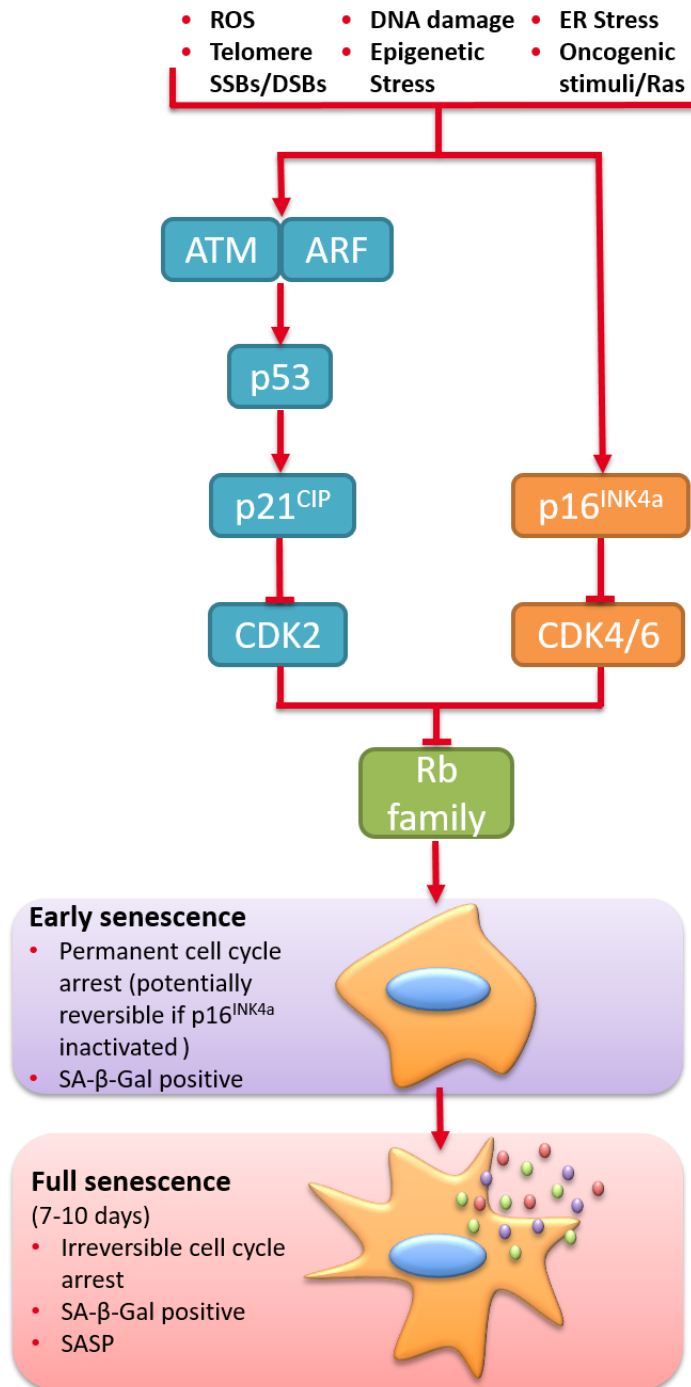


Figure 1.5 Activation of senescence.

Diagram showing stress stimuli activating p53/p21^{CIP} and p16^{INK4a} pathways ultimately leading to Rb inhibition, exit from the cell cycle and initiation of senescence. If senescence becomes fully established it develops the SASP, and if not cleared (aka chronic senescence) will lead to tissue dysfunction. Acute senescence is beneficial for processes such as wound repair and tumour suppression. Adapted from Childs et al (Childs *et al.*, 2015).

1.5.5 Classical senescence marker

Senescence-associated β -galactosidase has been the most prevalent biomarker used for senescence, mainly because it is simple to detect and many senescent cell types have shown up-regulation of the lysosomal β -galactosidase at pH6.0. At this pH, this biomarker is found to only be expressed by senescent cells and not by cells in any other state both *in vitro* and *in vivo*. The colorimetric assay using the substrate X-Gal detects the level of β -galactosidase in situ. Developed in 1995, this assay has been used and reported extensively in over 2,400 publications to detect cellular senescence (Lee *et al.*, 2006; Campisi and d'Adda di Fagagna, 2007; Itahana *et al.*, 2013).

Despite its universal utilisation, the role of SA- β -Gal in senescence has not been completely defined and some studies challenge its efficiency and suitability. There are some studies that found this assay generated false positive data, or did not generate consistent, reproducible results. As senescence is a multi-factorial process, and considering the issues surrounding the SA- β -Gal assay, it is wise to use this biomarker in combination with other biomarkers of senescence (Lee *et al.*, 2006).

1.6 Senescence, age-related disease and the senescence-associated secretory phenotype

Senescence drives the ageing phenotype (McHugh and Gil, 2018). A number of studies from this lab and others have demonstrated that senescence via OS plays a role in organ dysfunction in a number of different tissue systems, including the liver, lungs, brain and heart (Passos *et al.*, 2010; Jurk *et al.*, 2014; Birch *et al.*, 2015; Ogrodnik *et al.*, 2017; Anderson *et al.*, 2018; Anderson *et al.*, 2019; Ogrodnik *et al.*, 2019b; Walaszczyk *et al.*, 2019). A hallmark of senescent cells is the production of the senescent-associated secretory phenotype (SASP). The SASP is a complex combination of numerous factors including growth factors, cytokines, chemokines, ECM factors, proteases and many others that have potent signalling properties and are released from the senescent cell. It can act in both an autocrine manner, to maintain senescence in the cell, and a paracrine fashion to drive the establishment of senescence in neighbouring cells (Figure 1.6) (Acosta *et al.*, 2008; Coppé *et al.*, 2008; Kuilman *et al.*, 2008; Coppé *et al.*, 2010; Rodier and Campisi, 2011; Watanabe *et al.*, 2017). The SASP is initiated by the DDR and has been demonstrated to take around

7-10 days to fully develop at which point the cell is irreversibly senescent (Coppé *et al.*, 2008; Passos *et al.*, 2009).

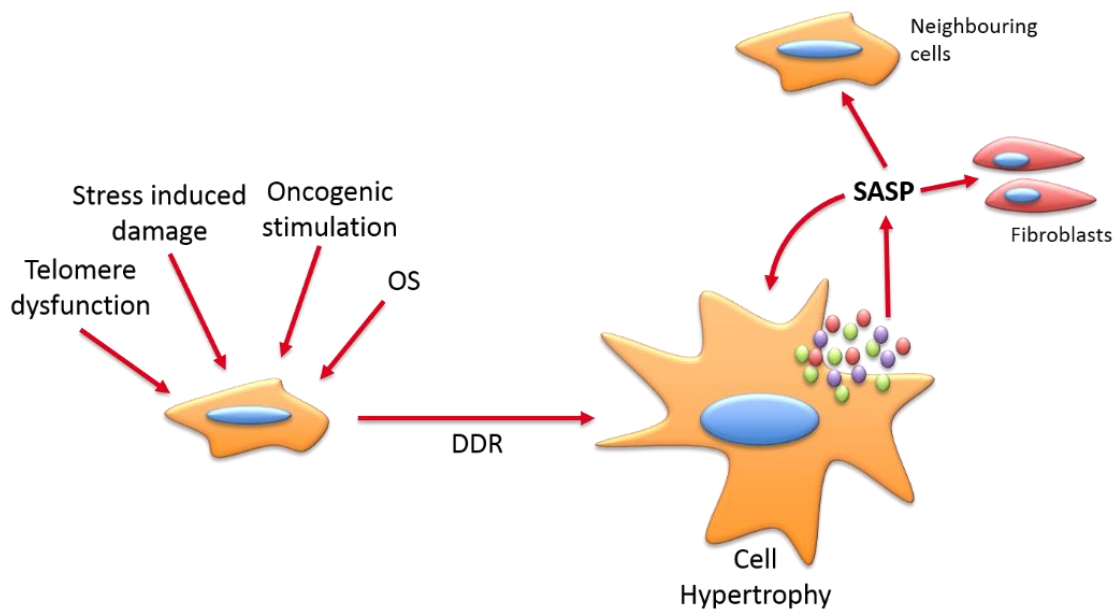


Figure 1.6 Cellular changes after induction of senescence.

Initiation of senescence from different stimuli elicits DNA damage that in many cases activates the DDR causing the cell to become senescent, adopting many hallmarks of senescence including hypertrophy and the SASP. The SASP can act in an autocrine and paracrine manner to initiate senescence in different cell types.

The SASP can be highly detrimental in some scenarios and can: cause and maintain chronic inflammation; promote tumours depending on the oncogenes involved and whether p53 is deficient; and also hinder tissue repair and alter tissue architecture which are both related to the ageing process (Demaria *et al.*, 2015; Velarde and Demaria, 2016; Watanabe *et al.*, 2017). Evidence has shown that senescence can initiate malignant tumour formation *in vivo* through the accumulation of certain types of senescent cells, in particular senescent fibroblasts, and via components of the SASP communicating with activated oncogenes (Coppé *et al.*, 2010; Rodier and Campisi, 2011; Childs *et al.*, 2015). These components include IL-6 and interleukin-8 (IL-8), however, the SASP is incredibly complex and not all SASP proteins stimulate cancer development (Rodier and Campisi, 2011).

Regardless of the SASP factors involved and the final outcome, an important definition of a senescent cell is its ability for paracrine communication with other cells. The presence of the SASP is what separates a non-senescent cell that has exited the cell

cycle, for example a quiescent or terminally differentiated cell, to a senescent cell (Watanabe *et al.*, 2017).

In terms of ageing and disease, the SASP drives tissue dysfunction via ECM deterioration, disrupting stem cell function, deregulating cell differentiation and promoting inflammation (Figure 1.7) (van Deursen, 2014). Proteases are components of the SASP and their cleavage activity on receptors, ligands and the ECM disrupts the integrity of the tissue (Parrinello *et al.*, 2005; Laberge *et al.*, 2012). Tissue function can also be adversely affected by induction of a SASP due to components, such as IL-6 and IL-8, promoting tissue fibrosis and inflammation (van Deursen, 2014). The SASP is a cocktail of up to 40-80 signalling factors many of which have known pro-inflammatory roles (Coppé *et al.*, 2010; Freund *et al.*, 2010), and can impact normal cell differentiation, as demonstrated by senescent fibroblasts in *in vitro* co-cultures leading to aberrant epithelial differentiation, proliferation and migration, mostly via the activity of the SASP factor matrix metalloproteinase-3 (MMP-3) (Parrinello *et al.*, 2005). Additionally, senescent fibroblasts and the SASP factors they secrete can promote the process termed epithelial-mesenchymal transition (van Deursen, 2014). Epithelial and mesenchymal cells act synergistically to create an epithelial barrier in organs stabilised by the ECM produced by mesenchymal cells, however, cytokines released from senescent fibroblasts can stimulate them to change their phenotypes. In cancer this process is important in the generation of tumour cells. As well as this, epithelial-mesenchymal transition enables tumour cells to migrate and invade alternative tissues progressing the tumour to a metastatic cancer (Laberge *et al.*, 2012). This process has also been shown to be involved in a range of other diseases of the pulmonary system, including asthma, chronic obstructive pulmonary disease and idiopathic pulmonary fibrosis (Bartis *et al.*, 2014), to the gastrointestinal, renal and digestive system, affecting the pathogenesis of Crohn's disease (Jiang *et al.*, 2017), glomerulonephritis (Jinde *et al.*, 2001) and liver fibrosis (Zeisberg *et al.*, 2007b). All the above processes initiated by a SASP led to tissue dysfunction which is associated with ageing and age-related pathologies (Childs *et al.*, 2015).

Stem cell dysfunction has also been attributed to senescence and the SASP (van Deursen, 2014). The BubR1 mouse is a model of accelerated ageing with a hypomorphic *BubR1* allele reducing the activity of this mitotic checkpoint regulator resulting in mice displaying several hallmarks of progeria and ageing phenotypes

(Baker *et al.*, 2004). In the muscle and adipose tissue from the BubR1 mouse, the stem cell populations were strongly affected by a senescent environment and levels were around 3-fold lower than in age-matched wild type mice (Baker *et al.*, 2013). This data supports the idea that with ageing senescence induces tissue dysfunction by preventing efficient regeneration of tissues (van Deursen, 2014)

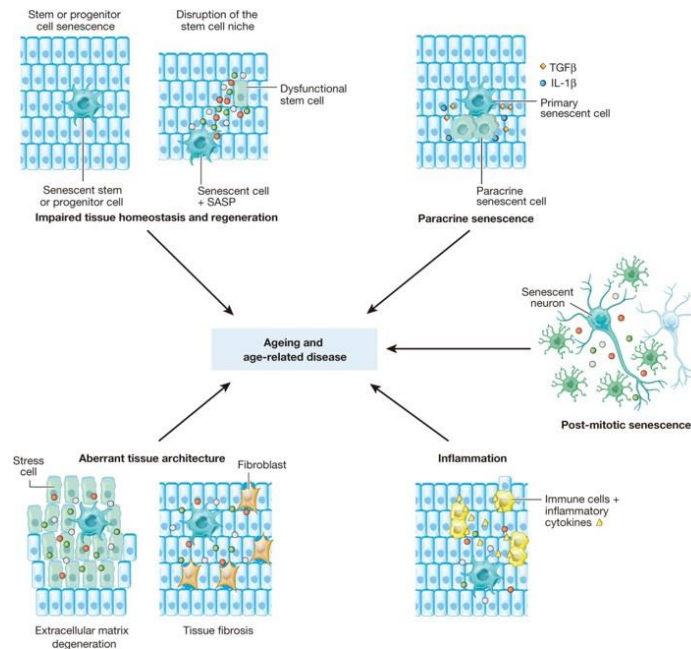


Figure 1.7 Age-related cellular disorders.

Cellular senescence is associated with many aspects of ageing, chronic diseases and tissue dysfunction. This occurs via several pathways that utilise the SASP, which allows a senescent cell to signal in a paracrine fashion to neighbouring cells to impair regeneration, trigger inflammation, and alter cellular architecture through the ECM, fibrosis and abnormal cell differentiation. Taken from van Deursen, J. (van Deursen, 2014).

A model that supports the hypothesis of a SASP contributing directly to ageing and tissue dysfunction is the INK-ATTAC mouse (Baker *et al.*, 2011). As described above, administration of the compound AP20187 leads to activation of caspase 8 in p16^{Ink4a} expressing cells resulting in the targeted clearance of p16^{Ink4a} positive, senescent cells (Baker *et al.*, 2011; Baker *et al.*, 2016). When crossed onto the BubR1 line, treatment with AP20187 led to a reduction in senescence and SASP markers in the skeletal muscle, eye, adipose, kidney and heart, correlating with fewer events of sarcopenia, cataracts, accumulated adipose tissue, kidney dysfunction, glomerulosclerosis, CM hypertrophy and cardiac death (Baker *et al.*, 2011; Baker *et al.*, 2016). This result has also been replicated in an INK-ATTAC mouse crossed with the MAPT^{P301SPS19} line,

which displays elevated levels of tau in neurons resulting in neurodegenerative symptoms (Bussian *et al.*, 2018). Tau plays a structural role in the formation and stabilisation of microtubules that are components of neuronal cytoskeletal system, as well as a signalling role in maintaining homeostasis in the brain. Therefore, mutations to tau can cause either loss of function or aberrant gain of function that is toxic to the neuron (Gendron and Petrucelli, 2009; Rosenmann *et al.*, 2012). These mice were shown to accumulate factors relating to the SASP and senescent astrocytes and microglia, both mitotic cells of the nervous system (Streit, 2006; Gonzalez-Perez and Quiñones-Hinojosa, 2012), and their clearance improved neuron density and other characteristics of neurodegeneration (Bussian *et al.*, 2018). When INK-ATTAC mice were fed a high fat diet or dosed with the insulin receptor antagonist S961 (Vikram and Jena, 2010), they developed insulin resistance and were utilised as a model of Type II diabetes (Aguayo-Mazzucato *et al.*, 2019). These mice also displayed an augmented SASP profile yet after AP20187, or pharmacological clearance of senescence, SASP factors were significantly reduced correlating to improvements in diabetes associated pathologies suggesting the SASP does play a role in disease (Aguayo-Mazzucato *et al.*, 2019).

1.7 Senescence and the heart

Cardiovascular diseases are also associated with ageing as a significant risk factor (Dhingra and Vasan, 2012; Niccoli and Partridge, 2012; Balakumar *et al.*, 2016). Despite studies showing an association between CVDs and senescence hallmarks, there are uncertainties regarding senescence as a causative factor in CVDs *in vivo*, and how exactly the role senescence plays may be detrimental to the heart (Serrano and Andrés, 2004b; Erusalimsky and Kurz, 2005).

This may be in part be due to the concept that replicative senescence occurring as a result of telomere shortening during cell proliferation and DNA division has been considered the major contributor to the accumulation of senescence with age (Childs *et al.*, 2015; McHugh and Gil, 2018). While this can explain the accumulation of senescence in rapidly dividing tissues it seems unlikely that this would be the primary driver of senescence in the heart which is relatively quiescent (Anderson *et al.*, 2019).

However, there is data that suggests that if telomere dysfunction is induced this is associated with changes in the heart that are characteristic of myocardial ageing. In comparison to humans, mice possess very long telomeres that are five-ten times longer than human telomeres (Calado and Dumitriu, 2013). Therefore, to model human ageing because of telomere dysfunction due to replicative senescence an mTERC^{-/-} transgenic mouse, was established. These mice lack an RNA component of telomerase, the enzyme that maintains telomere length (Blasco *et al.*, 1997; Toussaint *et al.*, 2002) and as such all the cells in these mice, including the germ cells, lack the ability to extend or maintain their telomeres (Blasco *et al.*, 1997). Therefore, telomere length is inherited with each generation and with each generation mice offspring display progressive telomere shortening which by generation 3 (G3) results in critically short telomeres and chromosomal instability (Artandi *et al.*, 2000) resembling replicative senescence.

Mice from G3 or later generations have a premature ageing phenotype with increased incidence of tumours (Artandi *et al.*, 2000). These mice also displayed characteristics of cardiomyopathies, comprising of increased end diastolic pressure, decreasing LV mass : volume ratio and CM hypertrophy in the LV (Leri *et al.*, 2003), hallmarks which are associated with ageing in humans (Villari *et al.*, 1997). This suggests that ageing by telomere attrition and induced senescence can be causative to CVD development (Leri *et al.*, 2003). While in the normal physiological state replicative senescence may not be the mechanism of cardiac senescence (Anderson *et al.*, 2019) the mTERC^{-/-} mouse supports the observation that the induction of senescence through shortening telomeres is associated with remodelling in the heart which is detrimental to cardiac health. (Leri *et al.*, 2003; Deng *et al.*, 2008). In addition, mice lacking *Sirtuin 1* or *Bmi*, genes that antagonise the senescence program, develop cardiac dysfunction, hypertrophy, fibrosis and subsequently a dilated cardiomyopathy (Tong *et al.*, 2013; Gonzalez-Valdes *et al.*, 2015). In contrast, global deletion of p53, a master transcriptional regulator of both senescence and apoptosis, protects against pressure overload and MI induced heart failure (Matsusaka *et al.*, 2006; Sano *et al.*, 2007).

Other evidence that senescence may be detrimental to myocardial health is the link between cardiomyopathy and chemotherapies including doxorubicin. Doxorubicin is an anthracycline often used to treat some types of cancer. It is known to trigger senescence in CMs and leads to cardiomyopathies sometimes years after treatment

has ended depending on the dose of the drug (Maejima *et al.*, 2008; Spallarossa *et al.*, 2009; Piegari *et al.*, 2013). Doxorubicin induces senescence by targeting telomeric binding factors that under normal physiological conditions aid in telomere and chromosomal stability and by increasing p53 levels. Downregulation of these telomeric binding factors led to senescence, however, if the level of downregulation exceeded a certain threshold then the cell may go down the apoptosis pathway (Spallarossa *et al.*, 2009). This model provides further evidence that drug therapies such as doxorubicin can induce senescence in CMs, and that hypertrophy and a loss of regeneration potential can result in cardiomyopathies and heart failure (Spallarossa *et al.*, 2009).

More recently, our lab has also begun to dissect the mechanism by which senescence contributes to myocardial ageing. Our data suggests that CM senescence not only accumulates with age but also promotes myocardial remodelling dysfunction. Senescence induced dysfunction was caused both directly as the senescent phenotype is directly associated with CM hypertrophy and also indirectly via the production of a SASP which promotes myofibroblast differentiation and inhibits proliferation of different cardiac cell lineages *in vitro* (Anderson *et al.*, 2019). We have described a mechanism by which rarely cycling or even post-mitotic CMs accumulate senescence with age. These data suggest that OS, because of mitochondrial dysfunction, induces DNA damage in telomeric regions leading to the formation of TAF. In both mice and humans these TAF are a persistent form of DDR and induce CM senescence through the classical senescence-inducing pathways, p21^{CIP} and p16^{INK4a} (Anderson *et al.*, 2019).

Senescence has been reported to drive the ageing phenotype (McHugh and Gil, 2018), and CVDs are also associated with ageing as a significant risk factor (Balakumar *et al.*, 2016). Despite studies showing an association between CVDs and senescence hallmarks, there are uncertainties regarding senescence as a causative factor in CVDs *in vivo*, and how exactly the role senescence plays may be detrimental to the heart in terms of numerous cardiovascular pathologies (Serrano and Andrés, 2004a; Erusalimsky and Kurz, 2005).

1.7.1 Senescence, ageing and regeneration

There is a clear association between senescence, impaired regenerative potential with age and the progression of degenerative diseases in other self-renewing tissues (Sahin and Depinho, 2010). Studies investigating CM turnover in mice and humans have presented data suggesting the same may be true of the heart. Wild type and mdx mice (a model of cardiomyopathy) both demonstrated the ability to undergo CM renewal, which was reduced with age (Richardson *et al.*, 2015a) and in their CM studies Bergmann *et al.* demonstrated in humans CMs retain the potential to regenerate throughout life, however, CM turnover decreases from approximately 0.8% at 20 years to around 0.3% at 70 years (Figure 1.8) (Bergmann *et al.*, 2015). While the direct contribution of senescence to age-related impaired CM regeneration is unclear, there are a number of possible mechanisms by which this may occur.

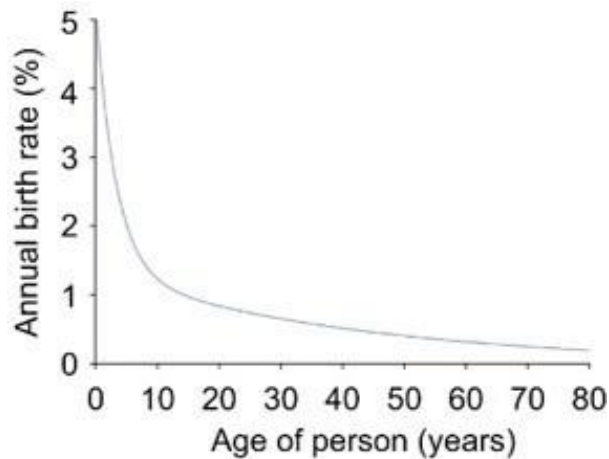


Figure 1.8 Turnover of human cardiomyocytes.

Graph illustrating the exponential decrease in CM renewal rates with age. By the second decade of life the CM turnover rate is <1%, at about 0.8%, which declines to around 0.3% in later life (70-80 years). Taken from Bergmann *et al.* (Bergmann *et al.*, 2015).

CM proliferation contributes directly to CM turnover (Hsieh *et al.*, 2007; Loffredo *et al.*, 2011; Malliaras *et al.*, 2013; Senyo *et al.*, 2013), therefore it is possible that CM senescence of the subpopulation of proliferative CMs may directly impair myocardial function through cyclin kinase inhibitor expression and cell cycle exit (Alam *et al.*, 2019a). It has also been demonstrated that the accumulation of senescence with age is not exclusive to the CM population. Lewis-McDougall *et al.* show with age the human cardiac stem cell progenitor population that are c-kit^{pos}/CD31^{neg}CD45^{neg} also can

become senescent and accumulate in the heart (Lewis-McDougall *et al.*, 2019). Expression of p16^{INK4A}, SA-β-Gal and DNA damage markers in these stem progenitor cells increased proportionally with age. Those stem progenitor cells positive for senescence markers were not positive for proliferation markers, and when transplanted into young mice that were subjected to permanent LAD ligation the rates of progression to heart failure correlating with attenuated regeneration was elevated when compared to young mice receiving proliferative progenitor cells in this MI model. Additionally, *in vitro* senescent stem progenitor cells generated a SASP that induced the bystander effect in healthy cultures by increasing senescence induction and preventing proliferation (Lewis-McDougall *et al.*, 2019). This combined with the data from our lab also showing senescence and the SASP accumulates with age, attenuates proliferation and is associated with cardiac dysfunction but in the CM population (Anderson *et al.*, 2019) supports the hypothesis that senescence within many cardiac cell lineages results in a diminished regenerative potential that contributes to dysfunction with age or after injury.

This data regarding senescence in the cardiac stem cells could also potentially explain the failure of pre-clinical trials to translate clinically into regenerative therapies (Lewis-McDougall *et al.*, 2019). Preclinical studies focus on the use of young healthy animals (Hsieh *et al.*, 2007; Malliaras *et al.*, 2013) whereas using aged subjects would be more clinically relevant (Redgrave *et al.*, 2016). The epidemiology of CVDs shows that the prevalence of CVDs increases in a linear fashion with age (Yazdanyar and Newman, 2009), and thereby most individuals will have a higher level of background myocardial senescence (McHugh and Gil, 2018; Anderson *et al.*, 2019) that would create an unfavourable environment via the SASP hindering the success of regeneration transplant strategies (Lewis-McDougall *et al.*, 2019; Oldershaw *et al.*, 2019).

1.7.2 Role of senescence in cardiac remodelling

During our previous studies, we have demonstrated even in young animals induced senescence contributes to adverse myocardial remodelling and cardiac dysfunction (Anderson *et al.*, 2019). As discussed earlier, OS and ROS generation are known inducers of cellular senescence. Using a mouse model for cardiac specific overexpression of monoamine oxidase-A (MAO-A), an oxidative enzyme that generates ROS in the form of hydrogen peroxide (H₂O₂) (Lairez *et al.*, 2009; Sturza *et*

al., 2013), we demonstrated that young mice CM overproduction of OS was associated with increased CM senescence, as demonstrated by the formation of TAF. These mice also demonstrated CM hypertrophy and cardiac dysfunction all of which could be rescued in part by treatment with the anti-oxidant N-acetyl cysteine (NAC) (Anderson *et al.*, 2019). Data which demonstrates a direct association between OS, senescence, myocardial remodelling and cardiac function (Anderson *et al.*, 2019).

Senescence-associated secretory phenotype factors, however, have a range of effects depending on the circumstances, resulting in the heterogeneous nature of senescent cells (Coppé *et al.*, 2010). For example, senescence and the SASP are also central components in embryonic development and initiating tissue repair. In development, senescence acts in a regulatory manner in tissue development and patterning, including the pharyngeal arches that give rise to the aortic arch (Muñoz-Espín *et al.*, 2013; Storer *et al.*, 2013; Phillips *et al.*, 2019). Interfering with senescence and SASP factors resulted in patterning defects across both murine, chick, zebrafish, human other species' embryos, demonstrating that senescence is a conserved and essential event to control development (Storer *et al.*, 2013; Rhinn *et al.*, 2019). In tissue repair, wounds stimulate migration of fibroblasts to the injured tissue that differentiated into myofibroblasts. These myofibroblasts proliferate for a period of time depositing ECM to begin the process of wound closure, followed by transient induction of senescence in the myofibroblasts that express a SASP. This switch to the senescent phenotype serves to limit myofibroblast proliferation and SASP, which includes MMPs that degrade ECM proteins, limiting fibrosis and promoting clearance of these senescent myofibroblasts (Jun and Lau, 2010a; Rodier and Campisi, 2011; Demaria *et al.*, 2015; Watanabe *et al.*, 2017).

However, in other disease settings fibroblast senescence is associated with the production of a SASP that contributes to chronic inflammation and is pro-fibrotic. In the liver, senescence within the hepatocyte population correlated with liver steatosis, or fat accumulation, predisposing the mouse to elevated inflammation and fibrosis (Jurk *et al.*, 2014; Ogrodnik *et al.*, 2017). The same trends have been observed in models of pulmonary fibrosis (Schafer *et al.*, 2017; Waters *et al.*, 2018) and kidney disease (Valentijn *et al.*, 2018) (Chawla and Kimmel, 2012; Knoppert *et al.*, 2019).

Similar data has been reported for the heart. The heart is a multicellular organ, and the contribution of senescence in other cardiac cell types should also be taken into

account. Senescence induction and regulation within the fibroblast population is essential for the formation of a scar, which is needed to prevent cardiac rupture, and also to limit excessive fibrosis, which is important in order to retain as much cardiac function as possible (Leask, 2015; Meyer *et al.*, 2016). The role of cardiac fibrosis after injury was resolved using murine models including transverse aortic constriction (TAC) and a p53/p16^{Ink4a} knockout model (Meyer *et al.*, 2016). In the TAC model, the aorta was surgically ligated to simulate pressure overload-induced cardiac hypertrophy and fibrosis (Rockman *et al.*, 1991), and in wild type mice this resulted in increased fibrosis, expression of a panel of senescence markers and evidence showing that mostly myofibroblasts were the cell type undergoing senescence. Next, TAC was performed on p53 and p16^{Ink4a} knockout mouse models to understand the role of these pathways in fibroblast senescence. Senescence markers were only decreased in double knockout mice and correlated with more extensive fibrosis and reduced cardiac function. Interestingly this severe phenotype was not achieved if only p53 or p16^{Ink4a} was knocked out (Meyer *et al.*, 2016). Due to the parallel nature of these two pathways (Figure 1.5), they may act in a compensatory manner when one is disrupted (Leong *et al.*, 2009) , however, dual-knockouts of both p53 and p16^{Ink4a} increase the risk of tumourigenesis (Sharpless *et al.*, 2002).

Fibroblasts have been shown to become senescent subsequent to MI and *in vitro* both ischaemia and hypoxia induce senescence in cardiac fibroblasts, indicated by increased expression of p53 and p21^{Cip} (Zhu *et al.*, 2013; Zhu *et al.*, 2015). It has also been suggested that senescence plays a role in limiting the extent of fibrosis post-MI as p53 inhibition increases myofibroblast proliferation and collagen production *in vitro*. Mice lacking expression of p53 have also been shown to have an increased scar size following MI compared to control but displayed an increased inflammation, including the expression of known SASP proteins including IL-1, chemokine ligand 1 (CXCL1), CXCL2, monocyte chemoattractant protein 1 (MCP-1), IL-6, granulocyte chemotactic protein 2 (GCP-2) and macrophage colony-stimulating factor (M-CSF) some of which are known inducers of fibrosis (Zhu *et al.*, 2013; Schafer *et al.*, 2018). As such, while in the short term senescence and the SASP may limit fibrosis, an accumulation of senescent fibroblasts post-MI might also contribute to chronic inflammation exacerbating ongoing cardiac collagen deposition and fibrosis formation. Therefore, the SASP plays a key role in mediating the effects, beneficial and detrimental,

observed during senescence in the heart (Zhu *et al.*, 2013; Zhu *et al.*, 2015). Additionally with age, clearance of senescent cells, especially via the immune system, deteriorates (Rodier and Campisi, 2011). As such inefficient removal of senescent fibroblasts may occur in the older patients who are most likely to suffer a MI. This may ultimately predispose this patient group towards chronic inflammation and fibrosis, which would be detrimental to cardiac function (Zhu *et al.*, 2013).

Traditionally the composition of the heart has been thought to primarily consist of fibroblasts, although recent evidence suggest that more than 50% of murine cardiac cells are endothelial cells and only around 12% are fibroblasts (Pinto *et al.*, 2017). As discussed previously, angiogenesis is an essential recovery and remodelling mechanism after MI to stimulate new blood vessel growth for revascularisation of damaged myocardium (He *et al.*, 2017). Senescence in the endothelial cell population has been shown to reduce angiogenesis and impair recovery in induced models of CVD (Sano *et al.*, 2007; Erusalimsky, 2009; Cameron *et al.*, 2016). In a mouse model of pressure overload in the LV, elevated levels of endothelial cell senescence markers were observed which was associated with vascular rarefaction (the loss of vasculature associated with hypertension (Gogiraju *et al.*, 2015; Cameron *et al.*, 2016). Removal of these senescence signals, using p53 knockout mice lines or pharmacologically targeting p53 using pifithrin- α , reversed this phenomena resulting in elevated angiogenesis as well as leading to other beneficial events associated with remodelling and function including reduced fibrosis and LV dilation (Sano *et al.*, 2007; Gogiraju *et al.*, 2015).

Endothelial cell senescence has also been attributed as causal to increased inflammation of the vascular networks (Shimizu and Minamino, 2019), OS and endothelial dysfunction (Donato *et al.*, 2018), which can result in a SASP mediated endothelial-to-mesenchymal transition (EndMT). This process describes the transition of a differentiated endothelial cell into an alternative cell type, and has been shown to contribute to the fibroblast population after injury in the heart (Zeisberg *et al.*, 2007a; von Gise and Pu, 2012; Pérez *et al.*, 2017). Detached endothelial cells shift their expression of endothelial markers, such as CD31, to a myofibrotic profile of markers composed of collagens and MMPs after stimulation from a range of signalling proteins (Twist, Slug, Snail and zinc finger E-box protein homeobox-1) (Stenmark *et al.*, 2016). As EndMT has been shown to occur after exposure to TGF- β 1 and contribute

significantly to cardiac fibrosis in the TAC model, EndMT has been suggested a novel target to limit fibrosis and attenuate disease progression (Piera-Velazquez *et al.*, 2011).

Although there are many detrimental effects of excessive OS, preventing OS entirely may be detrimental itself if vital signalling pathways required for homeostasis or repair are deterred. Evidence to support the dual-role of ROS paradigm is the failure of antioxidants to alleviate injury, for example MI, or extend lifespan (Sanz *et al.*, 2006). In models of *Drosophila* and *C.Elegans* ROS secreted from the mitochondria have been concluded to have contrary effects, as they can have both beneficial and detrimental signalling roles in modulating mitochondrial function and lifespan (Scialò *et al.*, 2016). In mammals, elevated ROS have a role in wound repair to promote many mechanisms including: vasoconstriction and initiation of thrombus generation; attracting neutrophils and other immune cells towards the site of injury; mediating phagocytosis to remove invading cells; and triggering repair mechanisms including angiogenesis and ECM formation (Dunnill *et al.*, 2017). Consideration of the advantageous as well as harmful ROS signalling effects should be made when therapeutically targeting OS in disease and ageing (Scialò *et al.*, 2016).

Hypoxia relating to OS brought about by DDR activation is known to act as a switch turning off and on proliferation in CMs. Although uncommon, there have been case-studies reporting MI events in neonates that share many characteristics with MI in adults, such as an altered S-T segment detected by ECG and detection of cTn I and T biomarkers. Though there is only about a 50% survival rate in new-borns, and most cases are preferentially treated using thrombolytics (Papneja *et al.*, 2017). There is one case of a new-born male suffering from MI immediately after birth followed by complete regeneration. The patient presented with cyanosis, abnormal ECG and elevated cTn biomarkers. The diagnosis was severe cardiac injury and doctors detected an occlusion caused by thrombosis in the left anterior descending (LAD) artery. The artery had been occluded for over 20 hours before therapy with thrombolytics commenced. Interestingly the patient's cardiac function improved and biomarker levels returned to normal. Heart function appeared fully restored and there were no apparent structural defects within 2 months of the event, with these findings confirmed at the 1 and 3 year follow-ups (Haubner *et al.*, 2016). This case study, along with a few others, confirm that CM regeneration accompanied by complete restoration

of cardiac function is achievable in neonates. Improving our understanding of the mechanisms involved gives the potential of translating this knowledge in the treatment of MI in adults (Murugan *et al.*, 2009; Farooqi *et al.*, 2012; Cesna *et al.*, 2013; Haubner *et al.*, 2016).

In post-natal CMs, ROS generated from mitochondria represent a key source of OS. The sudden loss of CM proliferation potential shortly after birth has been attributed to the shift from the hypoxic environment in the uterus to the post-natal environment and the associated mitochondrial ROS damage. In adults, for example during MI, there is a reduction in inspired oxygen correlated with a drop in ROS that is able to restart CM proliferation, and may be a viable target to stimulate cellular regeneration and proliferation (Nakada *et al.*, 2017). It is this train of thought that has halted the practice to administer oxygen in STEMI patients. Oxygen therapy was traditionally viewed as a method to reduce myocardial injury and reverse the effects of the MI, however, it is now considered to contribute to the injury by stimulating increased levels of ROS that causes IRI, senescence, and limits proliferation (Stub *et al.*, 2012; Stub *et al.*, 2015). In 1986, Murry *et al.* (Murry *et al.*, 1986) first described ischaemic preconditioning (IPC), an important discovery demonstrating that short periods of ischaemia and reperfusion could reduce the infarct size following MI (Hausenloy *et al.*, 2016). Despite many laboratories replicating IPC and publishing data that unravels some of the ambiguities surrounding IRI, the exact signalling pathways involved are not entirely known (Penna *et al.*, 2009; Hausenloy *et al.*, 2016). Limiting oxygen to therapeutically improve CM regeneration appears counter intuitive. However, ROS are known to have numerous effects, depending on the source, levels and type of ROS. It also appears that there is a small population of resident CMs that can be activated during hypoxia to proliferate (Nakada *et al.*, 2017), suggesting they may possess a degree of immunity to the detrimental effects of OS. Nakada *et al.* (Nakada *et al.*, 2017) reported that in a mouse model of permanent MI (that has not been allowed to reperfuse and therefore has not suffered from IRI) the chronic hypoxia led to a significantly increased heart : body weight ratio, had smaller fibrotic scars, and a recovered LV systolic function that was not achieved in the non-hypoxic controls (Jun and Lau, 2010a).

Oxidative stress is complex, playing roles in both maintaining tissue homeostasis during health (Sanz *et al.*, 2006) but also during disease in promoting inflammation, fibrosis and adverse remodelling (Hybertson *et al.*, 2011). The data from our lab

supports the hypothesis of accumulating OS driving CM senescence with ageing (Anderson *et al.*, 2019), and given the contribution of OS to the pathogenesis of IRI post-MI (Kurian *et al.*, 2016), potentially CMs may enter a state of senescence in response to MI with IRI, however, to date it has not been thoroughly investigated. If senescence is involved following IRI, given the breadth of damaging effects that (Figure 1.9) senescence has on multiple cardiac cell populations, cellular senescence is therefore a potentially highly favourable and novel cardiac therapeutic target.

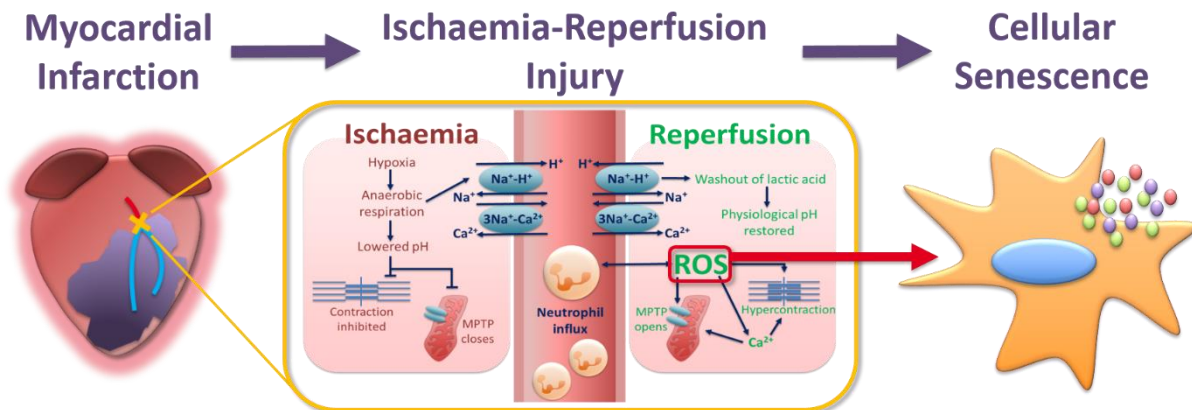


Figure 1.9 Hypothesised association between myocardial infarction, ischaemia-reperfusion injury, oxidative stress and cellular senescence.

After MI, the gold-standard therapy is to undergo timely reperfusion via PPCI. Although this salvages any viable myocardium it can stimulate IRI, which is associated with generating a state of OS that is also known to drive cellular senescence.

1.7.3 Targeting senescence therapeutically

Cellular senescence is a complex process that when established can have many different outcomes depending on the delicate balance of various factors expression, that can initiate both beneficial and detrimental events. However, it is an important and central event in many pathologies and therefore research is being conducted into many potential therapeutic targets (Munoz-Espin and Serrano, 2014; van Deursen, 2014).

The SASP is a key hallmark of senescence and has been shown to exert a variety of effects on senescent cells (Coppé *et al.*, 2010; Campisi, 2013). As mentioned earlier, in the heart following MI the SASP is controlled by p53 expression. Therefore, p53 could be a potential therapeutic target to control senescence in cardiac fibroblasts to mediate scar formation and avoid rupture, but also to ensure fibrosis doesn't accumulate and become detrimental to heart function (Zhu *et al.*, 2013). Although other

studies that administered SASP inhibitors in both animal models and humans demonstrated they can have beneficial effects and reverse some characteristics of senescence, SASP inhibitors operate via numerous mechanisms. Because of this it is not always clear exactly how the SASP inhibitors exerted their effects, and in some cases they cause unfavourable side effects (Kirkland and Tchkonja, 2017).

Due to OS being an established link between IRI and senescence, antioxidants as therapeutic agents have also been considered. Quercetin, a senolytic drug, operates as a potent antioxidant, however, the effects were limited to only some cell types making it not ideal for general use to target senescence (Soto-Gamez and Demaria, 2017). Other antioxidant research focuses on MAO-A. In the mitochondrial outer membrane is MAO-A, an enzyme that catalyses oxidative deamination of monoamines and produces the ROS by-product, H₂O₂. In the heart and other ageing models, MAO-A has been suggested to be an OS source and associated with other markers of senescence (Villeneuve *et al.*, 2013). Data from this lab focused on MAO-A in an ageing senescence study. A mouse was generated to have a CM specific overexpression of MAO-A, and showed to have increased markers of senescence, including TAFs, and cardiac dysfunction. Therapy with the antioxidant NAC rescued the phenotype (Anderson *et al.*, 2019). However, elucidating the specific ROS sources and how to target them may represent a superior way to therapeutically target OS, as antioxidant therapies have given inconsistent results across many IRI and senescence trials (Giordano, 2005; Hausenloy and Yellon, 2013).

Considering the efficiency of the mouse model INK-ATTAC with an inducible clearance system for p16^{Ink4a}, this model was also utilised by this lab to address if there was a direct link between senescent CMs and hypertrophy (Anderson *et al.*, 2019). Initially, young INK-ATTAC mice were irradiated to stimulate TAF formation and then underwent a regime of AP20187, the drug that leads to dimerization of caspase 8 in p16^{Ink4a} expressing cells triggering apoptosis (Baker *et al.*, 2011; Baker *et al.*, 2016). Irradiation was demonstrated to lead to an increase in the mean number of TAFs, percentage of TAF positive CMs and CM hypertrophy, all of which were restored with AP20187 therapy. This confirms that cells expressing p16^{Ink4a} influence DNA damage associated with CM hypertrophy (Anderson *et al.*, 2019).

However, the INK-ATTAC mouse is bred onto a mouse line that is associated with augmented cardiovascular dysfunction (BubR1) which may be too severe to allow

senescence cell clearance to improve life expectancy. This cardiovascular dysfunction is unrelated to cellular senescence and p16^{Ink4a} expression, therefore it cannot be ruled out that targeting senescence in CVDs may improve cardiac function and disease pathogenesis (Baker *et al.*, 2011; Naylor *et al.*, 2013). Indeed, this lab has also demonstrated that in an aged wild type mouse, senescence is directly detrimental to recovery and function following MI. If treated with a senolytic drug pre-emptively before permanent MI, the cardiac function of mice was improved and mortality rates due to surgery reduced to that reflecting a young mouse (Walaszczyk *et al.*, 2019).

A potential drug therapy to clear senescence cells are senolytics. Senolytic drugs act by triggering activation of apoptotic pathways in senescent cells resulting in senescent cell clearance. This is not targeted to specific cell types, rather they act to target components of anti-apoptotic pathways to inhibit cellular survival (Table 1.1) (Zhu *et al.*, 2015; Kirkland and Tchkonina, 2017; Short *et al.*, 2019). So far the components that have been trialled as potential therapeutic targets have included B-cell lymphoma (Bcl)-2/Bcl-X_L, P13K/Akt, p53/p21^{CIP}, tyrosine kinases and hypoxia inducible factor-1 α (HIF-1 α). However, as with any clinical trial for a developed drug, there are many associated complications with translating senolytics into therapies. As senescence is associated with ageing, it becomes trickier to test the effects of senolytics with defined endpoints at suitable time periods, which may be years after treatment began. Considerations also have to be made regarding the benefit of the therapy against any potential risks or side effects. A set of guidelines have been defined specifically for clinical trials involving senolytics (Burd *et al.*, 2016; Justice *et al.*, 2016).

However, senolytics are undergoing trials for use in many diseases related to senescence. One group has demonstrated improved cardiac function in mice with senolytic treatment (Dasatinib and Quercetin) but the results were variable (Zhu *et al.*, 2015). Some of the more promising senolytic agents have progressed from preclinical into clinical trials, including navitoclax (Health, 2017; Kirkland and Tchkonina, 2017).

Navitoclax (ABT-263) is a senolytic drug that targets the intrinsic apoptotic pathway (Figure 1.10). The intrinsic pathway, which is also known as the mitochondrial pathway, is triggered when sub-lethal damage to the cell is detected, stimulating activity from the anti-apoptotic class of regulatory proteins termed BCL-2 proteins (Montero and Letai, 2018). This BCL-2 family of apoptosis inhibitors including BCL-2, BCL-X_L (which are both class I anti-apoptotic members) and BCL-W are categorised according to their

Table 1.1 Table of senolytics, based on (Kirkland *et al.*, 2017; Kim and Kim, 2019).

Senolytic	Target	Outcomes	Side effects	References
Navitoclax (ABT-263)	Bcl-2 family (Bcl-2, -XL, -W)	Increase haematopoietic and muscle stem cell function Reduce atherosclerotic lesion formation	Thrombocytopenia	(Chang <i>et al.</i> , 2016; Zhu <i>et al.</i> , 2016)
Venetoclax (ABT-199)	Bcl-2	<i>Not yet tested in vivo as a senolytic</i>	-	(Souers <i>et al.</i> , 2013; Li <i>et al.</i> , 2019)
ABT-737	Bcl-2 family (Bcl-2, -XL, -W)	Increase hair follicle stem cell function Reduce IRI in lung	Thrombocytopenia	(Stamelos <i>et al.</i> , 2012; Yosef <i>et al.</i> , 2016)
A1331852	Bcl-XL	Reduce liver fibrosis	Neutropenia	(Zhu <i>et al.</i> , 2017; Moncsek <i>et al.</i> , 2018)
Dasatinib & Quercetin	Tyrosine kinase pathways	Increase cardiac function, vasomotor function and lifespan Reduce atherosclerosis, osteoporosis, hepatic steatosis, pulmonary fibrosis	Gastrointestinal discomfort Headache	(Zhu <i>et al.</i> , 2015; Roos <i>et al.</i> , 2016a; Farr <i>et al.</i> , 2017; Ogrodnik <i>et al.</i> , 2017; Schafer <i>et al.</i> , 2017; Xu <i>et al.</i> , 2018; Justice <i>et al.</i> , 2019)
Tanespimycin (17-AAG)	HSP90	Increase healthspan Reduce age-related symptoms	Hepatotoxicity	(Jhaveri <i>et al.</i> , 2012; Fuhrmann-Stroissnigg <i>et al.</i> , 2017)
Fisetin	PI3K/AKT	Increase lifespan, liver and pancreas function	<i>None reported – is a natural compound</i>	(Maher, 2015; Zhu <i>et al.</i> , 2017; Yousefzadeh <i>et al.</i> , 2018)
Piperlongumine	Multiple pathways	<i>Not yet tested in vivo as a senolytic</i>	-	(Wang <i>et al.</i> , 2016; Go <i>et al.</i> , 2018)
FOXO4-related peptide	p53 p21 ^{Cip} serpine	Increased renal function and hair growth Reduced liver toxicity from doxorubicin and frailty	<i>No reported adverse effects</i>	(Baar <i>et al.</i> , 2017)

BCL-2 homology domains. Class I proteins comprise BH1 to BH4 (Kelekar and Thompson, 1998). Together these domains create a hydrophobic groove that is constructed from two α -helices that are hydrophobic and six which are amphipathic (Liu *et al.*, 2016). The high sequence homology between BCL-2 proteins indicates that the groove structure is highly conserved and alterations to BH1, 2 or 3 result in a loss of anti-apoptotic activity as heterodimerisation with other BCL-2 proteins is unfeasible (Muchmore *et al.*, 1996; Liu *et al.*, 2016).

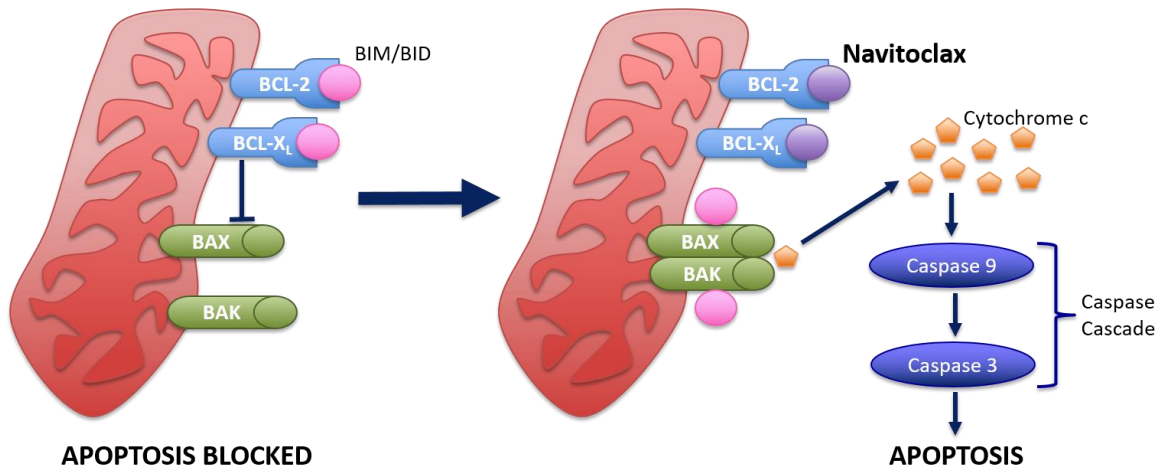


Figure 1.10 Navitoclax mechanism of action.

Illustration of navitoclax mechanism of action. It binds to anti-apoptotic proteins BCL-X_L/2 to displace pro-apoptotic factors such as BIM and BID. Once released, BIM and BID can bind to BAX and BAK generating a pore in the outer mitochondrial membrane and stimulate the release of cytochrome c from the mitochondria to activate the caspase cascade, via caspases 9 and 3, to trigger apoptosis of the senescent cell. Adapted from Rosell, R. *et al* and Montero, J. and Letai, A. (Rosell *et al.*, 2013; Montero and Letai, 2018).

The BH3 domain is highly important for the BCL-2 proteins to bind and act antagonistically on proteins that stimulate apoptosis, termed class II and III proteins. Neither class possesses either BH1 or 2, but BH3 is present (class II also have BH4, whereas class III are also referred to as BH3-only proteins) (Kelekar and Thompson, 1998). In the class I and II proteins, BH4 can bind to and form a heterodimer with BCL-2 associated X protein (BAX). Evading apoptosis in this manner differs to the classical binding and inhibition of BH3 pro-apoptotic proteins, and requires further investigation (Liu *et al.*, 2016) as preventing cell death via BAX binding may not always be sufficient (Hanada *et al.*, 1995).

In contrast, the class III proteins apoptotic-promoting activity is essential in efficiently regulating apoptosis. This group of proteins is extensive and diverse including the proteins BCL-2 interacting mediator of cell death (BIM) and BH3-interacting domain death agonist (BID) amongst many others (Shamas-Din *et al.*, 2011). Both these pro-apoptotic proteins during homeostasis are sequestered and inactivated via binding to anti-apoptotic proteins such as BCL-2 and BCL-X_L. Upon stimulation from an apoptotic signal BIM and BID are released, or administration of a BH3-mimetic such as navitoclax will preferentially displace BIM and BID releasing them into the cytoplasm (Zhu *et al.*, 2016), and once unbound BIM and BID are then able to bind to BAX and BCL-2 homologous antagonist killer (BAK). Binding directly initiates oligomerisation of BAX and BAK generating pores and mitochondrial outer membrane permeabilisation (MOMP). Once this occurs proteins that reside in the inner membrane space of mitochondria including cytochrome c are able to migrate into the cytoplasm signalling the “point of no return” for the cell (Kelekar and Thompson, 1998; Shamas-Din *et al.*, 2011). Once in the cytoplasm, cytochrome c can form complexes and activate caspase 9, which is the first caspase in the caspase cascade and ultimately results in apoptosis of the cell (Figure 1.10) (Kelekar and Thompson, 1998; Rosell *et al.*, 2013; Edlich, 2018).

Currently there is no published data investigating navitoclax action on CMs in a model of IRI. However, it is the first senolytic drug that demonstrated high potency, high specificity and high efficiency for binding to its target, in multiple different senescent cell types (Chang *et al.*, 2016), and promising data from trials of navitoclax on aged mice heart function both with and without permanent MI (Walaszczyk *et al.*, 2019), therefore led to navitoclax being selected for trial on CMs in this project.

Another therapeutic option would be to target the pathways activating senescence. The p16^{INK4a} pathway is an important pathway triggering senescence (Figure 1.6). The INK-ATTAC mouse model demonstrated highly efficient clearance of p16^{INK4a} expressing senescent cells (Baker *et al.*, 2011) and previous work confirmed that these senescent cells are associated with DNA damage inducing hypertrophy (Anderson *et al.*, 2019). Because of this evidence, targeting p16^{INK4a} specifically in the CMs may be an efficient mechanism to clear detrimental senescence without impacting other cell types, for example fibroblasts that require senescence to drive wound healing (Rodier and Campisi, 2011). For this study, a novel CM-specific knockout model for p16^{INK4a}

was developed to investigate the specific role p16^{Ink4a} has in initiating CM senescence and the contribution of CM senescence to cardiac dysfunction after MI with IRI.

1.8 Aims

Considering the evidence in the literature supporting a detrimental role and critical need to target IRI post-MI, the strong association of IRI and cellular senescence to OS, and how CMs retain a small regeneration and proliferation potential that can be influenced by the degree of ROS, all led to the hypothesis and primary aims of this project. This project focused on the CMs in the BZ following IRI and investigated the role of senescence of these CMs and how they impact infarct size and cardiac function.

The aims and hypotheses of this project are defined below:

1. Quantify senescence in an *in vivo* model of MI and IRI using LAD ligation.

Reperfusion after MI leads to IRI generating ROS which triggers senescence in cardiomyocytes and other cardiac cell lineages.

2. Investigate the potential utilisation of the senolytic compound navitoclax therapeutically post-MI and IRI in an *in vivo* mouse model.

Senescence induced following IRI in the heart contributes to adverse remodelling and is detrimental to recovery. Clearance of senescent cells pharmacologically using a senolytic will attenuate adverse remodelling and cardiac function will improve. Therefore, progression to heart failure will be delayed or prevented.

3. Generate a novel transgenic model in which p16^{Ink4a} is specifically knocked out of the CM population and to test if recovery is improved following MI and IRI when CM senescence is attenuated.

Cardiomyocytes have been observed to senesce in a model of MI with IRI. Preventing activation of the p16^{Ink4a} pathway via floxing exon 1α of p16^{Ink4a} will stop CM senescence and attenuate adverse remodelling resulting in improved cardiac function.

4. Examine the contribution of non-CMs in the myocardium to cardiac dysfunction and adverse remodelling. Develop *in vitro* models of cardiac fibroblast senescence to study the effects of a fibrotic SASP on numerous cardiac cell types when senescence is induced.

Cardiac cells as well as CMs, including fibroblasts, are undergoing senescence resulting in excessive fibrosis and a reduction in reparative and regeneration mechanisms.

Chapter 2. Materials and Methods

All mice used for the following experiments were male C57BL/6 (3-4 months of age, purchased from Charles River) and treated accordingly to the UK Home Office Animals Scientific Procedures Act, 1986 (UK Government, 1986). Mice were housed in the Functional Genetics Unit in the Institute of Genetic Medicine, Newcastle University, unless otherwise stated.

2.1 Coronary artery ligation mouse model

Surgical occlusion of the LAD coronary artery, a major coronary artery of the LV, is deemed to be a reproducible and representative model of MI, and is the standard model currently used (Salto-Tellez *et al.*, 2004). All surgeries were carried out according to a Home Office approved protocol (P011C564C – Protocol 8) (Redgrave *et al.*, 2016) under appropriate conditions by a microsurgeon, Dr Rachael Redgrave.

In brief, intra-operative analgesia was induced by pre-treating mice with fentanyl/fluanison (0.4ml/kg, Hypnorm) prior to anaesthesia using isoflurane, which was maintained using mechanical ventilation following endotracheal intubation (2.5% isoflurane/97.5% oxygen, 130-140 stroke rate, stroke volume initially 5ml/kg – increased to 7.5ml/kg post-thoracotomy). At the fourth intercostal space, left-side thoracotomy was executed to allow removal of the pericardium and enable a 7-0 prolene suture to be placed around the LAD and loosely tied. An infarction was simulated by inserting a piece of 1-2mm PE-10 tubing into the suture loop and tightening the suture knot to terminate blood flow for 60 minutes (Figure 2.1). After this period the PE-10 tubing was removed to allow the LAD to be reperfused. Reperfusion was visually confirmed before the chest cavity was closed and anaesthesia discontinued. Mice were extubated once breathing spontaneously and received buprenorphine (0.05mg/kg, Vetergesic) for post-operative analgesia. Whilst recovering, the mice were placed in a 33°C incubator until they regained normal physical activity.

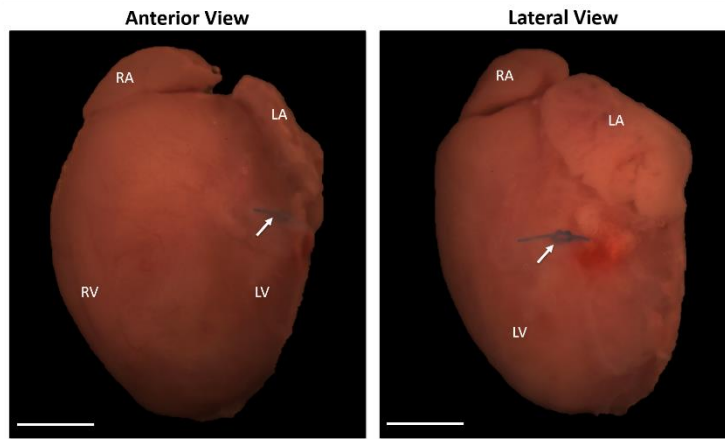


Figure 2.1 Position of suture around the left anterior descending coronary artery.

Tubing tied in the suture compresses the LAD ceasing blood flow for 60 minutes, simulating MI and producing an ischaemic region. After this, the tubing is removed to allow reperfusion and IRI to occur. The suture is left (indicated by the arrow) to minimise damage to the ventricle wall and allow easy identification of the affected region. Scale bar = 2mm.

2.2 Navitoclax treatment

Navitoclax was prepared in a lipid vehicle solution consisting of EtOH, polyethylene glycol and Phospal 50 PG in a 1:3:6 ratio respectively, according to Chang *et al* (Chang *et al.*, 2016). During the Navitoclax treatment, mice also received a dose of 5-ethynyl-2-deoxyuridine (EdU) at 100µg/mg of body weight (BW), via intraperitoneal injection (IP) for 7 days, to allow for identification of newly generated cells.

Details regarding the specific experimental procedures are outlined in section 4.3 but in brief mice were provided Navitoclax (ABT263, A10022, AdooQ Bioscience LLC) daily at a dose of 50mg/kgBW/day from day four post-LAD ligation for 7 days via oral gavage. Control mice for this study also had LAD ligation surgery but received a lipid-vehicle control (EtOH, glycol and Phospal 50 PG alone in a 1:3:6 ratio respectively) via oral gavage for the treatment period as well as EdU via IP.

2.2.1 Cardiac magnetic resonance imaging

Magnetic Resonance Images (MRI) were generated at 3 and 5 weeks post-LAD ligation on the horizontal bore 7.0T Varian microimaging system (Varian Inc., Palo Alto, CA, USA) (Davison, 2014; Redgrave *et al.*, 2016) situated at the Campus for Ageing and Vitality, Newcastle University. During scanning mice were housed in the Keith Unit

on site. The MRI scans were performed by Dr Simon Tual-Chalot, Dr Anna Walaszczyk, and Emily Dookun (E.D.); E.D. solely performed the analysis and interpretation of images.

Mice were anaesthetised using isoflurane (3.5% initially and once unconscious isoflurane reduced to 1.5% with 1L/min oxygen) administered by facemask then placed on a specially designed stage with integrated electrocardiographic, cutaneous, temperature and respiratory monitors. To ensure that the orientation of the heart was optimal for imaging, a scout image was performed. Once correctly orientated, the whole heart was imaged using FLASH cine MR sequence. Each MR sequence is initiated by the R wave of the electrocardiogram (ECG), which corresponds to end diastole. Short, continuous axis slices with a 1mm thickness were acquired so that the whole LV could be visualised (Davison, 2014; Redgrave *et al.*, 2016).

2.2.2 Magnetic resonance imaging analysis

Images were analysed using Image J (NIH) using a previously published methodology in accordance with (Schneider *et al.*, 2006; Davison, 2014; Redgrave *et al.*, 2016). All images for each individual axis slice were combined to give a stack image showing the heart at that axis throughout the cardiac cycle. At the point of end diastole and end systole, the area of the epicardium and endocardium were measured (Figure 2.2). From this the total myocardial area for that slice could be calculated. Other variables relating to ventricular volumes and cardiac function were calculated and are outlined in Table 2.1.

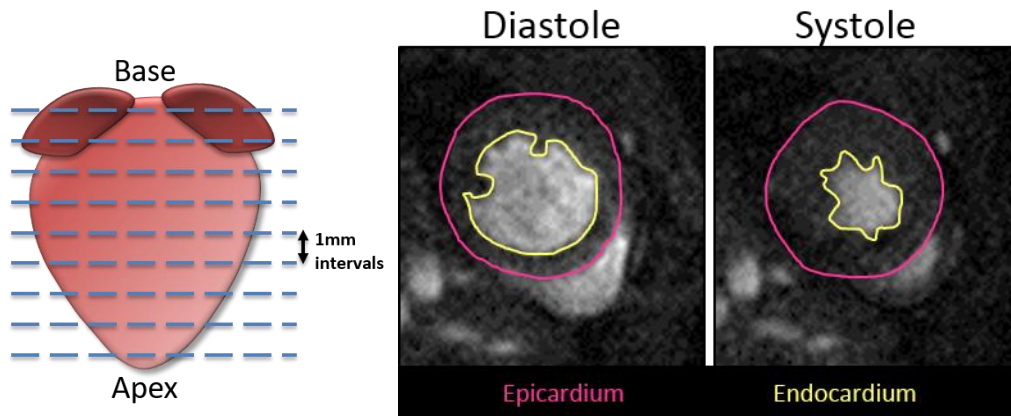


Figure 2.2 Measurements taken for magnetic resonance imaging analysis. Images were taken in a series of stacks at 1mm intervals from apex to base. The border of the LV epicardium (pink) and endocardium (yellow) were measured in each stack to quantify the area of myocardium and other subsequent variables outlined in Table 2.1 analysed from the MRIs.

Table 2.1 Variables quantified from magnetic resonance imaging analysis.
Calculations used to determine variables assessed from MRI analysis.

Variable	Equation
Total Myocardial Volume (mm ³)	Myocardial Area per slice (mm ²) x Number of slices throughout ventricle x Slice thickness (1mm/slice)
Left Ventricle Mass* (mg)	Myocardial Volume (mm ³) x Myocardial Specific Gravity (1.05mg/mm ³)
Left Ventricle Volume per slice (mm ³)	Endocardial Area (at end diastole or end systole)(mm ²) x Slice thickness (1mm/slice)
End Diastolic Volume (LV-EDV) (μl)	Σ Left Ventricle Volume per slice at end diastole
End Systolic Volume (LV-ESV) (μl)	Σ Left Ventricle Volume per slice at end systole
Stroke Volume (SV) (μl)	LV-EDV (μl) – LV-ESV (μl)
Ejection Fraction (EF) (%)	[SV (μl) / LV-EDV (μl)] x 100
Cardiac Output (CO) (ml/min)	[SV (μl) x Heart Rate (BPM)] / 1000

*Presented as the average of LV mass independent of end diastolic and end systolic measurements

2.3 Novel transgenic mouse generation

While the above pharmaceutical approaches should provide insight into the therapeutic potential of senolytic treatments for IRI, since they influence senescence systemically they are insufficient to address questions regarding the direct contribution of CM senescence to myocardial remodelling. To address this, I developed a novel transgenic model in which *p16^{Ink4a}* is specifically knocked out in the CM population. This model has been achieved by crossing two established transgenic mouse models; the *αMHC-MerCreMer* line (ID 005657, The Jackson Laboratory) and the *p16Ink4a^{fllox/fllox}* line (ID B6.129(Cg)-Cdkn2a^{tm2.1Nesh/Nci}, NCI Mouse Repository).

The α MHC-MerCreMer line works on the principal of the cardiac specific promoter myosin heavy chain (α MHC) controlling the expression of Cre recombinase (Laboratory, 2017). Cre recombinase has been widely utilised across many research fields due to the simplicity in purifying and expressing this enzyme (Sauer, 2002; Gilbertson, 2003; Kos, 2004; Brault *et al.*, 2007; Wirth *et al.*, 2007; Birling *et al.*, 2009; Wang *et al.*, 2011; Lanza *et al.*, 2012). It acts by genetically altering or mutating transgenes by inserting DNA cassettes into chromosomes. It is predominantly used to orchestrate the removal of a gene that is flanked with *loxP* sites. These sites are bound with a high affinity to Cre leading to dimer formation bringing the *loxP* sites together and excision of the gene (Van Duyne, 2015). In this case, α MHC-MerCreMer was an inducible form of Cre that was activated upon administration of a synthetic ligand, tamoxifen or 4-hydroxytamoxifen (4-OHT). (Kam *et al.*, 2012). Therefore, in this system the Cre expression can be precisely stimulated at certain time-points to clear senescence expression specifically in CMs.

The p16^{Ink4a}^{flox/flox} line has been created with *loxP* sites flanking exon 1 α of *p16^{Ink4a}* (B6.129(Cg)-*Cdkn2a*^{tm2.1Nesh/Nci}, 01XBU, NCI Mouse Repository). Therefore, when crossed with the Cre mouse (B6.FVB(129)-*A1cfTg*^{(Myh6-cre/Esr1*)1Jmk/J}, 005657, The Jackson Laboratory), these exons are spliced out leaving a truncated version of *p16^{Ink4a}* (*p16^{-/-}*, Figure 2.3). Once recombined with Cre, previous studies were unable to detect any levels of p16^{Ink4a} protein in this mouse model (Monahan *et al.*, 2010), which implies that the truncated p16^{Ink4a} protein is likely to be unstable.

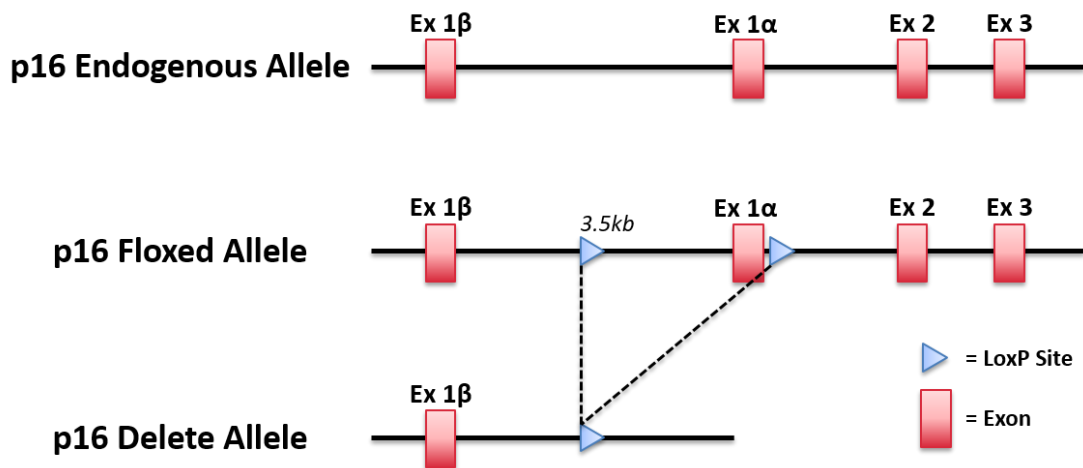


Figure 2.3 Schematic of generation of $p16^{Ink4a}$ floxed mice from crossing the $p16^{Ink4a^{flox/flox}}$ line with the Myh6-MerCreMer line.

Upon administration of tamoxifen therapy, Cre recombinase was activated to splice out the $p16^{Ink4a}$ exon 1 α that is flanked by *loxP* sites.

2.3.1 Genotyping polymerase chain reactions

For identification and genotyping purposes, ear notches were taken from transgenic mice. To extract the DNA, the notches were incubated in 75 μ l of Hotshot Lysis buffer (25mM NaOH, 0.2mM EDTA, pH 12, in purified water (ddH₂O)) in a 95°C heat block for at least one hour, or until the notch has dissolved. At this stage, the notches in solution were cooled to 4°C for 10 minutes before 75 μ l of Hotshot Neutralising buffer (40mM trizma hydrochloride, pH5, in ddH₂O) was added. Extracted DNA was stored at 4°C for the short term (up to 1 month) and -20°C for long-term storage.

Once DNA was extracted, genotyping polymerase chain reactions (PCRs) were performed to identify the mice genotypes. The following PCRs were used: to detect the floxed $p16^{Ink4a}$ ($p16^{ff}$) allele primers (diluted 1:2 in ddH₂O) for $p16^{Ink4a}$ common Reverse, $p16^{Ink4a}$ wild-type Forward and $p16^{Ink4a}$ floxed Forward were used; S1X A and B Cre primers (diluted 1:10 in ddH₂O) identified MerCreMer positive and negative mice; and $p16^{Ink4a}$ LCred PCR used primers (diluted 1:10 in ddH₂O) specifically designed to generate a product if $p16^{Ink4a}$ exon 1 α had been successfully floxed out (Monahan *et al.*, 2010). Sequences for these primers can be found in Table 2.2.

Table 2.2 Sequences for primers used for genotyping polymerase chain reactions.

Name	Primer Sequence
p16 ^{lnk4a} f/f F	GTATGCTATACGAAGTTATTAGGTA CTGC
p16 ^{lnk4a} wild-type F	GTTTTGGAGCAGCAGGGATT
p16 ^{lnk4a} common R	CTATGTCAGATTTGGCTAGGGAGT
S1X-A Cre F	TAACCAGTGAAACAGCATTGCTG
S1X-B Cre R	GGACATGTTTCAGGGATCGCCAGGCG
p16 ^{lnk4a} LCred F	TACCACAGTTTGAACAGCGTGA
p16 ^{lnk4a} LCred R	AACCAACTTCCTCCTTCCCC

For all PCRs, a previously verified (by E.D.) positive control was used if available and ddH₂O used as negative control to ensure no contaminant or false positive bands were observed. Master mix solutions were prepared according to the template in Table 2.3 and 18µl of completed master mix added to 2µl of extracted DNA.

Table 2.3 Polymerase chain reaction master mix reagent volumes.

Volume	Reagent
(X=number of samples)	
Xµl	F primer (dilutions above)
Xµl	R primer (dilutions above)
10Xµl	Dream Taq 2X (K1082, ThermoFisher Scientific)
6Xµl	ddH ₂ O

PCR products were identified by gel electrophoresis using a 2% agarose in Tris-acetate-EDTA (TAE) gel containing ethidium bromide (EtBr). Samples (8µl) were run

against a 100bp ladder (4µl) at 125V for 30 minutes and imaged using a UV transilluminator. The product sizes for genotyping PCRs are outlined in Table 2.4. Only homozygous floxed mice were used for experimentation, with or without Cre to generate floxed allele mice (p16^{f/f}) or deleted allele mice (p16^{-/-}).

Table 2.4 Polymerase chain reaction product sizes.

Name		Product size
p16 ^{f/f} genotyping	Wild-type (WT)	194bp
(Monahan <i>et al.</i> , 2010)	LoxP (f/f)	261bp
p16 ^{-/-} identification	LCred (-/-)	≈300bp (or unamplifiable product of 3.9kb if floxed exon 1α not deleted)
(Monahan <i>et al.</i> , 2010)		
Cre		280bp

2.4 Tissue collection and processing

If the heart was not to be used for histological analysis, some animals underwent cardiac puncture to obtain ≤1ml blood immediately prior to being culled. Animals were anaesthetised using isoflurane and a 25G needle inserted along the midline of the abdomen through the diaphragm and into the heart.

At the end of each *in vivo* study, mice were culled by a Schedule 1 method; dislocation of the neck. Hearts for histological analysis were dissected after termination immediately and placed into a 50mM solution of potassium chloride to stop heart contractions at diastole (to allow the accurate measurement of hypertrophy). The hearts were then washed in phosphate buffered saline (PBS), trimmed to remove any excess fat, connective tissue, outflow tract vessels, and then weighed before embedding.

For some studies, upper ventricles and atria superior to the LAD ligation suture were removed, placed in Trizol and stored at -80°C for RNA analysis. For other studies, upper ventricles and atria superior to suture, right ventricle inferior to suture and LV inferior to suture were placed in RIPA buffer for protein analysis. When required, additional organs including liver, lungs, kidneys, muscle and testis, were also collected,

cryo-embedded and snap frozen for RNA or histological analysis. To enable the subsequent controlling for mouse size in the MRI analysis (e.g. LV mass) legs were removed from all mice, tibias dissected and tibia length recorded (Yin *et al.*, 1982).

2.4.1 Tissue embedding

For cryo-embedding, hearts and other organs were cryo-protected by incubating in 30% sucrose and at 4°C with agitation for 6 hours. Tissues were then embedded in optimal cutting temperature compound (OCT), in the appropriate orientation, on dry ice and stored at -80°C.

For wax embedding, hearts were first fixed in a solution of 4% paraformaldehyde (PFA) at 4°C overnight with gentle agitation. After several washes with PBS, tissues were dehydrated using an ethanol (EtOH) gradient (50% 3 hours room temperature (RT), 70% 2 hours RT, 70% overnight 4°C, 95% 1 hour RT, followed by 4 repeated washes for 2 hours in 100% EtOH). Once dehydrated, the hearts were placed into glass vials and left in HistoClear for two 1 hour incubations, before replacing with HistoClear wax for 4 hours. The hearts were then equilibrated in repeated changes of paraffin over 3-4 days at 60°C and then finally embedded in the desired orientation.

The hearts were sectioned to produce 10µm thick transverse sections on a cryostat or 5µm thick transverse sections on a microtome, and collected as sister sections on Superfrost Plus slides (Thermo Scientific). All hearts, LAD ligated and controls, were cut fully from apex to atrium. The ischaemic region of ligated hearts was defined as the region of the heart inferior to the LAD ligature.

2.5 Histology and immunofluorescence

Heart sections embedded in OCT first were thawed at RT. Paraffin-embedded heart sections underwent de-paraffination (two 10 minute HistoClear incubations), followed by rehydration (100%, 90%, 70% and 50% EtOH for 2 minutes each), and antigen-retrieval (in a pressure cooker for 5 minutes in 0.01M Citrate buffer (pH6.3)) prior to staining.

For immunofluorescence, all sections were fixed in 4% PFA for 20 minutes, followed by several PBS washes. Samples were permeabilised in a 0.5% Triton-X solution, washed in PBS, and then blocked in 10% Foetal Calf Serum (FCS) for 1-2 hours at RT. Slides were incubated with primary antibody (1°Ab) overnight at 4°C or for 1 hour at RT. After more PBS washes the next day, the secondary antibody (2° Ab) was applied to the slides and incubated for 1-2 hours at RT in the dark. Once stained, slides were washed in PBS and coverslips were mounted using Vectashield Antifade Mounting Medium with DAPI (H-1500, VectorLab). A complete table of all antibodies used can be found in Table 2.5.

Table 2.5 List of antibodies use for all analyses.

	Antibody	Dilution	Raised in/ wavelength	Catalogue number	Company
1° Ab	Anti-p21 ^{Cip}	1:4	Rat	Hugo291	Abcam
	Anti-troponin C	1:400- 800	Goat	ab30807	Abcam
	Anti-p16 ^{Ink4a}	1:200	Rabbit	100401170	Rockland
	Anti-vimentin	1:200	Mouse	Ab8978	Abcam
	Anti-γH2Ax	1:200	Rabbit	9718	Cell Signalling
	Anti-ETS-related gene (ERG)	1:1000	Rabbit	ab92513	Abcam
2°Ab	Donkey anti-rat	1:200	594nm	A21209	Life Technologies
	Donkey anti-goat	1:200- 500	488nm	A11055	Life Technologies
	Donkey anti-rabbit	1:500	594nm	R37119	Life Technologies
	Donkey anti- mouse	1:500	647nm	A31571	Life Technologies
	Goat anti-rabbit IgG biotinylated	1:200		PK-6101	Vectorlab
Misc	DSC-Fluorescein	1:500	488nm	A-2001	Vectorlab
	DAPI	1:500	358nm	MBD0015	Sigma
	WGA	1:500	594/647nm	W11262/ W32466	Invitrogen

2.5.1 p21^{Cip} and troponin C dual staining

For staining of p21^{Cip}, the cleanest staining was achieved when using paraffin sections. The 1°Abs used were anti-p21^{Cip} (1:4 using supernatant, rat, Hugo291, Abcam), the CM marker troponin C (1:400, goat, ab30807, Abcam), and 2° Abs used were donkey anti-rat (1:200, 594nm, A21209, Life Technologies) and donkey anti-goat (1:200, donkey anti-goat, 488nm, A11055, Life Technologies). After 2° Ab incubation, slides were washed a minimum of five times in PBS and then mounted in Vectashield Antifade Mounting Medium with DAPI (H-1500, VectorLab).

2.5.2 p16^{Ink4a}, troponin C and vimentin triple staining

The protocol above in 2.5 was adapted and optimised since I encountered problems with non-specific membrane staining of the p16^{Ink4a} antibody. Consequently, for p16^{Ink4a} antibody labelling, cryo-embedded sections were incubated in 0.5% Triton-X for 10 minutes and washed once in PBS for 5 minutes prior to fixing. The sections were then fixed in 4% PFA, PBS washed and permeabilised in 0.5% Triton-X as described above. Sections were then blocked using 10% donkey serum (D9663, Sigma) as the 2° Abs used are both raised in donkey. Primary Ab incubation was carried out overnight at 4°C or for 1 hour at RT using anti-p16^{Ink4a} (1:200, rabbit, 100401170, Rockland), anti-troponin C (1:800, ab30870, Abcam) and anti-vimentin (1:200, mouse, ab8978, Abcam). Slides were washed in PBS and incubated in 2° Abs: donkey anti-rabbit (1:500 at 594nm against p16^{Ink4a}, R37119, Life Technologies); donkey anti-goat (1:500 at 488nm against troponin C, A11055, Life Technologies); and donkey anti-mouse (1:500 at 647nm against vimentin, A31571, Life Technologies), containing DAPI (1:500, MBD0015, Sigma) for 45 minutes at RT. After 2° Ab incubation, slides were washed a minimum of five times in PBS and then mounted in Dako Fluorescence Mounting Media (Agilent, S3023).

2.5.3 Senescence-associated β -galactosidase staining

Cryo-embedded sections were stained using the SA- β -Gal Staining Kit (#9860, Cell Signaling Technology) as per the manufacturer's instructions (Cell Signaling Technology, 2016) with the following modifications for tissue sections: 1) Slides were thawed at RT; 2) fixed using the provided fixative solution for 15 minutes and washed

three times in PBS; 3) β -Galactosidase staining solution was prepared at pH 6 and added to each slide; 4) slides were incubated at 37°C until the blue colour had developed (at approximately 48 hours after application; 5) slides were washed with PBS, dehydrated in 95% and 100% ethanol solutions, washed in Histoclear and mounted with Histomount.

As the cells of interest were CMs, a triple stain was optimised for SA- β -Gal, troponin C and wheat germ agglutinin (WGA). After SA- β -Gal staining, as above, the slides were fixed in 4% PFA for 20 minutes, membrane permeabilised with 0.5% Triton-X for 20 minutes and incubated with 1°Ab for troponin C (1:400, goat, ab30807, Abcam) and WGA (1:500, 574nm, Invitrogen) in 0.1% FCS/PBS overnight. Slides were washed and then incubated for 2 hours with 2° Ab (1:200, donkey anti-goat, 488nm, A11055 Life Technologies) and then mounted in Vectashield Antifade Mounting Medium with DAPI (H-1500, VectorLab).

2.5.4 Telomere-associated DNA damage foci staining

Telomere-Associated DNA Damage Foci were detected by performing Immuno-FISH, as previously described (Passos *et al.*, 2007), on cryo-embedded heart sections.

Sections that were cryo-embedded were fixed in 4% PFA, washed in PBS, treated with 70% EtOH, blocked in 8% bovine serum albumin (BSA) in PSB-TT (0.5% Tween-20, 0.1% Triton X-100), washed in PBS-TT, and incubated in 1°Ab at 4°C overnight. The 1°Ab used was rabbit monoclonal anti- γ H2Ax (1:200, 9718, Cell Signalling).

Slides were subsequently washed in PBS-TT before the 2° Ab was added for 1 hour at RT. The 2° Ab used was goat anti-rabbit IgG Biotinylated (1:200, PK-6101, VectorLab). PBS washes were then followed by a 20 minute incubation with DSC-Fluorescein (1:500, A-2001, VectorLab) and three PBS washes. The sample was then cross-linked using 4% PFA for 20 minutes, washed, dehydrated in ice cold 70%, 90% and 100% EtOH before air-drying. Next, 10 μ l of probe hybridisation mix (Table 2.6) was applied to the slides and left in a dark, humidified chamber overnight. Afterwards, the samples underwent a series of washes; 20 minutes in 70% formamide/2x saline-sodium citrate buffer (SSC), twice in 2xSSC for 10 minutes each, and 10 minutes PBS. Samples were stained with WGA (1:500, 674nm, W32466, Invitrogen) for 1 hour prior

to mounting coverslips with prolong Gold Antifade Mountant with DAPI (P36935, ThermoFisher Scientific).

Table 2.6 Probe hybridisation mix reagent volumes.

Volume	Reagent
175µl	Formamide deionized
33.6µl	ddH ₂ O
21.4µl	MgCl Buffer
2.5µl	1M Tris pH7.2
12.5µl	1x Roche Blocking Buffer made up in Malic acid pH 7.5
5µl	PNA probe (25µg/ml Cy3-labelled telomere-specific (CCCTAA) peptide nuclei acid probe (F1002, Panagene))

2.5.5 Masson's Trichrome staining

Masson's trichrome staining was performed to visualise the infarct (collagen stain) produced following MI and reperfusion (Bogatryov *et al.*, 2013). Hearts were sectioned to give up to 5 sets of slides, 10 slides per set. The first slide from each set were stained for this analysis and a minimum of 4 sections per slide were analysed.

Cryo-sections were fixed for 1 hour in 4% PFA followed by overnight incubation in Bouin's solution (HT10132, Sigma), both at RT. The next day, slides were washed in running tap water, and nuclei were stained for 5 minutes in Weigert's Haematoxylin solution consisting of equal parts Haematoxylin Solution A and Solution B (HT1079, Sigma). Following a further wash in running tap water, cytoplasm staining was achieved by 5 minutes in Beibrich Scarlet-Acid Fuchsin Solution (HT151, Sigma). Slides were washed in ddH₂O and to allow uptake of the stain, slides were incubated in phosphotungstic/phosphomolybdic acid solution with ddH₂O in a 1:1:2 solution retrospectively. Slides were incubated in Aniline Blue Solution (b8563, Sigma) for 5 minutes, washed in ddH₂O and placed in 1% glacial acetic acid for 1-2 minutes. This solution fades the stain allowing the colours to be more distinguishable. Slides were washed with ddH₂O and dehydrated via an EtOH gradient from 70% to 100% EtOH,

washed in HistoClear (HS-202, National Diagnostics) and mounted using Histomount (HS-103, National Diagnostics).

2.5.6 Wheat Germ Agglutinin staining

Cryo-sections were stained with WGA (1:500, 594nm, W11262, Invitrogen) and DAPI (1:500, MBD0015, Sigma) for 1 hour at RT after 20 minutes fixation in 4% PFA and PBS washes. Slides were mounted in Dako Fluorescence Mounting Medium (Agilent, S3023).

2.5.7 5-Ethynyl-2-deoxyuridine staining

Staining for EdU to assess proliferation was achieved using the Invitrogen Click-iT EdU Alexa Fluor 594 Imaging Kit (C10339). Sections (cryo-embedded) were stained for troponin C, as above, or for the endothelial marker ERG (rabbit anti-ERG, 1:1000, Ab92513, Abcam, counter stained with donkey anti-rabbit, 1:200, R37118, Life technologies). Following troponin C/ERG staining, sections were washed in 3% BSA and then treated with 0.5ml of 1X Click-iT reaction cocktail, prepared according to manufacturer's protocol (Invitrogen, 2011) for 30 minutes in the dark. Afterwards, the reaction cocktail was removed and slides washed again in 3% BSA followed by PBS. Sections were also stained for WGA (1:400, 647nm, W32466, Invitrogen) for a 30 minutes incubation period. Sections were labelled with DAPI (1:500, MBD0015, Sigma), washed in PBS and mounted in Dako Fluorescence Mounting Medium (Agilent, S3023).

2.5.8 RNAscope

RNAscope was performed to verify the results obtained from p16^{Ink4a} staining in Section 2.5.2 according to the manufacturer's protocol (RNAscope® Multiplex Fluorescent Kit v2 User Manual, 323100-USM, ACD) (Diagnostics, 2018). Cryo-sections were initially fixed in 4% PFA for 15 minutes at 4°C followed by an EtOH dehydration gradient (5 minutes each at RT in 50%, 70% and two 100% washes). Sections were left to air dry, a hydrophobic barrier was created around the sections and then covered in RNAscope hydrogen peroxide (PN322381, ACD) and incubated

in the HybEZ humid tray for 10 minutes, at RT. Next, slides were washed five times for 2 minutes each in PBS, the excess liquid was removed and one drop/section of Protease IV (PN322381, ACD) added for a 30 minute incubation in the HybEZ tray at RT. Slides were then washed again in several changes of PBS. Then one drop/section of p16^{Ink4a} probe (Mm-Cdkn2a-tv2, 447491, ACD, C1 probe) was applied and sections placed in the HybEZ oven set at 40°C for 2 hours. Following two washes in 1X wash buffer (PN310091, ACD), slides could be stored overnight at RT in 5X SSC.

The next day, sections were washed twice in 1X wash buffer and then incubated at 40°C with one drop/section of the following reagents: RNAscope Multiplex Flv2Amp1 for 30 minutes; RNAscope Multiplex Flv2Amp2 for 30 minutes; RNAscope Multiplex FlvAmp3 for 15 minutes; RNAscope Multiplex Flv2 HRP-C1 for 15 minutes; 100µl of TSA Plus Cy3 (1:750 in TSA buffer (322809, ACD), 594nm, NEL744001KT, PerkinElmer) for 30 minutes; and finally RNAscope Multiplex Flv2 HRP blocker for 15 minutes (PN323110, ACD). Between each incubation slides were washed twice in 1X wash buffer. Afterwards, slides underwent counterstaining for troponin C (anti-troponin C, 1:800, ab30870, Abcam) for 1 hour at RT, washes in PBS, incubation with the 2^o Ab donkey anti-goat (1:500 at 488nm against troponin C, A11055, Life Technologies) with DAPI (1:500, MBD0015, Sigma) for 1 hour at RT, final washes in PBS and sections mounted in Dako Fluorescent Mounting Medium (S3023, Agilent).

2.5.9 4-Hydroxynonenal staining

To assess OS levels, staining with the marker 4-hydroxynonenal (4-HNE) was carried out. This work was performed by a collaborator's lab, Dr Jeanne Mialet-Perez's. Tiled images of 4-HNE stained heart sections were analysed by measuring the fluorescence intensity and normalising the intensity to myocardial area.

2.5.10 TUNEL staining

For the detection of DNA fragmentation during cellular apoptosis, TUNEL staining was performed (In situ Cell Death Detection Kit, TMR Red, 12156792910, Roche). In brief, wax sections underwent de-paraffination, rehydration and antigen retrieval as described above (2.5), prior to blocking in 5% BSA for 30 minutes and then a 1 hour incubation in TUNEL Reaction mixture. After labelling, slides were washed in PBS and

stained for the CM marker, troponin C (1:800, ab30870, Abcam) for 1 hour at RT. Slides were again washed in PBS and then incubated in the 2°Ab donkey anti-goat (1:500 at 488nm against troponin C, A11055, Life Technologies) with DAPI (1:500, MBD0015, Sigma) for 45 minutes at RT. Slides were then washed in PBS and mounted in Dako Fluorescence Mounting Media (Agilent, S3023).

2.6 Microscopy and image analysis

All images were taken on a Axiolmager with apotome microscope (Zeiss) and analysed using ZEN 2.3 (Zeiss).

Slides that underwent staining for TAF were imaged using a DM5500 microscope (Leica), z-stacks taken at x63 magnification, and analysed using Fiji (ImageJ).

Slides stained with SA-β-Gal were imaged at x10 to generate a titled image of the whole transverse heart section.

The area of interest imaged for each senescence marker was the border zone (BZ); this is defined as the region proximal to the infarct. All images were taken of CMs in this region, within the LV (Figure 2.4.A, red region), and images of controls with no LAD ligation were taken throughout the LV. Other areas that have been imaged were the right ventricle (RV) and distal septum termed remote zone (RZ) (Figure 2.4.A, blue region). If healthy controls were not available, the RZ was used as a comparison to the BZ in some cases. The RZ was accepted as being unaffected as it was too distant to the infarct region.

A minimum of 20 images/mouse at x63 were analysed with 10 images/section over 5 sections being imaged.

For Masson's Trichrome, the first slide of each sister set of 10 slides was stained and 4 sections analysed per slide at x10. Slides were scanned and analysed using the Leica Digital Image Hub. The LV area was calculated by measuring the epicardial area and subtracting the endocardial area. The infarct area was then measured and the percentage of LV that is infarct calculated to analyse scar size (Figure 2.4.B).

For WGA staining to assess CM hypertrophy, again 10 images/section were taken within the BZ but at x20 across 4 sections. All CMs surrounded by three capillaries

were presumed to be in the same orientation, and the area of these CMs in a similar orientation were measured for this analysis (Walaszczyk *et al.*, 2019).

Quantification for markers (eg p21^{Cip}, p16^{Ink4a}, RNA-scope p16^{Ink4a}, Ki67, TUNEL) is expressed at the percentage of CMs that are positive for that marker (ie number of CMs positive for the marker divided by the total number of CMs and multiplying by 100), unless otherwise stated. For TAF there were two types of analyses performed: the first was “Mean TAF number in CMs” which was calculated by averaging the TAF counts per CM; and “Percentage of CMs positive for TAF” which was calculated by dividing the number of CMs that contained 5 or more TAF by the total number of CMs.

In each image taken, between 10-50 CMs were visible and quantified, therefore between 200 and 2500 CMs were analysed per mouse for each marker investigated. On average over 800 CMs were counted per mouse for each analysis. For analysis of *in vitro* experiments between 80 and 200 cells were included.



Figure 2.4 Images of a transverse heart section.

- A)** The BZ is outlined in red, surrounding the infarct (blue stained region in LV), and the RZ shown in blue covering the distal septum and RV.
- B)** Masson's Trichrome stained transverse section outlining the epicardium (pink), endocardium (yellow) and infarct border (blue).

2.7 Characterisation of a cardiomyoblast senescence-associated secretory phenotype *in vitro*

To model CMs, an established cardiomyoblast H9C2 cell line was utilised (Branco *et al.*, 2015). The H9C2 line was originally derived from embryonic BD1X rat heart tissue in 1976 (Kimes and Brandt, 1976), and have since been used regularly for *in vitro* studies given their embryonic CM-like morphology (Zordoky and El-Kadi, 2007; Tan *et al.*, 2010; Watkins *et al.*, 2011; Branco *et al.*, 2015; Kuznetsov *et al.*, 2015; Witek *et al.*,

2016). All *in vitro* experiments performed in this study using H9C2 cardiomyoblasts were incubated in normoxic conditions at 37°C and 5%CO₂.

2.7.1 Cell culture of H9C2 cells

H9C2s were cultured in DMEM (Dulbecco's Modified Eagle Medium, 13345364, Gibco, Life Technologies) supplemented to contain 12.5% foetal bovine serum (FBS) (10500056, Gibco, Life Technologies), 2mM L-glutamine (25030024, Gibco, Life Technologies) and 1% Penicillin-Streptomycin (P/S) (15070063, Gibco, Life Technologies). Cells were grown in 7ml of supplemented DMEM in treated T75 flasks and either split at 70-80% confluence or for experiments grown to confluence.

2.7.2 Irradiation of H9C2 cells

Once cells had reached confluence, they underwent irradiation for 2 minutes at 10Gy. Immediately after irradiation, media was replaced and changed every 3-4 days. Cells were left for 10 days for senescence to become fully established (Hewitt *et al.*, 2012) (Basisty *et al.*, 2020). To confirm irradiated cultures had become senescent, cells were stained with SA-β-Gal (#9860, Cell Signaling Technology) as per the manufacturer's instructions (Cell Signaling Technology, 2016). For conditioned media experiments, 48 hours prior to collection cells were serum starved in media containing no FBS, and at day 10 this conditioned media was collected and H9C2 cells trypsinised and added to Trizol.

2.7.3 H9C2 cells treatment with navitoclax

To assess cell viability and senescence expression after treatment with navitoclax, H9C2s were cultured as previously described (Anderson *et al.*, 2019) to reach confluence and underwent irradiation. Ten days post-irradiation, experimental cultures were treated with navitoclax prepared in 0.1% dimethyl sulfoxide (DMSO) in PBS at 0.5μM, 1.0μM and 1.5μM concentrations for 2 days.

On day 12, cells were either fixed in 2% PFA for staining to analyse expression of SA-β-Gal, or collected for viability analysis (Figure 2.5). To assess viability, H9C2s were trypsinised and resuspended in 100μl of 1X prepared Annexin binding buffer (5X stock,

V13246, Life Technologies) and 25µl loaded onto a Tali cellular analysis slide (T10795, Invitrogen). Slides were analysed using a Tali image-based cytometer (Invitrogen) with images taken from 20 fields and set to quantify cells expressing propidium iodide.

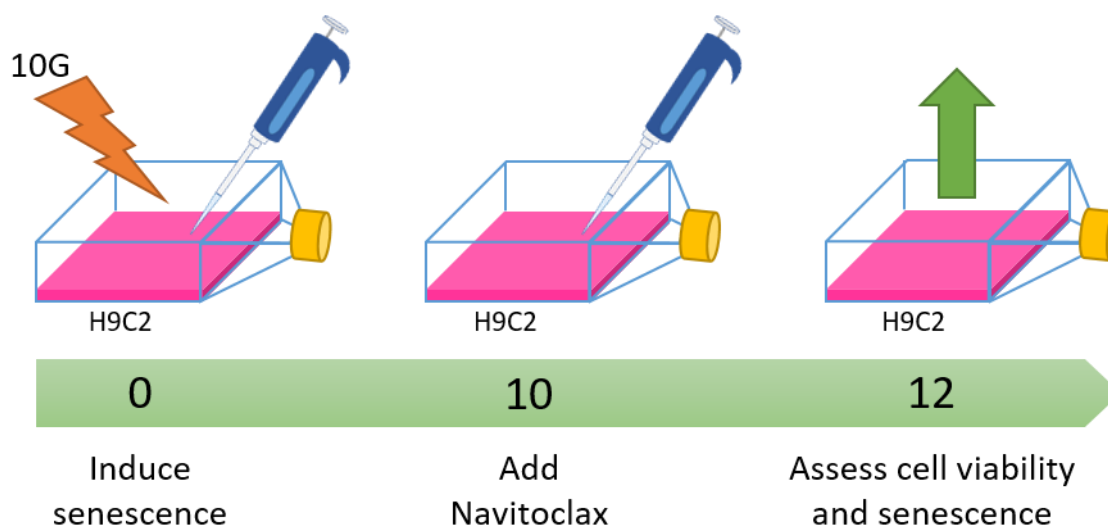


Figure 2.5 Experimental timeline of navitoclax study on H9C2s *in vitro*.

H9C2s were cultured to confluence in T75 flasks and irradiated to induce senescence. Ten days post-irradiation navitoclax at varying concentrations (0.5µM, 1.0µM and 1.5µM) was added to cultures and at day 14 cells assessed for viability and senescence, by expression of the marker SA-β-Gal.

2.8 Characterisation of fibroblast senescence *in vitro*

As the heart is a heterogeneous organ, it was of interest to investigate the impact of other cell types within the heart after they undergo senescence. To investigate the impact of a fibroblast senescence and the SASP they produce, fibroblast cell lines and primary fibroblasts were cultured *in vitro* for assessment. All *in vitro* experiments were incubated in normoxic conditions at 37°C and 5%CO₂.

2.8.1 Cell culture of MRC5 cells

An established human foetal lung-derived fibroblast cell line, the MRC5 line, was utilised to establish methodology and used as a positive control. This line was derived from lung tissue taken from a 14 week male foetus by Jacobs, J. P and colleagues (Jacobs *et al.*, 1970), and has been used for over the last 50 years as a fibroblast model (Friedman and Koropchak, 1978; McSharry *et al.*, 2001; Farah *et al.*, 2013).

Cells were cultured in non-treated T75 flasks in DMEM (Dulbecco's Modified Eagle Medium, 41966029, Gibco, Life Technologies) containing 10% FBS (10500056, Gibco, Life Technologies), 2mM L-glutamine (25030024, Gibco, Life Technologies) and 1% P/S (15070063, Gibco, Life Technologies). Cultures were split sub-confluent (70-80%).

2.8.2 MRC5 cell treatment with navitoclax

To determine the effect of Navitoclax on the clearance of senescent fibroblasts, MRC5s were cultured as above until confluent, irradiated and left for 10 days to become senescent. Then cultures were treated with navitoclax prepared in 0.1% DMSO in PBS at 1.5 μ M and 5 μ M concentrations for 48 hours. After treatment, cells were again fixed and stained for SA- β -Gal or counted for viability analysis, as described in 2.9.3 and Figure 2.5.

2.8.3 Isolation of primary adult mouse cardiac fibroblasts

Trials to isolate primary cardiac fibroblasts (CFs) from adult mice were also performed. Hearts from culled mice were excised, finely minced with a blade and placed within a media solution (DMEM + 0.5mg/ml BSA, 1% P/S) containing collagenase II (300U/ml) and incubated at 37°C for 1 hour. The collagenase solution was then transferred, carefully to avoid tissue debris, and fresh solution added to remaining tissue. This process was repeated three times and supernatant was centrifuged at 400G for 6 minutes to collect a cell pellet. The pellet was then washed and finally resuspended in 10ml of media (DMEM + 10% FBS, 1% P/S) and seeded into T25 flasks or chamber slides. After 4 hours, the media was removed containing CMs and other cell types, leaving only fibroblasts adhered to the culture-ware, and fresh media applied.

Cells were allowed to reach confluence and slides were fixed in 2% PFA prior to staining. Staining was performed to verify the cell types isolated to ensure whether it was a pure population of primary fibroblasts or also contained CMs and other cell types. Slides were stained for cellular markers, according to protocols outlined above in 2.5 for cryosections. Primary antibodies used included: anti-vimentin (1:500, mouse, ab8978, Abcam) and anti- α -smooth muscle actin (1:1000, mouse, conjugated 488nm, ab184675, Abcam) as markers of fibroblasts, anti-troponin C (1:800, goat, ab30807,

Abcam) as a marker of CMs and anti-ERG (1:1000, goat, ab92513, Abcam) as a marker of endothelial cells.

2.8.4 Irradiation of MRC5 and primary adult mouse cardiac fibroblast cells to obtain conditioned media

Once confluent, MRC5s and CFs were irradiated at 20Gy to induce senescence. Media was changed immediately after irradiation and replaced every 3-4 days. At day 8 media was replaced for serum free media (DMEM containing no FBS) for 48 hours prior to sample collection on day 10. Conditioned media was aspirated off and centrifuged to remove debris before storage at -80°C. Cells were trypsinised and resuspended in 1ml of Trizol before storage at -80°C.

Conditioned media from senescent fibroblast cell lines was then added to cultures of healthy cells to assess whether the SASP released from the irradiated fibroblasts acts in a paracrine fashion to stimulate senescence of a healthy cell population (Figure 2.6).

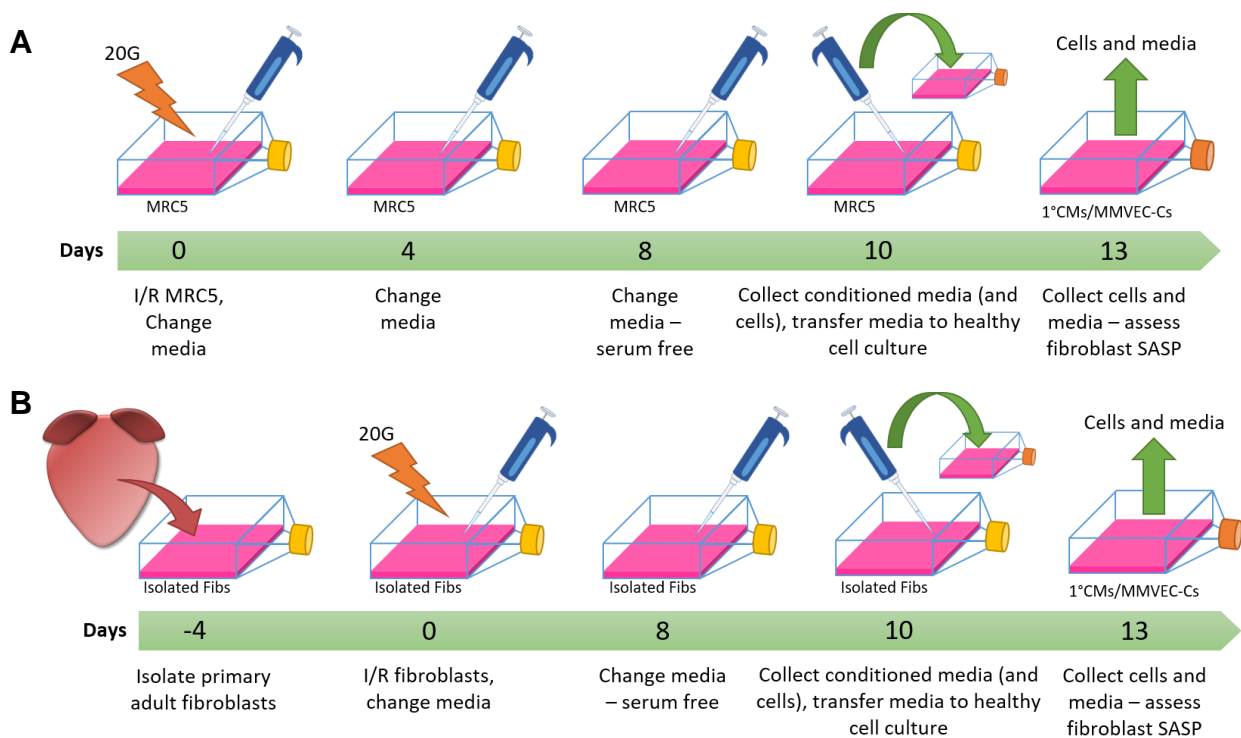


Figure 2.6 Experimental timeline of irradiating the fibroblast cell lines MRC5 and primary cardiac fibroblasts to investigate a fibrotic senescence-associated secretory phenotype.

- A)** MRC5 cells were cultured and irradiated at 20Gy. On day 8, 48 hours prior to collection, media was replaced for serum free media. Cells and conditioned media was collected on day 10, and conditioned media transferred to healthy cell cultures. This was tested on other cell types including primary CMs and the endothelial cell line MMVEC-Cs.
- B)** CFs were isolated from adult mouse hearts, also irradiated at 20Gy and cultured and samples collected the same as (A) for MRC5s.

2.8.5 Endothelial cell culture

Conditioned media experiments using an endothelial cell line, mouse coronary microvascular endothelial cells (MMVEC-Cs, Lonza), was performed by an mRes student, L. Donastorg Sosa, and cells were supplied by and experiments conducted in Dr. David Grieve's lab of Queen's University Belfast. Cultures of MMVEC-Cs were seeded in 12-well plates at a density of 5×10^4 per well.

2.8.6 Isolation of primary embryonic mouse cardiomyocytes

Primary embryonic murine CMs were utilised as a CM model. Embryos were dissected at E16.5-17.5 and hearts placed into ice-cold cardiomyocyte balanced salt buffer

(CBSB) (Table 2.7). Each heart was cut into 3-4 segments and all fragments transferred to enzyme solution without trypsin (Table 2.7) and incubated for 5 minutes in a water bath at 37°C. After 37°C incubations, the supernatant was transferred to a new collection tube, centrifuged at 700G for 15 minutes, supernatant discarded and cell pellet resuspended in 2ml of FBS and stored at 4°C between centrifugations. Once the supernatant from the tube containing heart fragments had been removed, fresh enzyme solution containing trypsin (Table 2.7) was added and fragments incubated for 30 minutes at 37°C.

Fragments were continuously incubated in enzyme solution with regular supernatant collections to isolate dissociated cells until the fragments had completely disintegrated. After the last centrifugation to collect cells, the pellet was resuspended in 7ml of cardiomyocyte growth media (CM-GM) (Table 2.7) and transferred to a T75. Cells were pre-plated for 1-2 hours and kept in a 37°C incubator set to 5% oxygen to allow any fibroblasts to adhere to the flask. Media containing CMs (not adhered to T75 flask) was removed, cells counted using a haemocytometer and resuspended in the appropriate volume of CM-GM for plating onto pre-treated collagen coated culture vessels containing coverslips (Table 2.7). For a 12-well plate, 1×10^6 CMs and cardiac derived cells were plated per well.

Table 2.7 Solutions for isolation of primary embryonic cardiomyocytes.

Solution	Protocol
Cardiomyocyte Balanced Salt Buffer (CBSB) For 1L:	<ul style="list-style-type: none">• 6.8g Sodium Chloride (NaCl)• 20ml HEPES 1M• 120mg Sodium Dihydrogen Phosphate (NaH₂PO₄)• 400mg Potassium Chloride (KCl)• 100mg Magnesium Sulfate (MgSO₄)• pH to 7.4 with Sodium Hydroxide (NaOH)• Make up to 1L with dH₂O• Autoclave and store at 4°C
Enzyme Solution For 600ml:	<ul style="list-style-type: none">• 150ml CBSB• 1.62ml Glucose 1M• 100mg Collagenase II (240U/mg)• Filter with a 0.2µm filter• Place 25ml of filtered solution into 50ml falcon and make up to 50ml with CBSB• Store at 4°C, heated to 37°C in water bath before use, add 2.5% Trypsin (100X) when needed (ie add 500µl Trypsin per 50ml Enzyme solution)
Cardiomyocyte Growth Media (CM-GM) Makes 202ml:	<ul style="list-style-type: none">• 136ml DMEM• 34ml Medium 199• 10ml FBS• 20ml Horse serum• 2ml P/S• Stored at 4°C, heated to 37°C in water bath before use
Collagen coated culture vessels	<ul style="list-style-type: none">• Collagen (1mg/ml) dilute 1:10 in sterile water• Add: 500µl/well to a 12-well plate with coverslips; 3ml to a T25; or 5ml to a T75• Incubate culture vessel for several hours at RT or overnight at 4°C• Remove excess fluid and allow to dry overnight at 4°C• Rinse with CBSB before introducing cells in CM-GM

2.8.7 Analysis of irradiated primary fibroblast senescence-associated secretory phenotype

Isolated embryonic CMs were left for 24 hours to adhere to the wells and proliferate. At 24 hours after seeding, conditioned media from proliferative and irradiated MRC5 and CFs cultures was filtered using a 0.2µm filter and diluted 1:1 in CM-GM before being added to CMs cultures. Cells were assessed every 24 hours, and after 72 hours in conditioned media the CMs were fixed for 10 minutes in 2% PFA and stored at 4°C in PBS until stained.

Cultures of MMVEC-C cells were also cultured for 72 hours in conditioned media from proliferative and irradiated MRC5s that had been filtered and diluted 1:1 in high glucose DMEM supplemented with 1% 4-(2-hydroxyethyl)-1-piperazineethanesulfonic acid (HEPES) and 5% FCS. At the end of the experiment cells were fixed for 10 minutes in 4% PFA and again stored at 4°C in PBS until staining.

Coverslips with CMs were stained for either Ki67 (1:500, rabbit, ab15580, Abcam) with troponin C to assess impact of conditioned medias on proliferation, or with SA-β-Gal to investigate whether the conditioned media contained components from a fibrotic SASP that could induce senescence in the CMs.

Coverslips with MMVEC-Cs were also stained for the proliferation marker Ki67 (1:500, rabbit, ab15580, Abcam) or for dihydroethidium (DHE, 10µM, D7008, Sigma) which is a superoxide probe that detects the presence of ROS, and once oxidised will emit a signal detectable at 594nm (Sigma Aldrich, 2019). For DHE, unfixed cells are incubated for 30 minutes at 37°C in a humidified dark chamber and imaged

For all stains the protocols used can be found in section 2.5 and 10 images taken per coverslip at x10 magnification.

2.9 Gene expression analysis

To evaluate the levels of gene expression from cell and tissue samples stored in Trizol, samples underwent RNA isolation, followed by cDNA synthesis and then samples analysed by qRT-PCR.

2.9.1 RNA isolation

RNA was extracted from cell pellets stored at -80°C using Qiagen RNeasy Mini Kit (74106, Qiagen) according to the manufacturer's protocol (Qiagen, 2012). First $350\mu\text{l}$ of Buffer RLT was used to suspend the cells. The lysate was homogenised by placing it on a QIA shredder spin column and centrifuged at 14,000 RPM for 2 minutes. $350\mu\text{l}$ of 70% EtOH was added to the lysate and the sample transferred to an RNeasy spin column and spun at 10,000 RPM for 15 seconds. The flow through was discarded, $700\mu\text{l}$ of Buffer RW1 applied to spin column, column spun at 10,000 RPM again for 15 seconds. Flow through was again discarded and $500\mu\text{l}$ of Buffer RPE was added to the spin column. The column was spun for 2 minutes at 10,000 RPM to ensure it was dry and RNA was eluted from the column by adding $15\mu\text{l}$ of RNase-free H_2O and centrifuging at 10,000 RPM for 1 minute. The H_2O containing RNA was passed through the column twice to ensure maximal RNA elution.

RNA was also extracted from tissue. Upper ventricles and atria stored in Trizol were made up to 1.5ml of Trizol before being homogenised at a low power. To fresh eppendorfs, $800\mu\text{l}$ of homogenised tissue in Trizol was added to $200\mu\text{l}$ of chloroform, inverted vigorously for 15 seconds, left to settle for 3 minutes and the centrifuged for 15 minutes at 12,000G (all centrifuges carried out at 12,000G). The aqueous phase was carefully removed, ensuring that the interphase was not disturbed, and added to a fresh Eppendorf with $500\mu\text{l}$ of isopropanol and mixed gently with a P1000 pipette before a 10 minute incubation at RT. To RNeasy spin columns, $700\mu\text{l}$ were added and spun for 30 seconds and repeated for remaining sample, discarding all flow through. Once all the sample was added to the spin column, $50\mu\text{l}$ of DNase was added to the column and left for 15 minutes at RT. Next $700\mu\text{l}$ of Buffer RW1 was applied to the column, column spun for 30 seconds, then $500\mu\text{l}$ of Buffer RPE was added, the column spun for 30 seconds and then an additional $500\mu\text{l}$ of RPE added and the column spun for 2 minutes. The column was dried by centrifuging for 1min before the column was placed in a collection tube and $50\mu\text{l}$ of RNase-free H_2O added to the column. The H_2O containing RNA was passed through the column a second time to maximise RNA elution.

To measure RNA content, $1\mu\text{l}$ of elute was run on a nanodrop. Concentrations were accepted if there was a 260/280 ratio of 1.8-2.1 and a regular plot on an absorbance

spectrum, as this indicated high purity of the RNA. Samples were stored at -80°C until further use.

2.9.2 cDNA synthesis

cDNA was synthesised using the RevertAid First Strand cDNA synthesis kit (K1622, ThermoFisher Scientific). The volume required to contain 2µg of RNA was added to 1µl of Random Hexamer Primers and made up to a total volume of 12µl with ddH₂O. To this 12µl mix, the following reagents were added in order: 4µl of 5X reaction buffer; 1µl of RiboLock RNase Inhibitor; 2µl of 10mM dNTP mix; and 1µl of RevertAid Reverse Transcriptase. Samples were run on a PCR programme with the following stages: 5 minutes at 25°C; 45 minutes at 50°C, 15 minutes at 70°C; then kept at 4°C.

2.9.3 Quantitative reverse transcriptase polymerase chain reaction

qRT-PCR was performed for markers of interest: p16^{Ink4a} and p21^{Cip}. Housekeeping genes used were glyceraldehyde 3-phosphate dehydrogenase (GAPDH) and hypoxanthine phosphoribosyltransferase (HPRT), with data presented normalised to GAPDH. A master mix is prepared to contain 0.5µl of TaqMan primers (containing F and R, Table 2.8), 5µl of TaqMan Universal mix and 3.5µl of ddH₂O. To this 9µl reaction mix, 1µl of cDNA diluted 1:40 is added onto and 384well plate and run on QuantStudio 7 Flex System for a standard Comparative CT run.

Table 2.8 TaqMan probes, ThermoFisher Cat. Number 4331182.

Gene	Taqman probe	Probe spans exons
GAPDH	Mm99999915_g1	2-3
p21 ^{Cip} (Rasa3)	Mm00436272_m1	5-6
p16 ^{Ink4a} (Cdkn2a)	Mm00494449_m1	2-3

2.10 Protein expression analysis

For the assessment of protein expression from blood and tissue samples, samples were processed for analysis by cytokine/chemokine array, by Eve Technologies.

2.10.1 Serum isolation from whole blood

To isolate serum from whole blood obtained from cardiac puncture, 250µl-500µl blood was left in an eppendorf to clot at RT for at least 30 minutes before centrifugation for 10 minutes at 1,000G at 4°C. The upper aqueous phase composing of serum was transferred to a fresh Eppendorf and stored at -20°C.

Additional blood (≤600µl) was processed using a BD Microtainer SST serum separator tube (BD 365979, Becton Dickerson). The tube containing blood was inverted 5 times, left for 30 minutes, spun at 14,000G for 1.5 minutes and serum aspirated off and stored at -20°C until analysis.

2.10.2 Protein isolation from tissue

Portions of heart (superior to suture, affected RV and affected LV) were placed in 1ml of RIPA buffer (R0278, Sigma) prepared to contain protease inhibitors (58927091001, cOmplete ULTRA Tablets, 1 tablet dissolved in 10ml RIPA buffer) and left on ice for at least 20 minutes. Tissue was then homogenised and centrifuged for 20 minutes at 12,000 G at 4°C. Supernatant was transferred to a fresh Eppendorf and stored at -20°C.

To normalise protein content, a bicinchoninic acid (BCA) assay was performed according to manufacturer's instructions (Thermo Scientific, 2019). Samples were diluted 1:10 and 1:100 in RIPA buffer, and 25µl in duplicate loaded onto a flat-bottomed 96-well plate, alongside 25µl of BSA protein for the standard curve (concentrations at 2000ng/µl, 1500ng/µl, 1000ng/µl, 750ng/µl, 500ng/µl, 250ng/µl, 125ng/µl and 25ng/µl). To all duplicate samples, 200µl of working reagent (50 parts BCA Reagent A with 1 part BCA Reagent B) was added and the plate incubated for 30 minute at 37°C in the dark. Once cooled to RT, the plate was loaded into the plate reader, the plate was shaken for 5 seconds at 500rpm, and then the absorbance of samples analysed at 562nm. Concentrations were determined according to the standard curve generated from the BSA samples.

2.10.3 Cytokine/Chemokine array

For analysis by Eve technologies on a Mouse Cytokine Array/Chemokine Array 44-Plex (MD44) and TGFbeta 3-Plex Array (TGFb1-3), protein samples were normalised to contain 2mg/µl. Serum for analysis by these Arrays was diluted 1:1 in PBS. All samples were run in duplicate for both assays.

Heat maps showing expression levels were generated on www.heatmapper.ca/expression and results displayed with Average Linkage Clustering method with Pearson Distance Measurement method.

2.11 Statistical analysis

Data analysis was carried out using the flow chart in Figure 2.7. Initially data analysis was performed using a T-Test of ANOVA. These statistical tools assume that residuals (defined as actual – fitted) are normally distributed with mean 0 and a constant variance. Normality of the residuals was assessed via visual inspection of QQ plots and by carrying out a Shapiro Wilk test on the residuals. A QQ Plot arranges the data collected (*y*-axis) against the theoretical values for a normally distributed population (*x*-axis). The straight line across the graph represents a perfect fit to the normal distribution (Figure 2.8.A) (Pleil, 2016). In cases where QQ plots exhibited non-linearity (Figure 2.8.B), a nonparametric test such as a Mann Whitney or Kruskal-Wallis was carried out as per Figure 2.7.

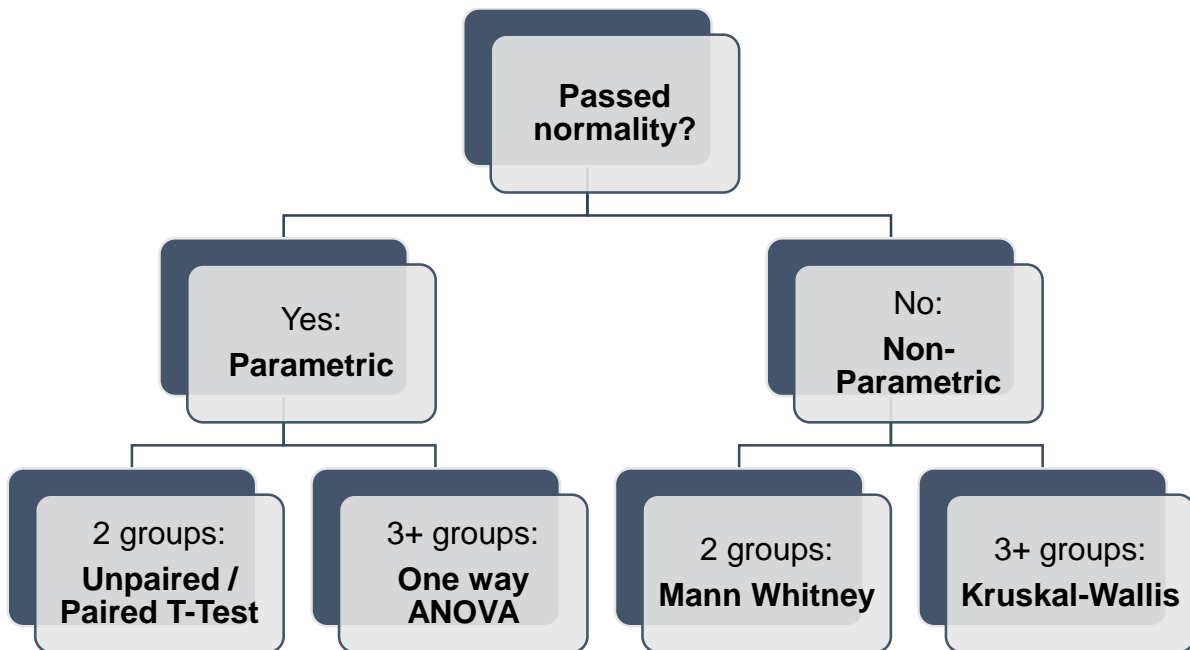


Figure 2.7 Flow chart to determine appropriate statistical test to perform according to the outcome from a Shapiro-Wilk test.

If the data set residuals from the fitted model passed normality, then a parametric test was performed: Unpaired/ Paired T-Test for two groups; or One-way ANOVA for \geq three groups. If the data sets didn't pass normality, then a non-parametric test was carried out: Mann Whitney for two groups; or Kruskal-Wallis for \geq three groups. P values obtained from each test are represented as follows: not significant/ns = >0.05 , * = ≤ 0.05 , ** = ≤ 0.01 , *** = ≤ 0.001 , **** = ≤ 0.0001 .

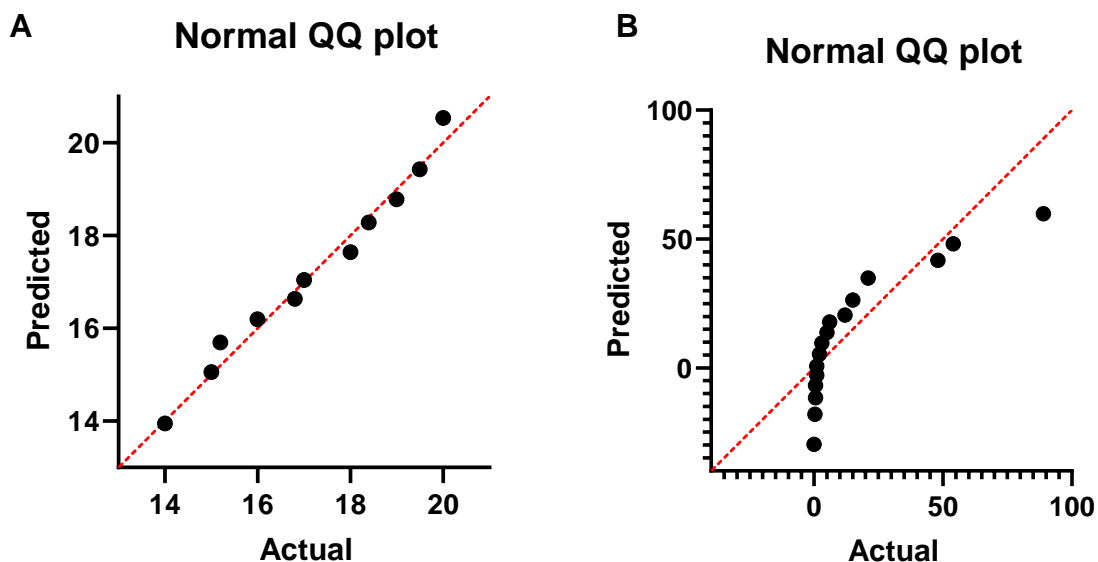


Figure 2.8 Example of a QQ Plot showing the distribution of the data residuals against a theoretical normally distributed population.

A) Data has passed Shapiro-Wilk test.

B) Data has not passed Shapiro-Wilk test.

For MRI analysis, if analysing data collected from the same mouse at different time-points and a parametric test was appropriate, then a paired T-test was used. For all other analyses, an unpaired T-test was utilised if performing a parametric test to compare two groups.

A One-Way ANOVA or Kruskal-Wallis with multiple comparisons was performed comparing only the mean of the “Non-LAD” control group against the mean of the “IRI” and “IRI + Nav” groups at the 3 week and 5 week time-points separately. Differences between the IRI untreated and IRI Navitoclax treated groups, either against each other or comparing the data between time-points, was assessed using a T-Test as appropriate, outlined above.

Chapter 3. Cardiomyocyte senescence post-myocardial infarction and subsequent reperfusion in a mouse model of ischaemia-reperfusion injury

3.1 Introduction

Myocardial infarction is the leading cause of death and disability in developed countries (Roger, 2007). The gold-standard intervention is timely reperfusion via PPCI (Terkelsen *et al.*, 2009; National Clinical Guideline Centre (UK). 2013), which can limit acute MI injury by salvaging viable myocardium, and the introduction of PPCI has led to dramatic improvements in patient survival rates from MI. Paradoxically, reperfusion itself can cause damage to the myocardium due to the phenomenon termed IRI (Lønborg, 2015; Doost Hosseiny *et al.*, 2016), which encompasses numerous events including ECM remodelling and stimulation of an inflammatory response (Ibarrola *et al.*, 2019). Together these processes all contribute to adverse myocardial remodelling of the LV accelerating progression to heart failure (Joost *et al.*, 2016; Westman *et al.*, 2016; Ibarrola *et al.*, 2019).

Ischaemia-reperfusion injury is associated with multiple forms of genotoxic stress, including OS, which is known to be central to many adverse processes occurring as a result of IRI (Kalogeris *et al.*, 2012; Hausenloy and Yellon, 2013). Mild OS can accelerate telomere shortening rates (von Zglinicki, 2002) whereas high OS can lead to senescence independently of telomere length (Dumont *et al.*, 2000). More recently it has been shown that OS induces DNA damage at telomeric regions, resulting in activation of a persistent DNA damage response (Hewitt *et al.*, 2012). Senescence is thought to contribute to ageing in multiple organ systems (Kirkland and Tchkonja, 2017; de Magalhães and Passos, 2018) including the heart (Anderson *et al.*, 2019; Lewis-McDougall *et al.*, 2019; Walaszczyk *et al.*, 2019) and is also associated with age-related disorders (Childs *et al.*, 2015). There is now growing evidence linking senescence with CVDs including atherosclerosis, pressure overload-induced cardiac hypertrophy and heart failure (Meyer *et al.*, 2016; Childs *et al.*, 2018; Anderson *et al.*, 2019; Shimizu and Minamino, 2019). Senescent cells are thought to contribute to ageing via release of ROS that can cause damage to surrounding cells (Nelson *et al.*, 2012), the secretion of a SASP (Coppé *et al.*, 2008), which is pro-inflammatory, pro-

fibrotic and can also promote senescence in surrounding cells (Acosta *et al.*, 2013), along with limiting stem cell function and altering the ECM (Coppé *et al.*, 2008; van Deursen, 2014; McHugh and Gil, 2018).

While the heart has a limited regenerative potential, the majority of CMs are considered to be post-mitotic cells and were traditionally believed to be incapable of becoming senescent (Sapieha and Mallette, 2018). Recently it has been demonstrated that with age, an accumulation of OS drives telomere dysfunction and senescence in CMs irrespective of telomere length (Anderson *et al.*, 2019). Damage in telomere regions has been shown to induce a persistent DNA damage response (Hewitt *et al.*, 2012). Mechanistically, it is thought that shelterin components such as TRF2 inhibit non-homologous end joining (NHEJ) impairing repair (Fumagalli *et al.*, 2012). Telomere associated DNA damage foci have been shown to accumulate in multiple tissues during aging (Hewitt *et al.*, 2012; Birch *et al.*, 2015; Anderson *et al.*, 2019; Victorelli *et al.*, 2019) and increased in mouse models of increased OS (Anderson *et al.*, 2019).

Formation of TAF has been shown to contribute to a senescent-like phenotype in CMs, portraying a hypertrophic phenotype, expression of cyclin-dependent kinases p21^{Cip}, p16^{Ink4a} and p15^{Ink4b} and generating an atypical SASP, which does not involve pro-inflammatory cytokines and chemokines such as Il-6 and Cxcl1 (Anderson *et al.*, 2019). This atypical SASP is believed to initiate remodelling events, as *in vitro* taking conditioned media from aged CMs for culture on healthy fibroblasts and neonatal CMs demonstrated increases in myofibroblast differentiation and CM hypertrophy which are both prominent characteristics of adverse remodelling (Anderson *et al.*, 2019). In a model of mitochondrial dysfunction (MAO-A mouse) where the enzyme monoamine oxidase A, which is a promoter of OS, was specifically upregulated in the CM population resulted in increased OS and markers of senescence including TAF compared to age-matched controls. Treatment with the antioxidant NAC recovered TAF and senescence levels in the transgenic MAO-A mouse. Additionally, alternative mouse models deficient in antioxidant enzymes catalase and manganese superoxide dismutase showed increased TAF in CMs compared to age-matched controls. These models implied that OS directly causes senescence and telomere dysfunction of CMs (Anderson *et al.*, 2019).

A senescent environment generated from the SASP has been shown to attenuate regeneration (Lewis-McDougall *et al.*, 2019) and contributes to the pathophysiology of

adverse remodelling by promoting fibrosis and hypertrophy (Anderson *et al.*, 2019; Walaszczyk *et al.*, 2019). To date, it is unknown whether IRI post-MI instigates cardiac and CM senescence and if, as in aged hearts, senescence contributes to myocardial remodelling via the SASP.

It was hypothesized that the genotoxic stress associated with IRI will induce cellular senescence (Figure 3.1). To investigate this hypothesis, I used the LAD ligation with reperfusion model of IRI and characterised senescence using the markers TAF, SA- β -Gal and expression of the CDK inhibitors p21^{Cip} and p16^{Ink4a} (Carnero, 2013).

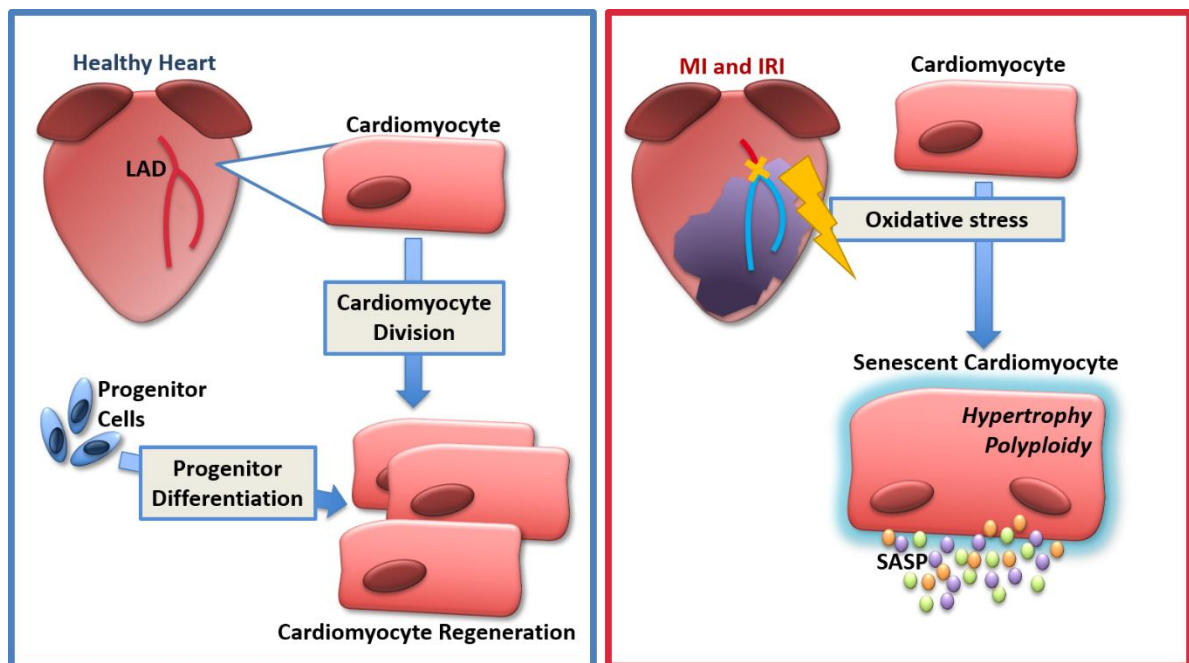


Figure 3.1 Graphical hypothesis.

The healthy heart (left) has a limited but measurable potential for CM regeneration, a process that involves both CM proliferation as well as contribution from progenitor cells, which has the potential to contribute to a restricted recovery following MI. Following MI with reperfusion (right), IRI and the subsequent increase in OS drives DNA damage and senescence in the CM population via persistent activation of the DDR.

3.2 Experimental model

To establish whether MI with IRI induced CM senescence, a murine model in which the LAD is surgically occluded for 1 hour and then allowed to reperfuse (Figure 2.1) was utilised. Male C57BL/6 mice at 3-months old were used for all experiments. Male mice were used as other studies have reported differences between male and female mice in the progression of myocardial repair and remodelling after MI (Redgrave *et al.*,

2016). These differences are due to variations in the inflammatory and fibrotic responses resulting in female mice demonstrating lessened remodelling (Cavasin *et al.*, 2004; Gao *et al.*, 2005; Fang *et al.*, 2007; Wang *et al.*, 2007; Redgrave *et al.*, 2016). Also studies using male subjects may be of more relevance as the proportion of patients in a clinical setting that have an MI that are male is higher than the incidence of MI in females (Dunlay and Roger, 2012; Bhatnagar *et al.*, 2015).

Hearts were then excised, collected and processed at 24 hours, 72 hours, 1 week and 4 weeks (Figure 3.2) after IRI and embedded either in wax or OCT to allow histological analysis for a range of markers for OS, telomere dysfunction and senescence.

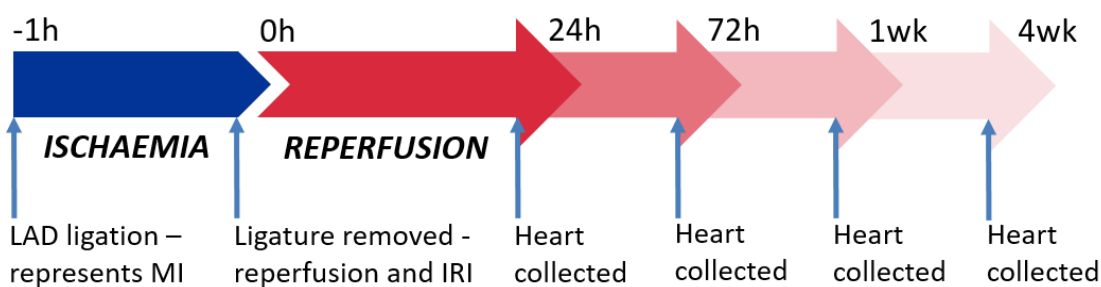


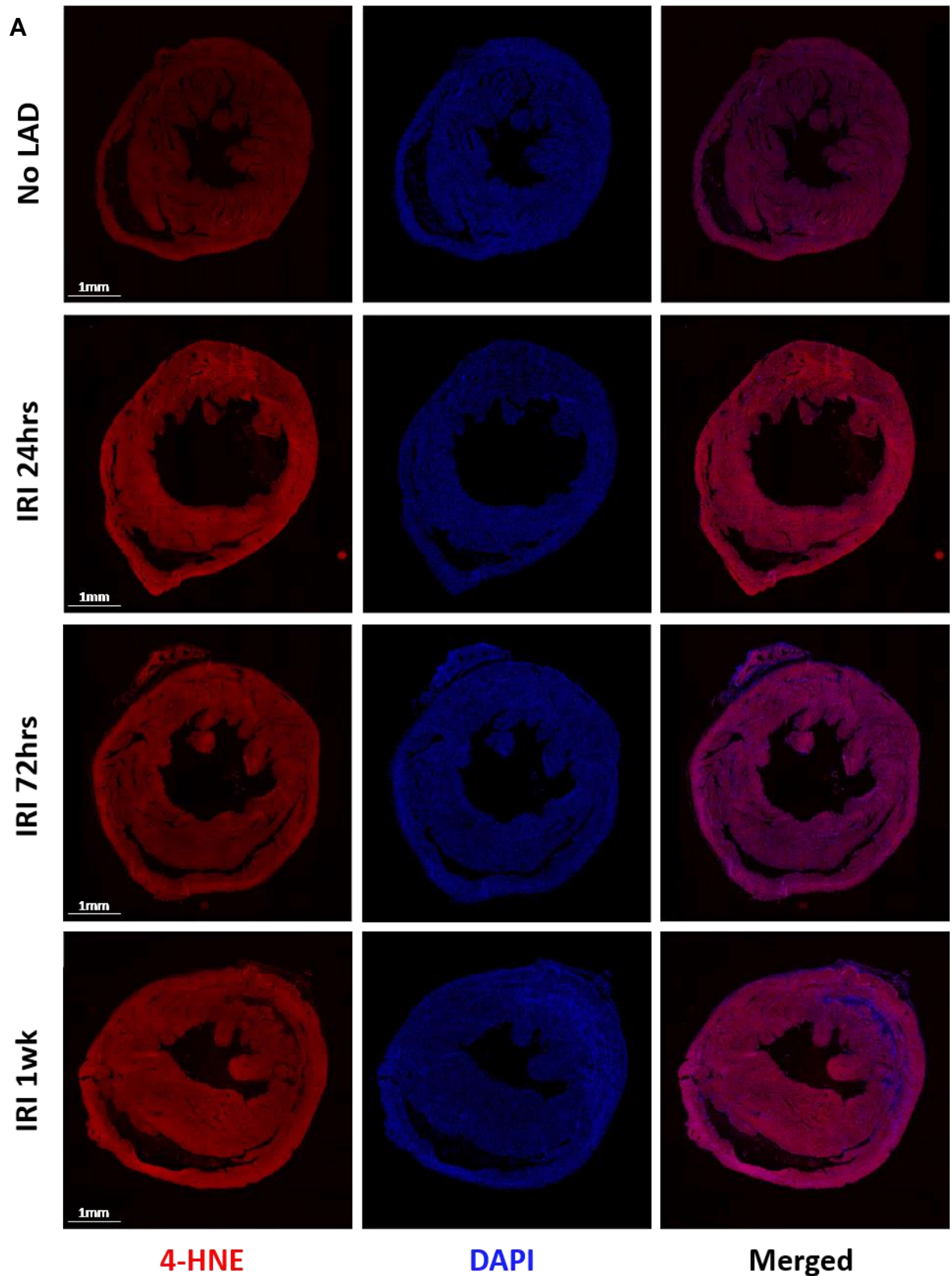
Figure 3.2 Experimental timeline.

After 1 hour ligation of the LAD the LAD was allowed to be reperfused and hearts collected at numerous time-points (24 hours, 72 hours, 1 week and 4 weeks, N=3-5 for each time-point) post-surgery for senescence analysis.

3.3 Detection of senescence in a model of ischaemia-reperfusion injury

3.3.1 Oxidative stress markers are increased post-ischaemia-reperfusion injury

In this model it was first confirmed whether OS levels were increased as a result of LAD ligation and IRI. Within 24 hours after IRI, levels of the OS marker 4-HNE (Pradeep *et al.*, 2013) significantly increased ($p=0.0043$). At baseline in healthy, non-ligated mice, the intensity of 4-HNE fluorescence normalised to myocardial area was measured at $4.73\text{AU} \pm 0.68$, and by 24 hours post-LAD ligation, levels were raised to $8.01\text{AU} \pm 0.70$. By 72 hours, 4-HNE levels had lowered to $6.78\text{AU} \pm 0.08$ but this elevated level of OS was maintained by 1 week after infarct with detected levels of $6.71\text{AU} \pm 0.99$ (Figure 3.3). Fluorescence of 4-HNE at 24 hours was particularly elevated within the region of the LV predicted to be affected and generate an infarct. The corresponding region in hearts analysed 1 week after IRI demonstrated a loss of the myocardium in the medial LV wall which is likely infarct. (Figure 3.4).



B

Intensity of 4-HNE fluorescence after IRI

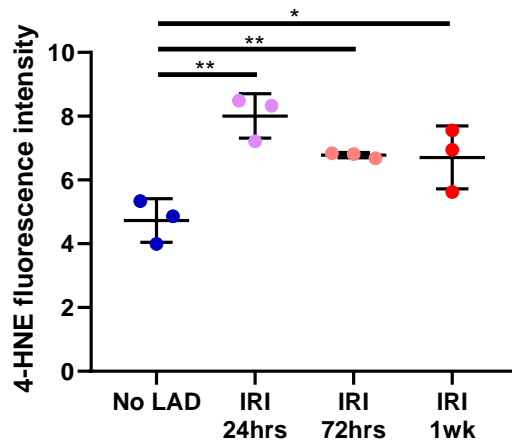


Figure 3.3 Fluorescence intensity of 4-hydroxynonenal as a marker of oxidative stress increases at 24 hours after surgery and elevated levels are maintained up to a week.

- A)** Images of 4-HNE (left column), DAPI (middle column) and merged (right column) channels in a non-LAD ligated heart (first row), and IRI hearts at 24 hours (second row), 72 hours (third row) and 1 week post-IRI (fourth row). Fluorescence intensity is greatest in the heart at 24 hours.
- B)** Graph shows there is a significant increase in 4-HNE intensity at 24 hours ($p=0.0043$) and these elevated levels reduced slightly by 72 hours (0.0068) and are sustained by 1 week (0.0466).

N=3 for each experimental condition. NS \geq 0.05, * p <0.05, ** p <0.01, *** p <0.001, **** p <0.0001 using Two-Tailed T Test and One-way ANOVA.

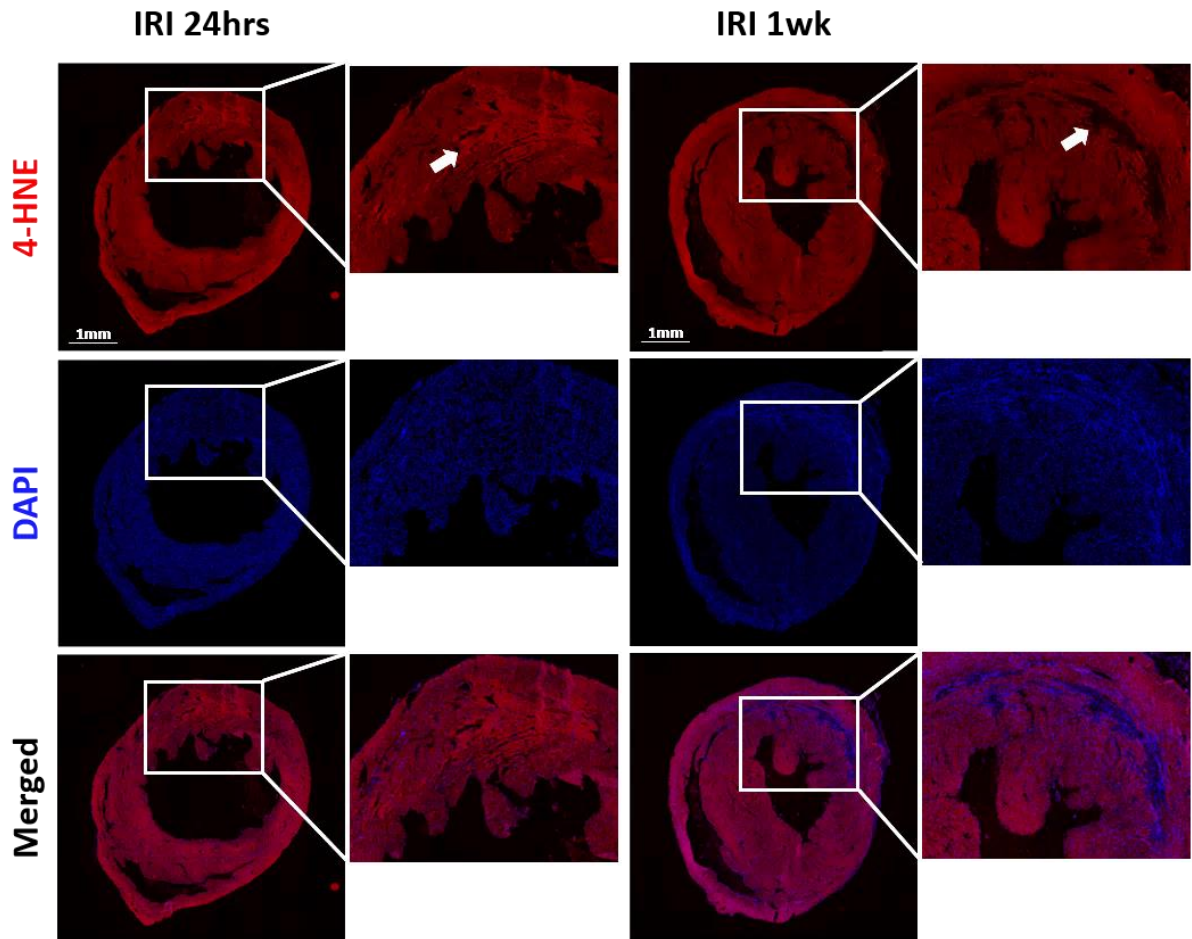


Figure 3.4 At 24 hours after ischaemia-reperfusion injury , 4-hydroxynonenal intensity was elevated in the region of the left ventricle predicted to become infarct.

Images of 4-HNE, DAPI and merged channels from hearts at 24 hours and 1 week after IRI. In the heart at 24 hours the intensity of 4-HNE fluorescence is greater within the LV myocardium (arrow). This region is the area predicted to be affected by MI and would become infarct. Zoomed image at 1 week shows that the equivalent region (arrow) has an infarct.

3.3.2 Presence of telomere-associated DNA damage is elevated after ischaemia-reperfusion injury

It is commonly accepted that OS triggers genomic DNA damage leading to activation of the DDR (Correia-Melo *et al.*, 2014). Our previous studies have shown that during ageing, mitochondrial dysfunction and increased OS leads to DNA damage at telomere regions. This TAF accumulation is persistent and has been suggested to contribute directly to myocardial remodelling (Anderson *et al.*, 2019). On the basis of the aforementioned findings, I hypothesised that the OS associated with IRI induced TAF.

To assess levels of TAF, immuno-FISH was carried out on hearts taken from mice at 1 week post-operation. At this time-point, levels of the OS marker had been elevated over the 7 days (Figure 3.3) and corresponds to when senescence would be starting to become fully established (Correia-Melo *et al.*, 2014). TAFs were identified by the co-localisation of γ H2Ax foci (green) and telomere C domain probe-foci (red) within a nucleus (blue). The region of infarct was located using WGA, which also stained the membranes of the CMs (cyan) (Figure 3.5.A-F). The WGA was also used to discriminate the CM nuclei from other cell types, based on cell size and morphology for analysis. In each image, the total number of CMs, the number of CMs positive for TAFs, and the number of TAFs per nuclei were quantified. The TAFs were counted by moving through the z-stack and recording the number of overlapping foci in the green and red channel within each nucleus. Figure 3.5.B-F is an example of a TAF positive nuclei.

In the BZ surrounding the infarct at 1 week, CMs demonstrated a significantly higher ($p=0.0095$) number of total TAF (6.86 ± 1.84) compared to the RZ (3.70 ± 1.18). Levels in the BZ was also significantly higher than in healthy non-ligated controls (1.98 ± 0.48 , $p=0.0006$) (Figure 3.5.G). At this time-point, the percentage of CMs containing a TAF was significantly higher after IRI ($p<0.0001$), with the percentage of TAF positive CMs increasing from $16.33\% \pm 5.79$ pre-IRI to $67.88\% \pm 0.83$ in the BZ (Figure 3.5.H).

TAF analysis was also performed at 4 weeks post-LAD ligation to assess residual senescence still present after CM death. At this time-point mean TAF number and percentage of CMs positive for TAF had reduced in comparison to the 1 week time-point to 4.35 ± 0.70 and $35.52\% \pm 7.95$ respectively (Figure 3.5.G-H).

An additional point to consider when analysing TAF is the organ-specific TAF threshold for initiating senescence. In hepatocytes, it has been demonstrated that considering 3 or more TAF is a robust marker of senescence induction (Jurk *et al.*, 2014; Ogradnik *et al.*, 2017), but suggested that this threshold may vary between tissue types and be higher in the heart (Anderson, 2016). If this data was analysed to calculate the percentage of CMs positive for 5 or more (≥ 5) TAF, then only $1.53\% \pm 0.45$ of healthy CMs contained ≥ 5 TAF, which was significantly increased ($p=0.0001$) to $54.00\% \pm 20.52$ by 1 week post-IRI and levels were lower by 4 weeks at $17.71\% \pm 7.67$ ($p=0.0402$, Figure 3.5.H).

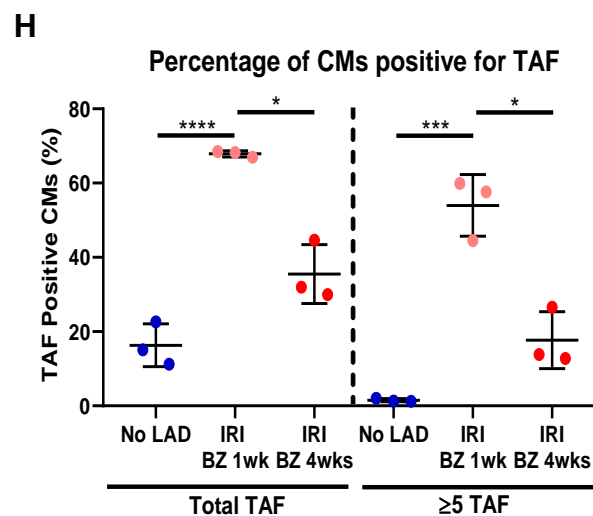
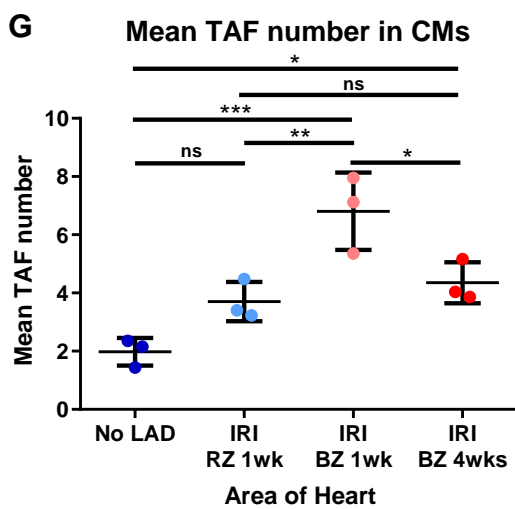
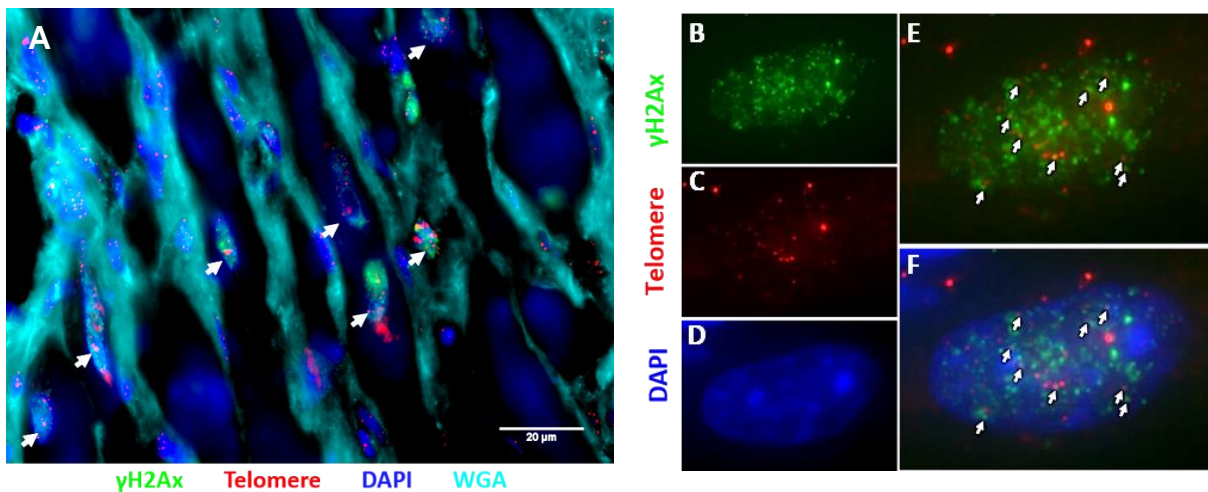


Figure 3.5 Proximal to the infarct cardiomyocyte nuclei are positive for telomere-associated DNA damage foci.

A) Representative image taken from the BZ in a heart collected 1 week post-LAD ligation. CMs with TAF positive nuclei are highlighted with white arrows.

B) Individual channel for γ H2Ax.

C) Individual channel for Telo-c probe.

D) Individual channel for DAPI.

E) Example of γ H2Ax and Telo-c channels merged, to allow for identification of TAF, which are highlighted with white arrows.

F) Merged channels including DAPI showing TAF localise within the nuclei.

G) Graph showing mean TAF number in CMs in no-LAD ligation control, the RZ in LAD ligated samples at 1 week and the BZ in LAD ligated samples at 1 and 4 weeks. There were significantly more TAFs in all IRI groups compared to no-LAD ligated control. In the BZ, the mean TAF number was higher at 1 week than at 4 weeks.

H) Graph showing the percentage of CMs positive for total and more than 5 TAF without LAD and at 1 and 4 weeks. There were significantly more CMs positive for TAF in the IRI groups compared to no-LAD ligated control.

N=3 for each experimental condition. NS \geq 0.05, * p <0.05, ** p <0.01, *** p <0.001, **** p <0.0001 using Two-Tailed T Test and One-way ANOVA.

3.3.3 Cardiomyocytes are positive for senescence-associated β -galactosidase activity 1 week post-ischaemia-reperfusion injury

Having observed elevated levels of OS (Figure 3.3) and this correlating with an accumulation of TAF within the CM population (Figure 3.5) additional markers of senescence were tested. SA- β -Gal staining was used for these initial studies as it is an established marker of senescence (Dimri *et al.*, 1995; Itahana *et al.*, 2013).

In the uninjured control hearts, no SA- β -Gal was detected. Conversely, SA- β -Gal activity was observed in all hearts subjected to LAD ligation and at all time-points SA- β -Gal staining was restricted to the LV (Figure 3.6).

At 24 hours post-IRI numerous SA- β -Gal positive cells were found throughout the myocardium in the region which I hypothesised would be affected. These observed positive cells were small and located within the interstitial cells of the myocardium. At this time-point no cells with a CM morphology were found to be stained for SA- β -Gal (Figure 3.6.B.i).

By 72 hours, the infarct was more readily defined (Figure 3.6.C.ii). Positive staining for SA- β -Gal was observed throughout this region as well as within interstitial cells of the myocardium adjacent to the infarct in a region subsequently referred to as the infarct BZ (Figure 3.6.C.i). This region of positive staining correlated to the same region observed in Figure 3.4 that had elevated expression of the OS marker, 4-HNE.

At 1 week the SA- β -Gal staining remained similar to the 72 hour time-point, located in the infarct and interstitial cells of the BZ, although the staining appeared more intense (Figure 3.6.D.ii). In addition, throughout the BZ of the hearts at 1 week post-operation, cells positive for SA- β -Gal with a CM morphology were identified (Figure 3.6.D.i). These cells were always observed peri to the infarct and were not observed in the myocardium remote to the infarct. It should also be noted that this staining was also performed on sections collected 4 weeks after LAD ligation, however, little to no positive staining could be detected (Figure 3.6.E).

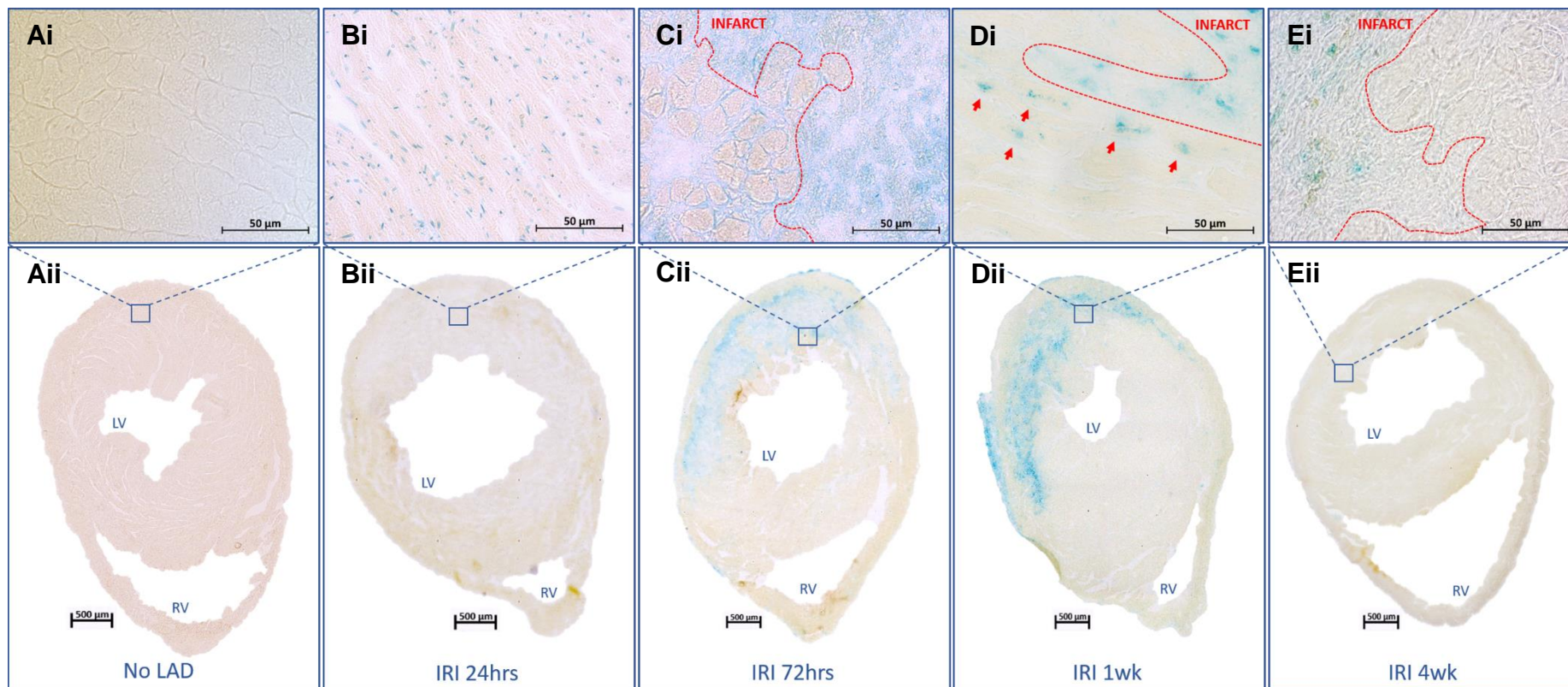


Figure 3.6 Senescence-associated β -galactosidase expression is observed within the infarct and cardiomyocyte population post-ischaemia-reperfusion injury.

Upper row Ai, Bi, Ci, Di and Ei) High power images of the BZ at each time-point. **Di)** SA- β -Gal positive cells with CM morphology (red arrows).

Lower row Aii, Bii, Cii Dii and Eii) Tiled images of a whole heart section with the distribution and intensity of positive SA- β -Gal staining throughout the heart. BZ = CMs proximal to the infarct. N=3 for each time-point.

My next aim was to validate that SA- β -Gal staining was in the CM population by using two established markers of CMs: autofluorescence at 488nm; and via expression of the CM specific protein troponin C. Cardiomyocytes are autofluorescent at 488nm allowing their discrimination from other cardiac cell lineages (Chorvat *et al.*, 2005). In the BZ, SA- β -Gal positive cells which demonstrated a high degree of auto-fluorescence at 488nm were observed. The presence of sarcomere-like structures further indicated that these cells were CMs (Figure 3.7.A-B). Troponin C is a protein that is a component of the troponin complex expressed in CMs, and functions to sense and bind to calcium triggering CM contraction (Li and Hwang, 2015). Cells stained with both troponin C and SA- β -Gal were again identified in the BZ at 1 week post-IRI indicating that CMs peri to the infarct may be induced to senescence as a result of IRI (Figure 3.7.C-D).

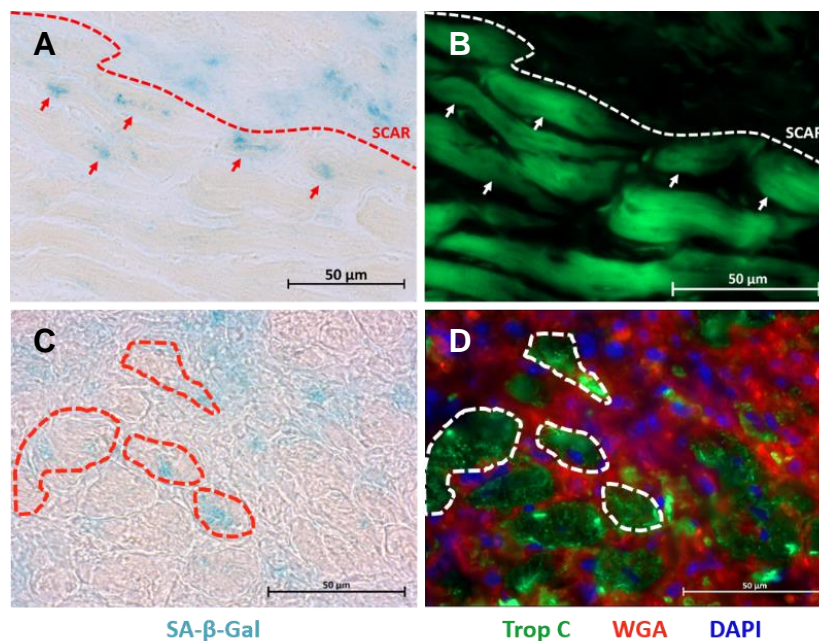


Figure 3.7 A sub-population of cardiomyocytes are positive for senescence-associated β -galactosidase 1 week after ischaemia-reperfusion injury.

A and B) Images showing the same cells to be positive staining for SA- β -Gal (A) and autofluorescence in the 488nm channel (B). These cells also appeared striated, another characteristic of CMs. This hypothesis could only be confirmed by developing a dual stain using a CM marker.

C and D) Images showing the same cell to be positively stained for SA- β -Gal (C) and the CM specific sarcomeric protein, troponin C (D). Image A and C are bright field images showing SA- β -Gal labelled cells (blue). Images B and D are immunofluorescence images: troponin C (in green, wavelength 488nm), WGA (in red, wavelength 594nm), and DAPI (in blue, wavelength 461nm). The cells outlined are CMs that are positive for SA- β -Gal and troponin C.

As detailed above there is no universal marker for cellular senescence. While SA- β -Gal is an established senescence marker, as an indicator of the increased lysosomal activity at pH 6.0 (Lee *et al.*, 2006), utilising multiple markers leads to a more robust analysis (Biran *et al.*, 2017), and these markers were further investigated at the 4 week post-LAD ligation time-point.

3.3.4 RNA levels for p21^{Cip} and p16^{Ink4a} are also increased following ischaemia-reperfusion injury

To further test the hypothesis that senescence was induced by IRI and to establish if senescence was persistent up to 4 weeks post-IRI the transcript expression of p21^{Cip} and p16^{Ink4a}, additional biomarkers of cellular senescence, were quantified using qRT-PCR. At 4 weeks post-infarct hearts were removed (n>4) and each LV was dissected into two regions: 1) the region posterior to the ligation containing the infarct and BZ; and 2) the region superior to the ligation containing only myocardium remote to the infarct. The same regions were collected from control uninjured hearts. Following collection, mRNA was isolated and expression of p21^{Cip} and p16^{Ink4a} was quantified using TAQman probes (Table 2.6). qRT-PCR revealed there was a significant 2-fold increase in p21^{Cip} expression at 4 week post-LAD ligation compared to uninjured control (2.04 ± 0.56 vs 1.00 ± 0.34 , $p=0.0291$, Figure 3.8.A) and over a 4-fold increase in p16^{Ink4a} expression in IRI hearts vs control (4.61 ± 1.74 vs 1.00 ± 0.30 , $p=0.0033$, Figure 3.8.B).

This data showing the expression of p16^{Ink4a} and p21^{Cip} in the BZ was compared to the expression in the remote myocardium at 4 weeks post-IRI. By doing so this identified if senescence was restricted to the infarct area and also provided a control to demonstrate that increased senescence was indeed due to IRI and not simply a result of the surgery. Contrary to the LV containing infarct, no significant difference was observed in the mRNA isolated from tissue collected superior to the ligation for either p21^{Cip} (1.00 ± 0.11 without LAD ligation and 1.26 ± 0.41 post-LAD, Figure 3.8.C) or p16^{Ink4a} expression (1.00 ± 0.40 to 1.719 ± 0.66 , Figure 3.8.D). This result supports my hypothesis that the affected myocardial region is restricted to the BZ and suggests that IRI directly contributes to senescence induction.

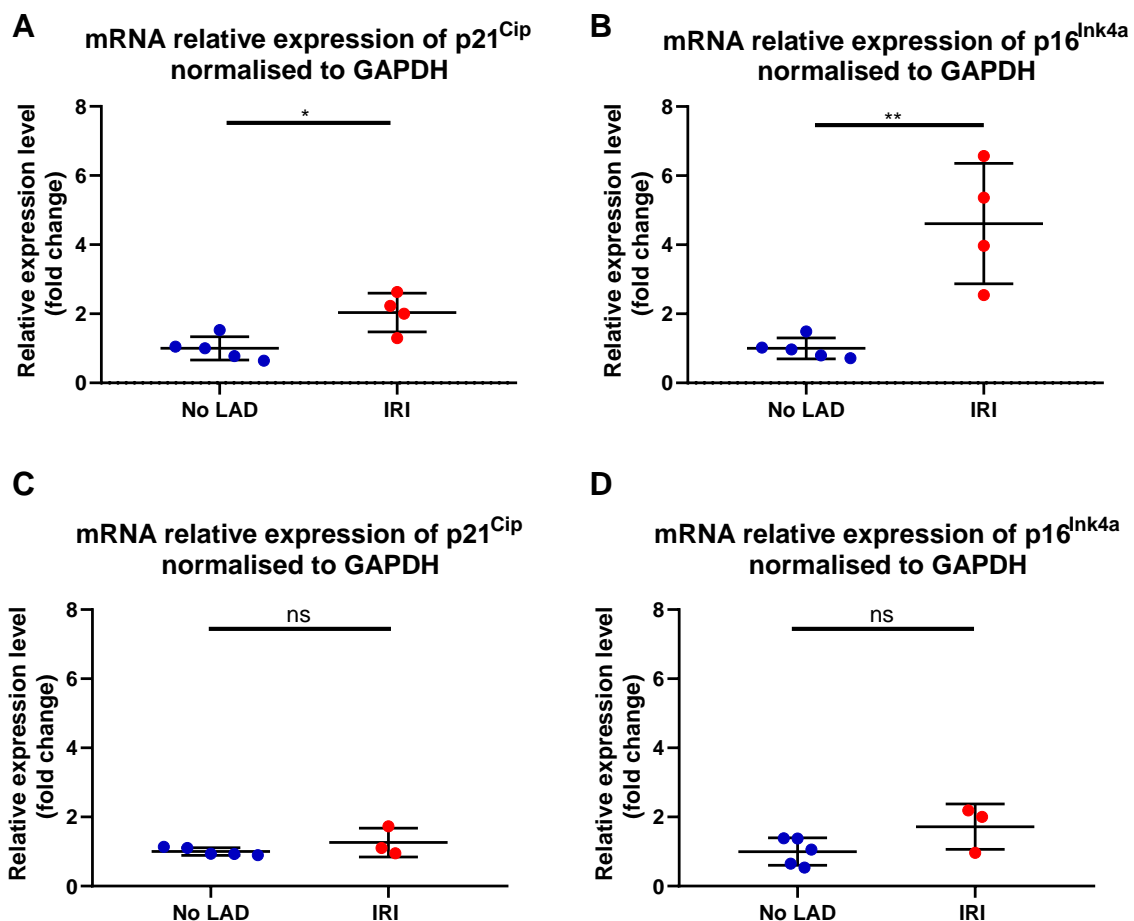


Figure 3.8 mRNA expression of p21^{Cip} and p16^{Ink4a} from tissue samples collected from regions proximal and distal to the infarct.

- A)** Expression of p21^{Cip} was significantly increased in mRNA samples collected from the LV of LAD ligated hearts posterior to the suture of LAD ligated hearts.
- B)** Expression of p16^{Ink4a} was significantly increased in mRNA samples collected from the LV of LAD ligated hearts posterior to the suture of LAD ligated hearts.
- C)** Expression of p21^{Cip} shows no significant change in mRNA samples collected from the LV and atria superior to the suture of LAD ligated hearts.
- D)** Expression of p16^{Ink4a} shows no significant change in mRNA samples collected from the LV and atria superior to the suture of LAD ligated hearts.

N=3-5. NS≥0.05, *p<0.05, **p<0.01, ***p<0.001, ****p<0.0001 using Two-Tailed T Test.

3.3.5 In the border zone proximal to the infarct, cardiomyocytes remain positive for p21^{Cip} and p16^{Ink4a}

A vital CDK inhibitor that lies downstream of p53 to evoke the SASP and cell cycle arrest is p21^{Cip} (Lieberman *et al.*, 2017). Sections from hearts collected at 4 weeks post-IRI were dual stained by immunofluorescence for p21^{Cip} and troponin C. Troponin C expressing CMs which were also positive for p21^{Cip} were identified in the BZ at this

time-point. Expression of p21^{Cip} was observed as a typical punctate staining located specifically in the nuclei (Figure 3.9.B). Quantitative analysis revealed a statistically significantly ($p=0.0003$) increase in the number of p21^{Cip} positive troponin C expressing CMs in the BZ of LAD-ligated hearts compared to the same region of myocardium of age-matched uninjured controls ($18.47\% \pm 2.62$ vs $0.46\% \pm 0.56$ respectively, Figure 3.9.D).

At 4 weeks the remote myocardium remained absent of p21^{Cip} expression further suggesting that CM senescence was a result of proximity with the infarct. Additionally, at this time-point the cells within the infarct did not express p21^{Cip}. There were interstitial cells present that were autofluorescent at both 488nm and 594nm, which were postulated to be erythrocytes as they are autofluorescent at both wavelengths following PFA fixation (Davis *et al.*, 2014). However, none of the interstitial cells were positive for p21^{Cip} at 594nm.

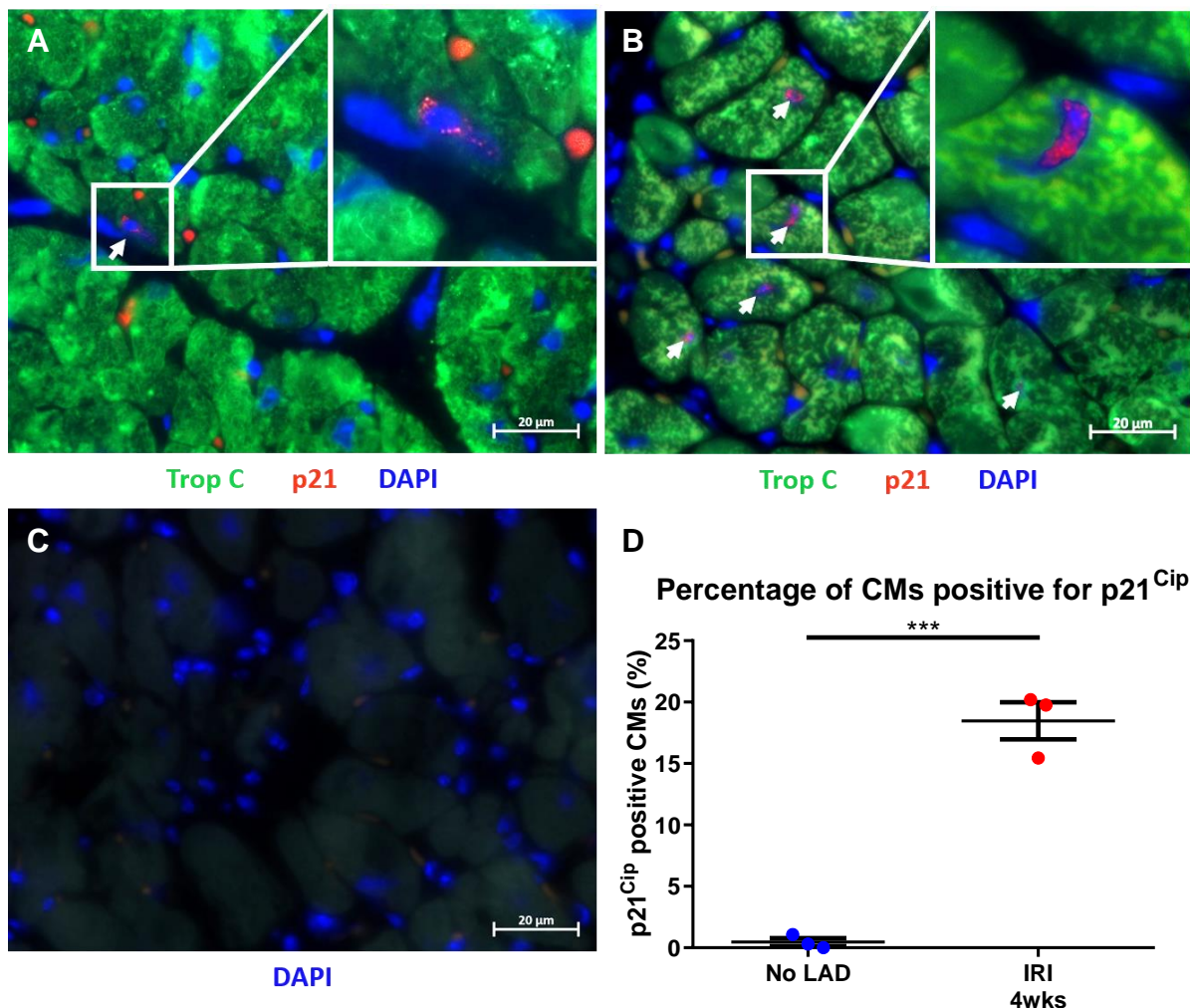


Figure 3.9 Cardiomyocytes express p21^{Cip} post-ischaemia-reperfusion injury.

- A)** Immunofluorescence staining in control, non-LAD ligated hearts. Slides stained with CM marker troponin C (in green, wavelength 488nm), senescence marker p21^{Cip} (in red, wavelength 594nm) and nuclei (in blue with DAPI, wavelength 461nm). All images for this analysis were taken in the BZ. CMs positive for p21^{Cip} are highlighted with a white arrow.
- B)** Immunofluorescence staining in hearts post-IRI. Slides stained with CM marker troponin C (in green, wavelength 488nm), senescence marker p21^{Cip} (in red, wavelength 594nm) and nuclei (in blue with DAPI, wavelength 461nm). All images for this analysis were taken in the BZ. CMs positive for p21^{Cip} are highlighted with a white arrow.
- C)** Negative control for both 1°Abs, slides were incubated in PBS instead. Cells autofluorescent are postulated to be erythrocytes as they are autofluorescent in both 488nm and 594nm channels following PFA fixation (Davis *et al.*, 2014).
- D)** Quantification of CMs expressing p21^{Cip} in no-LAD ligation ctrl vs IRI hearts. The percentage of p21^{Cip} positive CMs was significantly increased.

N=3 for each experimental condition. NS≥0.05, *p<0.05, **p<0.01, ***p<0.001, ****p<0.0001 using Two-Tailed T Test.

Senescent cells are maintained in G1 arrest by expression of p16^{Ink4a} which inhibits the phosphorylation of Rb (Gil and Peters, 2006). It is also proposed that p16^{Ink4a} expression acts as a safety mechanism to maintain cellular arrest in the event of Rb being phosphorylated, as in this scenario DNA synthesis is restarted but p16^{Ink4a} expression blocks cytokinesis and cell proliferation (Takahashi *et al.*, 2007). Consequently, p16^{Ink4a} is essential for both the initiation and maintenance of senescence and therefore a marker of both of these processes.

At 4 weeks post-IRI p16^{Ink4a} expression was observed in a pattern similar to p21^{Cip}. Expression of p16^{Ink4a} was by troponin C positive CMs in the BZ while being absent from the remote myocardium. There were approximately three times more troponin C expressing CMs co-expressing p16^{Ink4a} within the BZ of the infarct post-LAD (Figure 3.10.B) than the same region of LV in uninjured control (Figure 3.10.A), (6.61% ± 2.16 to 23.91% ± 1.75, p=0.0002, Figure 3.10.D). In contrast to p21^{Cip}, interstitial cells in the BZ and within the infarct that expressed p16^{Ink4a} were also observed.

Together this data for p21^{Cip} and p16^{Ink4a} expression supports the qRT-PCR data for both CDKs, confirming elevated expression of these senescent markers within cells proximal to the infarct (Figure 3.8.A-B).

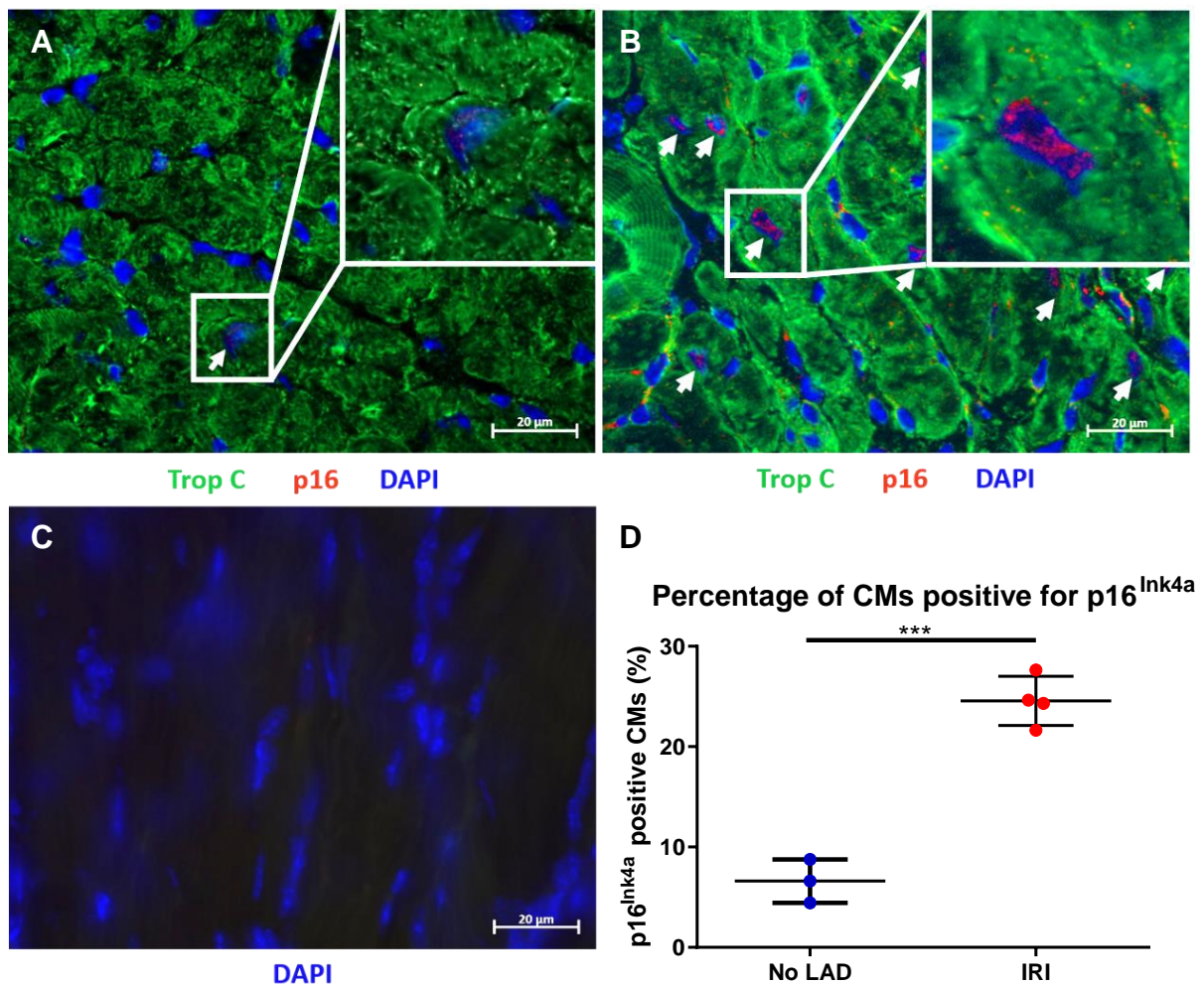


Figure 3.10 Cardiomyocytes express p16^{Ink4a} post-ischaemia-reperfusion injury.

A) Immunofluorescence staining in control, non-LAD ligated hearts. Slides stained with CM marker troponin C (in green, wavelength 488nm), senescence marker p16^{Ink4a} (in red, wavelength 594nm) and nuclei (in blue with DAPI, wavelength 461nm). All images for this analysis were taken in the BZ. CMs positive for p16^{Ink4a} are highlighted with a white arrow.

B) Immunofluorescence staining in hearts post-IRI. Slides stained with CM marker troponin C (in green, wavelength 488nm), senescence marker p16^{Ink4a} (in red, wavelength 594nm) and nuclei (in blue with DAPI, wavelength 461nm). All images for this analysis were taken in the BZ. CMs positive for p16^{Ink4a} are highlighted with a white arrow.

C) Negative control for both 1°Abs, slides were incubated in PBS instead.

D) Quantification of CMs expressing p16^{Ink4a} in no-LAD ligation ctrl vs IRI hearts. The percentage of p16^{Ink4a} positive CMs was significantly increased.

N=3 for each experimental condition. NS≥0.05, *p<0.05, **p<0.01, ***p<0.001, ****p<0.0001 using Two-Tailed T Test.

3.4 Discussion

In this study it was hypothesised that OS from IRI would induce genotoxic stress in the form of TAF, triggering senescence within the CMs proximal to the infarct after LAD ligation with reperfusion. My data shows that post-IRI there is an increase in OS which is associated with an increased number of TAF and senescence markers. While I do not show a direct causality between OS inducing TAF or TAF inducing senescence in the current study, it has been previously demonstrated that in the MAO-A, manganese superoxide dismutase, and catalase knockout transgenic models, which have elevated CM OS, induce TAF independently of age (Anderson *et al.*, 2019). Similarly, it was demonstrated that TAF independent of other senescent stimuli is able to trigger cellular senescence (Anderson *et al.*, 2019). Moreover TAF have been shown to induce senescence in multiple cell types (Jurk *et al.*, 2014; Ogradnik *et al.*, 2019b) and are an established marker of senescence (Hewitt *et al.*, 2012; Ogradnik *et al.*, 2019a). On the basis of my findings elevated OS in the myocardium induces senescence in multiple cell populations including CMs following IRI in young male mice which is consistent with the hypothesis.

The formation of TAF and expression of senescence markers is a dynamic process and after LAD ligation their levels are augmented and then reduced in both the infarct and surrounding CMs in the border zone. I observed a considerable generation of TAFs within CMs in the BZ by 1 week post-LAD ligation which was significantly decreased by 4 weeks. DNA damage not only stimulates senescence induction but if extensive enough, it can lead to either programmed cell death via apoptosis or even necrosis (d'Adda di Fagagna, 2008). Following MI the heart undergoes a dynamic repair process which occurs for several weeks after injury (Blankestijn *et al.*, 2001). The process of wound repair can be divided into four phases, the first of which includes death by apoptosis and necrosis (Blankestijn *et al.*, 2001). In rabbits following LAD ligation with reperfusion, TUNEL staining identified extensive CM apoptosis from 2 days post-LAD, but levels were much lower level by 2 and 4 weeks after surgery (Takemura *et al.*, 1998). From my data, the peak in TAF at 1 week post-LAD ligation and then reduction by 4 weeks may be in part due to apoptosis and necrosis of these CMs containing TAF. Senescent cells are also known to recruit immune cells via the SASP paracrine signalling in order to stimulate immune clearance (Vicente *et al.*, 2016;

Prata *et al.*, 2019). As such, it is also possible that the reduction in CMs containing TAF is due to clearance of this population by immune cells.

Also a decline in TAF number may be due to them being repaired. Double-stranded breaks, can be repaired via NHEJ (Lieber, 2010; Davis and Chen, 2013). Once a DSB is identified, a complex formed of NHEJ components forms to stabilise the break and provide a scaffold for recruited DNA end processing enzymes. These enzymes, including the nuclease Artemis, process the ligated end of the DNA in preparation for ligation by DNA Ligase IV (Davis and Chen, 2013). However, after senescence induction, senescence-associated heterochromatin foci can form making TAFs less accessible by the NHEJ reparative machinery and results in TAF being persistent (Adams, 2007; Mao *et al.*, 2016). An alternative mechanism that can result in TAF repair via homologous recombination has been proposed. Homologous recombination, however, is activated during S and G2 stages (Davis and Chen, 2013) and therefore can only occur during cell proliferation. Although most CMs are post-mitotic, regeneration does occur at a low level (Kikuchi and Poss, 2012) and as such it is possible that TAF may be repaired by homologous recombination in this rare population of proliferating CMs, leading to reduction in total TAF over time.

As well as CM proliferation contributing to regeneration, stem cells have also been shown to play a role (Beltrami *et al.*, 2003; Ellison *et al.*, 2013). As such, TAF reduction may result from a dilution of TAF positive CMs due to formation of new CMs from resident stem cell populations. While at homeostasis the levels of CM renewal from stem or progenitor cells is low this increases considerably following injuries including MI (Hsieh *et al.*, 2007; Malliaras *et al.*, 2013). It has been shown that in the border zone post-MI between 0.7% and 4% CMs may be replaced (Hsieh *et al.*, 2007; Loffredo *et al.*, 2011; Malliaras *et al.*, 2013).

Senescence associated- β -galactosidases activity was observed throughout the myocardium at 24 hours post-IRI within the region consistent with the infarct area. During skin wound healing, senescent fibroblasts and SASP signalling trigger myofibroblast differentiation that migrate to the infarct and play a role during wound repair and later modulate fibrosis (Jun and Lau, 2010b; Demaria *et al.*, 2015). Studies focused on the heart have shown that CMs can recruit fibroblasts via expression of fibronectin (Ulrich *et al.*, 1997; Blankesteyn *et al.*, 2001), and by 48 hours post-MI populations of senescent myofibroblasts have been observed in the injured region

(Baum and Duffy, 2011). Therefore, the SA- β -Gal positive cells observed at 24 hours in my study may well be this myofibroblast population.

By 72 hours post-IRI there is a clearly defined region of SA- β -Gal staining restricted to the infarct. The infarct at this time-point is composed of granulation tissue containing myofibroblasts, inflammatory cells and blood vessels (Ulrich *et al.*, 1997; Blankesteyn *et al.*, 2001). At 72 hours post-infarct, the secondary inflammation phase of wound repair is starting to diminish as the third phase marked by proliferation and granulation formation starts to peak around day 5 post-injury (Midwood *et al.*, 2004; Jun and Lau, 2010b).

At 1 week post-IRI this infarct region is more prominently stained with SA- β -Gal suggesting a high number of senescent cells are present throughout the infarct. However, by 4 weeks little to no SA- β -Gal staining was evident. A study on cutaneous wound repair observed that senescent cells, identified by SA- β -Gal staining, contained within the granulation tissue at 7 days post-injury were virtually undetectable by 12 days (Jun and Lau, 2010b). Additionally, in a rat model of MI, it was demonstrated that by 4 weeks post-surgery most of the viable cells in the infarct had been cleared. Only 9% of the scar was composed of myofibroblasts whereas 80% of the infarct was composed of collagen (Bogatyryov *et al.*, 2013). These studies together with my data suggest that the absence of SA- β -Gal staining at 4 weeks may be due to a reduction in β -galactosidase activity by this time-point, or simply resulting from a reduction in the total number of viable cell in the infarct.

Additionally, at 1 week post-IRI I observed the presence of SA- β -Gal positive CMs. Previous studies have reported on the ability of CMs to become senescent (Maejima *et al.*, 2008; Cai *et al.*, 2012; Anderson *et al.*, 2018; Cui *et al.*, 2018; Alam *et al.*, 2019b; Anderson *et al.*, 2019). For example, in a model of doxorubicin induced cardiomyopathy, it resulted in premature activation of senescence in CMs which may play a role in cardiac dysfunction (Maejima *et al.*, 2008). However, to date no other studies have demonstrated that IRI can potentially induce senescence in the CM population.

The above data clearly demonstrates that post-MI the process of senescence accumulation is a dynamic process during infarct formation and wound repair. This potentially raises two important considerations: 1) the levels of senescence that occurs

at early time-points may not reflect persistent senescence following injury; and 2) this also may suggest that any detrimental effects of senescence occur during this early phase of repair.

Given that senescence is dynamic I concentrated my subsequent analysis of senescent markers at the 4 weeks post-LAD ligation, which comprise persistently senescent cells. Considering the novelty of the above observations of senescent CMs, I continued my analysis of additional senescent markers p21^{Cip} and p16^{Ink4a} with a focus on the CMs population. Cardiomyocyte senescence was persistent at 4 weeks after LAD ligation and levels of p21^{Cip} and p16^{Ink4a} were comparable to the levels of TAF, supporting my use of ≥ 5 TAF as a marker of CM senescence, both within healthy hearts and ligated hearts at 4 weeks post-IRI.

An observation from these analyses was that interstitial cells appeared to not be positive for the marker p21^{Cip} at 4 weeks yet some were positive for p16^{Ink4a}. One explanation could be non-specific binding of the primary antibody against p16^{Ink4a} leading to false positive results. However, the antibody was applied in a blocking solution and levels of p16^{Ink4a} in the CMs were comparable to levels of p21^{Cip} in CMs. Also the antibody was verified on p16^{Ink4a} knockout tissue (chapter 5). Moreover, this histological data which suggests that more cell types express p16^{Ink4a} than p21^{Cip} is consistent with the qRT-PCR data demonstrating a larger increase in p16^{Ink4a} mRNA expression than p21^{Cip} following IRI.

Another explanation as to why the interstitial cells were only positive for p16^{Ink4a} may be that after several weeks after the initial insult, only those myofibroblasts that are under activation of p16^{Ink4a}-induced senescence are persistently present. Senescent myofibroblasts have been described to act in a self-limiting effect during wound repair (Demaria *et al.*, 2014). In the heart myofibroblasts have been shown to be resistant to apoptosis (Richardson *et al.*, 2015b) and can be identified in infarcts decades after MI (Blankestijn *et al.*, 2001). It has also been reported that cells initially exiting the cell cycle is due to p21^{Cip} expression, leading to a temporary state of senescence for DNA damage to be repaired, but if the damage persists, p16^{Ink4a} expression will result in sustained cell cycle arrest and permanent senescence (Childs *et al.*, 2014). It may well be that these apoptotic-resistant myofibroblasts are in a persistent senescent state via p16^{Ink4a} activation rather than p21^{Cip}.

Alternatively as it has been shown that senescence can occur due to activation of either the p16^{Ink4a} or p21^{Cip} pathways independently (Mirzayans *et al.*, 2012) and fibroblasts have been shown to be capable of obtaining the senescent phenotype in the absence of p21^{Cip} (Serrano 1999). Furthermore, different stimuli activate the different pathways. For example the p53/p21^{Cip} pathway is considered a genotoxic stress activated pathway, whereas the p16^{Ink4a}/Rb pathway stimulation predominantly occurs due to other cellular stressors, including those resulting from SASP (Zhu *et al.*, 2013). The difference in p21^{Cip} and p16^{Ink4a} expression in interstitial cells and CMs may reflect which pathways are responsible for driving senescence in each cell type as well as the stimuli acting on them. To confirm this hypothesis, additional studies are required to sequentially characterise senescence markers expression across all cardiac cell types specifically. Determination of this would benefit knowledge of cardiac repair mechanisms and how to modulate scar formation. This information would ensure that cardiac rupture is avoided yet the scar doesn't progress so far as to reduce cardiac function to the point of heart failure.

Regardless, this data provides strong evidence that following MI with IRI multiple cell populations, including CMs, obtain a senescent phenotype. Given the documented detrimental influence that senescent cells have on the function of other tissue systems, targeting these CMs for clearance may be of therapeutic benefit post-MI with IRI and requires further investigation. Therefore, clearing senescent cells after MI with IRI and measuring cardiac function would help ascertain if senescence is detrimental to recovery in the heart. If clearance is of benefit, then understanding which mechanisms are responsible for cardiac recovery would help identify potential therapeutic targets for IRI.

Chapter 4. Pharmacological clearance of senescence modulates ischaemia-reperfusion injury and cardiac remodelling

4.1 Introduction

Senescence accumulation and the associated SASP has been demonstrated to be detrimental to tissue function in a number of age related diseases of multiple organs including in the heart (Childs *et al.*, 2015; Anderson *et al.*, 2019). However, genetic and pharmacological clearance of senescent cells was shown to be highly favourable to recover cardiac function and mitigate remodelling in models of cardiac ageing with associated heart failure, atherosclerosis and MI (Zhu *et al.*, 2015; Childs *et al.*, 2018; Anderson *et al.*, 2019; Walaszczyk *et al.*, 2019). Additionally, pharmacological clearance of senescent cells using the senolytic navitoclax in aged mice reduced components of the SASP, attenuated remodelling and resulted in improving cardiac function as well as survival and recovery to myocardial infarct (Walaszczyk *et al.*, 2019). Senolytics exploit senescent cells overexpressing BCL-2 proteins, which serves as a protective, anti-apoptotic mechanism, but as such make senescent cells primed for apoptosis (Childs *et al.*, 2014).

Navitoclax is a small molecule inhibitor that targets the BCL-2 family of proteins. As a BH3 mimetic, navitoclax preferentially binds to BCL-2, BCL-X_L or BCL-W, releasing BH3, pro-apoptotic proteins. These proteins are then able to bind to and activate oligomerisation of BAX and BAK forming a pore within the outer mitochondrial membrane making it permeable and cytochrome c relocates into the cytoplasm. In the cytoplasm they create an apoptosome via binding to APAF-1 and caspase-9 triggering the caspase cascade and apoptosis, and senescent cells are removed in a targeted fashion (Kipps *et al.*, 2015; Montero and Letai, 2018). The drug navitoclax is orally-bioavailable and currently in Phase I and II clinical trials for the treatment of a range of cancers including acute lymphoblastic leukaemia, small-cell lung cancer and other solid tumours (Tse *et al.*, 2008; Wilson *et al.*, 2010).

Studies using navitoclax have been performed in models of ageing and disease not relating to cancer. These studies demonstrated navitoclax acts in a senolytic fashion on numerous BCL-2 family proteins, in both human and mouse models, across many

cell types *in vitro* and *in vivo* (Chang *et al.*, 2016; Zhu *et al.*, 2016; Walaszczyk *et al.*, 2019). Navitoclax induced apoptosis was confirmed in a cell line of human umbilical vein endothelial cells (HUVECs), human lung fibroblasts (IMR90s), mouse embryonic fibroblasts (MEFs) that had been induced to senescence (Zhu *et al.*, 2016), as well as human renal epithelial cells (Chang *et al.*, 2016) and *in vivo* senescent cells were cleared via apoptosis from the lungs, skeletal muscle, brain, liver and heart of the p16-3MR mouse (Chang *et al.*, 2016). In a model of aged mice, navitoclax significantly reduced markers of senescence and hypertrophy, and when given pre-emptively before permanent MI, EF was increased and survival rates were improved to that of a young mouse (Walaszczyk *et al.*, 2019).

Having demonstrated that IRI results in an accumulation of senescence post-IRI in chapter 3, and given the documented contribution of senescence and the SASP to dysfunction including the induction of myocardial remodelling (Shimizu and Minamino, 2019; Walaszczyk *et al.*, 2019) I hypothesised that the accumulation of senescence post-IRI contributes to ongoing myocardial remodelling, including CM hypertrophy and fibrosis, and ultimately impacts on cardiac function. As such targeting senescence may be a therapeutic strategy for patients post-MI with IRI who often progress to heart failure (Minicucci *et al.*, 2011; Torabi *et al.*, 2014). Therefore, I aimed to establish in this chapter if navitoclax treatment would reduce senescence post-IRI and investigate if this had any influence on recovery in terms of myocardial remodelling and cardiac function. (Figure 4.1).

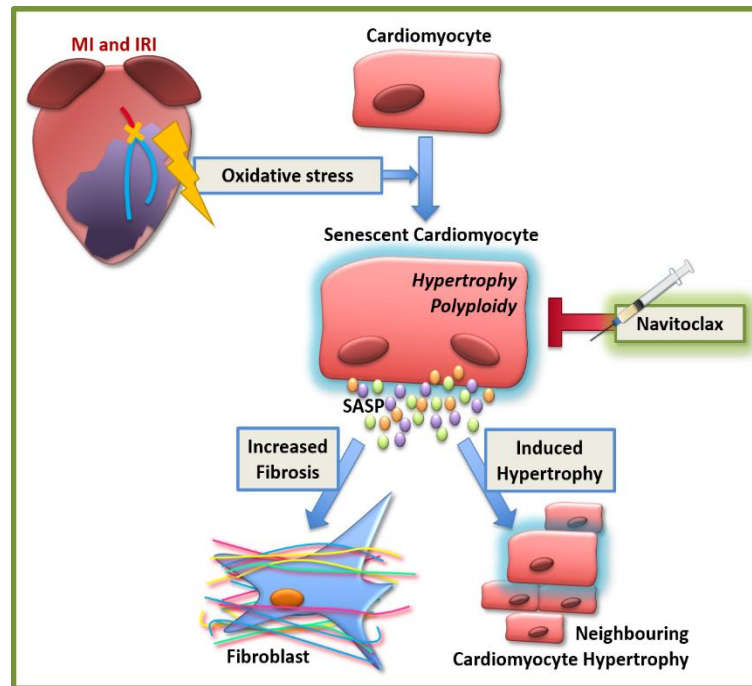


Figure 4.1 Graphical hypothesis.

Myocardial infarction and subsequent IRI initiate senescence in the heart, in particular CMs. Treatment with the senolytic navitoclax will clear senescent CMs and other cardiac cells to reduce CM hypertrophy, dysfunction, SASP generation and fibrosis all leading to attenuated remodelling and improved cardiac function.

4.2 Navitoclax treatment reduces viability of senescent but not proliferative cardiomyoblasts *in vitro*

Having demonstrated that following MI with IRI senescence was induced in the CM population, I first aimed to establish if navitoclax induced apoptosis in an established CM *in vitro* cell model, the H9C2 rat cardiomyoblast line (Branco et al., 2015).

Rat myoblasts (H9C2 line) were treated with 10Gy x-ray irradiation to induce senescence or were sham irradiated as a proliferative control. At 10 days post-irradiation, proliferative and irradiated cell cultures (n=3 for each experimental group) were then treated with increasing concentrations of navitoclax (0 μ M, 0.5 μ M, 1.0 μ M and 1.5 μ M) for 2 days.

Senescence was confirmed in a cohort of cells by staining with SA- β -Gal (Figure 4.2.A), and only irradiated H9C2s stained positively for SA- β -Gal (Figure 4.2.A.lower panels). Viability was assessed using the Tali Image-Based Cytometer to count viable cell numbers. Senescent H9C2 cardiomyoblasts demonstrated a dose dependent

decrease in viability, however, the viability of the proliferative H9C2 cultures remained unchanged ($p=0.0001$, <0.0001 and <0.0001 respectively, Figure 4.2.B). This datum suggests that navitoclax selectively promotes apoptosis in senescent CM-like-cells and has no detrimental effect on healthy, proliferative cells, and has been now published in Anderson, R. *et al* (Anderson *et al.*, 2019).

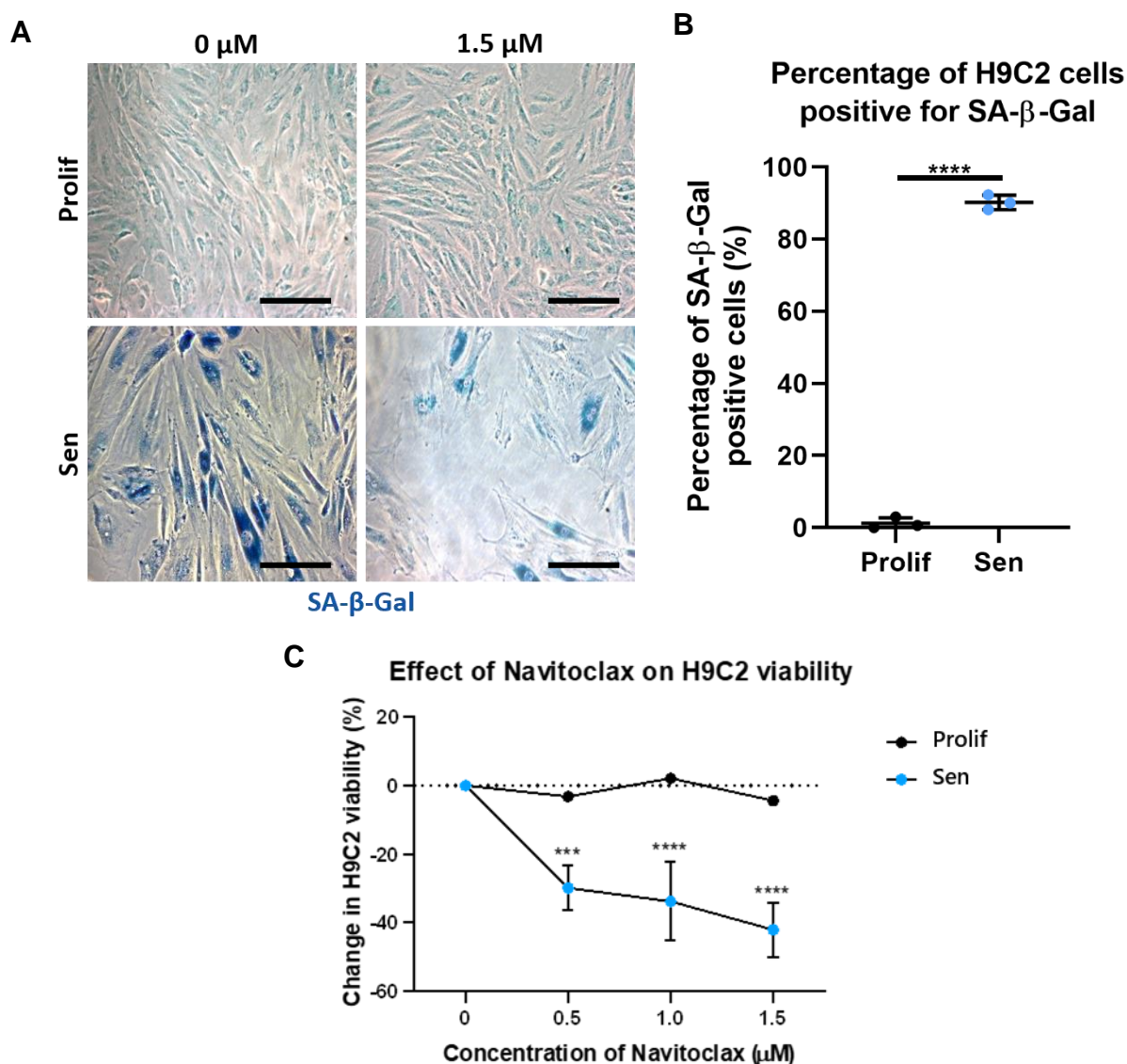


Figure 4.2 Treatment with navitoclax specifically reduces the viability of senescent (irradiated) H9C2 cultures that are positive for senescence-associated β -galactosidase. Navitoclax has no effect on the viability of healthy, proliferative (non-irradiated) H9C2s.

- A)** SA- β -Gal staining. Top row shows no positive staining or change in cell density in proliferative culture, both untreated and 1.5 μ M navitoclax treated. Bottom row shows positive staining in senescent culture and reduced cell density in culture treated with 1.5 μ M navitoclax. Scale bar equal to 50 μ m.
- B)** Percentage of proliferative and senescent MRC5s positive for SA- β -Gal.
- C)** H9C2 percentage viability is stable in proliferative group with all doses of navitoclax. Senescent H9C2 cultures show a dose dependent reduction in cell viability.

N=3 for each experimental condition. To control for ongoing proliferation and cell death as a result of irradiation, viability for each condition (proliferative or irradiated) was calculated relative to the number of cells in the untreated culture for that condition. NS \geq 0.05, * p <0.05, ** p <0.01, *** p <0.001, **** p <0.0001 using One-Way ANOVA. Data from Anderson, R et al. (Anderson et al., 2019).

4.3 *In vivo* model to investigate the effect of navitoclax on recovery post-ischaemia-reperfusion injury

It has previously been demonstrated that in the aged heart an accumulation of senescent CMs contributes to age related myocardial remodelling, possibly as a result of SASP inducing fibrosis and hypertrophy. In addition, treatment of aged mice with navitoclax reduced the number of senescent CMs, attenuated characteristics of age related remodelling and improved function and survival to permanent MI (Anderson *et al.*, 2019; Walaszczyk *et al.*, 2019).

Ischaemia-reperfusion injury can promote adverse myocardial remodelling (Kurian *et al.*, 2016), an accumulation of senescence has been shown to occur in multiple cell populations (Burton, 2009) and senescent cells are sensitive to navitoclax (Anderson *et al.*, 2019). I therefore aimed to establish if reactive navitoclax treatment would eliminate senescence post-IRI and to establish the effect of senescence elimination on recovery. Young, male C57BL/6 mice underwent LAD ligation, as outlined in 2.1, and then were allowed 72 hours to recover from surgery to initiate vital wound repair responses in the myocardium (Gough, 2015). On day 4 post-IRI mice were randomised and provided with either navitoclax (at 50mg/kg BW per day) or lipid only control (2.2) via oral gavage for 7 days. To allow retrospective analysis of DNA synthesis as an indication of cell turnover, mice were also provided with a 7 day dosing regimen of EdU (at 100µg/mg BW per day) starting at day 4. After this treatment period, mice were transferred and left for a further week to recover before MRI scanning began. The preliminary scan was performed at 3 weeks post-LAD ligation and a subsequent MRI scan 2 weeks after this, at week 5 post-surgery. Following the 5 week MRI scan, hearts were collected and processed accordingly for analysis (2.4, Figure 4.3).

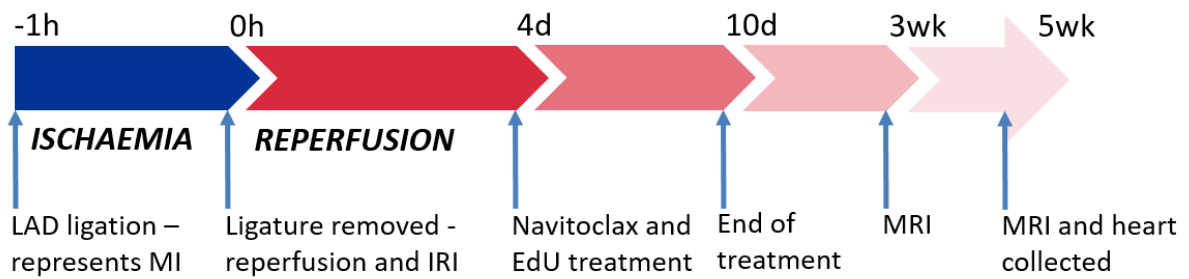


Figure 4.3 Experimental timeline.

The LAD was ligated for 1 hour and then the heart allowed to reperfuse. To ensure tissue repair mechanisms were initiated, mice were left to recover for 3 days and then on day 4 a 7 day daily dosing regimen of navitoclax (50mg/kg BW per day) and EdU (100µg/mg BW per day) was started. Mice were then transferred to the Keith Unit for MRIs at weeks 3 and 5 post-surgery.

4.4 Navitoclax treatment reduces senescence markers expression in cardiomyocytes

To ascertain if navitoclax treatment eliminated senescent cells following IRI *in vivo* I quantified several senescence markers in sections of vehicle control and navitoclax treated hearts by immunohistochemistry at 5 weeks post-IRI (4 weeks post-navitoclax treatment).

Initially I investigated whether the TAF positive CM population was lessened as a result of navitoclax dosing. After IRI, 14.22% ± 2.34 CMs were positive for ≥5 TAF, and navitoclax treatment significantly reduced levels to 6.41% ± 1.63 (p=0.003, Figure 4.4.C). The datum for the IRI cohort was slightly reduced in comparison to the IRI cohort in Figure 3.5 (17.71% ± 7.67), but not significantly so (p=0.3596). When assessing TAF number within CM nuclei, the mean number of TAF was significantly lowered (p=0.0124) from 4.18 ± 0.30 after IRI to 3.47 ± 0.40 following navitoclax treatment (Figure 4.4.D).

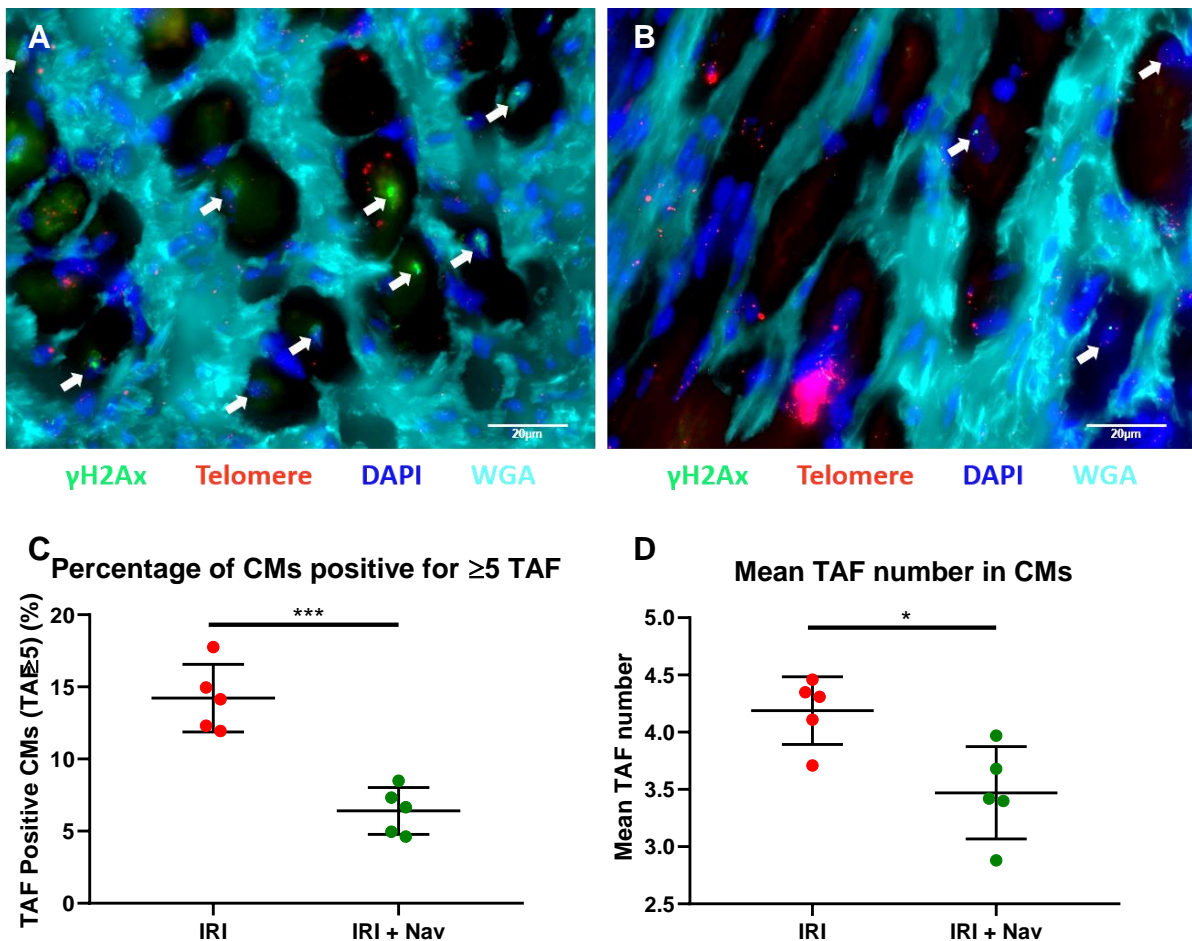


Figure 4.4 Navitoclax reduces the percentage of cardiomyocytes positive for telomere-associated DNA damage foci and mean foci number.

- A)** Immunofluorescence staining in heart post-IRI without navitoclax treatment. Slides stained with γ H2Ax (in green, wavelength 488nm), telomere-c probe (in red, wavelength 594nm), nuclei (in blue with DAPI, wavelength 461nm) and WGA (in teal, wavelength 647nm). All images for this analysis were taken in the BZ. Cardiomyocytes positive for TAF are highlighted with a white arrow.
- B)** Immunofluorescence staining in LAD ligated heart with navitoclax treatment. Slides stained with γ H2Ax (in green, wavelength 488nm), telomere-c probe (in red, wavelength 594nm), nuclei (in blue with DAPI, wavelength 461nm) and WGA (in teal, wavelength 647nm). All images for this analysis were taken in the BZ. Cardiomyocytes positive for TAF are highlighted with a white arrow.
- C)** Quantification of CMs expressing ≥ 5 TAF in IRI hearts vs IRI and navitoclax. Navitoclax treatment significantly reduced the percentage of CMs positive for TAF post-IRI.
- D)** Quantification of mean TAF number in CMs post-IRI and navitoclax. Navitoclax treatment significantly reduced the CM mean TAF number.

N=3 and 4 for each experimental condition. NS \geq 0.05, * p <0.05, ** p <0.01, *** p <0.001, **** p <0.0001 using Two-Tailed T-Test.

Overall senescence analysis based on SA- β -Gal staining demonstrated that although CMs positive for SA- β -Gal were observed within the BZ of hearts taken from the untreated cohort, these were not observed in navitoclax treated hearts (Figure 4.5). Staining for SA- β -Gal was observed in the interstitial cells and cells in the infarct in both experimental groups. Staining for SA- β -Gal was diffuse and variable in intensity throughout individual hearts making quantification difficult. Furthermore, it is difficult to use staining protocols such as SA- β -Gal for the accurate discrimination between different cell types. Therefore, a more detailed and quantified analysis using alternative markers of senescence and CMs was executed.

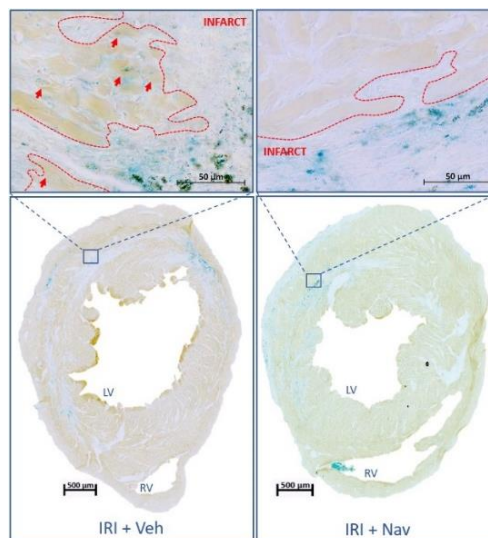


Figure 4.5 Senescence-associated β -galactosidase staining in the ischaemia-reperfusion injury model with and without navitoclax treatment.

SA- β -Gal activity could still be detected in areas within the infarct in both the untreated (IRI + Veh) and treated (IRI + Nav). Some CMs within the BZ were observed to be SA- β -Gal positive in the untreated cohort, however, the intensity of staining was highly reduced compared to sections stained at 1 week post-IRI (Figure 3.6).

4.4.1 Both $p21^{Cip}$ and $p16^{Ink4a}$ are significantly reduced following treatment with navitoclax

As described in chapter 3, multiple markers of senescence should be used to gain an accurate understanding of senescence activity. Based on previous data from aged mice that showed navitoclax eliminated senescence CMs (Walaszczyk et al., 2019) and the observations that navitoclax specifically eliminated cardiomyoblasts *in vitro* (Anderson et al., 2019), I quantified the relative numbers of cells expressing the CDK

inhibitors p21^{Cip} and p16^{Ink4a}, with a focus on the CM population in the three experimental groups.

As observed in the chapter 3, IRI resulted in increased expression of p21^{Cip} within the troponin C expressing CM population. With the percentage of troponin C expressing CMs increasing from 0.46% ± 0.56 in non-LAD ligated controls (data shown in Figure 3.9) to 20.00% ± 1.57 at 5 weeks following IRI ($p < 0.0001$, Figure 4.6.A-D), this frequency was consistent with the data presented in chapter 3 (Figure 4.6, 18.47% ± 2.62 of CMs).

Following navitoclax treatment, the percentage of troponin C CMs positive for p21^{Cip} significantly decreased when compared to the IRI group to 7.12% ± 0.94 ($p < 0.0001$, Figure 4.6.B/D) indicating an approximately 3-fold reduction in p21^{Cip} expressing CMs.

Quantification of p16^{Ink4a} expression revealed similar changes after navitoclax treatment to those observed for p21^{Cip}. Ischaemia-reperfusion injury as a result of LAD ligation significantly increased the percentage of p16^{Ink4a} expressing, troponin C positive CMs (24.56% ± 2.46, Figure 4.7.D) compared to non-LAD ligated controls (6.61% ± 2.16, $p < 0.0001$), again consistent to the p16^{Ink4a} data obtained in chapter 3. Treatment with navitoclax after IRI significantly reduced the percentage of CMs that were expressing p16^{Ink4a}, with a reduction to 12.95% ± 1.28 ($p = 0.0002$, Figure 4.7.D) representing a 1.90-fold decrease in p16^{Ink4a} expressing CMs. Taken together these data suggest that navitoclax following MI with IRI can eliminate senescent CMs, presumably as a result of the induction of apoptosis.

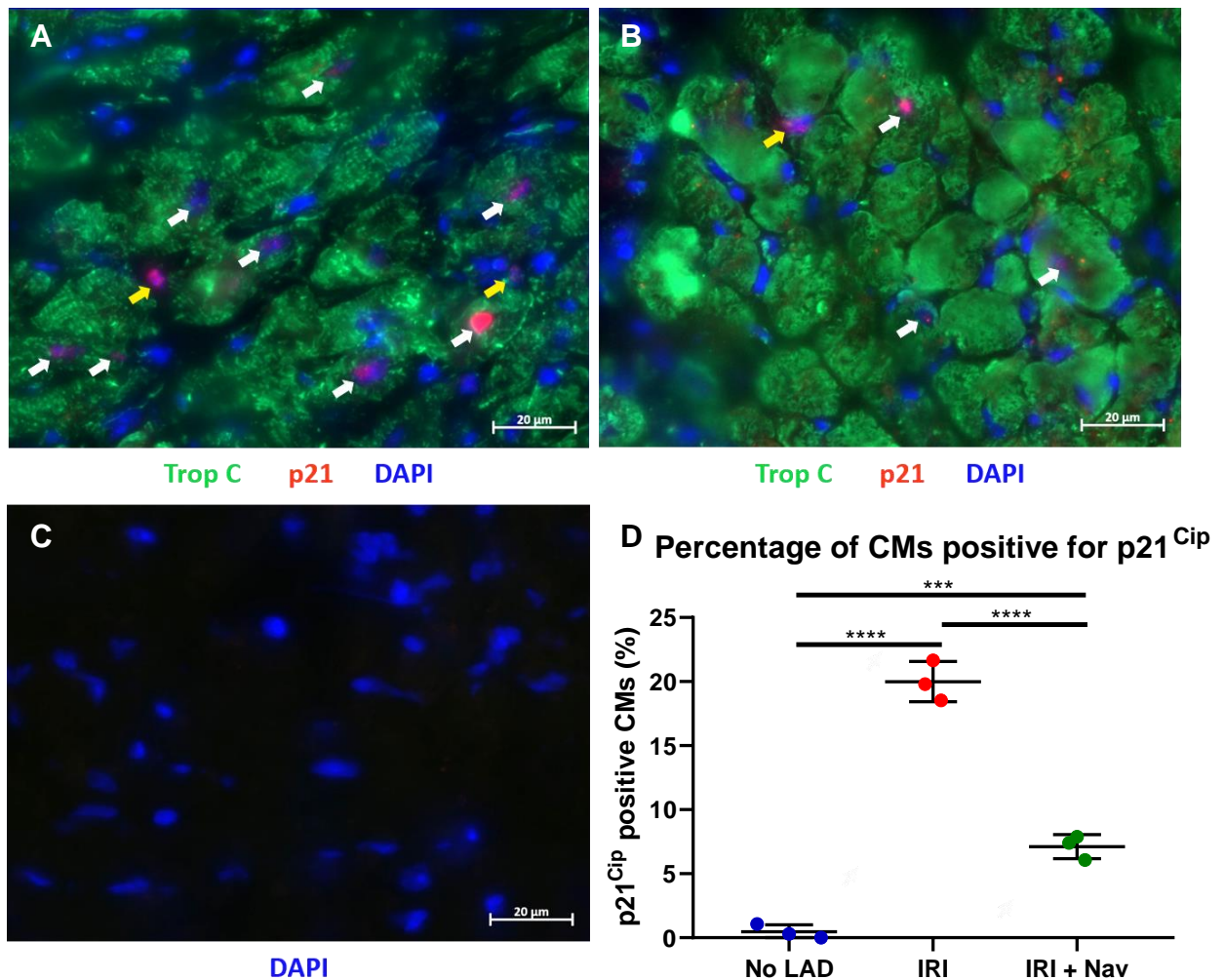


Figure 4.6 Navitoclax reduces percentage of cardiomyocytes positive for p21^{Cip} after ischaemia-reperfusion injury.

- A)** Immunofluorescence staining in hearts post-IRI without navitoclax treatment. Slides stained with CM marker troponin C (in green, wavelength 488nm), senescence marker p21^{Cip} (in red, wavelength 594nm) and nuclei (in blue with DAPI, wavelength 461nm). All images for this analysis were taken in the BZ. Cardiomyocytes positive for p21^{Cip} are highlighted with a white arrow. Interstitial cells positive for p21^{Cip} are highlighted with a yellow arrow.
- B)** Immunofluorescence staining in LAD ligated hearts with navitoclax treatment. Slides stained with CM marker troponin C (in green, wavelength 488nm), senescence marker p21^{Cip} (in red, wavelength 594nm) and nuclei (in blue with DAPI, wavelength 461nm). All images for this analysis were taken in the BZ. Cardiomyocytes positive for p21^{Cip} are highlighted with a white arrow. Interstitial cells positive for p21^{Cip} are highlighted with a yellow arrow.
- C)** Negative control for both 1^o Abs, slides were incubated in PBS instead.
- D)** Quantification of CMs expressing p21^{Cip} in no-LAD ctrl vs IRI hearts vs IRI and navitoclax. There was a significantly higher percentage of CMs positive for p21^{Cip} post-IRI than no-LAD ligated controls, however, navitoclax treatment significantly reduced the percentage of CMs positive for p21^{Cip} post-IRI.

N=3 and 4 for each experimental condition. NS≥0.05, *p<0.05, **p<0.01, ***p<0.001, ****p<0.0001 using One-way ANOVA.

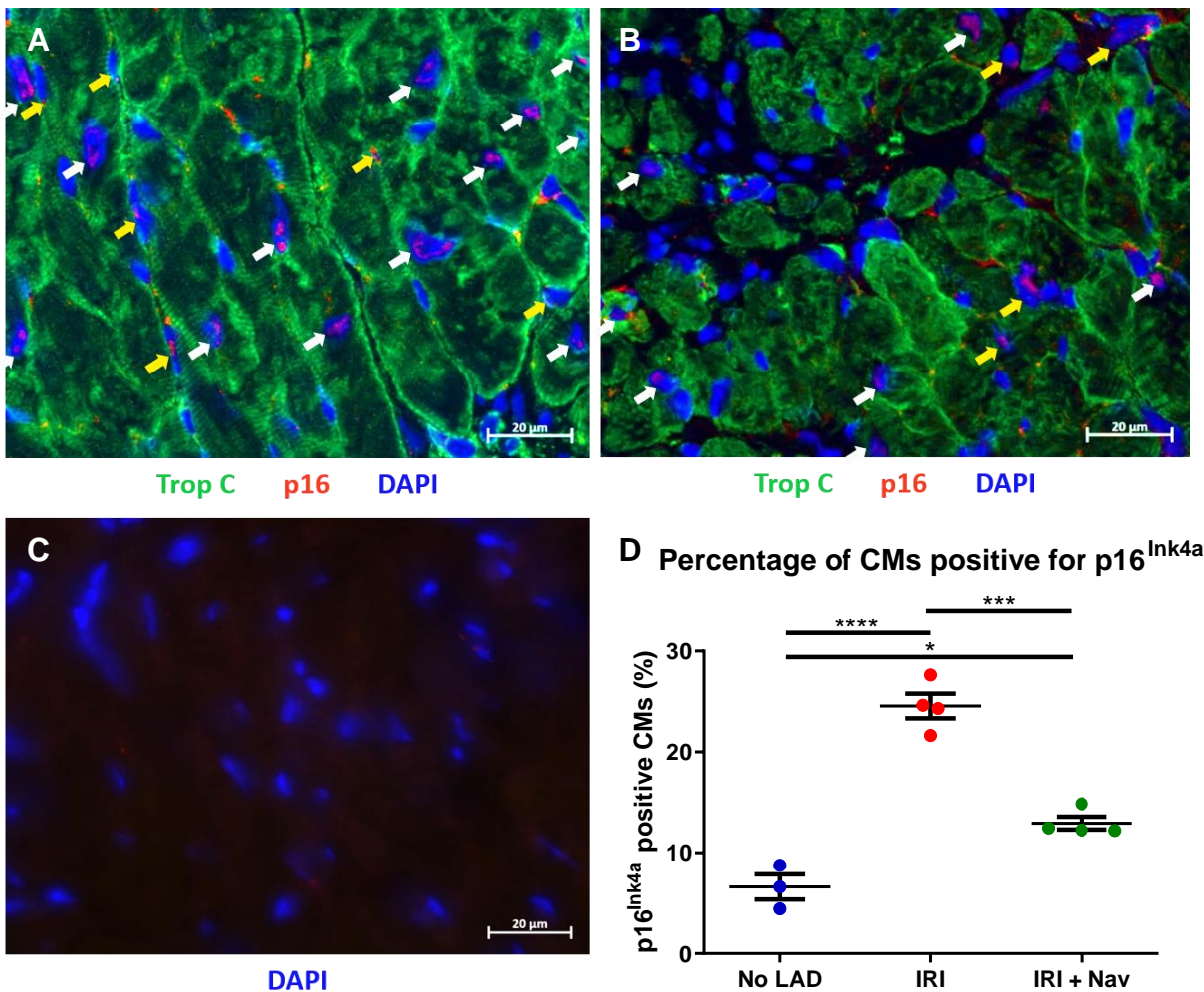


Figure 4.7 Cardiomyocytes positive for p16^{Ink4a} after ischaemia-reperfusion injury is reduced by navitoclax.

- A)** Immunofluorescence staining in hearts post-IRI without navitoclax treatment. Slides stained with CM marker troponin C (in green, wavelength 488nm), senescence marker p16^{Ink4a} (in red, wavelength 594nm) and nuclei (in blue with DAPI, wavelength 461nm). All images for this analysis were taken in the BZ. Cardiomyocytes positive for p16^{Ink4a} are highlighted with a white arrow. Interstitial cells positive for p16^{Ink4a} are highlighted with a yellow arrow.
- B)** Immunofluorescence staining in hearts post-IRI with navitoclax treatment. Slides stained with CM marker troponin C (in green, wavelength 488nm), senescence marker p16^{Ink4a} (in red, wavelength 594nm) and nuclei (in blue with DAPI, wavelength 461nm). All images for this analysis were taken in the BZ. Cardiomyocytes positive for p16^{Ink4a} are highlighted with a white arrow. Interstitial cells positive for p16^{Ink4a} are highlighted with a yellow arrow.
- C)** Negative control for both 1°Abs, slides were incubated in PBS instead.
- D)** Quantification of CMs expressing p16^{Ink4a} in no-LAD ctrl vs IRI hearts vs IRI and navitoclax. There was a significantly higher percentage of CMs positive for p16^{Ink4a} post-IRI than no-LAD ligated controls, however, navitoclax treatment significantly reduced the percentage of CMs positive for p16^{Ink4a} post-IRI.

N=3 and 4 for each experimental condition. NS≥0.05, *p<0.05, **p<0.01, ***p<0.001, ****p<0.0001 using One-way ANOVA.

4.5 Treatment with navitoclax improves functional outcome

To assess cardiac function, mice underwent MRIs at 3 and 5 weeks post-LAD, in a longitudinal study, allowing analysis of progressive changes in cardiac function and to investigate any effect of navitoclax treatment on multiple parameters of cardiac function. Specifically, LV mass, CO, EDV, ESV, SV and EF were analysed. These data were calculated from measuring the LV epicardial and endocardial areas of slices taken throughout the heart at diastole and systole (examples in Figure 4.8).

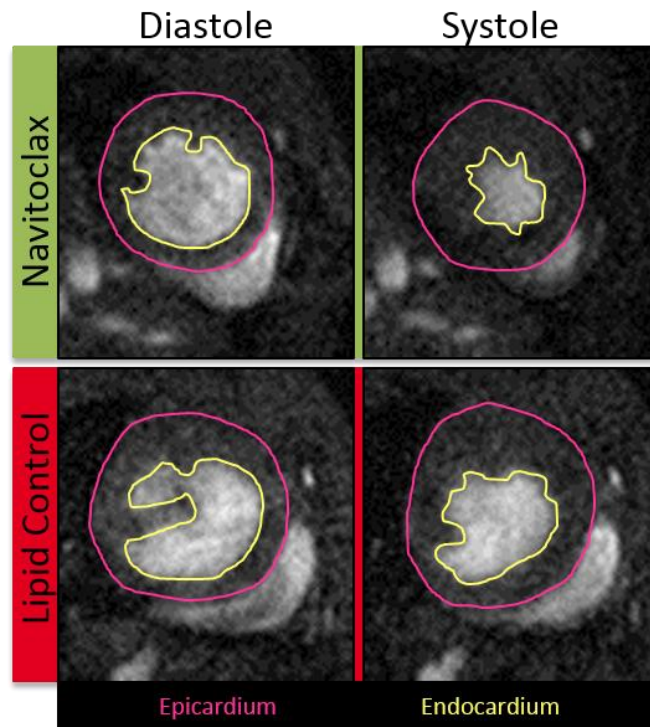


Figure 4.8 Example of measurements taken for each magnetic resonance imaging slice at diastole and systole from ischaemia-reperfusion injury (lipid control) and navitoclax treated mice.

Pink line denotes the epicardial area measured and the yellow line indicates the endocardial area of the LV measured for analysis.

Cohort data was compared to results obtained from an aged-matched group of controls who did not undergo LAD ligation.

4.5.1 Left ventricular mass is unchanged following ischaemia-reperfusion injury and is unaffected by navitoclax treatment

Initially LV mass was investigated. Increases in LV mass can be indicative of CM hypertrophy, myofibroblast proliferation and increased interstitial fibrosis which are characteristics of adverse remodelling of the LV (Konstam *et al.*, 2011). Adverse LV remodelling is observed in numerous patients following MI with reperfusion via PPCI and is a prognostic marker of declining clinical outcomes and onset of heart failure (Bulluck *et al.*, 2017).

Left ventricular mass was not significantly different in any experimental groups at either time-point including the no LAD control group ($p=0.9918$, Figure 4.9.A). The mean LV mass of the no LAD controls was $112.4\text{mg} \pm 7.75$. In the IRI cohort at 3 weeks and 5 weeks the LV mass was $114.5\text{mg} \pm 16.61$ and $111.6\text{mg} \pm 19.46$ respectively. In the navitoclax treated cohort LV mass was $111.4\text{mg} \pm 21.91$ and $110.9\text{mg} \pm 15.79$ at 3 and 5 weeks respectively.

To see if there was any change in LV mass in each individual heart I calculated the delta change in LV mass between 3 and 5 weeks. Similarly, no significant change in LV mass was observed in this paired analysis. ($p=0.7442$ and 0.7014 , Figure 4.9.B).

In summary, this data demonstrated in this model of IRI in young mice, myocardial mass is not altered post-LAD ligation and navitoclax has no effect on mass.

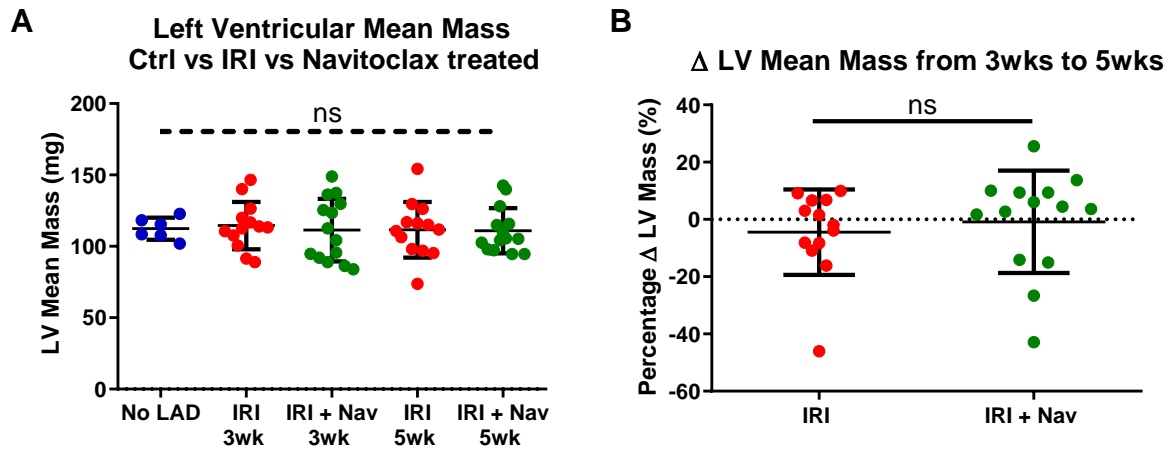


Figure 4.9 Left ventricular mass remains unchanged after ischaemia-reperfusion injury and navitoclax treatment.

- A)** Data shows non-significant change in LV mass was observed between healthy non-LAD ligated mice, IRI mice and IRI mice with navitoclax treatment. This indicated that in this cohort LV mass was not affected by IRI or navitoclax dosing.
- B)** Quantification of the change in LV mass between week 3 and 5 for both the IRI and navitoclax groups. Non-significant differences were observed between the two cohorts and between the mice within each cohort across the two time-points.

N=6, 13 and 14 for each experimental condition. NS \geq 0.05, * p <0.05, ** p <0.01, *** p <0.001, **** p <0.0001 using One-Way ANOVA, Unpaired and Paired T-Test.

4.5.2 Navitoclax treatment improves systolic but not diastolic function post-myocardial infarction

Increased EDV is used as a clinical indicator of LV remodelling post-STEMI. Patients demonstrating a $\geq 20\%$ increase in EDV, when compared to baseline, are diagnosed as having LV remodelling and are predicted to have a poorer prognosis, in terms of increased incidences of CV-related death or congestive heart failure (Sutton *et al.*, 1997; Bolognese *et al.*, 2002; Bulluck *et al.*, 2017; Rodriguez-Palomares *et al.*, 2019). Congestive heart failure is defined as a syndrome arising from any event that compromises the ventricles from filling or ejecting blood (Figueroa and Peters, 2006). End systolic function is also used to forecast survival and outcome post-MI, with an increase in ESV indicating an inability of the myocardium to contract efficiently and as such is also associated with a poorer prognosis (White *et al.*, 1987; Wu *et al.*, 2008; McManus *et al.*, 2009). Increases in EDV and ESV, resulting in congestive heart failure, can indicate enlargement of the LV cavity as well as cardiac remodelling (Redgrave *et al.*, 2016).

Following LAD ligation EDV was increased significantly from $61.29\mu\text{l} \pm 7.74$ in control animals, to $82.83\mu\text{l} \pm 21.98$ at 3 weeks post-IRI ($p=0.0341$) and remained increased at $85.01\mu\text{l} \pm 21.41$ at 5 weeks post-IRI ($p=0.0186$, Figure 4.10.A). These data also show that EDV does not progressively change between the MRIs at the times I investigated (Figure 4.10.B). Although marginally lower, navitoclax does not appear to have any impact on EDV as differences between the IRI groups were not significant. Similar to vehicle controls, no difference in mean EDV was observed between the week 3 ($71.35\mu\text{l} \pm 22.77$) and week 5 ($72.11\mu\text{l} \pm 21.02$) in the navitoclax treated animals (Figure 4.10). Calculation and analyses of the delta changes in EDV in individual mice between the experimental groups demonstrated there was no difference in change from 3 to 5 weeks between the experimental groups. Furthermore, from the data of individual mice in each cohort, neither experimental group showed a significant change in EDV between 3 and 5 week (Figure 4.10.B).

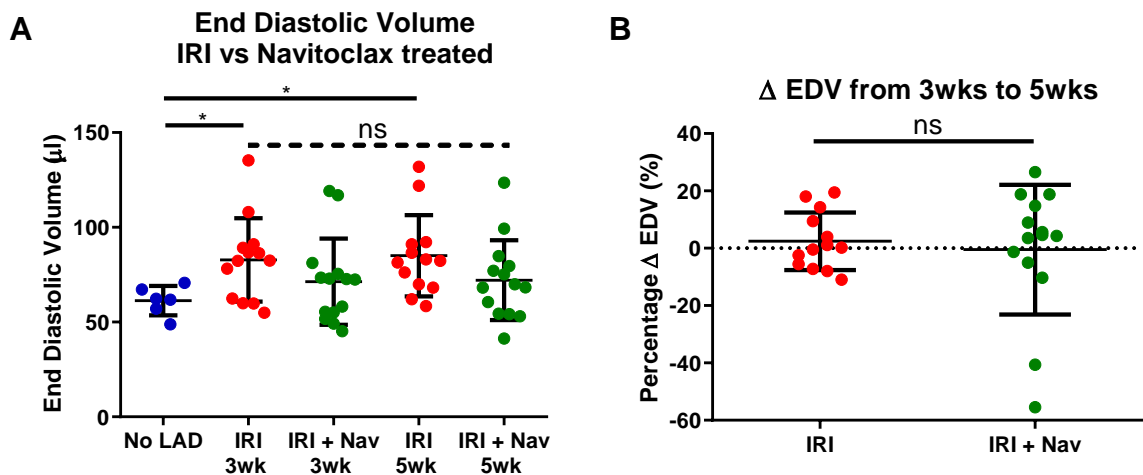


Figure 4.10 End diastolic volume increases after ischaemia-reperfusion injury but remains unchanged following navitoclax treatment.

- A)** Data showing EDV was significantly increased following IRI compared to healthy controls. However, non-significant changes were observed between healthy non-LAD ligated mice or IRI mice against IRI mice treated with navitoclax.
- B)** Quantification of the change in EDV between week 3 and 5 for both the IRI and navitoclax groups. Non-significant differences were observed between the two cohorts or between the mice across the two time-points, indicating that at the time-points investigated EDV remains stable and is unaffected by navitoclax treatment.

N=6, 13 and 14 for each experimental condition. NS \geq 0.05, * p <0.05, ** p <0.01, *** p <0.001, **** p <0.0001 using One-Way ANOVA, Unpaired and Paired T-Test.

End systolic volume was significantly increased from $12.84\mu\text{l} \pm 4.33$ in control mice at both 3 weeks post-LAD and 5 weeks post-LAD ($47.43\mu\text{l} \pm 23.64$ and $55.92\mu\text{l} \pm 20.47$ respectively, $p=0.0041$ and 0.0002). Navitoclax treated animals had a significantly larger ESV than uninjured controls at week 3 ($40.57\mu\text{l} \pm 16.94$ at 3 week, $p=0.0302$, and $36.32\mu\text{l} \pm 17.38$ at 5 weeks, $p=0.0931$), but navitoclax treated mice had a significantly smaller ESV than the LAD-ligated vehicle treated mice at 5 weeks ($p=0.0126$, Figure 4.11.A). In addition, there was a significant difference in the delta change in ESV from 3 to 5 weeks between the experimental groups. These significant changes were a function of both a significant increase in ESV in the vehicle animals ($17.44\% \pm 18.59$, $p=0.0040$) and a significant decrease in ESV ($-19.74\% \pm 30.92$, $p=0.0186$) over the 2 week period between MRI scans, as demonstrated by a paired analysis of the delta change in ESV of the individual mice of each group (Figure 4.11.B).

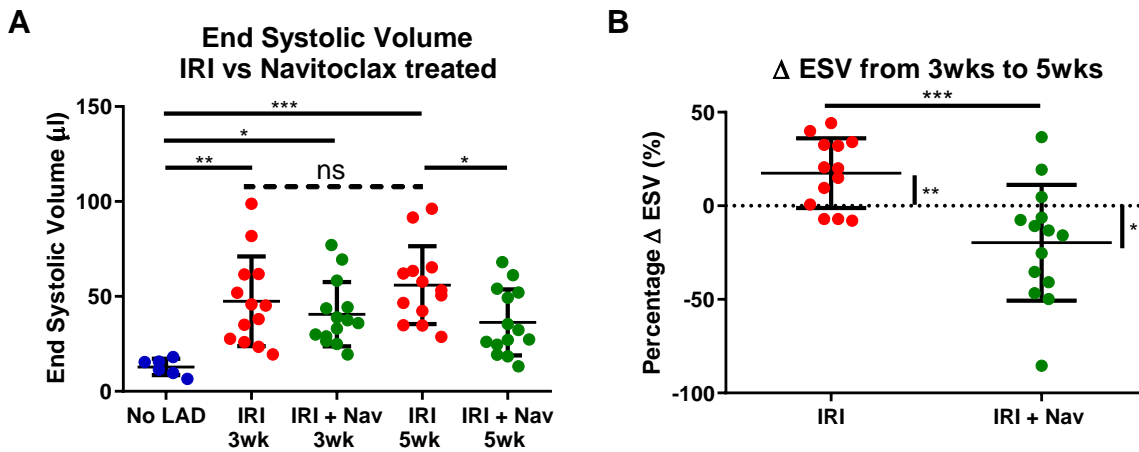


Figure 4.11 End systolic volume increases after ischaemia-reperfusion injury and continually increases from weeks 3 to 5. Navitoclax treatment is able to stabilise or reduce end systolic volume over this time frame.

- A)** Data showing ESV was significantly increased following IRI compared to healthy controls. ESV was also increased post-IRI with navitoclax dosing compared to the no LAD controls at the initial time-point analysed (3 weeks). Non-significant differences were observed between the IRI group data and against the navitoclax cohort at week 3. At week 5 there was a significant difference between the two groups.
- B)** Quantification of the change in ESV between week 3 and 5 for both the IRI and navitoclax groups revealed that the ESV was increasing in the IRI group with time. Significantly, the navitoclax cohort demonstrated a conflicting trend, where most mice either maintained or significantly reduced their ESV over the 2 weeks between MRIs.

N=6, 13 and 14 for each experimental condition. NS \geq 0.05, *p<0.05, **p<0.01, ***p<0.001, ****p<0.0001 using One-Way ANOVA, Unpaired and Paired T-Test.

4.5.3 Navitoclax significantly increased stroke volume.

Another variable assessed was SV. This is closely related to EDV and ESV, as it denotes the volume of blood ejected from the heart with each contraction, as calculated by EDV minus ESV (Redgrave *et al.*, 2016).

All groups that were subjected to IRI had a significantly reduced SV in comparison to the non-ligated control cohort at $48.45\mu\text{l} \pm 3.83$ ($p=0.0063$). This is consistent with the clinical situation where patients display a lowered SV as a result of less efficient contractions, which has been shown to be a result of scar formation and increased myocardial stiffness (Richardson *et al.*, 2015b).

A significant difference in the mean stroke volume was observed between the vehicle treated ($35.39\mu\text{l} \pm 6.15$ to $29.09\mu\text{l} \pm 6.83$, $p=0.0210$) but not the navitoclax treated animals ($p=0.2369$, Figure 4.12.A). In the navitoclax group there was a trend towards an increase in SV between the 3 and 5 week time-point ($30.78\mu\text{l} \pm 10.96$ to $35.79\mu\text{l} \pm 10.93$, $p=0.0704$, Figure 4.12.A). Consistent with the reduction in ESV between 3 and 5 weeks post-IRI in the navitoclax treated animals, comparisons of the delta change in SV also demonstrated a significant difference between the experimental groups ($-15.77\% \pm 22.47$ in the vehicle vs $16.17\% \pm 38.75$ following navitoclax, $p=0.0080$, Figure 4.12.B). These data were again a function of both a significant decrease in SV in the vehicle group ($p=0.0216$) and the significant increase in SV in the navitoclax animals ($p=0.0090$, Figure 4.12.B).

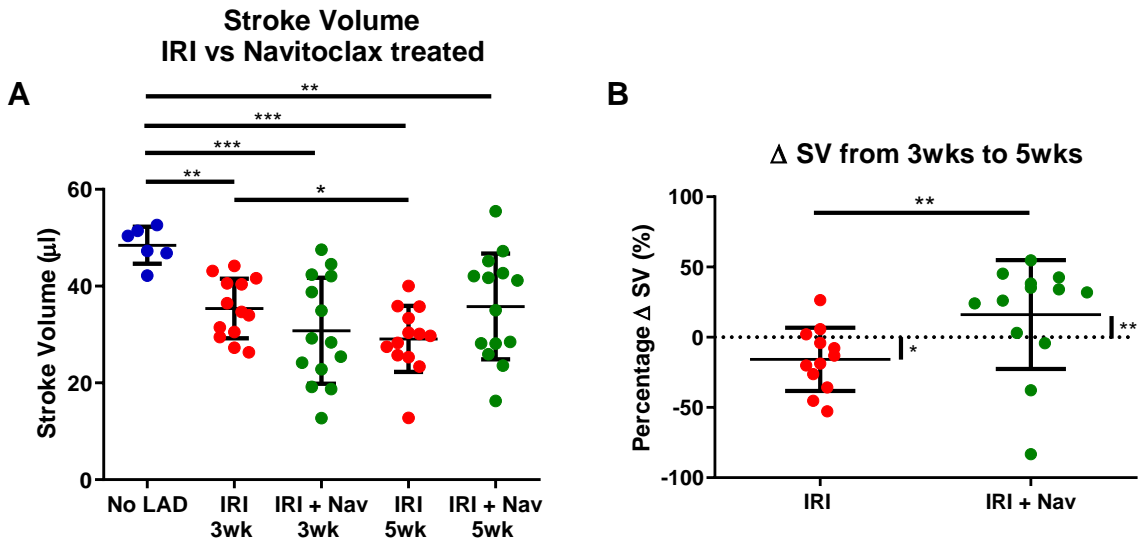


Figure 4.12 Stroke volume continuously declines after ischaemia-reperfusion injury, however, navitoclax treatment is able to partially recover stroke volume.

A) Data showing SV was significantly reduced following IRI compared to healthy controls, and continued to significantly decline between weeks 3 and 5. Navitoclax treatment had no significant effect on raw SV values.

B) Quantification of the significant change in SV between week 3 and 5 for both the IRI and navitoclax groups. On average the IRI cohort showed a significant trend for a decreasing SV, whereas navitoclax treatment improved the SV of the cohort.

N=6, 13 and 14 for each experimental condition. NS \geq 0.05, * p <0.05, ** p <0.01, *** p <0.001, **** p <0.0001 using One-Way ANOVA, Unpaired and Paired T-Test.

4.5.4 Navitoclax treatment after ischaemia-reperfusion injury significantly increased cardiac output

In direct relation to SV is CO that demonstrated a similar profile, and describes the volume of blood ejected by the LV per minute (Borzage *et al.*, 2017).

Cardiac output was significantly reduced in all groups following IRI, and was significantly higher in the navitoclax mice than vehicle controls at 5 but not 3 weeks ($p= 0.0226$, Figure 4.13.A). As CO is calculated from multiplying SV and heart rate, this difference in CO at 5 weeks may be due to differences in heart rate. The heart rates were not significantly changed between the healthy control cohort at $467.00\text{bpm} \pm 31.62$ and all mice after IRI, both with and without navitoclax and at both time-points. In the IRI only group, the average heart rates were $432.10\text{bpm} \pm 70.78$ at week 3 and slightly lower at $417.10\text{bpm} \pm 112.10$ at week 5. In the navitoclax group at week 3 the average heart rate was $445.00\text{bpm} \pm 70.79$ which was marginally faster at week 5 with an average heart rate of $470.30\text{bpm} \pm 108.6$ (Figure 4.13.C). Although non-significant, these marginal changes could have considerable effects on CO overall.

Analysis of the change in CO between 3 and 5 weeks post-IRI also showed similar results to the SV data with a significant difference in the mean change in CO being observed between the experimental groups ($p=0.0356$). However, this appeared to be primarily as a result of a decrease in CO in the vehicle cohort ($p=0.0015$) as no significant change in CO was observed in the navitoclax treated animals ($p=0.1766$, Figure 4.13.B). Overall, IRI had a highly detrimental impact on CO which progressively declined even over 2 weeks, whereas navitoclax prevented the decline in CO due to IRI from continually progressing.

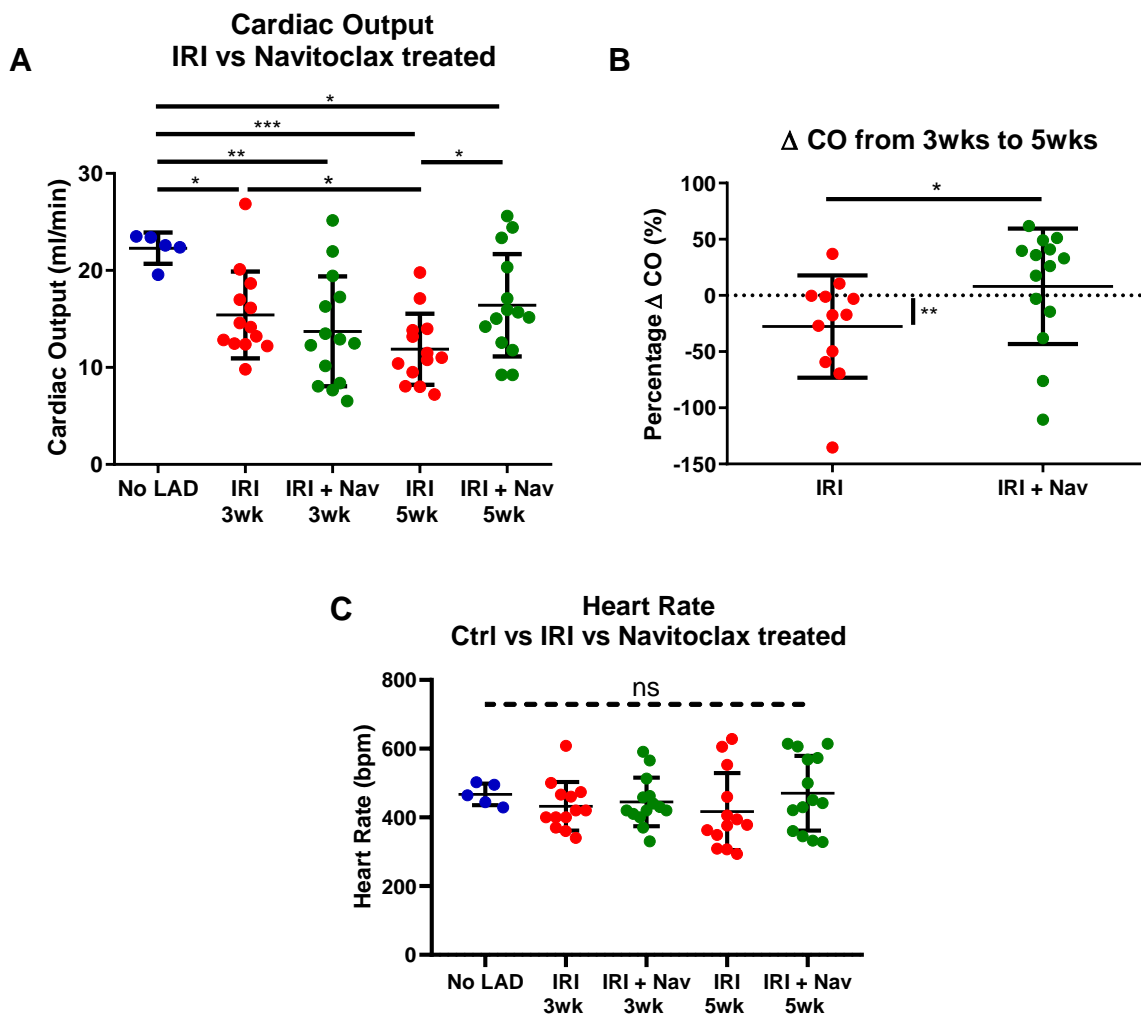


Figure 4.13 Cardiac output continuously declines after ischaemia-reperfusion injury, however, navitoclax treatment is able to maintain cardiac output and prevent this observed continuous decline.

- A)** Data showing CO was significantly reduced following IRI compared to healthy controls, and continued to significantly decline between weeks 3 and 5. Navitoclax treatment significantly rescued CO by 5 weeks post-IRI.
- B)** Quantification of the significant change in CO between week 3 and 5 for both the IRI and navitoclax groups. On average the IRI cohort showed a significant trend for a decreasing CO, whereas navitoclax treatment maintained a steady CO.
- C)** Graph showing the heart rate between no LAD and IRI with and without navitoclax at weeks 3 and 5 is unchanged, although is slightly higher in the navitoclax cohort at 5 weeks compared to IRI alone.

N=6, 13 and 14 for each experimental condition. NS \geq 0.05, * p <0.05, ** p <0.01, *** p <0.001, **** p <0.0001 using One-Way ANOVA, Unpaired and Paired T-Test.

4.5.5 Navitoclax treatment following ischaemia-reperfusion injury improves ejection fraction.

The final variable assessed by MRI was EF which is used clinically to classify systolic dysfunction (Ponikowski *et al.*, 2016).

In all groups subjected to LAD ligation EF was significantly reduced ($p=0.0001$, Figure 4.14.A), similar to SV and CO (Figure 4.12-Figure 4.13). In the uninjured control cohort, the mean EF was $79.52\% \pm 4.86$. At 3 weeks post-IRI there was a non-significant difference in the EF of the vehicle control ($44.87\% \pm 14.16$) and navitoclax ($42.67\% \pm 11.75$) groups suggesting there were no differences in the initial infarct in the two experimental groups. However, the mean EF of the navitoclax cohort was significantly higher than vehicle controls at 5 weeks ($53.47\% \pm 12.53$ vs $37.15\% \pm 9.27$; $p=0.0013$, Figure 4.14.A).

I next calculated the delta change in EF in the individual mice and identified a difference in the mean delta change from 3 to 5 weeks between the experimental groups. This difference was as a result of a significant increase in EF in the navitoclax group (mean change in EF $18.30\% \pm 19.41$, $p=0.0026$) and a significant reduction in EF in the vehicle control animals (mean change in EF $-20.34\% \pm 24.63$, $p=0.0047$). Specifically, in the IRI group, only three mice were able to demonstrate an improvement in their EF, with the greatest recovery being 10.21%. Conversely in the navitoclax group, only two mice demonstrated a reduction in their EF, one at 17.94% and the other at 1.19% (Figure 4.14.B).

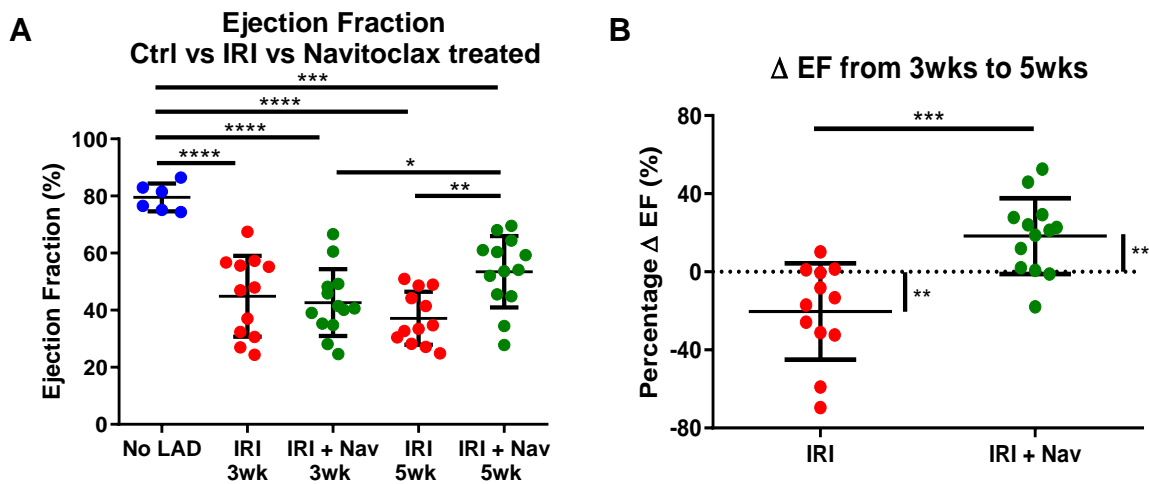


Figure 4.14 Ejection fraction continuously declines after ischaemia-reperfusion injury, however, ejection fraction is stabilised or improved following navitoclax treatment.

- A)** Data showing EF was significantly reduced following IRI compared to healthy controls. Navitoclax treatment significantly rescued EF by 5 weeks post-IRI both compared to the week 3 data and to IRI cohort at 5 weeks.
- B)** Quantification of the significant change in EF between week 3 and 5 for both the IRI and navitoclax groups. On average the IRI cohort showed a significant trend for a decreasing EF, whereas navitoclax treatment significantly increased EF.

N=6, 13 and 14 for each experimental condition. NS \geq 0.05, *p<0.05, **p<0.01, ***p<0.001, ****p<0.0001 using One-Way ANOVA, Unpaired and Paired T-Test.

4.6 Navitoclax treatment post-ischaemia-reperfusion injury reduces infarct size but has no effect on cardiomyocyte hypertrophy

In aged mice navitoclax has been previously shown to improve age-related cardiac dysfunction by attenuating remodelling, specifically via attenuating CM hypertrophy and reducing fibrosis (Walaszczyk *et al.*, 2019). To ascertain if the improved systolic function following IRI was also due to attenuated remodelling, next infarct size and hypertrophy were analysed using histological techniques. An infarct results from detrimental alterations to the myocardium and excessive CM death. As such a larger infarct directly reduces cardiac function and the degree of scarring is the strongest predictor of function including EF subsequent to MI (Orn *et al.*, 2007).

To assess infarct size, heart sections were stained as per the Masson's Trichrome protocol (Takagawa *et al.*, 2007) outlined in 2.5.5 and infarct region was defined as the area of collagen staining as a percentage of total LV area. As expected no region of collagen staining was observed in the non-LAD ligated controls. In the navitoclax treated cohort scar size was significantly smaller ($p=0.0003$) than that of the vehicle controls, as a reduction from $18.50\% \pm 2.72$ to $12.47\% \pm 1.68$, suggesting that clearance of senescent cardiac cells is beneficial to attenuate fibrosis and adverse remodelling (Figure 4.15).

Cardiomyocyte hypertrophy is characteristic of the adaptive and ultimately maladaptive remodelling and occurs when the workload on the heart is increased. After MI, changes to CM area are due to strains on the heart from elevated pressure or volume and are as such termed "pathological" hypertrophy (Kehat and Molkentin, 2010; Grossman and Paulus, 2013; Shimizu and Minamino, 2016).

To establish if, as in an aged heart, elimination of senescent CMs post-IRI resulted in attenuated hypertrophy, hearts were labelled with WGA and CM cross sectional area measured as previously described (Walaszczyk *et al.*, 2019). In healthy controls, the mean area of CMs was $305.6\mu\text{m}^2 \pm 33.43$. After IRI this was significantly increased to $412.6\mu\text{m}^2 \pm 24.29$ ($p=0.0034$), and was marginally but not significantly reduced to $394.9\mu\text{m}^2 \pm 39.52$ following navitoclax treatment ($p=0.7358$, Figure 4.16).

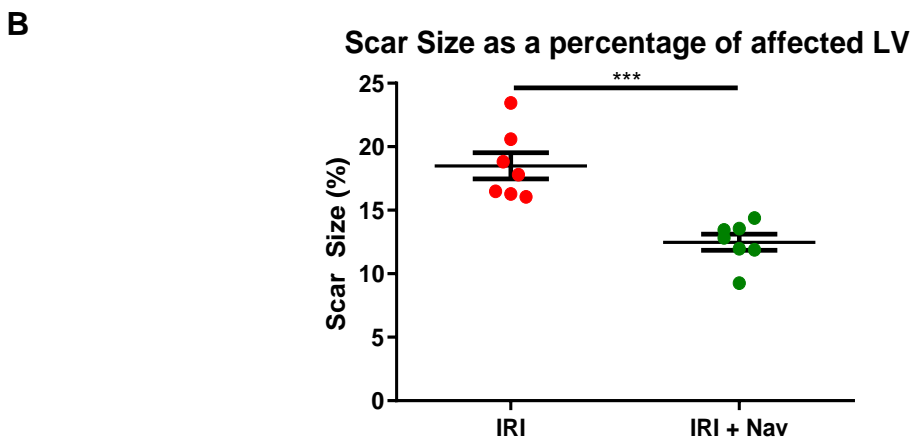
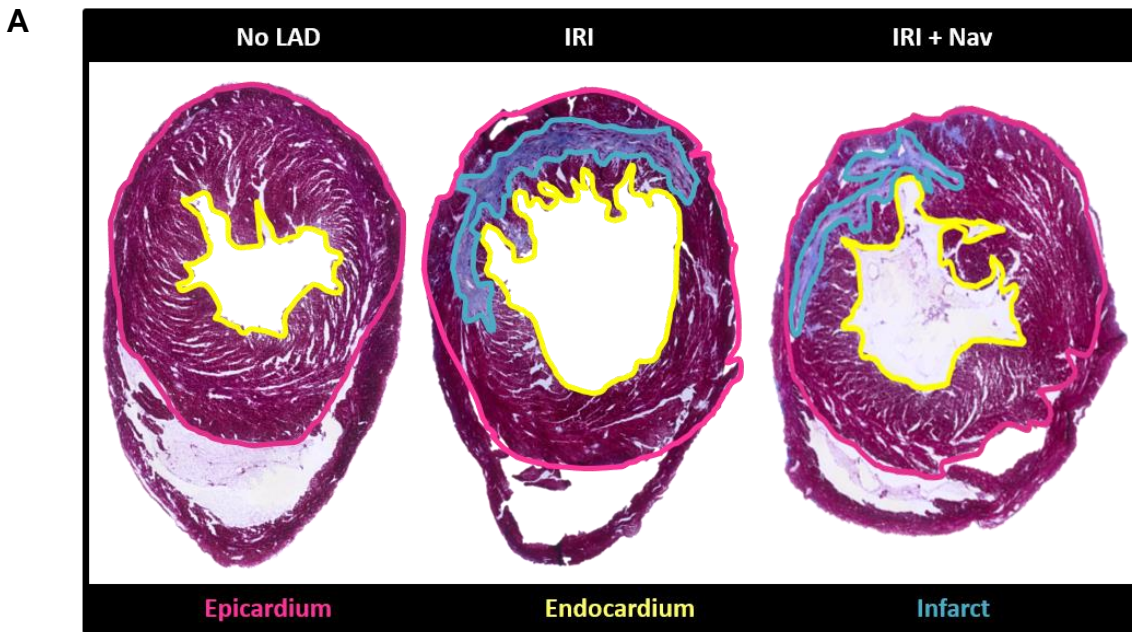


Figure 4.15 Navitoclax significantly reduces scar size within the left ventricle.

A) Tiles of transverse sections of hearts from healthy non-ligated control, LAD-ligated untreated and LAD-ligated navitoclax treated mice stained by Masson's Trichrome. The pink line highlights the LV epicardium and the yellow line highlights the LV endocardium. From these two measurements the LV area could be calculated. The blue line denotes the area of fibrosis in the LV as identified by the blue staining. From this, the percentage area of the LV composed of scar could be calculated. The non-LAD controls had no fibrosis detected, whereas all mice that had undergone LAD ligation (IRI and IRI + Nav) presented with an infarct.

B) Scar size as a percentage of the LV was calculated and found to be significantly decreased in the navitoclax treated cohort.

N=7 for each experimental condition. NS \geq 0.05, * p <0.05, ** p <0.01, *** p <0.001, **** p <0.0001 using Unpaired T-Test.

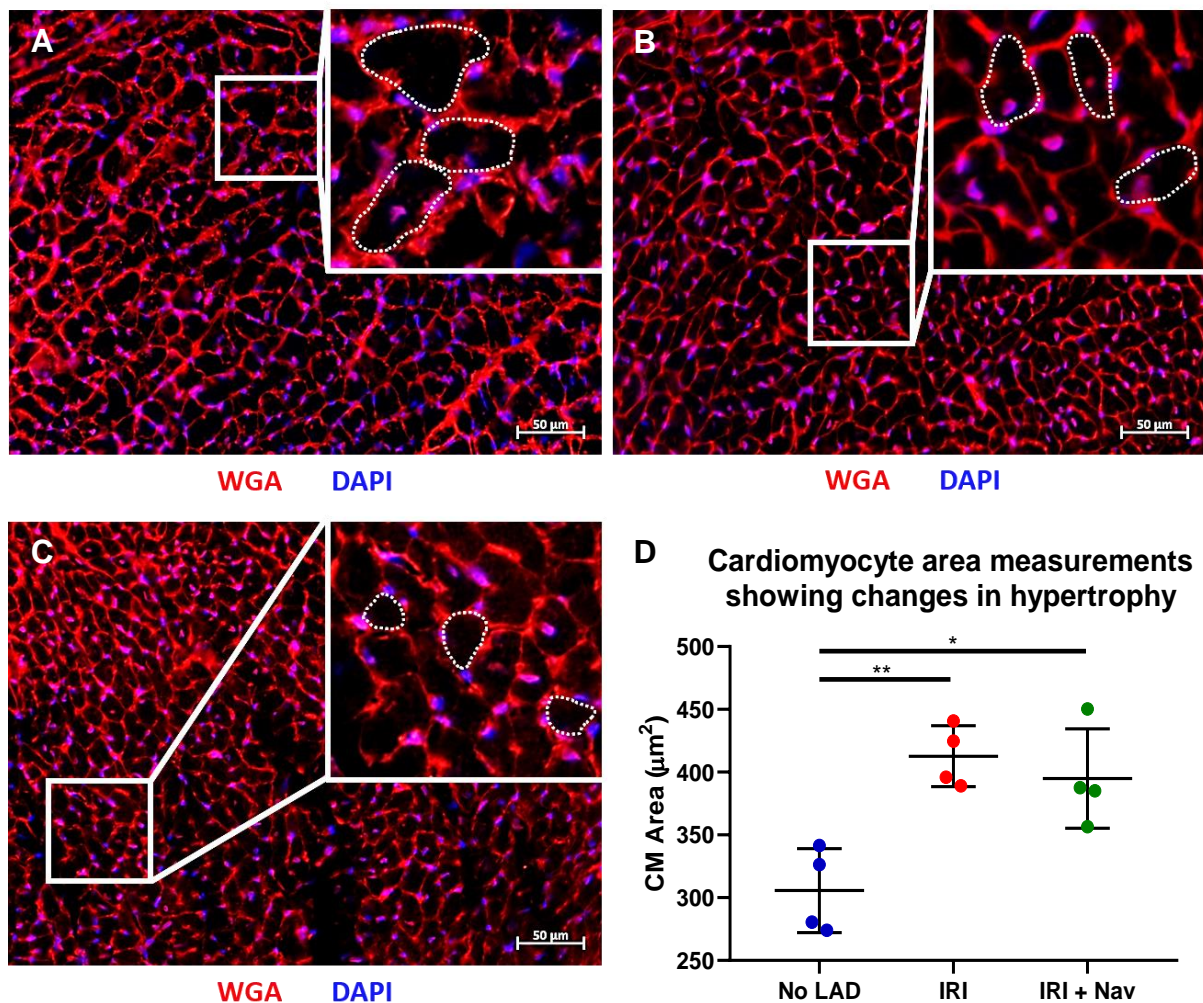


Figure 4.16 Ischaemia-reperfusion injury leads to significant changes in hypertrophy of the cardiomyocytes. Navitoclax slightly reduces hypertrophy, but insignificantly, compared to the ischaemia-reperfusion injury cohort.

A) WGA staining (red, 594nm) in heart after IRI, zoom figure shows measurements taken around CMs surrounded with 3+ capillaries so CMs in same orientation.

B) WGA staining (red, 594nm) in heart after IRI with navitoclax, zoom figure shows measurements taken around CMs surrounded with 3+ capillaries so CMs in same orientation.

C) WGA staining (red, 594nm) in heart with no LAD, zoom figure shows measurements taken around CMs surrounded with 3+ capillaries so CMs in same orientation.

D) Graph shows CM hypertrophy occurs due to IRI as CM area significantly increases. In the navitoclax cohort, the mean CM area is lowered slightly but is insignificant.

N=4 for each experimental condition. NS≥0.05, *p<0.05, **p<0.01, ***p<0.001, ****p<0.0001 using One-Way ANOVA.

4.7 Discussion

Mortality events after MI have reduced over the last few decades, yet MI still remains a major public health problem as IRI can result in heart failure (Lønborg, 2015). Indeed the number of patients suffering from heart failure has increased over the last 5 years (Conrad *et al.*, 2018). As such, there is considerable effect directed toward managing this problem.

In chapter 3 I demonstrated that IRI induces senescence, and given the documented association between senescence and tissue dysfunction including cardiomyopathy (Valiente-Alandi *et al.*, 2015), this raises the possibility that senescence may be a therapeutic target post-IRI. Previous studies from my lab have consistently shown that navitoclax in a range of *in vivo* and *in vitro* models clears senescence (Anderson *et al.*, 2019; Walaszczyk *et al.*, 2019), and therefore I used it for this study. Initially I confirmed that several senescence markers, including TAF, SA- β -Gal, p21^{Cip} and p16^{Ink4a} were reduced in the heart following navitoclax treatment.

For a treatment for IRI to be effective it is important that it has a positive impact on cardiac function, and so therefore I first looked to investigate whether navitoclax post-IRI would improve cardiac function. In depth analysis of the functional capacity of mice after IRI and IRI with navitoclax dosing led to some interesting and promising conclusions. Cardiovascular MRI is used clinically as an accurate and reproducible method for assessing LV measurements to determine cardiac function, LV remodelling and predict patient outcome (Bulluck *et al.*, 2017).

Ejection fraction is a clinically relevant variable when assessing cardiac function and is used to characterise systolic heart failure. In healthy humans, EF is reported between 50-70% (Rahmayani *et al.*, 2018; Kosaraju and Makaryus, 2019) and patients are diagnosed as having heart failure if their EF falls below 40%. Current European Society of Cardiology guidelines (Ponikowski *et al.*, 2016) state an EF of less than 40% is defined as systolic heart failure with reduced EF, and an EF equal to or greater than 50% is considered as normal and within healthy range and referred to as heart failure with preserved EF. An EF of 40-49% has traditionally been a “grey area” where patients are not considered as being in heart failure but at increased risk of many co-morbidities, and are now termed as heart failure mid-range EF (Ponikowski *et al.*, 2016).

In this study EF was considerably lowered after IRI in both the treated and untreated groups and at 3 weeks navitoclax had a marginal impact on EF compared to vehicle. Mice that received IRI with no treatment had a diminishing EF measurements between weeks 3 and 5. This indicates a detrimental shift towards worsening heart failure. Conversely, navitoclax treated animals showed a significantly improved EF over the same period. If this trend for a rescued EF continued or was sustained after 5 weeks, it potentially could prevent patients after MI progressing into heart failure and drastically improve morbidity and mortality post-MI.

In terms of developing murine models of heart failure with reduced EF, many models including the model used in this study are accepted as recapitulating the human disease, but there are many associated limitations. For example the baseline EF of young mice is around 66-80% (Stegger *et al.*, 2009; Schiattarella *et al.*, 2019), which is considerably higher than a healthy human. This discrepancy limits the comparison that can be made between raw values of cardiac function of mice and humans. Although the progression of disease and trends make this LAD ligation model suitable as a model of MI (Salto-Tellez *et al.*, 2004).

The improvement in EF observed in the navitoclax treated mice could be as a result of either recovered EDV, ESV or a combination of both. In other MI studies conducted with mice, EDV and ESV were increased post-MI (Shioura *et al.*, 2008; Redgrave *et al.*, 2016), with ESV reported as a strong marker to forecast adverse remodelling in mice (reflected in a progressively larger EDV (Redgrave *et al.*, 2016)) and survival after STEMI in patients (White *et al.*, 1987; Hassell *et al.*, 2017). In patients with heart failure, symptoms and mortality events were moderated correlating to interventions that reduced ESV (Cleland *et al.*, 2005).

Analysis of both EDV and ESV following IRI in both navitoclax treated and untreated animals led to an increase in EDV corresponding to dilation of the LV lumen and an increase in ESV due to an impairment of contractile ability. Examination of EDV showed no changes between 3 and 5 weeks in both cohorts whereas ESV significantly increased between 3 and 5 weeks in untreated mice indicating a progressive decline in systolic function. These trends in patients are associated with poorer outcomes including increased risk of heart failure and mortality (McManus *et al.*, 2009). In contrast, navitoclax treated mice demonstrated a significant reduction in ESV indicating an improved systolic function. It would be of interest to investigate the

progression of ESV over an extended longitudinal study to confirm whether or not ESV continually increases after IRI and if navitoclax can attenuate this to be of functional benefit. Together this data shows that the overall improvement in EF was in the most part due to navitoclax treatment rescuing systolic function.

The ability of navitoclax to reverse this trend for progressive systolic dysfunction advocates its use to improve or preserve cardiac function. Evidence supporting the use of navitoclax as a pharmacological intervention to improve cardiac function post-IRI was also the improvements observed in SV. This result was expected, as it quantifies the volume of blood ejected between EDV and ESV. As EDV was sustained in this cohort and ESV was lowered after navitoclax, it would result in a larger SV. Besides ESV, SV is also directly related to CO. As HR was unchanged between the IRI and navitoclax groups, the trends in CO mirrored those in SV. This supports the findings of the study by Janssen *et al* that showed a lowered CO in mice 4 weeks after MI was due to alterations in SV rather than HR changing (Janssen *et al.*, 2002). Progressive declines in CO have been connected to heart failure (McManus *et al.*, 2009; Jain and Borlaug, 2019), which was observed in the untreated IRI cohort. However, unlike ESV and SV, CO with navitoclax treatment was not significantly changed, but instead treatment stabilised CO and at the time-points tested here, prevented CO from worsening after IRI.

I demonstrated that IRI caused cardiac dysfunction, however, this was not associated with changes in LV mass. In patients following MI, LV mass is used as a prognostic indicator of disease progression (Bulluck *et al.*, 2017). The absence of a change in LV mass in mice may reflect their differences to humans in the way they respond to myocardial injury. A previous study using aged mice and a permanent ligation model (without reperfusion) did not show alternations in LV mass (Walaszczyk *et al.*, 2019), which supports my finding. It is possible that net LV mass is unchanged due to both an increase in hypertrophy in combination with LV wall thinning of infarcted area (Visser, 2003; Feygin *et al.*, 2008).

In support of this suggestion, hypertrophy and remodelling was investigated at a cellular level and I did detect an increase in CM hypertrophy after IRI. Despite the increase in CM hypertrophy, the LV wall dimensions were unchanged. Therefore, CMs are undergoing remodelling yet this does not affect the overall LV mass. Regardless,

as no change in hypertrophy was observed following navitoclax treatment, it is unlikely that attenuation of hypertrophy contributed to improve cardiac function in this cohort.

Another remodelling process after MI is the formation of scar tissue in the region of the infarct (Azevedo *et al.*, 2016) and I observed a significant reduction in infarct size following navitoclax treatment. Clinically the size of the infarct correlates directly with cardiac function with smaller infarcts being associated with improved functional outcome and decreased mortality risk. In patients, an infarct greater than 12% of the LV was associated with a mortality rate of 7% within 2 years of the MI event, whereas the rate was negligible if infarct was smaller than 12% (McAlindon *et al.*, 2015). Modulating infarct size represents a potential mechanism to improve patient outcome. The decrease in infarct size in the navitoclax treated cohort therefore likely contributed directly to improved function and highlights its potential as a therapeutic option.

A number of alternative therapeutic strategies that aim to reduce infarct size and improve function have been investigated, however, to date these strategies have failed to translate to the clinic (Bulluck *et al.*, 2016; Paradies *et al.*, 2018). Conditioning events have been trialled with the aim to initiate cardio-protective mechanisms. These include intermittent reperfusion, termed ischaemic postconditioning, or inducing short periods of ischaemia followed by reperfusion in distal regions of the arm or leg, termed remote ischaemic conditioning (Zhao *et al.*, 2003; Staat *et al.*, 2005; Sörensson *et al.*, 2010; Hahn *et al.*, 2013). However, there is conflicting data regarding the effectiveness of these treatments. Ischaemic postconditioning has been reported to reduce infarct size (Zhao *et al.*, 2003; Staat *et al.*, 2005), yet the outcomes from these studies have been challenged (Sörensson *et al.*, 2010; Hahn *et al.*, 2013). In preclinical models remote ischaemic conditioning yielded encouraging results (Bulluck *et al.*, 2016) and recently the COND12/ERIC-PPCI trial from centres across Denmark, Spain, Serbia and the UK investigating ischaemic conditioning in STEMI patients that underwent PPCI was completed (March 2019, (NIH U.S National Library of Medicine, 2019)). Although currently the outcomes of this study have not been published.

Alternative strategies also include the use of pharmaceuticals. Cyclosporin-A, an immunosuppressant to inhibit opening of the mPTP, was trialled in STEMI patients and drastically reduced scar size by up to a 40% (Piot *et al.*, 2008). This drug progressed to a Phase III clinical trial, however, did not demonstrate the same effects as mortality and LV remodelling were unchanged (Cung *et al.*, 2015). Furthermore, treatment with

exenatide, an anti-diabetic therapy, also limited infarct size in patients (Lønborg et al., 2012), but subsequent follow-up studies observed no beneficial effects (Roos *et al.*, 2016b). It is important that treatment strategies consider what an appropriate clinical outcome is. For example, adenosine diphosphate, which is a cardio-protective agent, reduced infarct size in a porcine model of MI, however, the treatment had no effect on cardiac function (Bune et al., 2013). A follow on clinical trial also did not observe any functional improvements (Nazir et al., 2016).

These studies highlight the need for novel treatment strategies but also raise potential problems in clinically translating findings from preclinical models. In order for a treatment to be successful clinically it must have the potential to improve function not just morphology. It has also been suggested that stratifying patients and therapies to target interventions to those patients with the greatest potential for benefit may have more positive outcomes. Alternatively, using a combination of agents or techniques may exert favourable effects that are reproducible across a heterogeneous population rather than a single intervention alone (Bulluck et al., 2016).

Combining senolytic agents has also been trialled to improve the efficacy for senescent cell clearance. In one study by Zhu, Y. *et al* (Zhu *et al.*, 2015) 46 compounds were tested *in vitro* on senescent preadipocytes and HUVECs, and dasatinib and quercetin (D&Q) in combination yielded the best results. When tested in an aged *in vivo* murine model (24 months), EF and fractional shortening were both substantially improved, but vascular endothelial function was not changed. This study concluded that clearance of senescence was postulated to be a potential therapeutic avenue to treat age-related declines in cardiovascular function, however, reported that D&Q was not specific for senescent cells as they observed that healthy cells were also induced to apoptose (Zhu *et al.*, 2015; van Willigenburg *et al.*, 2018).

Navitoclax has previously been shown to act in a senolytic fashion *in vitro* and *in vivo* (Chang *et al.*, 2016) and it was concluded that Bcl-2 family inhibitors act on a wider range of cell types (Zhu *et al.*, 2016). My data, along with previously published data (Anderson *et al.*, 2019; Walaszczyk *et al.*, 2019), support the hypothesis that cardiac-lineage cells are removed by navitoclax and targeting senescence can therapeutically benefit cardiac function. However, as discussed above, promising results in the lab don't always translate well into the clinic. Therefore, additional studies are necessary

to test navitoclax on senescent human cardiac cells and in human subjects, and maybe trialling navitoclax in combination with other agents may be more effective.

As discussed above, it is important to consider that data from mouse models does not always translate well into the clinic. However, the data included in this chapter is encouraging and based on a number of parameters of cardiac function indicate that senolytic treatment in the form of navitoclax may represent a potential therapy to improve outcome after IRI. Additionally, I have demonstrated that navitoclax eliminates senescent CMs, which was associated with improved function and limiting adverse remodelling as shown by scar size. As the functional unit of the heart, CM dysfunction directly influences cardiac function (Paradis *et al.*, 2014). Due to this study's findings along with previous data showing reduced senescence markers in CMs (Anderson *et al.*, 2019; Walaszczyk *et al.*, 2019), it was hypothesised that clearance of senescent and dysfunctional CMs may be the underlying mechanism behind the improvements in cardiac function. For this reason, a novel CM-specific knockout model was generated to stop expression of the protein p16^{Ink4a}. The aim of this model was to explore whether inhibition of CM senescence could recapitulate the beneficial outcome observed in this chapter after navitoclax therapy. If so, more targeted senolytic agents towards senescent CMs could be constructed to optimise clearance and improve function.

Chapter 5. Characterisation of a novel $p16^{Ink4a}$ cardiomyocyte specific transgenic knockout model to investigate outcome to ischaemia-reperfusion injury

5.1 Introduction

Senescence has been shown to play a role in the heart, however, it is still unclear which cell populations display senescent markers. I have shown that subsequent to 60 minute LAD ligation with reperfusion there is an increase in markers of cellular senescence in different cell populations, including CMs. Additionally, I have shown that treatment with the senolytic navitoclax post-LAD ligation resulted in an improved cardiac function which was associated with a diminishing scar size and reduction in the number of senescent CMs.

During mouse ageing it was previously demonstrated that markers of senescence accumulate in the CM population and this was not observed in other cell types (Anderson *et al.*, 2019). These senescent CMs expressed an atypical SASP including the factors Tgf- β 2, End3 and Gdf15. These SASP factors induced characteristics of myocardial remodelling both in combination and, to a certain extent, individually. With navitoclax treatment, aged mice had a reduction in senescent CMs which correlated with improved cardiac function and attenuated remodelling, in terms of increased CM regeneration and reduced fibrosis and hypertrophy. Therefore, it was concluded that the observed reduction in remodelling was due to the removal of senescent, hypertrophic CMs and their associated SASP that would escalate hypertrophy and fibrosis via the by-stander effect (Anderson *et al.*, 2019).

Additionally, it has been reported in multiple models that senescence in the fibroblast population actually limits fibrosis (Zhu *et al.*, 2013; Meyer *et al.*, 2016; Childs *et al.*, 2018; Meng *et al.*, 2019). In the TAC surgical model performed on transgenic p53/p16^{Ink4a} knockout mice, senescence markers in fibroblasts were reduced, however, the degree of fibrosis was higher than compared to wild type mice (Meyer *et al.*, 2016). This observation that inhibiting senescence improves expression of markers and inflammation but that there is excessive fibrosis was also confirmed in a model of MI on p53 knockout mice (Zhu *et al.*, 2013).

Taking these observations together, I hypothesised that following IRI, CM senescence is detrimental to recovery because of CM SASP-induced myocardial remodelling. To test this hypothesis, I aimed to establish a mouse model that allowed specific inhibition of senescence within the CM population.

p16^{Ink4a} is a dominant regulator of senescence by controlling the G1-S phase checkpoint. Expression of p16^{Ink4a} is a useful marker of senescence and was shown to increase after injury in multiple organs such as skin and liver (Krizhanovsky *et al.*, 2008; Jun and Lau, 2010a; Demaria *et al.*, 2014; Liu *et al.*, 2019). A number of studies have directly demonstrated that p16^{Ink4a} expressing cells are causal to ageing (Liu *et al.*, 2011; LaPak and Burd, 2014). By establishing the INK-ATTAC transgenic mouse, which allows for the selective but systemic killing of p16^{Ink4a} expressing cells, Baker, D.J. *et al.* demonstrated that genetic elimination of p16^{Ink4a} cells extended life-span and alleviated or delayed the onset of numerous age-related diseases (Baker *et al.*, 2011; Baker *et al.*, 2016). Using the same INK-ATTAC model, it was also shown that elimination of p16^{Ink4a} cells from aged mice reduced the number of senescent CMs, attenuated hypertrophy and reduced fibrosis. These results mirrored the effects of navitoclax treatment on the outcomes of aged mice (Anderson *et al.*, 2019).

Moreover, navitoclax has been studied using the p16-3MR transgenic mouse (Chang *et al.*, 2016). Transgenic p16-3MR mice contain a trimodality reporter fusion protein which includes renilla luciferase, a red fluorescent protein (mRFP), and truncated herpes simplex virus 1 thymidine kinase (HSV-TK) all driven by the p16^{Ink4a} promoter. The luciferase allows the detection of senescent cells by luminescence, mRFP permits cell sorting and identification of senescent cells (which is important as there are questions over the validity of antibodies for p16^{Ink4a} expression), and HSV-TK allows specific killing of senescent cells by ganciclovir. Following a non-lethal dose of irradiation, which induced a systemic increase in senescence, a comparison was made between the treatment with the suicide drug (ganciclovir) and treatment with navitoclax. Both treatments yielded similar results in terms of killing senescent cells (Chang *et al.*, 2016) demonstrating a relationship between the cellular target of navitoclax and p16^{Ink4a} expression.

These studies concluded the following: 1) p16^{Ink4a} activated senescence played a role in establishing CM senescence in aged mice; 2) p16^{Ink4a} expressing CMs contributed to myocardial remodelling during ageing; and 3) navitoclax treatment resulted in the

elimination of p16^{Ink4a} expressing cells in multiple tissue systems including the heart. Based on these observations and the data presented in chapter 4 showing a reduction in p16^{Ink4a} expressing CMs in IRI mice treated with navitoclax, to investigate the contribution of senescent CMs to remodelling and recovery post-IRI I targeted the p16^{Ink4a} expressing CM population (Figure 5.1).

To date, there is no model available to specifically remove individual cell lineages expressing p16^{Ink4a}. To inhibit senescence in the CM population I instead took the approach of establishing a transgenic model in which p16^{Ink4a} expression was knocked out in the CM population. The p16^{Ink4a} floxed mouse line (Cdkn2atm2.1Nesh line (p16^{Ink4a}^{ff}) (Monahan *et al.*, 2010)) was crossed with an inducible Cre line under activation of a CM specific promoter (*Myh6-cre/Esr1* (α MHC-*MerCreMer*)). The α MHC-*MerCreMer* mice carry a fusion transgene of *Cre* recombinase flanked by *Mer*, a mutated oestrogen receptor ligand-binding domain, driven by the cardiac α -myosin heavy chain promoter (encoded by *Myh6*). The p16^{Ink4a}^{ff} line carries *loxP* elements ~3.5 kb upstream of 5' to exon 1 α and immediately downstream of 3' to the p16^{Ink4a} exon 1 α . Once α MHC-*MerCreMer* :: p16^{Ink4a}^{ff} mice were established, *Cre* activation led to the excision of the *loxP* sites which resulted in selective p16^{Ink4a} exon 1 α excision permanently and specifically in the CM population. I crossed *MerCreMer*^{+/-} :: p16^{+/-} males with *MerCreMer*^{-/-} :: p16^{+/-} females to create α MHC-*MerCreMer*^{+/-} :: p16^{ff} (Containing both transgenes and referred to from here as *MerCreMer* :: p16^{ff}) and littermates *MerCreMer*^{-/-} :: p16^{ff} as controls (expressing the p16^{ff} transgene but lacking α MHC-*MerCreMer* and referred to as WT :: p16^{ff}).

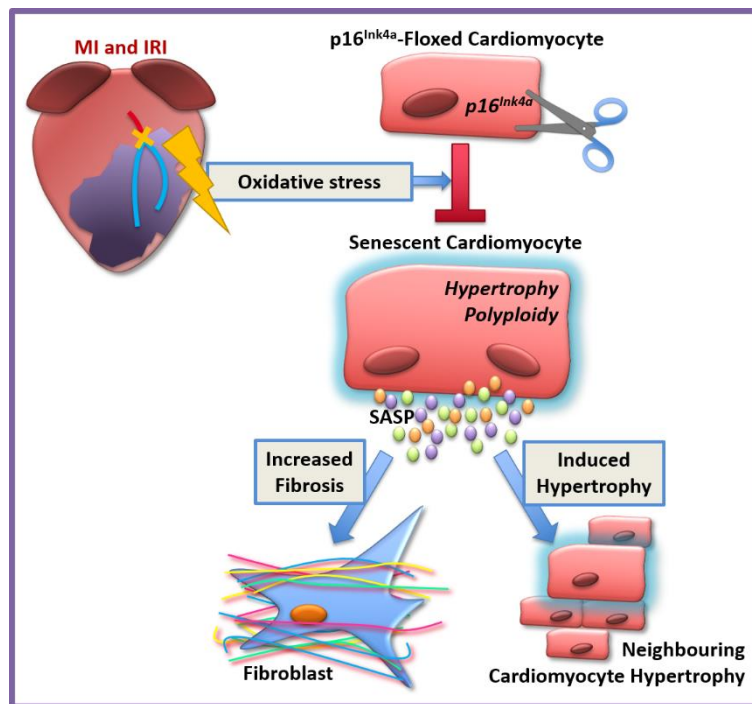


Figure 5.1 Graphical hypothesis.

$p16^{Ink4a}$ is a major regulator of senescence, and previously demonstrated to play a role in numerous age-associated disorders. I hypothesised that CM-specific knockout of $p16^{Ink4a}$ would attenuate CM senescence and thereby reduce myocardial remodelling and improve cardiac function post-IRI.

5.2 Experimental Design and Model Validation.

I established a novel $MerCreMer^{-/-} :: p16^{ff}$ transgenic model which allowed for a temporally controlled, CM-specific knockout of $p16^{Ink4a}$ to determine if an accumulation of CM senescence was primarily driving adverse cardiac remodelling and impacting on functional recovery post-IRI. Additionally, it would conclude whether elimination of this population was pivotal to the benefits observed following navitoclax treatment.

$MerCreMer^{-/-} :: p16^{ff}$ and littermate WT $:: 16^{ff}$ mice were genotyped and treated with tamoxifen for 2 weeks (0.5mg/ml/d 4-OHT) from the age of 3 months of age to allow translocation of Cre to the nucleus and the recombination of the *loxP* sites. Following 4-OHT treatment mice were rested for 2 weeks to allow full and efficient recombination to occur. Mice then underwent LAD ligation as previously described (2.1) and were transferred to the Keith Unit at the Campus for Ageing and Vitality for MRI scanning which were performed at weeks 3 and 5 post-LAD ligation. On the day of the 5 week MRI mice were humanely killed and hearts were collected for analysis and processed accordingly (Figure 5.2).

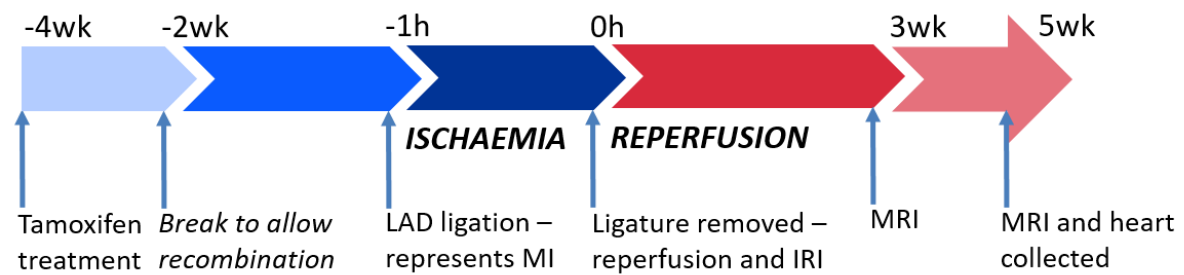


Figure 5.2 Experimental timeline.

Mice were dosed with 4-OHT for 2 weeks to activate Cre recombinase and flox out exon 1 α of $p16^{Ink4a}$, and therefore CMs no longer expressed $p16^{Ink4a}$ at a protein level. Then they had surgery where the LAD was ligated for 1 hour and then the heart allowed to reperfuse. Mice were then transferred to the Keith Unit for MRIs at weeks 3 and 5 post-surgery.

5.3 Validation of exon 1 α excision from $p16^{Ink4a}$ in cardiomyocytes

Although mice had already been genotyped prior to experiment, a second genotyping was undertaken post-tissue collection to confirm the correct genotype. DNA was isolated from the atria of both $MerCreMer :: p16^{ff}$ and $WT :: p16^{ff}$ mice and PCRs were performed for Cre and the $p16^{Ink4a}$ transgene (2.3.1), which confirmed that both $MerCreMer :: p16^{ff}$ and $WT :: p16^{ff}$ mice were homozygous for the $p16^{Ink4a^{ff}}$ allele and only $MerCreMer :: p16^{ff}$ mice expressed the Cre allele (product sizes 261bp (data not shown) and 280bp respectively, Figure 5.3.A). Next I confirmed that excision of $p16^{Ink4a}$ exon 1 α had occurred at a genetic level in the $MerCreMer :: p16^{ff}$ mice subjected to 4-OHT treatment. To confirm excision of exon 1 α , p16LCred primers were used that are designed to anneal to DNA at regions flanking the *loxP* sites. As such, if exon 1 α had been excised, then a product of 270bp would be amplified (Monahan *et al.*, 2010). All 15 $MerCreMer :: p16^{ff}$ mice which had been treated with 4-OHT and expressed Cre had a band present from the p16LCred at the expected molecular weight (Figure 5.3.B). Having demonstrated the excision of $p16^{Ink4a}$, these mice are subsequently referred to as $p16^{-/-}$. The 8 $WT :: p16^{ff}$ mice that were negative for Cre were also negative for the p16LCred product. Having confirmed the genotype of these mice, they are subsequently referred to as $p16^{ff}$.

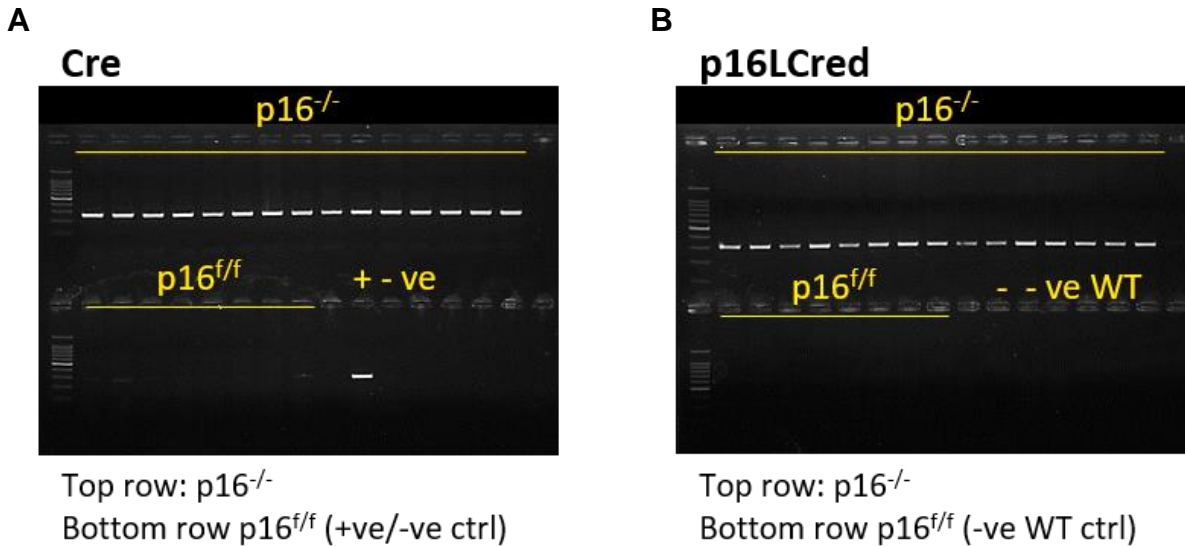


Figure 5.3 Genotyping polymerase chain reactions to confirm the presence of Cre and that it had been activated to flox *p16^{Ink4a}* exon 1 α .

- A)** PCR for Cre. A white band at 280bp confirmed the presence of Cre within the genome of the mouse. On the top row all 15 experimental mice (p16^{-/-}) had a positive result. On the bottom row none of the 8 control mice (p16^{f/f}) generated a product and were negative for expression of Cre. Samples were tested against a sample previously confirmed to be Cre positive (+ve) and a ddH₂O negative control (-ve).
- B)** PCR to confirm Cre was activated and had successfully floxed *p16^{Ink4a}* exon 1 α . A positive result of a band present at 270bp was observed in the same 15 mice (top row) with a positive result from the Cre PCR. On the lower row there was no product formed in the 8 experimental mice, which correlated with no Cre present in A. Samples were run against WT mice with no Cre of floxed *p16^{Ink4a}* (-ve WT).

5.3.1 *p16^{Ink4a}* and *p21^{Cip}* are significantly reduced in the mouse cohort with cardiomyocytes not expressing *p16^{Ink4a}*

Next I aimed to confirm that *p16^{Ink4a}* knockout resulted in reduced *p16^{Ink4a}* protein expression. Post-ischaemia-reperfusion injury expression of *p16^{Ink4a}* in the CMs from the p16^{f/f} cohort was 20.09% \pm 2.29, which was similar to levels observed in wild type mice at the same time-point post-IRI (4-5 weeks). However, *p16^{Ink4a}* expression was significantly reduced ($p < 0.0001$) in the p16^{-/-} cohort with 6.51% \pm 2.29 CMs being positive for *p16^{Ink4a}* staining. This reduction corresponds to 67.60% fewer *p16^{Ink4a}* positive, troponin C expressing CMs being present in the p16^{-/-} hearts compared to the p16^{f/f} heart (Figure 5.4). This result is consistent to previous studies which have demonstrated a 70-80% efficiency in *loxP* recombination when using the *MerCreMer* transgenic mouse (Sohal *et al.*, 2001).

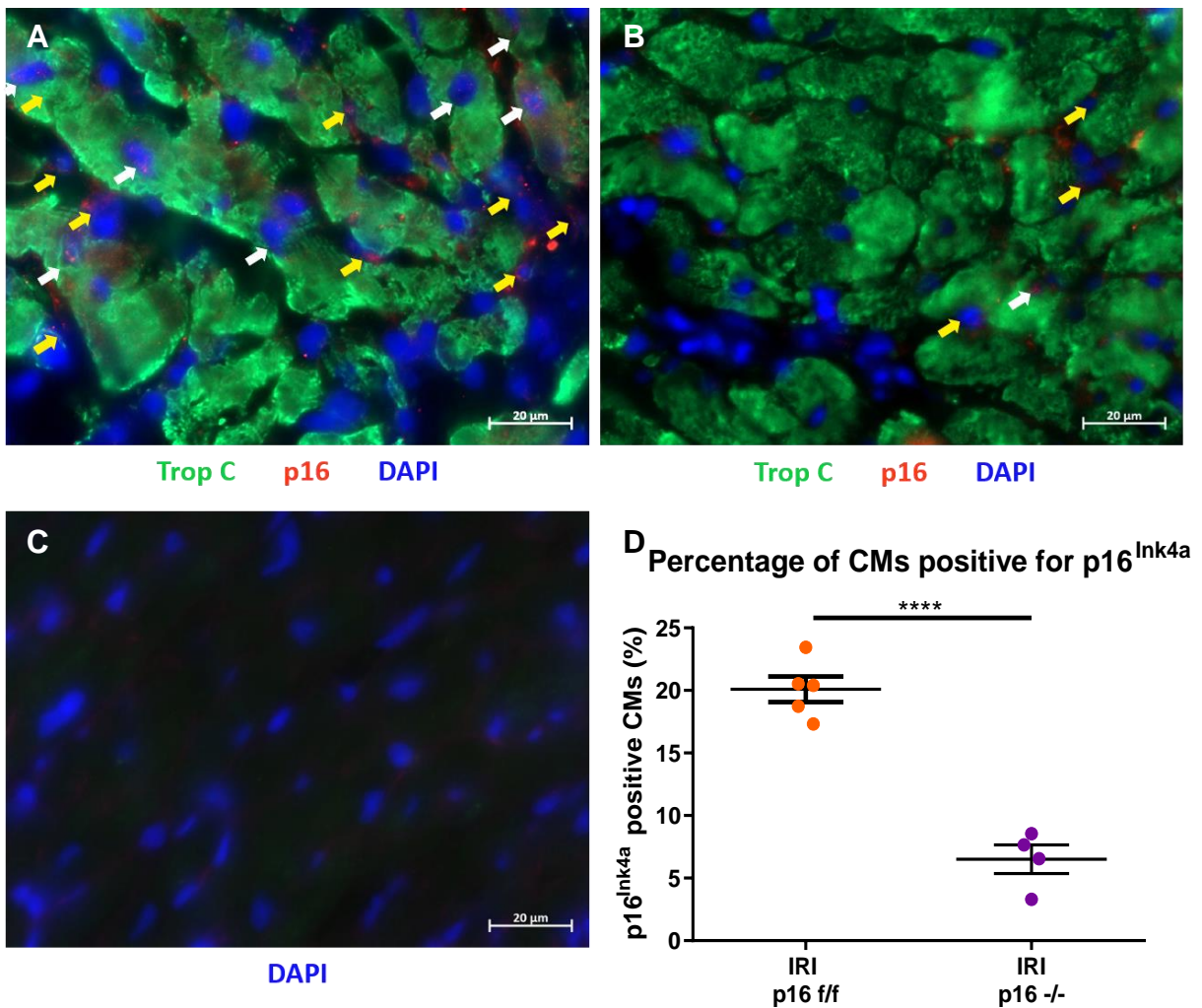


Figure 5.4 Cardiomyocytes have reduced expression of p16^{Ink4a} following floxing of p16^{Ink4a} after ischaemia-reperfusion injury.

A) Immunofluorescence staining in p16^{f/f} hearts post-IRI. Slides stained with CM marker troponin C (in green, wavelength 488nm), senescence marker p16^{Ink4a} (in red, wavelength 594nm) and nuclei (in blue with DAPI, wavelength 461nm). All images for this analysis were taken in the BZ. Cardiomyocytes positive for p16^{Ink4a} are highlighted with a white arrow. Interstitial cells positive for p16^{Ink4a} are highlighted with a yellow arrow.

B) Immunofluorescence staining in p16^{-/-} hearts post-IRI. Slides stained with CM marker troponin C (in green, wavelength 488nm), senescence marker p16^{Ink4a} (in red, wavelength 594nm) and nuclei (in blue with DAPI, wavelength 461nm). All images for this analysis were taken in the BZ. Cardiomyocytes positive for p16^{Ink4a} are highlighted with a white arrow. Interstitial cells positive for p16^{Ink4a} are highlighted with a yellow arrow.

C) Negative control for both 1°Abs, slides were incubated in PBS instead.

D) Quantification of CMs expressing p16^{Ink4a} in p16^{f/f} IRI hearts vs p16^{-/-} IRI hearts. Floxing of p16^{Ink4a} from CMs significantly reduces the percentage of CMs positive for p16^{Ink4a} post-IRI.

N=4 and 5 for each experimental condition. NS≥0.05, *p<0.05, **p<0.01, ***p<0.001, ****p<0.0001 using Unpaired T-Test.

To validate the antibody, sections were also stained via RNAscope which is a method of in situ hybridisation. Following normalisation to the negative control, RNAscope analysis revealed that in the $p16^{ff}$ mice hearts the percentage of troponin C positive CMs co-expressing $p16^{Ink4a}$ transcript RNA ($33.11\% \pm 2.48$) was higher than those expressing $p16^{Ink4a}$ protein. Importantly, the percentage of troponin C positive CMs expressing $p16^{Ink4a}$ was reduced in the $p16^{-/-}$ cohort to $5.54\% \pm 3.80$ ($p=0.005$, Figure 5.5). These findings added further evidence that $p16^{Ink4a}$ expression was reduced in the CMs of the $p16^{-/-}$ mice.

Having confirmed that knockout of $p16^{Ink4a}$ resulted in decreases of both $p16^{Ink4a}$ transcript and protein expression, next I established if absence of $p16^{Ink4a}$ results in a decrease in CM senescence. Alternative senescent markers were then quantified in the CM population, with heart sections stained with the $p21^{Cip}$ antibody. At 5 weeks post-IRI the percentage of troponin C positive CMs co-expressing $p21^{Cip}$ in the $p16^{ff}$ mice was $20.17\% \pm 1.53$, comparable with wild type animals in chapter 3 and chapter 4 ($18.47\% \pm 2.62$ and $20.00\% \pm 1.57$). $p16^{Ink4a}$ knockout in the $p16^{-/-}$ mice led to a significant decrease in CM $p21^{Cip}$ expression to $13.55\% \pm 0.45$ (Figure 5.6), however, not to the same degree as observed following navitoclax treatment in chapter 4 ($7.12\% \pm 0.94$).

I also performed staining for TAF to investigate whether DNA damage was affected in this mouse model. However, neither the percentage of CMs positive for TAF ($p=0.2487$) or mean TAF number in CM nuclei ($p=0.0733$) were significantly changed after floxing of $p16^{Ink4a}$ exon 1 α (Figure 5.7).

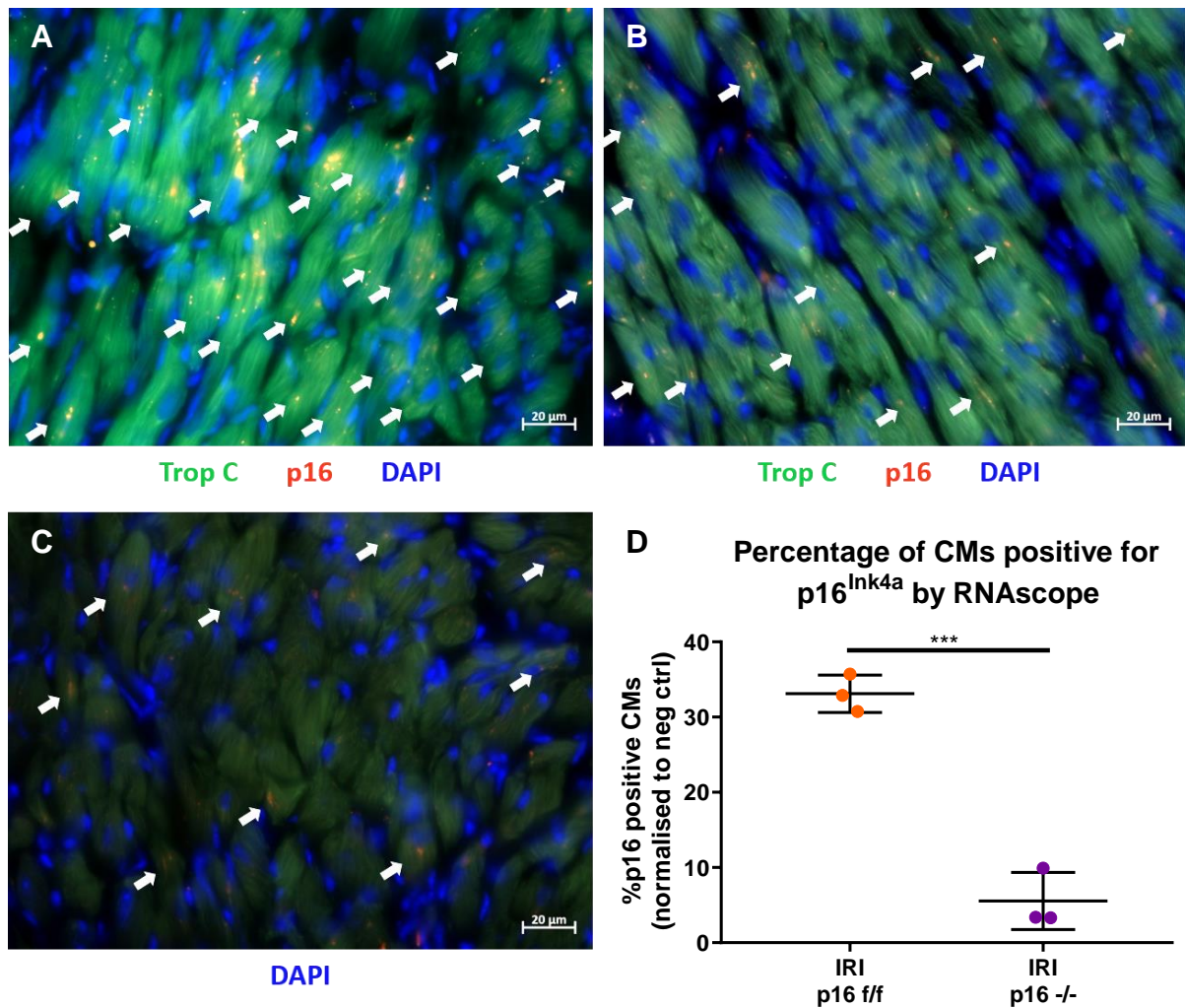


Figure 5.5 p16^{Ink4a} expression by RNAscope is significantly decreased in knockout mice, and levels are comparable to those quantified by immunofluorescence when normalised to the negative control.

- A)** RNAscope staining in p16^{f/f} hearts post-IRI. Slides were stained with the probe for p16^{Ink4a} RNA (in red, wavelength 594nm) and counter stained for the CM marker troponin C (in green, wavelength 488nm) and nuclei (in blue with DAPI, wavelength 461nm). All images for this analysis were taken in the BZ. Cardiomyocytes positive for p16^{Ink4a} are highlighted with a white arrow.
- B)** RNAscope staining in p16^{-/-} hearts post-IRI. Slides were stained with the probe for p16^{Ink4a} RNA (in red, wavelength 594nm) and counter stained for the CM marker troponin C (in green, wavelength 488nm) and nuclei (in blue with DAPI, wavelength 461nm). All images for this analysis were taken in the BZ. Cardiomyocytes positive for p16^{Ink4a} are highlighted with a white arrow.
- C)** Negative control for the RNAscope probe. Background staining in the CMs are highlighted with a white arrow.
- D)** Graph showing the percentage of troponin C expressing CMs positive for the probe against p16^{Ink4a} normalised against the negative control in p16^{f/f} and p16^{-/-} mice.

N=3 for each experimental condition. NS≥0.05, *p<0.05, **p<0.01, ***p<0.001, ****p<0.0001 using Unpaired T-Test.

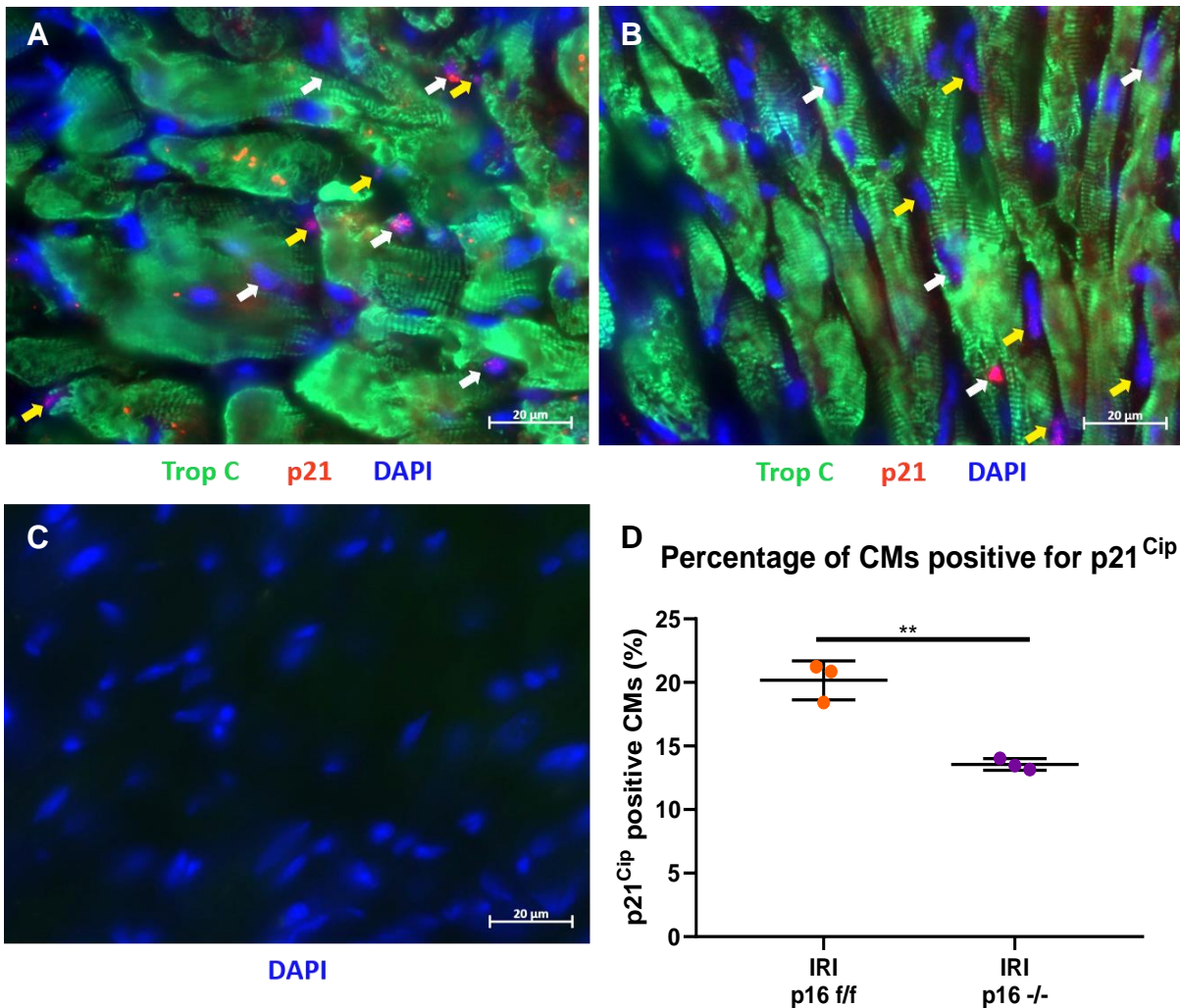


Figure 5.6 Floxing $p16^{Ink4a}$ from cardiomyocytes reduces the percentage of cardiomyocytes positive for $p21^{Cip}$ after ischaemia-reperfusion injury.

- E)** Immunofluorescence staining in $p16^{f/f}$ hearts post-IRI. Slides stained with CM marker troponin C (in green, wavelength 488nm), senescence marker $p21^{Cip}$ (in red, wavelength 594nm) and nuclei (in blue with DAPI, wavelength 461nm). All images for this analysis were taken in the BZ. Cardiomyocytes positive for $p21^{Cip}$ are highlighted with a white arrow. Interstitial cells positive for $p21^{Cip}$ are highlighted with a yellow arrow.
- F)** Immunofluorescence staining in LAD ligated $p16^{-/-}$ hearts. Slides stained with CM marker troponin C (in green, wavelength 488nm), senescence marker $p21^{Cip}$ (in red, wavelength 594nm) and nuclei (in blue with DAPI, wavelength 461nm). All images for this analysis were taken in the BZ. Cardiomyocytes positive for $p21^{Cip}$ are highlighted with a white arrow. Interstitial cells positive for $p21^{Cip}$ are highlighted with a yellow arrow.
- G)** Negative control for both 1°Abs, slides were incubated in PBS instead.
- H)** Quantification of CMs expressing $p21^{Cip}$ in $p16^{f/f}$ IRI hearts vs $p16^{-/-}$ IRI hearts. In mice with floxed $p16^{Ink4a}$ from CMs $p21^{Cip}$ is significantly reduced in CMs post-IRI.

N=3 for each experimental condition. NS \geq 0.05, * p <0.05, ** p <0.01, *** p <0.001, **** p <0.0001 using Unpaired T-Test.

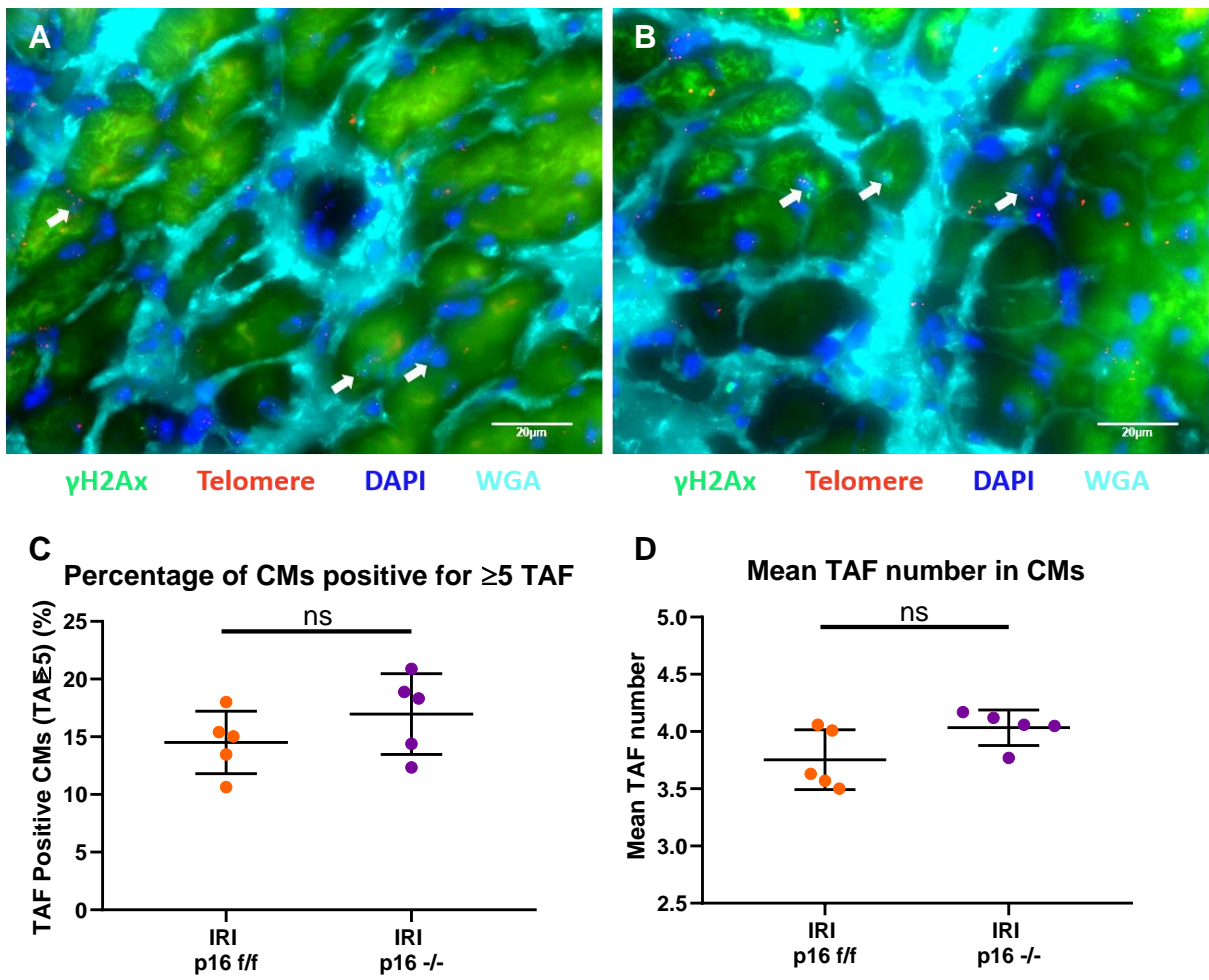


Figure 5.7 Floxing of $p16^{Ink4a}$ has no effect on telomere-associated DNA damage foci in cardiomyocytes.

A) Immunofluorescence staining in $p16^{ff}$ heart post-IRI. Slides stained with γ H2Ax (in green, wavelength 488nm), telomere-c probe (in red, wavelength 594nm), nuclei (in blue with DAPI, wavelength 461nm) and WGA (in teal, wavelength 647nm). All images for this analysis were taken in the BZ. Cardiomyocytes positive for TAF are highlighted with a white arrow.

B) Immunofluorescence staining in $p16^{-/-}$ heart post-IRI. Slides stained with γ H2Ax (in green, wavelength 488nm), telomere-c probe (in red, wavelength 594nm), nuclei (in blue with DAPI, wavelength 461nm) and WGA (in teal, wavelength 647nm). All images for this analysis were taken in the BZ. Cardiomyocytes positive for TAF are highlighted with a white arrow.

C) Quantification of CMs expressing ≥ 5 TAF in $p16^{ff}$ and $p16^{-/-}$ IRI hearts. Removal of $p16^{Ink4a}$ had no effect on the percentage of CMs positive for TAF.

D) Quantification of mean TAF number in CMs post-IRI in $p16^{ff}$ and $p16^{-/-}$ hearts. Removal of $p16^{Ink4a}$ had no effect on the CM mean TAF number.

N=3 and 4 for each experimental condition. NS \geq 0.05, * p <0.05, ** p <0.01, *** p <0.001, **** p <0.0001 using Two-Tailed T-Test.

5.4 Cardiac function remains unchanged in this model

To assess cardiac function, mice underwent an MRI to investigate their LV mass, EDV, ESV, SV, CO and EF. Mice had an initial MRI at 3 weeks after surgery to establish a baseline function post-IRI and then a follow-up MRI 2 weeks later to evaluate any developments in these variables. As in section 4.5, these variables were calculated from measurements of the epicardial and endocardial areas of each MRI slice at diastole and systole. An example of these measurements can be found in Figure 5.8.

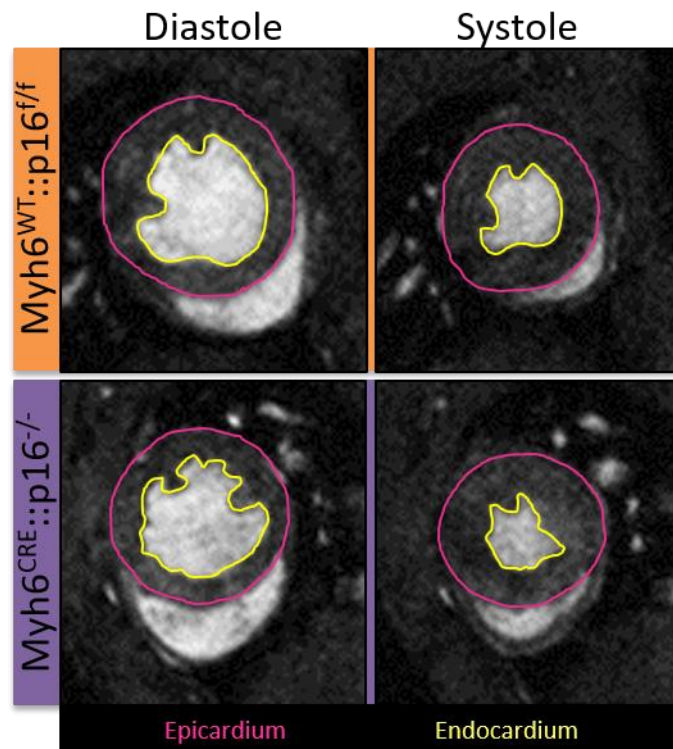


Figure 5.8 Example of measurements taken for each magnetic resonance imaging slice at diastole and systole after ischaemia-reperfusion injury.

Pink line denotes the epicardial area measured and the yellow line indicates the endocardial area measured for analysis.

5.4.1 Left ventricular mass is unaltered with the removal of $p16^{Ink4a}$ expression from cardiomyocytes

As described in 4.5.1, the variable LV mass can be used to identify signs of hypertrophy and fibrosis that drive adverse remodelling (Konstam *et al.*, 2011).

Across all groups post-IRI, LV mass was not significantly altered ($p=0.3223$). At week 3 LV mass was $125.4\text{mg} \pm 10.71$ in the $p16^{f/f}$ mice and $122.7\text{mg} \pm 13.45$ for the $p16^{-/-}$

mice, and at 5 weeks the p16^{ff} cohort had a mean LV mass of 122.0mg ± 12.89 and this was 123.4mg ± 22.20 in the p16^{-/-} mice (Figure 5.9.A).

The delta change in LV mass was assessed in addition to the raw values for LV mass. The percentage change in LV from weeks 3 to 5 was marginally larger in the p16^{ff} cohort at -3.09% ± 6.68 than the p16^{-/-} cohort at -0.78% ± 10.06. The change for each individual mouse within both cohorts was not significantly different either within each group or between the groups (p=0.1315, Figure 5.9.B).

These data reflect the results from section 4.5.1 that show the mean LV mass is largely unaffected in this model of IRI, but also demonstrates that inhibiting CMs from activating p16^{Ink4a} has no effect on LV mass post-LAD ligation.

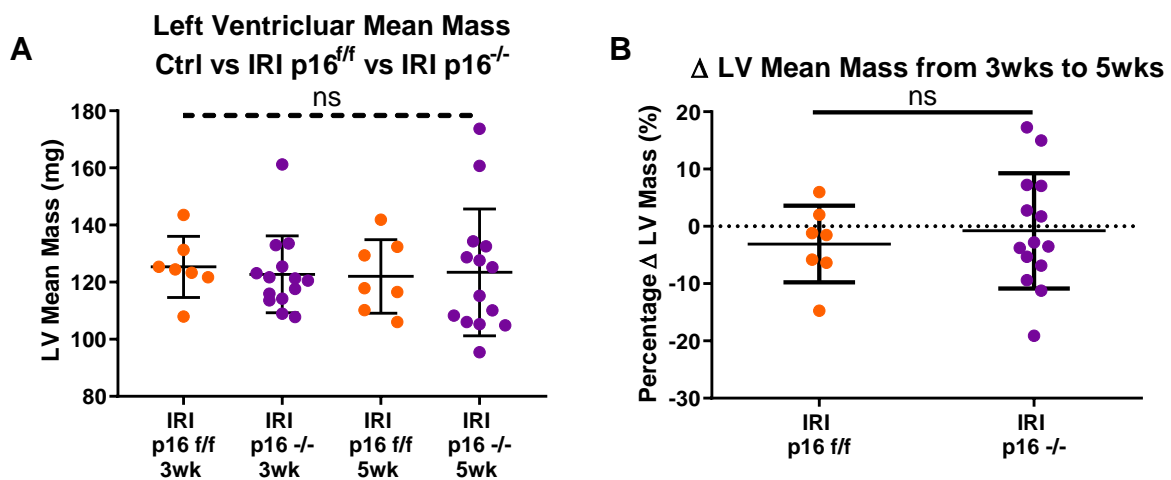


Figure 5.9 Left ventricular mass is unchanged after ischaemia-reperfusion injury in both cohorts.

- A)** Data showed no significant changes when comparing all groups, indicating that LV mass was not affected by floxing p16^{Ink4a} from the CM population.
- B)** Quantification of the change in LV mass between week 3 and 5 for both the IRI p16^{ff} and p16^{-/-} groups. No significant differences were observed either between the two cohorts or between the mice within each cohort across the two time-points.

N=7 and 14 for each experimental condition. NS≥0.05, *p<0.05, **p<0.01, ***p<0.001, ****p<0.0001 using One-Way ANOVA, Unpaired and Paired T-Test.

5.4.2 End diastolic volume and end systolic volume are not affected by floxing out p16^{Ink4a} from cardiomyocytes

Another set of variables that can elude to LV remodelling and predict outcome following MI are EDV and ESV (McManus *et al.*, 2009; Redgrave *et al.*, 2016; Bulluck *et al.*, 2017).

Ischaemia-reperfusion injury via LAD ligation led to significant increases in EDV. At 3 weeks the EDV of the p16^{ff} group was 98.61 μ l \pm 17.73 and 94.80 μ l \pm 30.35 for the p16^{-/-} group. At the 5 week MRI the mean EDV had marginally changed, with both IRI groups slightly decreased to 88.87 μ l \pm 18.28 (p=0.3829) and 90.80 μ l \pm 34.90 respectively (p=0.2649, Figure 5.10.A).

Although the mean EDV decreases were not significant when the raw values were compared, the changes in EDV was significant in the p16^{ff} cohort (p=0.0006). All mice demonstrated a reduction in their EDV (Figure 5.10.B), with an average reduction of -11.55% \pm 5.80 in the p16^{ff}. However, the reduction of -6.73% \pm 15.82 in the p16^{-/-} cohort was not significant (p=0.0790) and across the group mice showed increases and decreases in their EDV. The p16^{-/-} group reflects what would be expected to occur after IRI, and inhibiting p16^{Ink4a} in the CMs has not prevented the progression of EDV.

Similar to EDV, ESV also showed no significant differences between the IRI cohorts. At 3 weeks there was no significant difference between the p16^{ff} and p16^{-/-} groups with ESVs of 68.23 μ l \pm 19.23 and 61.34 μ l \pm 31.91 (p=0.6078). Similarly, at week 5 there was no difference in the ESVs (65.05 μ l \pm 25.19 and 64.58 μ l \pm 32.60 respectively, p=0.7952, Figure 5.11.A).

Looking at the changes in ESV between the MRIs also showed no significant changes within or between the groups. In the p16^{ff} group the mean percentage change in ESV was -10.57% \pm 32.62 (p=0.3664) and the p16^{-/-} had a stable ESV with a mean change of -2.07% \pm 50.72 (p=0.8226, Figure 5.11.B). This result demonstrates that removal of p16^{Ink4a} expression has no effect on ESV, as all mice in both groups did not show a trend in their ESV.

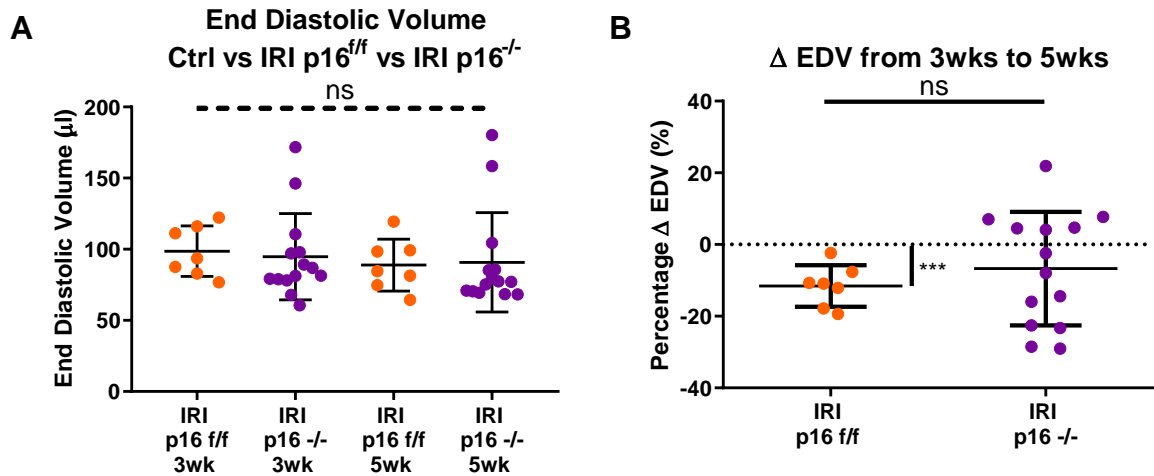


Figure 5.10 End diastolic volume increases after ischaemia-reperfusion injury but is not affected by $p16^{Ink4a}$ expression in cardiomyocytes.

- A)** Data showing no significant change in EDV was observed between IRI p16^{fl/fl} and p16^{-/-} mice.
- B)** Quantification of the change in EDV between week 3 and 5 for both the p16^{fl/fl} and p16^{-/-} groups. In the p16^{fl/fl} group all mice showed a decline in their EDV, and this change was significant between weeks 3 and 5. However, the p16^{-/-} showed a general trend for a smaller EDV at week 5, but individual responses varied and this reduction was not significant.

N=7 and 14 for each experimental condition. NS≥0.05, *p<0.05, **p<0.01, ***p<0.001, ****p<0.0001 using One-Way ANOVA, Unpaired and Paired T-Test.

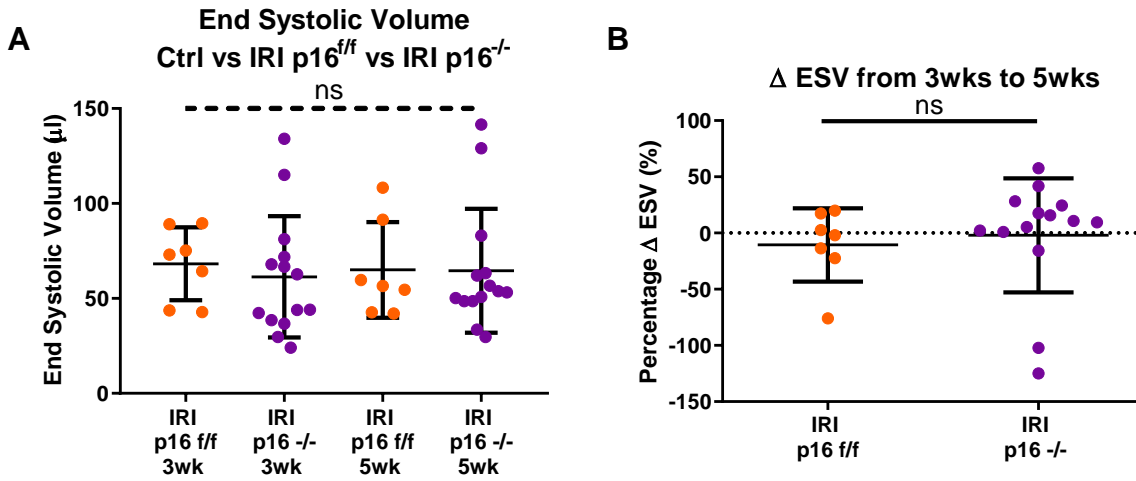


Figure 5.11 End systolic volume increases after ischaemia-reperfusion injury but is also not affected by $p16^{Ink4a}$ expression in cardiomyocytes.

- A)** Data showing no significant change in ESV was observed between IRI p16^{ff} and p16^{-/-} mice.
- B)** Quantification of the change in ESV between week 3 and 5 for both the p16^{ff} and p16^{-/-} groups. No significant difference between the progressions of the groups was observed and neither group had a significant change in their ESV from week 3 to 5.

N=7 and 14 for each experimental condition. NS≥0.05, *p<0.05, **p<0.01, ***p<0.001, ****p<0.0001 using One-Way ANOVA, Unpaired and Paired T-Test.

5.4.3 Inhibition of p16^{Ink4a} expression in cardiomyocytes does not lead to any improvements in stroke volume

There were no significant differences between the SV of the p16^{fl/fl} and p16^{-/-} groups, although for both cohorts the SV was reduced between weeks 3 and 5. The p16^{fl/fl} had an SV of 30.38 μ l \pm 9.28 which fell to 23.82 μ l \pm 12.80 (p=0.2934), and the p16^{-/-} SV changed from 33.46 μ l \pm 12.16 to 26.22 μ l \pm 9.86 (p=0.0849, Figure 5.12.A). These reductions are due to the EDV for both cohorts reducing over time, and maintaining a relatively steady ESV, so as the LV capacity at diastole was reduced, the volume of blood ejected with each contraction was therefore consequently lessened.

As the trends in changes in EDV and ESV were very similar across both the p16^{fl/fl} and p16^{-/-}, the percentage changes in SV were also not significantly different. Both groups demonstrated roughly a 60% decline in their SV (67.93% \pm 95.71 in the p16^{fl/fl} group, p=0.3664, and 55.81% \pm 92.59 in the p16^{-/-} group, p=0.8226, Figure 5.12.B).

When evaluating the individuals in each cohort, the spread of change was highly variable in both groups, so this result is not attributed to single individuals, but due to variations within both. Therefore, SV is significantly worsened following IRI (48.45 μ l \pm 3.93 SV pre-IRI, p=0.0002, Figure 4.12) and is not improved by preventing CMs from expressing p16^{Ink4a}.

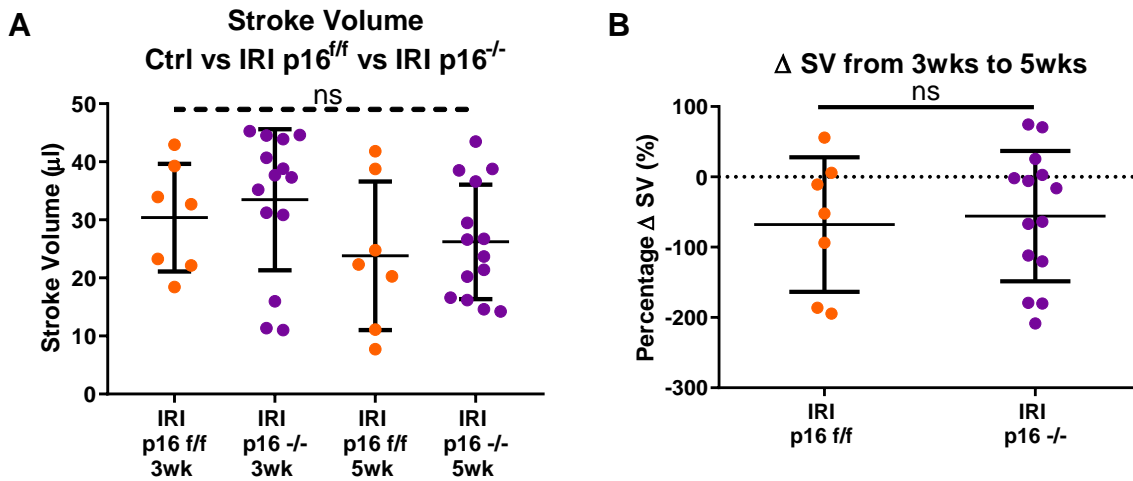


Figure 5.12 Ischaemia-reperfusion injury causes a reduction in stroke volume, however, altered $p16^{Ink4a}$ expression in cardiomyocytes has no effect.

- A)** Data showing no significant change in SV was observed between IRI p16^{ff} and p16^{-/-} mice.
- B)** Quantification of the change in SV between week 3 and 5 for both the p16^{ff} and p16^{-/-} groups. No significant difference between the progressions of the groups was observed and neither group had a significant change in their SV from week 3 to 5.

N=7 and 14 for each experimental condition. NS≥0.05, *p<0.05, **p<0.01, ***p<0.001, ****p<0.0001 using One-Way ANOVA, Unpaired and Paired T-Test.

5.4.5 Preventing cardiomyocytes from expressing $p16^{Ink4a}$ is insufficient to rescue ejection fraction post-myocardial infarction

The final variable assessed in these cohorts was EF. As previously described, EF is an important variable clinically, and an EF of <40% is defined as heart failure (Ponikowski *et al.*, 2016).

There was no significant difference in EF between the p16^{ff} or p16^{-/-} mice at either time-points. At 3 weeks, the mean EF of the IRI p16^{ff} cohort was 31.64% ± 11.28 and in the p16^{-/-} the mean EF was 37.78% ± 17.27 (p=0.4068). These data show that the IRI in these mice post-MI was very severe within 3 weeks of the MI. By 5 week, the mean EF for both cohorts had further declined to 28.30% ± 15.27 and 30.58% ± 13.06 respectively (p=0.6502 and 0.3761, Figure 5.13.A).

As per previous variables discussed above, the percentage change in EF was calculated. Both p16^{ff} and p16^{-/-} on average had a reduced EF with time, and this was

significantly reduced in the $p16^{-/-}$ cohort at $-44.03\% \pm 80.95$ ($p=0.0474$). The percentage change in the $p16^{ff}$ was even greater at $-52.35\% \pm 91.58$, though it was not significant ($p=0.1492$, Figure 5.13.B). With many variables, the data was often not closely grouped. This reflects either the variability in responses following IRI and that $p16^{Ink4a}$ floxed from CMs has no impact on reversing or reducing this variability, or raises concerns over the quality of the MRIs in this study. The responses at 5 weeks were unchanged for all variables and therefore assumed that the responses reported were biologically accurate.

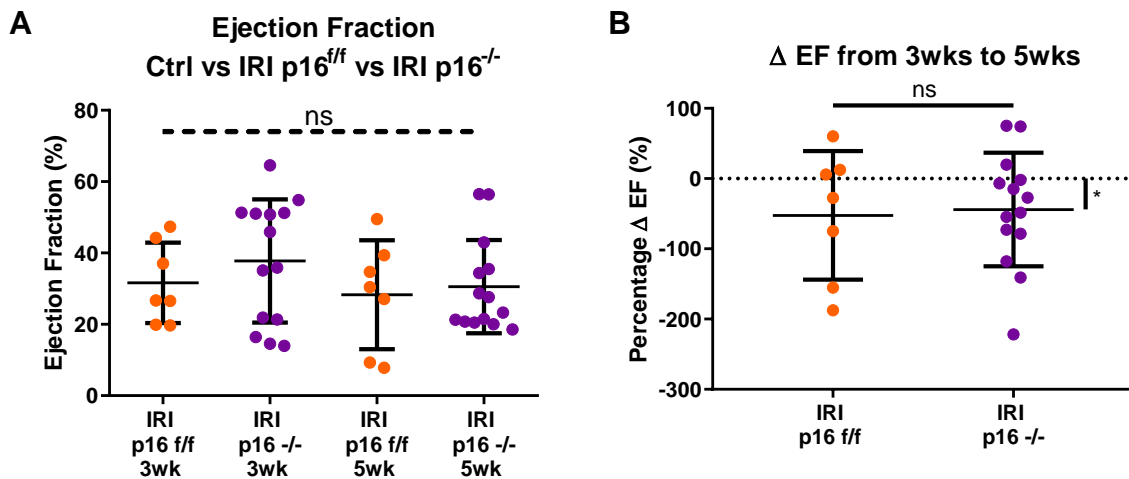


Figure 5.13 Ischaemia-reperfusion injury significantly reduces ejection fraction. Preventing $p16^{Ink4a}$ expression to reduce senescence has no effect on ejection fraction.

- A)** Data showing no significant change in EF was observed between IRI $p16^{ff}$ and $p16^{-/-}$ mice.
- B)** Quantification of the change in SV between week 3 and 5 for both the $p16^{ff}$ and $p16^{-/-}$ groups. No significant difference between the progressions of the groups was observed and neither group had a significant change in their SV from week 3 to 5.

$N=7$ and 14 for each experimental condition. $NS \geq 0.05$, $*p < 0.05$, $**p < 0.01$, $***p < 0.001$, $****p < 0.0001$ using One-Way ANOVA, Unpaired and Paired T-Test.

Overall, all variables remained unchanged with floxing $p16^{Ink4a}$ from CMs. In conclusion, $p16^{Ink4a}$ is either insufficient to inhibit CM senescence, or preventing CMs from becoming senescent is of no benefit functionally.

5.5 Transgenic model does not result in attenuated remodelling despite reduction of senescence markers

After investigating the cardiac function of these transgenic mice, I aimed to see if remodelling had been affected by floxing out $p16^{Ink4a}$ from CMs.

Samples were stained for Masson's Trichrome to assess the percentage of LV composed of infarct. In the IRI group, the infarct size was $15.83\% \pm 2.58$ of the LV and was similar to the previous cohort from chapter 4 which had an average scar size of $18.50\% \pm 2.72$. In the floxed mice, however, the region of infarct was $12.96\% \pm 5.79$ which was not significantly different ($p=0.4318$) to the control IRI group (Figure 5.14.B). This confirms that floxing $p16^{Ink4a}$ is insufficient to emulate the benefits of navitoclax at attenuating remodelling as I have demonstrated in chapter 4.

As an additional marker of remodelling, hypertrophy of the CMs was assessed (Kehat and Molkenin, 2010; Grossman and Paulus, 2013; Walaszczyk *et al.*, 2019). In healthy controls (Figure 4.16) CM area was $305.6\mu\text{m}^2 \pm 33.43$ and after IRI, CMs were hypertrophic. In this study the $p16^{ff}$ cohort had a mean area of $404.7\mu\text{m}^2 \pm 42.21$ (Figure 5.15). This measurement was comparable to the IRI cohort from Figure 4.16, which had a CM area of $412.6\mu\text{m}^2 \pm 24.29$. After $p16^{Ink4a}$ removal from the CMs, the mean CM area of the $p16^{-/-}$ mice was slightly smaller at $389.5\mu\text{m}^2 \pm 44.50$ but this was not significantly smaller than the $p16^{ff}$ group ($p=0.5936$, Figure 5.15). As both infarct size and hypertrophy measurements are unchanged after floxing $p16^{Ink4a}$ from the CMs, it indicates that this transgenic line is unable to attenuate remodelling alone.

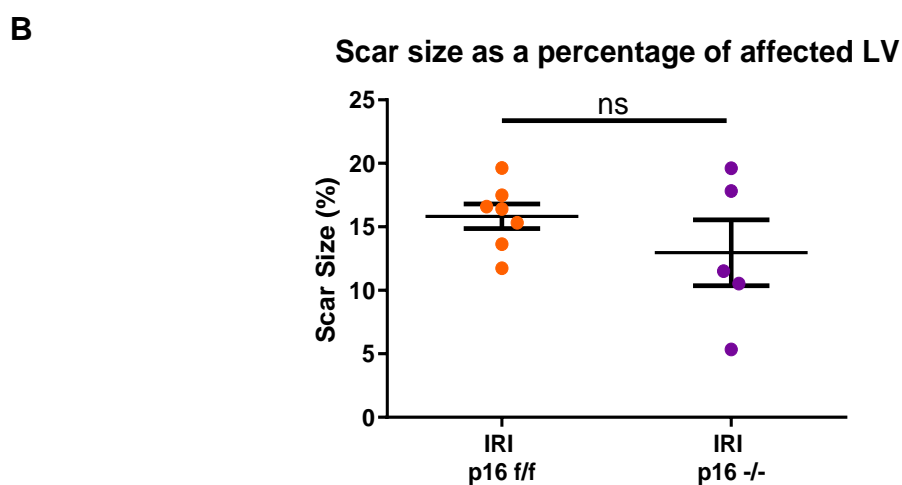
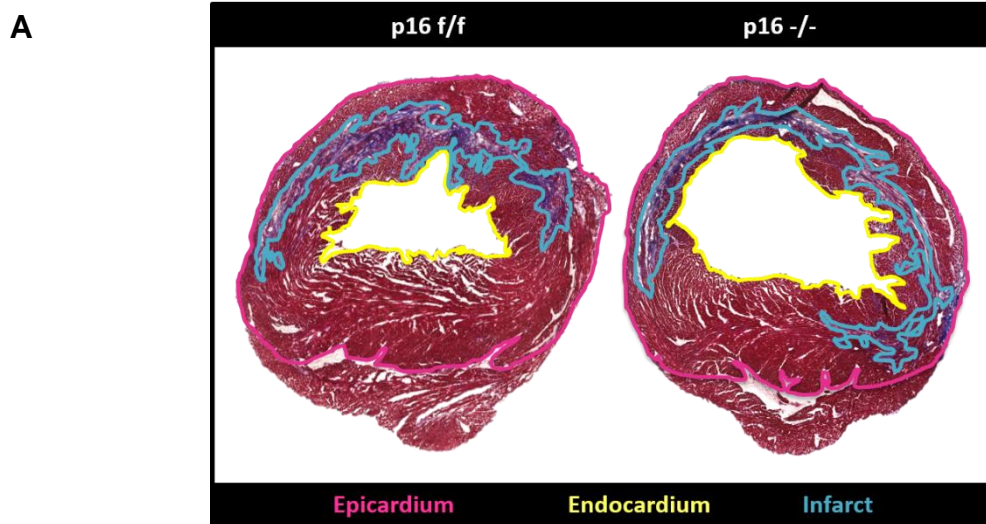
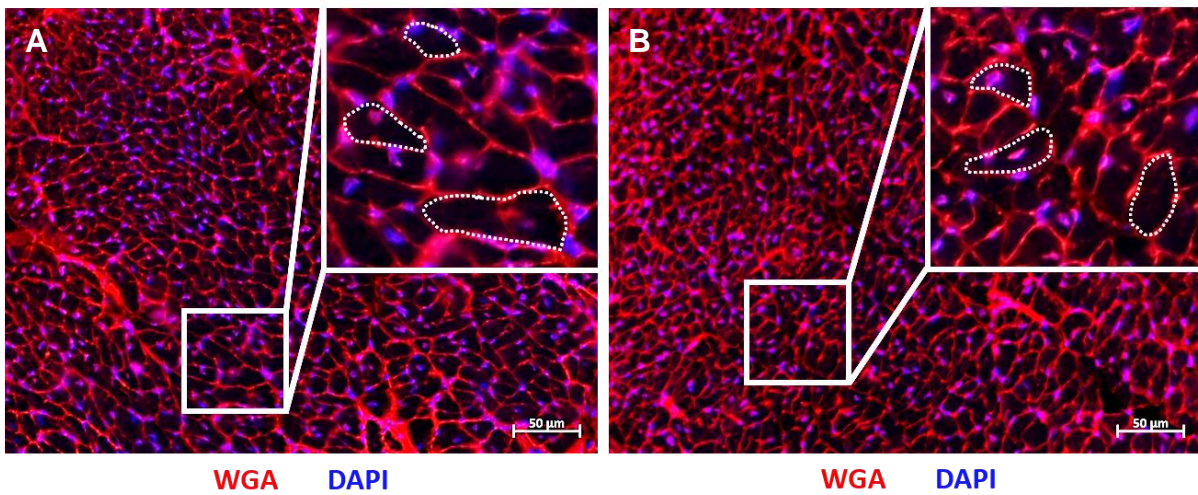


Figure 5.14 Scar size is unchanged after removal of $p16^{Ink4a}$ from cardiomyocytes.

A) Tiles of transverse sections of hearts from $p16^{f/f}$ and $p16^{-/-}$ mice post-LAD ligation stained by Masson's Trichrome. The pink line highlights the LV epicardium and the yellow line highlights the LV endocardium. From these two measurements the LV area could be calculated. The blue line denotes the area of fibrosis in the LV as identified by the blue staining. From these measurements the percentage area of the LV composed of scar could be calculated.

B) Calculated scar size as a percentage of the LV found to be not significantly different between cohorts. One $p16^{-/-}$ data point excluded according to a ROUT test for outliers.

N=5 and 7 for each experimental condition. NS \geq 0.05, * p <0.05, ** p <0.01, *** p <0.001, **** p <0.0001 using Unpaired T-Test.



C Cardiomyocyte area measurements showing changes in hypertrophy

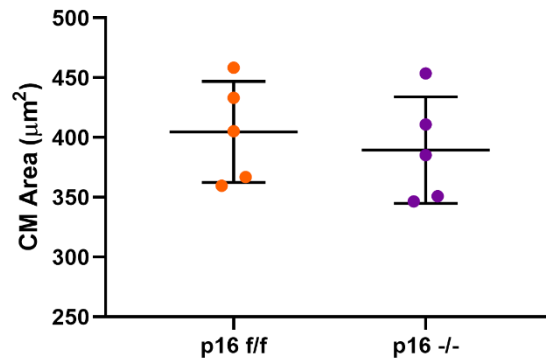


Figure 5.15 Cardiomyocyte area after inhibition of *p16^{Ink4a}* activity in the cardiomyocytes is not altered.

- A)** WGA staining (in red, wavelength 594nm) in p16^{fl/fl} heart after IRI, zoom figure shows measurements taken around CMs surrounded with 3+ capillaries so CMs in same orientation.
- B)** WGA staining (in red, wavelength 594nm) in p16^{-/-} heart after IRI, zoom figure shows measurements taken around CMs surrounded with 3+ capillaries so CMs in same orientation.
- C)** Preventing p16^{Ink4a} expression in the CM population (p16^{-/-}) does not change the CM area or reduce hypertrophy.

N=5 for each experimental condition. NS≥0.05, *p<0.05, **p<0.01, ***p<0.001, ****p<0.0001 using Unpaired T-Test.

5.6 Alternative hypothesis: persistent senescence signalling from fibroblasts may be responsible for a decline in heart function

Systemic clearance of all senescent cells pharmacologically using navitoclax improved heart function and structure (chapter 4). Yet specifically deleting $p16^{Ink4a}$ expression from CMs did not replicate any of these beneficial outcomes. This led me to hypothesise that other cell types within the heart play a greater role in adverse remodelling and it was clearance of these cell types by navitoclax that yielded benefits in terms of cardiac function and attenuation of remodelling.

By conducting SA- β -Gal staining, it appeared that there was less positive staining both within the infarct and in the CM population. Loss of these SA- β -Gal positive cells in the infarct may have an attenuated SASP which may be responsible for the observed lack of positive CMs (Figure 5.16).

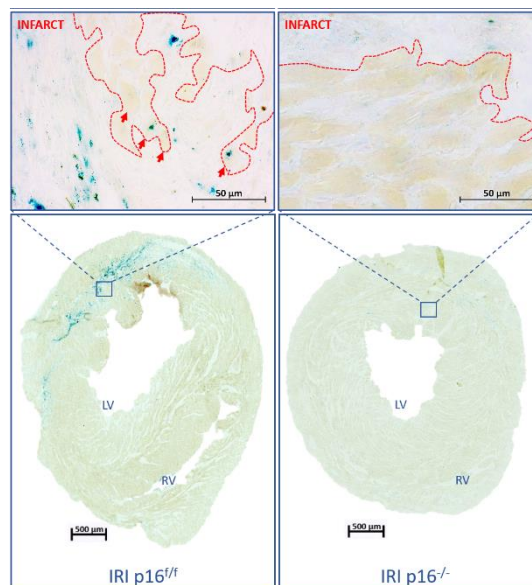


Figure 5.16 Senescence-associated β -galactosidase expression is lost in knockout mice.

At 5 weeks after IRI there is a small amount of residual SA- β -Gal staining observed in $p16^{f/f}$ mice, which is mostly within the region of infarct but some cells with a CM morphology in the BZ appeared positive. In mice without $p16^{Ink4a}$ expression, there is very little to no positive staining detected.

5.6.1 p16^{Ink4a} expression in non-cardiomyocytes is affected by preventing p16^{Ink4a} expression in cardiomyocytes

As already reported (3.3.5), expression of p16^{Ink4a} was observed within the interstitial cells. Many of these cells were also positive for the marker vimentin, also referred to as the fibroblast intermediate filament. However, vimentin is not considered to be cell-type specific and can be used as a marker for cell types other than fibroblasts including endothelial cells, macrophages, and lymphocytes amongst others (Robinson-Bennett and Han, 2006). Moreover, ischaemia can induce proliferation of cardiac endogenous mesenchymal stem cells to also express vimentin (Klopsch *et al.*, 2018).

Immunofluorescence staining with p16^{Ink4a} as carried out in 4.4.1 and 5.5.3 with the additional marker vimentin allowed for the quantification of vimentin positive cardiac cells also expressing p16^{Ink4a}. Vimentin was used as a fibroblast marker, but the possibility of cells included in the analysis being endothelial cells was considered.

From the immunofluorescence staining, the percentage of cardiac interstitial cells positive for p16^{Ink4a} was significantly higher in the p16^{f/f} group compared to p16^{-/-} group. The p16^{f/f} mice had a mean percentage of p16^{Ink4a} positive interstitial cells of 34.48% ± 5.28. Expression of p16^{Ink4a} from cells co-expressing vimentin in the p16^{-/-} mice significantly reduced (p=0.0078) to 24.29% ± 1.54 compared to the p16^{f/f} mice (Figure 5.17). This reduction in p16^{Ink4a} positive interstitial cells due to floxing of p16^{Ink4a} from the CMs implies that the CMs may have a SASP that does impact other cell types. However, the data from above suggest that it is not strong enough to be principally inducing the negative effects of senescence on the cardiac histology and function.

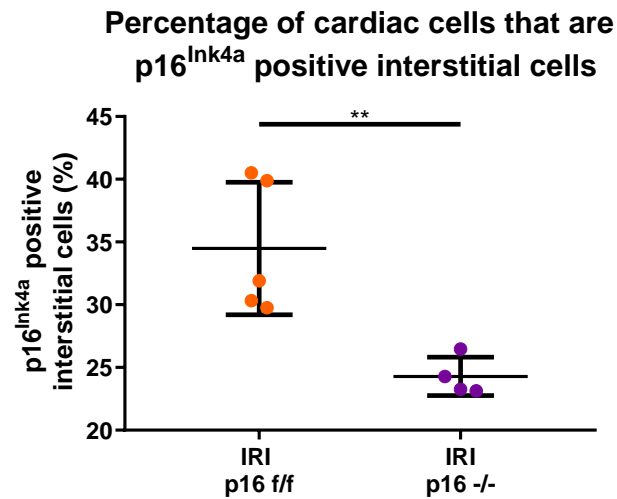


Figure 5.17 Preventing $p16^{Ink4a}$ expression in the cardiomyocytes leads to significantly fewer interstitial cells also expressing $p16^{Ink4a}$.

After IRI there are significantly more interstitial cells positive for $p16^{Ink4a}$ (data from staining in Figure 5.4). Floxing of $p16^{Ink4a}$ from CMs ($p16^{-/-}$) had the effect of significantly reducing $p16^{Ink4a}$ expression in the interstitial cells compared to the IRI cohort ($p16^{f/f}$), however, unlike navitoclax in Figure 4.7 levels were not restored to healthy baseline and remained significantly higher than the no LAD controls.

N=4 and 5 for each experimental condition. NS \geq 0.05, * p <0.05, ** p <0.01, *** p <0.001, **** p <0.0001 using Unpaired T-Test.

Therefore, a CM SASP could be important in propagating or maintaining cardiac senescence, but tests into the effects of a fibrotic SASP on CMs and other cardiac cell lineages should be investigated. The results of these studies would be important clinically, as determining the cell type chiefly responsible for the detrimental impacts of senescence and progression of adverse remodelling could allow for more targeted therapies to be developed, avoiding adverse and systemic effects of senolytics (van Deursen, 2019).

5.7 Discussion

In an attempt to understand the contribution of CM senescence to the pathophysiology of myocardial remodelling post-IRI I established a transgenic mouse model that lacked the expression of $p16^{Ink4a}$, but not $p19^{Arf}$, specifically in the CM population. Studies have shown that *Cre* inheritance from the maternal line can lead to a mosaic-pattern of recombination (Hayashi *et al.*, 2002; Heffner *et al.*, 2012). This can occur as in maternally-derived germline cells, the zygotes, *Cre* protein can accumulate and if fused with a sperm containing a floxed allele, recombination can aberrantly and prematurely occur from embryogenesis regardless of whether the zygote contains the *Cre* transgene (Hayashi *et al.*, 2002; Vincent and Robertson, 2003; Heffner *et al.*, 2012). To avoid this, only male *Cre* mice were used for breeding.

To validate the model and provide evidence that in this transgenic line $p16^{Ink4a}$ expression was absent from the CM population my initial analysis of senescence markers focused on the expression of $p16^{Ink4a}$. In $p16^{f/f}$ mice, which have the $p16^{Ink4a}$ floxed allele, but lacked *Cre* expression, the expression of $p16^{Ink4a}$ was at a similar level to the post-IRI wild type mice. In the $p16^{-/-}$ cohort, $p16^{Ink4a}$ levels were considerably lower. Specifically, in the CMs, $p16^{Ink4a}$ expression was reduced by 67% in the $p16^{-/-}$ animals compared with $p16^{f/f}$ littermate controls. This reduction in expression is consistent with the efficiency of the *MerCreMer*, as reported in the literature (Sohal *et al.*, 2001; Malliaras *et al.*, 2013).

Having demonstrated that $p16^{Ink4a}$ was reduced in the CM population I evaluated the effect this had on recovery to IRI. Overall, preventing the transcription of $p16^{Ink4a}$ within the CMs specifically led to no differences in any of the variables of cardiac function that were investigated.

Ejection fraction correlates to cardiac function and diagnosis of heart failure. A reduced EF is linked to a worse long-term outcome for patients, and as mortality rates post-MI 5 years after MI is approaching 50%, methods to improve EF are essential (Jones *et al.*, 2019). The response to navitoclax treatment was promising, however, the $p16^{-/-}$ mice did not demonstrate the same improvement in EF as navitoclax treated mice. Instead the $p16^{-/-}$ mice demonstrated a substantial decrease in EF between the time-points investigated and as such responded to IRI in a similar manner to both $p16^{f/f}$ mice

and wild type controls. Furthermore, no difference was observed in the EF of either p16^{fl/fl} or p16^{-/-} mice at either the 3 or 5 week time-point.

As with the navitoclax treatment, the p16^{-/-} mice showed no considerable change in EDV post-LAD between the cohorts, as well as no differences in ESV or SV at either time-point. So overall, p16^{Ink4a} expression in CMs does not affect systolic volume or function.

Although I observed no change in function in the p16^{Ink4a} knockout mice, it is possible that in this model cellular changes occur in the transgenic mice hearts but are insufficient to improve function. However, in my studies of myocardial remodelling, I found no differences between p16^{-/-} and p16^{fl/fl} mice in terms of infarct size and CM hypertrophy. In addition, the infarct which formed post-LAD ligation was of a comparable size to wild type mice following IRI. As infarct size was not smaller after p16^{Ink4a} was floxed from CMs, this may explain why there were no functional improvements. If the level of fibrosis was not reduced then the heart would likely have reduced elasticity, affecting its systolic function and recovery to contraction, in turn affecting CO and EF (Maekawa *et al.*, 2004). This result also opposes the hypothesis that post-IRI CM drives fibrosis via production of the SASP but rather suggests that fibrosis occurs independently of CM senescence and SASP.

Hypertrophy was also unchanged with the removal of p16^{Ink4a} from CMs. These data are particularly interesting as previous studies observed in aged mice that the CMs containing TAF are the most hypertrophic (Anderson *et al.*, 2019) and studies have also demonstrated that clearance of senescent cells from aged mice reduces hypertrophy (Childs *et al.*, 2018; Anderson *et al.*, 2019; Walaszczyk *et al.*, 2019). It is possible that senescence itself does not drive hypertrophy but rather may simply be associated with hypertrophy. As such, in this model the lack of p16^{Ink4a} has no influence on this aspect of remodelling. However, as I also saw no change in hypertrophy in my study with navitoclax, another explanation is that different mechanisms contribute to hypertrophy in the different settings, with senescence contributing to hypertrophy during ageing but not in response to injury. Therefore, other markers of senescence were investigated to ensure that p16^{Ink4a} expression was reduced and that CMs weren't activating a compensatory senescence pathway.

A marker used for senescence detection and quantification are TAFs (Hewitt *et al.*, 2012). From this cohort, TAF levels and percentage of CMs positive for TAFs were unchanged between the groups. This is likely because DNA damage, including TAFs, lie upstream of p16^{Ink4a} and p21^{Cip} activation (Childs *et al.*, 2015), and therefore floxing *p16^{Ink4a}* would not affect the induction of TAF. This result suggests that in this model, TAF generation results from stressors such as OS, and stimulate senescence as opposed to being a consequence of senescence.

Take together these data suggest that lack of *p16^{Ink4a}* expression in the CM population has no effect on the functional outcomes to IRI. In addition, these data may also suggest that in the navitoclax study the clearance of *p16^{Ink4a}* expressing senescent CMs may not play a major role in the observed improved function. However, there are alternative explanations for this.

It is possible that absence of *p16^{Ink4a}* alone may not be sufficient to inhibit CM senescence. My data showed that in the p16^{-/-} mice, the levels of p21^{Cip} were also reduced in comparison to the p16^{fl/fl} mice. This reduction indicated that absence of *p16^{Ink4a}* in the CM population attenuates both the p16^{Ink4a} and p21^{Cip}/p53 arms of the senescence pathway. However, the number of cells expressing p21^{Cip} remained higher than the number of p16^{Ink4a} expressing cells in the *p16^{Ink4a}* knockout mice with nearly 15% of CMs still expressing p21^{Cip}. Previously, it has been demonstrated when using the same Cdkn2atm2.1Nesh line as used in my study, both knockout of *p16^{Ink4a}* and *p53* were required to induce tumour formation in skin (Sharpless *et al.*, 2002). While these data illustrate that senescence is a multifactorial process that has a degree of redundancy, this is not indicative of senescence. It is well established that senescence can be initiated independently through either the p21^{Cip} and p16^{Ink4a} pathway (Prieur *et al.*, 2011). It is also possible that after genotoxic stress resulting from IRI, the p21^{Cip} pathway is more involved in the activation of senescence in the CMs than p16^{Ink4a}. Moreover, it has been shown that the p16^{Ink4a} and p53 pathways feedback on one-another (Leong *et al.*, 2009). In *p53*-knock down mouse fibroblasts, p16^{Ink4a} expression was up-regulated, and infecting cells with wild type p53 restored p16^{Ink4a} levels. However, in *p16^{Ink4a}* deficient cells, the effect on p53 levels was much smaller, suggesting that these pathways interact to limit cell proliferation (Leong *et al.*, 2009). Re-introducing p16^{Ink4a} in my p16^{-/-} mice after IRI to see if there was an effect on p21^{Cip} expression would be interesting to further dissect whether there was a feedback

mechanism between these two pathways. Regardless, with p21^{Cip} being activated in p16^{-/-} mice, this could highlight a flaw of this novel transgenic model. If senescence is being induced via the p21^{Cip} pathway in CMs directly, although attenuated by the lack of p16^{Ink4a}, then the model is not fully preventing CM senescence and their potential SASP to the degree expected.

Further complicating my findings is the possibility that a SASP from neighbouring senescent non-CMs was exerting detrimental effects, such as hypertrophy, on CMs irrespective of whether CMs could activate the p16^{Ink4a} pathway themselves.

To confirm the result from the p16^{Ink4a} immunofluorescence staining and validate both the antibody for p16^{Ink4a} and efficiency of this transgenic line, RNAscope was performed for p16^{Ink4a}. Once levels had been normalised to the negative control background, RNA p16^{Ink4a} levels were 1.65-fold higher than protein levels. This discrepancy between mRNA and protein levels may result from regulatory post-transcriptional mechanisms including modifications and degradation (Cho *et al.*, 2016; Chan *et al.*, 2018). The ratio between mRNA and protein content varies between tissue types (Chan *et al.*, 2018), and should be further analysed for cardiac tissue. Additionally, the *Cdkn2a* gene on chromosome 9p21 contains two reading frames that encode for two tumour suppressor genes, the first being p16^{Ink4a} that is transcribed from exons 1 α , 2 and 3, and the second being p19^{Arf} (p14^{ARF} in humans) that uses exon 1 β , which is located 20kb upstream of exon 1 α , and shares exon 2 with p16^{Ink4a} (Rayess *et al.*, 2012). The probe used for this analysis predominantly binds to regions within exon 1 α , however, could also bind to part of exon 2 and therefore potentially detect both transcripts. The resulting increased levels of mRNA could be in part be due to the detection of p19^{Arf} as well as p16^{Ink4a}. Regardless, as the fluorescent probe requires two target Z probes bound to the target region, RNAscope has been described as a specific and robust technique (Bingham *et al.*, 2017). Therefore, these data validate the specificity of the p16^{Ink4a} antibody and confirms that the floxed transgenic mouse did reduce p16^{Ink4a} in CMs.

The p16^{Ink4a} knockout also resulted in a small but substantial reduction in the expression of p16^{Ink4a} in the interstitial cell population. This response suggests that the CMs may have a small SASP that induces cell senescence in this population, although at a level that is insufficient to attenuate scar formation.

Also I was unable to include functional analysis of naive or sham p16^{-/-} and p16^{ff/ff} mice. Unfortunately, this was a result of time restraints and technical problems with the MRI equipment. Initially, establishment of the double transgenic lines took considerable time as the *Myh6-MerCreMer* line appears to breed slower and have smaller litters than wild type mice (Werfel *et al.*, 2014). While I did breed mice for MRI analysis of baseline cardiac function as the final experiments to complete my project, the MRI scanner quenched in July and remains out of service. The repair is scheduled to take place at the beginning of next year. If my studies had demonstrated differences in any variables of function or remodelling in the p16^{Ink4a} knockout, additional tamoxifen controls should have been performed. To ensure that the tamoxifen had no effects on function or histology, p16^{ff/ff}Cre⁺ mice would have had an IRI without tamoxifen treatment. However, as both p16^{-/-} and p16^{ff/ff} cohorts received tamoxifen this in part controls for the effects of tamoxifen and no difference was observed between the either experimental group in this study. In keeping with the 3Rs (Sneddon *et al.*, 2017), I saw no reason to subject additional mice to IRI as these data would add little to my findings.

If my studies were to continue there are possibly alternative approaches that could be used to reduce the time needed to perform similar studies. A group has published data on utilising an adeno-associated viral vector of serotype 9 that contains the *loxP* gene and can be directly inserted after injection intravenously and only requires one dose to induce recombination (Werfel *et al.*, 2014). Although when using a cardiac specific promoter there was a high efficiency of recombination in CMs, this technique did result in off-target effects, with recombination detected in the liver, lung and blood vessels (Werfel *et al.*, 2014).

So by addressing the issue of timing, this study highlighted a second general problem with *Cre* lines: off-target effects (Heffner *et al.*, 2012). However, the *Myh6-MerCreMer* line has been extensively tested in both embryos and adult hearts and showed that in the embryo, recombination as detected by β -galactosidase staining was restricted to the heart, and in adult tissues expression was only observed in the heart and not the aorta or pulmonary artery (Yan *et al.*, 2015). Crossing this *Cre* line with a reporter line also resulted in recombination only in cells co-expressing troponin T, an alternative CM marker, and not α -SMA positive, marker for smooth muscle, or PECAM, also known as CD31 an endothelial marker, positive cells. Additionally, in hearts expressing *Cre* that hadn't be dosed with tamoxifen showed a very low expression level of β -

galactosidase confirming that this line has negligible “Cre leakiness” (Yan *et al.*, 2015). Overall, these studies provide evidence that off-target effects do not represent a problem when using the *Myh6-MerCreMer* transgenic line.

It would also be possible to create a *Cre* knockout which may circumvent issues surrounding the efficiency of tamoxifen-inducible models. By using a *Cre* expressed in a specific cell population during embryogenesis this would result in the gene of interest not being expressed throughout life. For example, *Nkx2.5* or *troponin T* *Cre* lines could be used to knockout a gene permanently in the CM population (Iannello *et al.*, 1991; Moses *et al.*, 2001; Zhou *et al.*, 2013; Ranjbarvaziri *et al.*, 2017). However, as senescence has been shown to be important for development in a number of organs including the brain, neural tube, gut endoderm as well as digit formation (Muñoz-Espín *et al.*, 2013; Munoz-Espin and Serrano, 2014; Da Silva-Álvarez *et al.*, 2019), it is possible that senescence also plays a role in myocardial development. As such this type of developmental knockout could be associated with embryonic lethality or severe abnormalities depending on the gene targeted (Hong *et al.*, 2006; Feil *et al.*, 2009). Although, this in itself may be of interest scientifically.

Based on the data obtained in this chapter I hypothesised that clearance of senescent cardiac fibroblasts may be the primary mechanism by which navitoclax improves recovery post-IRI. This could contribute to attenuated fibrosis and a reduction in a pro-fibrotic SASP ultimately resulting in a smaller scar and improved cardiac function that was observed in the previous chapter. Therefore, the contributions of a fibrotic SASP to IRI pathogenesis should be further investigated.

Chapter 6. Interstitial cell senescence is postulated to exert a greater effect on the heart post-ischaemia-reperfusion injury

6.1 Introduction

My data thus far demonstrates that MI with IRI leads to an environment of OS, which induces DNA damage leading to a state of senescence in the myocardium. Clearance of senescent cells by navitoclax resulted in restored cardiac function and reduced infarct size, however, targeting only senescent CMs did not reproduce this pharmacologically-generated improvement.

In the heart, the majority of the mass is comprised of CMs, although they only account for roughly 30% of total cardiac cells. The composition of non-CM cardiac cells includes fibroblasts, endothelial cells and haematopoietic cells (Camelliti *et al.*, 2005; Nagalingam *et al.*, 2016; Pinto *et al.*, 2016). After injury including MI, fibroblasts are essential to deposit collagen and generate a scar to avoid cardiac rupture (Rouillard and Holmes, 2012; Chen and Frangogiannis, 2013). My findings support data from other researchers such as Zhu, F. *et al.* that have reported in the infarct the senescent cells primarily consist of fibroblasts (Zhu *et al.*, 2013). It has also been demonstrated that this OS induced fibroblast senescence acts to self-limit fibrosis and excessive collagen generation. This was suggested to be in part due to activation of the p21^{Cip}/p53 pathway leading to fibroblasts exiting from the cell cycle limiting proliferation and collagen disposition, as p53-deficient mice demonstrated to have larger infarcts post-MI (Zhu *et al.*, 2013). These data are consistent with studies that have demonstrated in young healthy mice senescence is required for optimal wound healing to injury to the skin and liver (Krizhanovsky *et al.*, 2008; Jun and Lau, 2010b; Demaria *et al.*, 2014). In terms of cutaneous injury, preventing senescence via the p16^{Ink4a} pathway or both p16^{Ink4a}/p21^{Cip} in mice delayed wound repair. This was due to myofibroblast numbers being depleted as fibroblasts were unable to secrete a SASP, including the SASP factor platelet derived growth factor (Pdgf) -AA, to activate myofibroblast differentiation which would lead to granulation and closure of the wound (Demaria *et al.*, 2014). In the heart, the study by Zhu, F. *et al.* also highlighted the importance of a fibrotic SASP activated via the p21^{Cip}/p53 pathway in regulating efficient fibrosis and inflammatory signalling after infarct (Zhu *et al.*, 2013). These data

suggest that long-term activation of the senescence pathways within the fibroblast population and increased SASP expression could promote chronic inflammation that contributes to the ongoing collagen deposition and fibrosis formation after MI.

In chapter 4 the study by design aimed to use navitoclax to clear senescent cells from the heart from a time-point after senescence had been established. Together with the fact that navitoclax should only cause apoptosis in senescent cells, have no impact on the development of senescence, the CM specific *p16^{Ink4a}* knockout model in chapter 5 lacked a phenotype, and the observed reduction in infarct size post-treatment led to following hypothesis. The observed beneficial effects of navitoclax were due to the elimination of the senescent fibroblasts and myofibroblasts in the infarct and thereby a reduction in inflammation via attenuation of the SASP.

In this chapter, I aimed to investigate the effect of navitoclax on the fibroblast population, to ascertain if elimination of senescent cells post-MI with IRI affected SASP expression *in vivo* and to establish if the fibroblast SASP could be detrimental to recovery following MI with IRI (Figure 6.1).

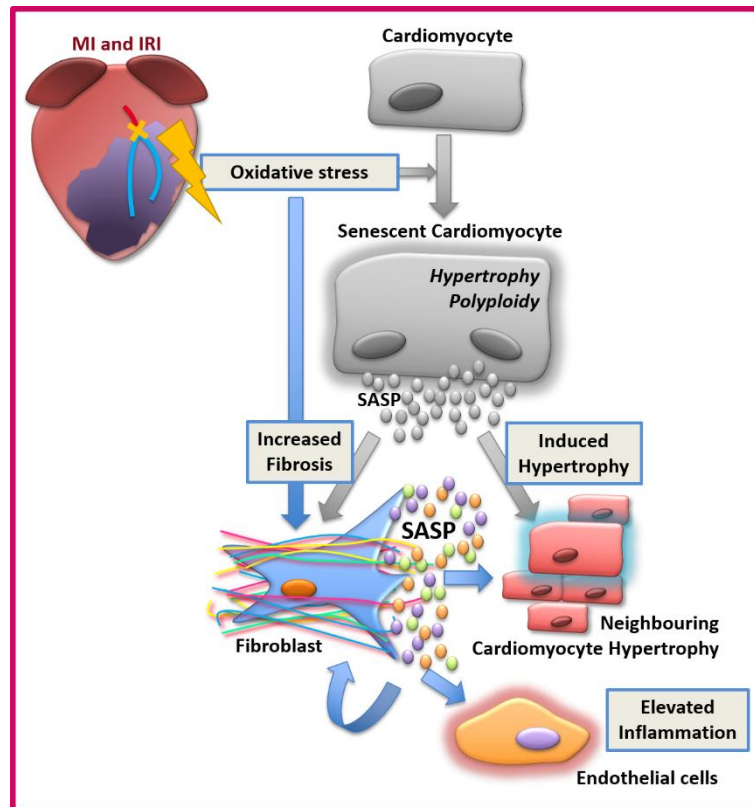


Figure 6.1 Graphical hypothesis.

Cardiac senescence post-MI with IRI is affecting the fibroblast population. Fibroblast senescence is important for wound repair, but chronic senescence activation and SASP production increases the level of cardiac fibrosis, induces senescence in the CM population and increases inflammation to limit angiogenesis.

6.2 *In vitro* irradiated fibroblasts are senescent and clearance by navitoclax is targeted to senescent cells

I next performed a similar experiment to 4.2 using the MRC5 fibroblast line. As previously described, MRC5 fibroblasts were induced to senescence using 10Gy X-ray irradiation, which was validated with SA- β -Gal staining at 12 days post-treatment. Sham irradiated MRC5s were used as a proliferative control. Given the previously published dose effects for navitoclax on an alternative fibroblast cell line, the IMR90 line (Zhu et al., 2016), I limited the treatment of MRC5s to 3 difference doses of navitoclax (0 μ m, 1.5 μ m, 5.0 μ m). As with H9C2 cardiomyoblasts, and previously published data by others using alternative fibroblast lines, navitoclax selectively reduced the viability of senescent and not proliferative MRC5s ($p=0.0026$ for 1.5 μ M and 0.0011 for 5 μ M, Figure 6.2) (Zhu *et al.*, 2016; Anderson *et al.*, 2019).

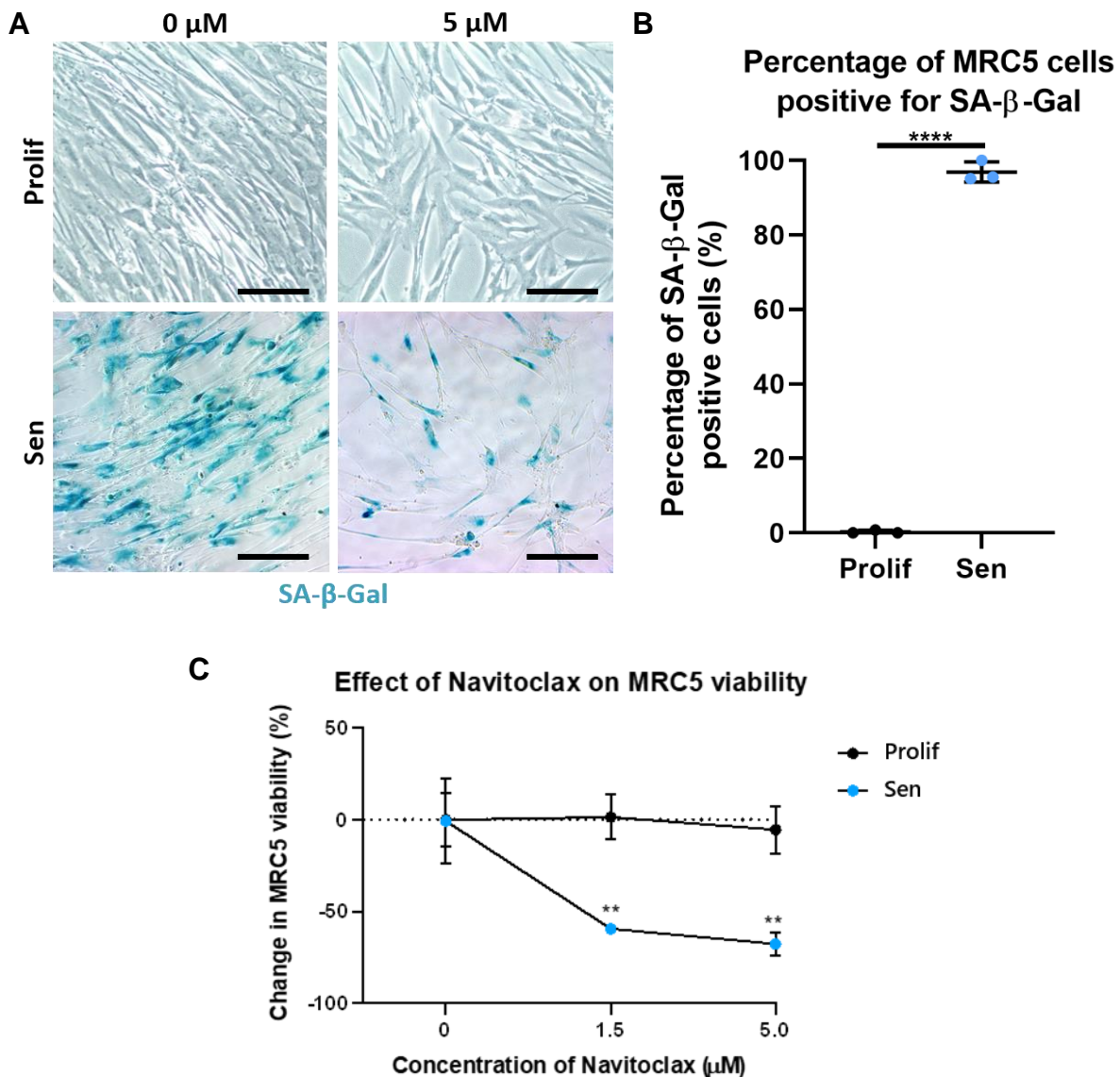


Figure 6.2 Treatment with navitoclax specifically reduces the viability of senescent (irradiated) MRC5 cultures that are positive for senescence-associated β -galactosidase. Navitoclax has no effect on the viability of healthy, proliferative (non-irradiated) MRC5s.

- A)** SA- β -Gal staining. Top row shows no positive staining or change in cell density in proliferative culture, both untreated and 5 μ M navitoclax treated. Bottom row shows positive staining in senescent culture and reduced cell density in culture treated with 5 μ M navitoclax. Scale bar equal to 50 μ m.
- B)** Percentage of proliferative and senescent MRC5s positive for SA- β -Gal.
- C)** MRC5 percentage viability is stable in proliferative group with all doses of navitoclax. Senescent MRC5 cultures show a dose dependent reduction in cell viability.

N=3 for each experimental condition. To control for ongoing proliferation and cell death as a result of irradiation, viability for each condition (proliferative or irradiated) was calculated relative to the number of cells in the untreated culture for that condition. NS \geq 0.05, * p <0.05, ** p <0.01, *** p <0.001, **** p <0.0001 using Two-Way ANOVA.

6.3 A fibroblast senescence-associated secretory phenotype influences the biology of different cardiac lineages *in vitro*

To investigate if the fibroblast SASP could impact the biology of other cell lineages in the myocardium in a detrimental manner post-IRI, conditioned media culture experiments were performed. Conditioned media was obtained as outlined in 2.10.4 from irradiated MRC5s and isolated primary murine CFs. This media was then transferred onto healthy, proliferative cultures of the endothelial cell line, MMVEC-Cs, or isolated primary murine embryonic CMs as described in Figure 2.6.

6.3.1 Conditioned media from senescent MRC5 fibroblasts inhibits endothelial cell proliferation and leads to senescence marker expression

Senescent cells and the SASP have been shown to attenuate proliferation and induce senescence in surrounding cells through the by-stander effect (Ritschka *et al.*, 2017; McHugh and Gil, 2018). To study the influence of the fibroblast SASP on endothelial cell function, I first quantified the proliferation of MMVEC-C cells cultured in media from either proliferating or senescence MRC5 fibroblasts. Ki67 protein is only expressed during proliferation, specifically the G1, S, G2 and M phases of the cell cycle and is not detectable during cell cycle arrest, and therefore is a widely used marker of proliferation (Li *et al.*, 2015; Juríková *et al.*, 2016). Following 3 days of culture the percentage of MMVEC-Cs positive for Ki67 in the proliferative conditioned media was 65.58% \pm 14.52. This was significantly lower ($p=0.0143$) when MMVEC-Cs were cultured with media from senescent fibroblasts for the same duration, with Ki67 expression reduced to 23.21% \pm 10.10 total cells (Figure 6.3.A-C).

As equal numbers of MMVEC-Cs were seeded ($5 \times 10^2/\text{mm}^2$), the total number of cells following 5 days of culture in media from proliferative or senescent fibroblasts were quantified to also assess cell proliferation. Significantly more endothelial cells were produced from the proliferative fibroblast media cultures compared to those cultured in media from senescent cells (4.07×10^3 cells/ $1\text{mm}^2 \pm 0.37$ vs 1.14×10^3 cells/ $1\text{mm}^2 \pm 0.41$, $p=0.0008$, Figure 6.3.D), supporting the trend observed with Ki67 expression in these cultures.

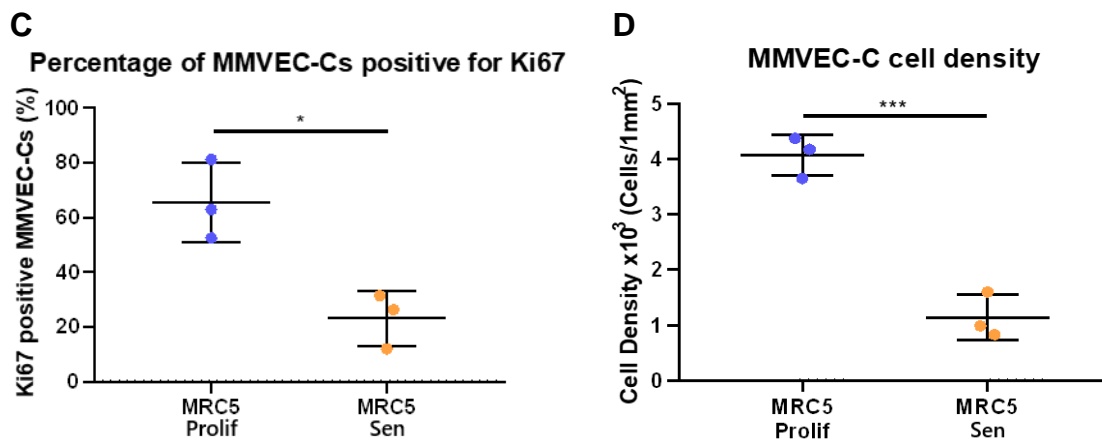
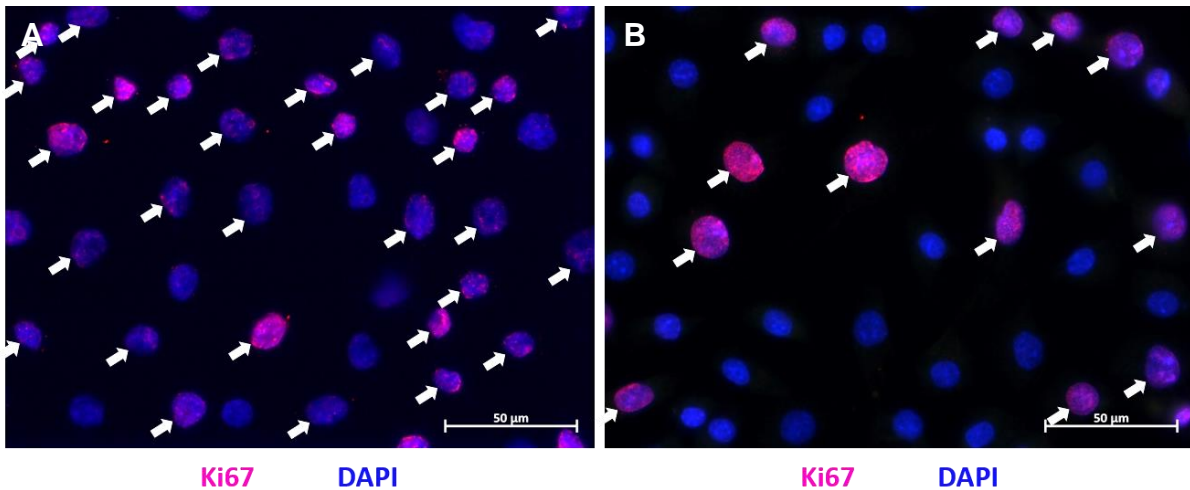


Figure 6.3 Proliferation of MMVEC-Cs is significantly reduced when exposed to irradiated MRC5 conditioned media.

- A) Image shows Ki67 expression in proliferative MMVEC-Cs treated with conditioned media from proliferative MRC5s.
- B) Image shows Ki67 expression in proliferative MMVEC-Cs treated with conditioned media from senescent MRC5s.
- C) Graph quantifying Ki67 expression in MMVEC-Cs. The percentage of MMVEC-Cs positive for Ki67 is significantly decreased following culture in irradiated MRC5 media.
- D) Graph shows the MMVEC-C cell density counts. MMVEC-C cells in proliferative MRC5 conditioned media proliferated at a significantly higher rate compared to cultures with irradiated MRC5 conditioned media.

N=3 for each experimental condition. NS≥0.05, *p<0.05, **p<0.01, ***p<0.001, ****p<0.0001 using Two-Tailed T-Test.

Next to see if the reductions in proliferation was due to increased senescence I studied the expression of both p16^{Ink4a} and p21^{Cip}. The relative expression of p16^{Ink4a} was unchanged between the MMVEC-Cs treated with proliferative and senescent conditioned media from MRC5 fibroblasts (1.00 ± 0.11 in proliferative media compared to 1.04 ± 0.19 in senescent media, p=0.7878, Figure 6.4.A). However, there was a significant increase (p=0.0006) in p21^{Cip} relative expression from MMVEC-Cs following culture in senescent conditioned media (3.80 ± 0.48, Figure 6.4.B) compared to proliferative media (1.01 ± 0.13, Figure 6.4.B). Therefore, the SASP from fibroblasts reduces endothelial cell proliferation and is associated with an upregulation of the senescent marker p21^{Cip}.

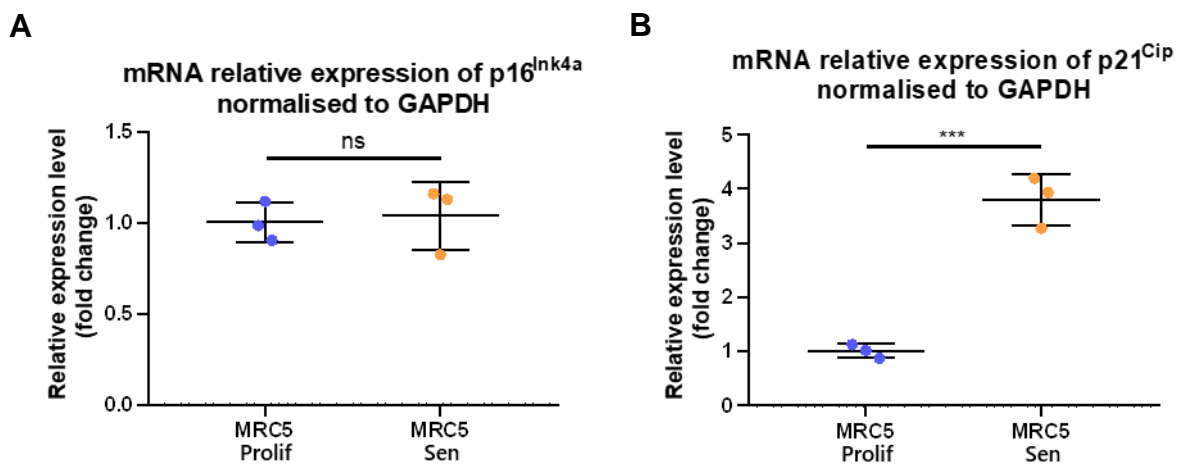


Figure 6.4 Expression of the senescence marker p21^{Cip} was significantly upregulated in MMVEC-C cells following exposure to conditioned media from irradiated senescent MRC5s.

- A)** Graph shows the relative expression of p16^{Ink4a} was unchanged between the conditioned media from proliferative MRC5s and senescent MRC5s containing a SASP.
- B)** Graph shows the relative expression of p21^{Cip} was significantly higher after culture in conditioned media from senescent MRC5s containing a SASP.

N=3 for each experimental condition. NS≥0.05, *p<0.05, **p<0.01, ***p<0.001, ****p<0.0001 using Two-Tailed T-Test.

Endothelial dysfunction has been associated with ageing, thrombosis, inflammation and heart failure amongst many other systemic disorders, and OS is frequently attributed to premature endothelial senescence the pathophysiology of endothelial dysfunction (Félétou and Vanhoutte, 2006; Bhayadia *et al.*, 2015; Khan *et al.*, 2017). Moreover, endothelial dysfunction has also been shown to be associated with increased ROS, superoxide production and increased OS (Hasdan *et al.*, 2002; Incalza *et al.*, 2018).

To assess if the fibrotic SASP that attenuated proliferation and increased senescence was associated with increased superoxide production, MMVEC-Cs after 5 days of culture in the conditioned media were stained with DHE. Dihydroethidium is a superoxide probe that generates a fluorescent product when oxidised by superoxides (Zhao *et al.*, 2005; Peshavariya *et al.*, 2007; Zhong *et al.*, 2010; Fernandes *et al.*, 2017). An example of DHE staining on MMVEC-Cs is shown in Figure 6.5.A-B. Quantification of the intensity of the fluorescence demonstrated a significantly higher level in the MMVEC-Cs treated with the media from irradiated MRC5s in comparison to the proliferative MRC5 media. The mean fluorescence intensity from the proliferative MRC5s was $15.12\text{AU} \pm 0.24$ but was more than doubled to $37.06\text{AU} \pm 8.294$ from irradiated MRC5 media ($p=0.0102$, Figure 6.5.C). This result demonstrated that a senescent fibroblast SASP induces superoxide formation from endothelial cells in a paracrine fashion.

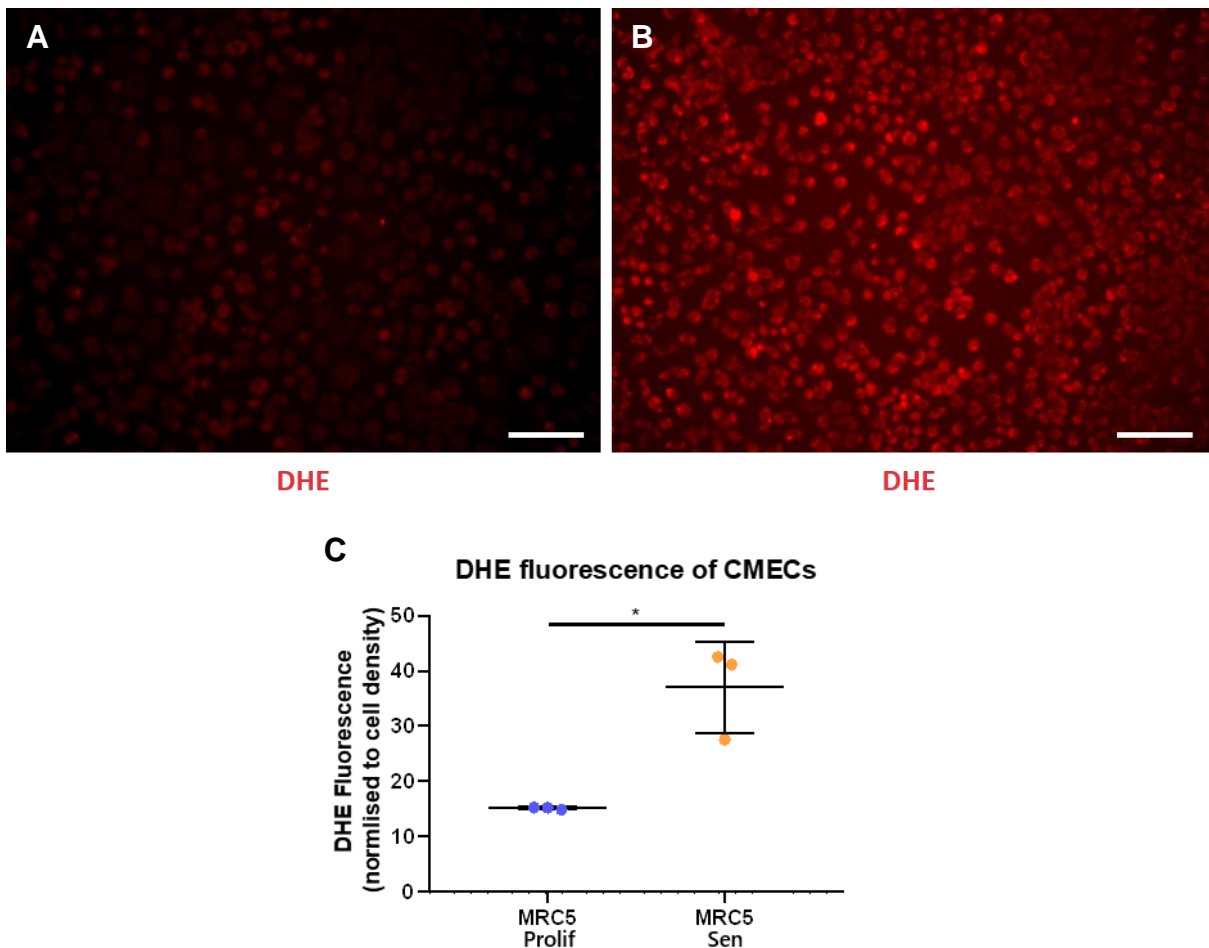


Figure 6.5 Irradiation of MRC5 cells significantly increases generation of the oxidative stress marker dihydroethidium in a paracrine fashion in MMVEC-C cell cultures.

- A)** Representative image from proliferative MMVEC-Cs treated with conditioned media from proliferative MRC5s. Red fluorescence equates to OS levels by superoxide.
- B)** Representative image from proliferative MMVEC-Cs treated with conditioned media from senescent MRC5s. Red fluorescence indicates OS elevated.
- C)** Graph quantifying fluorescence intensity normalised to cell density. Intensity is significantly increased in the culture with irradiated MRC5 media.

N=3 for each experimental condition. NS \geq 0.05, * p <0.05, ** p <0.01, *** p <0.001, **** p <0.0001 using Two-Tailed T-Test. Scale bar equal to 75 μ m.

6.3.2 Both irradiated MRC5 and primary cardiac fibroblast conditioned media constrains embryonic cardiomyocyte proliferation and triggers cardiomyocyte senescence

Having demonstrated that culture in conditioned media from irradiated MRC5 fibroblasts negatively reduced the proliferation of endothelial cells *in vitro* and was associated with an upregulation of the senescence marker p21^{Cip} and the superoxide marker DHE, conditioned media experiments were repeated to assess the effects of a fibrotic SASP on CMs.

It has been previously demonstrated that post-MI the heart can initiate a limited regenerative response including CM proliferation (Malliaras *et al.*, 2013), however, this mechanism is insufficient to fully repair the heart (Foglia and Poss, 2016). Previously it has been reported that the SASP generated from aged CMs inhibited the proliferation of neonatal fibroblasts and resulted in elevated expression of SA- β -Gal (Anderson *et al.*, 2019). Moreover, the regenerative potential of CMs declines with age (Bergmann *et al.*, 2015) and data from aged mice show that clearance of senescent cells, either using the Ink-ATTAC mouse or by navitoclax dosing, attenuated the SASP and promoted cardiac regeneration (Anderson *et al.*, 2019). Therefore, after MI with IRI a fibrotic SASP may negatively influence CM proliferation.

To ascertain if the fibroblast SASP could influence CM proliferation, primary CMs were isolated from mouse embryo hearts and cultured with conditioned media from proliferative or irradiated fibroblasts. For these experiments, two different fibroblast types were used: MRC5 fibroblasts as above; but also primary cardiac fibroblasts isolated from adult mouse hearts.

Ki67 was utilised to assess proliferation of the embryonic CMs. The conditioned media from both fibroblast types significantly reduced ($p=0.0053$) CM proliferation. Following 5 days of culture in the conditioned media from proliferative MRC5s, 20.82% \pm 2.79 of troponin C expressing CMs were positive for Ki67. At the same time-point proliferation of the CM cultures was significantly decreased to 11.58% \pm 0.80 when CM were treated with media from the senescent MRC5s.

When cultured in media from proliferative and irradiated primary adult CFs, the expression of Ki67 demonstrated similar trends (28.50% \pm 7.82 vs 11.66% \pm 0.97, $p=0.0207$, Figure 6.6) to the MRC5 media conditions, where there was a higher

percentage of CMs Ki67 positive following culture in the proliferative media from non-irradiated CFs.

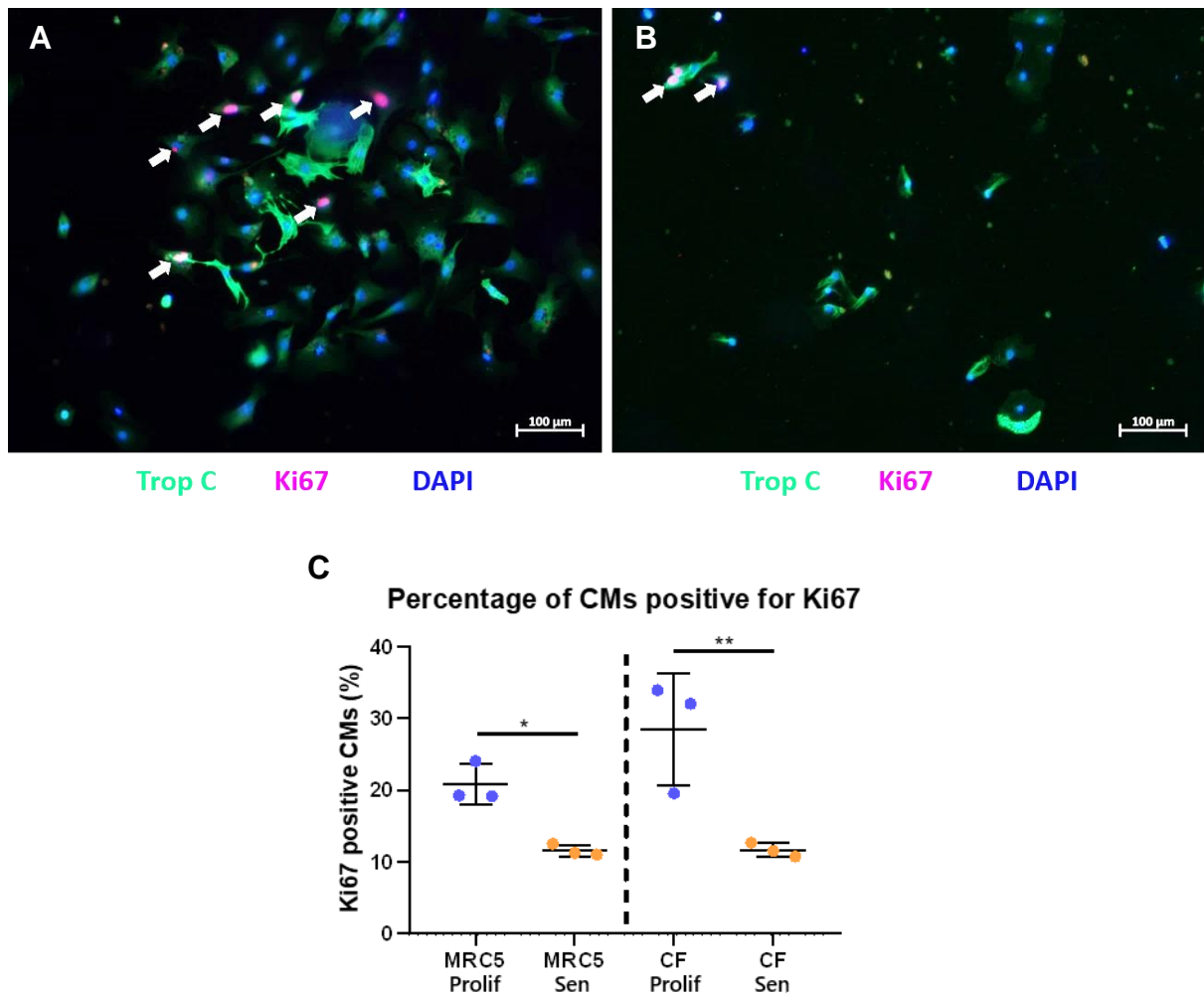


Figure 6.6 The senescence-associated secretory phenotype generated from cardiac fibroblasts is comparable to MRC5 fibroblasts, as both significantly reduce proliferation of isolated embryonic cardiomyocytes.

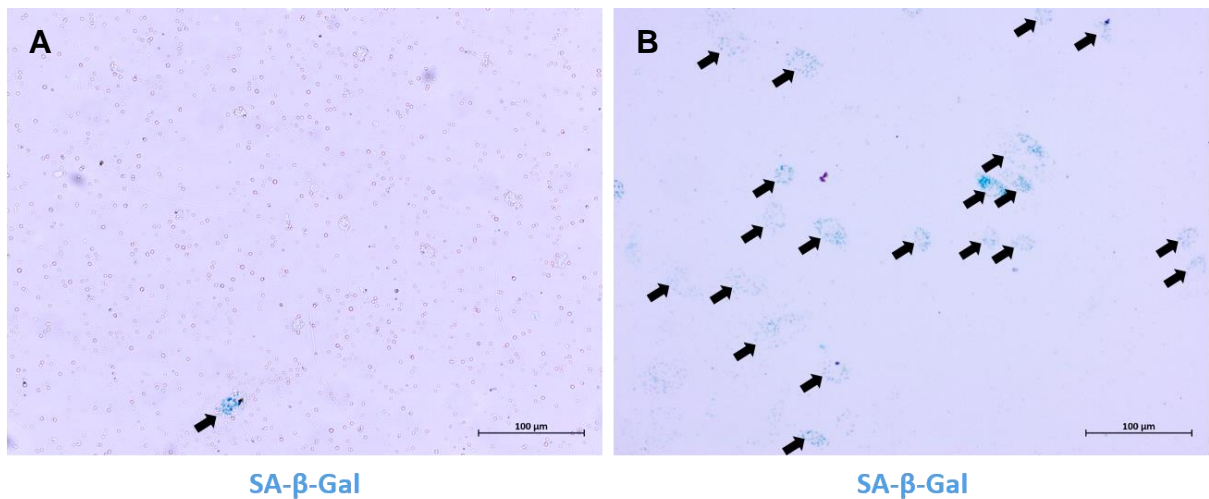
A) Image shows Ki67 expression in proliferative embryonic CMs treated with conditioned media from proliferative CFs (white arrows).

B) Image shows Ki67 expression in proliferative embryonic CMs treated with conditioned media from senescent CFs (white arrows).

C) Graph quantifying Ki67 expression in CMs. On the left is the data from proliferative and irradiated MRC5 cultures, and on the right from proliferative and irradiated CF cultures. The percentage of MMVEC-Cs positive for Ki67 is significantly decreased following culture with irradiated MRC5 and irradiated CF media.

N=3 for each experimental condition. NS \geq 0.05, * p <0.05, ** p <0.01, *** p <0.001, **** p <0.0001 using Two-Tailed T-Test.

To see if the fibroblast SASP reduced CM proliferation was due to induced senescence, embryonic CMs were also stained with SA- β -Gal. Again, similar trends between both conditions for the MRC5 and CF conditioned media were observed. In proliferative conditioned media, SA- β -Gal expression in CMs was 15.42% \pm 3.07 from MRC5s and 12.70% \pm 0.58 from CFs. Positive staining was increased to 47.24% \pm 10.15 in senescent MRC5 media and senescent CF media increased levels to 39.23% \pm 3.03 (Figure 6.7). However, due to one technical repeat failing, statistics could not be performed, and repeating the experiment with a greater sample size would determine whether the increase in this senescence markers following exposure to a fibrotic SASP was significant.



SA-β-Gal

SA-β-Gal

C Percentage of CMs positive for SAβGal

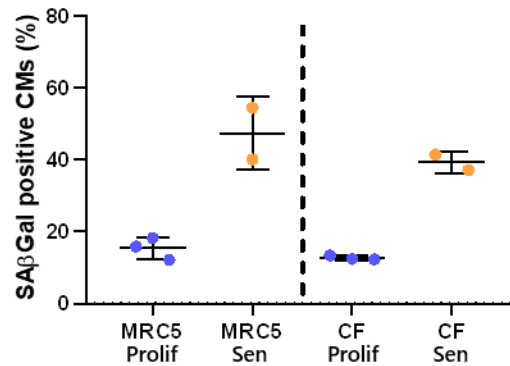


Figure 6.7 Levels of the senescence marker senescence-associated β-galactosidase were raised in cardiomyocytes cultured with irradiated media.

- A)** Image shows expression of SA-β-Gal in embryonic CMs treated with conditioned media from proliferative CFs.
- B)** Image shows expression of SA-β-Gal in embryonic CMs treated with conditioned media from irradiated CFs.
- C)** SA-β-Gal expression was increased following culture in irradiated conditioned media from either MRC5s or CFs compared to proliferative conditioned media. N=2 and 3 for each experiment condition.

6.4 Navitoclax treatment following ischaemia-reperfusion injury significantly reduced the number of p16^{Ink4a} and p21^{Cip} expressing myocardial interstitial cells

Having demonstrated that navitoclax can selectively kill fibroblasts and other cell types *in vitro* (Figure 4.2, Figure 6.2) I investigated the possibility that navitoclax treatment eliminated senescent fibroblasts located in the interstitial myocardium post-IRI. As such, the total number of cells expressing the senescence markers p16^{Ink4a} and p21^{Cip} were quantified in vimentin, a marker of fibroblasts, expressing cells in the interstitial regions of vehicle and navitoclax treated hearts, studied in chapter 3 at the 5 week post-LAD ligation time-point.

In all mice subjected to LAD ligation a significant increase in p16^{Ink4a} expression was observed in the vimentin expressing population (yellow arrows Figure 4.6.A-B). *In vitro* data demonstrated that navitoclax selectively cleared senescent fibroblasts, and in mouse hearts after IRI there was a considerable reduction in the percentage of vimentin expressing interstitial cells expressing p16^{Ink4a} observed in the navitoclax treated hearts. In summary, in the non-LAD ligated hearts 9.80% ± 0.82 vimentin expressing interstitial cells expressed p16^{Ink4a}. Expression of p16^{Ink4a} in vimentin positive cells increased to 19.76% ± 1.82 post-IRI (p=0.0014) in the vehicle control and was reduced to 8.90% ± 2.66 following navitoclax treatment (p=0.0005, Figure 6.8).

From Figure 5.17, levels of p16^{Ink4a} in the interstitial cells was larger after IRI in the p16^{fl/fl} mice compared to the IRI cohort in Figure 6.8. This difference could be due to either differences in responses to the surgeries in this study compared to the previous study, or as a result of 4-OHT dosing or the presence of Cre recombinase in the p16^{fl/fl} mice.

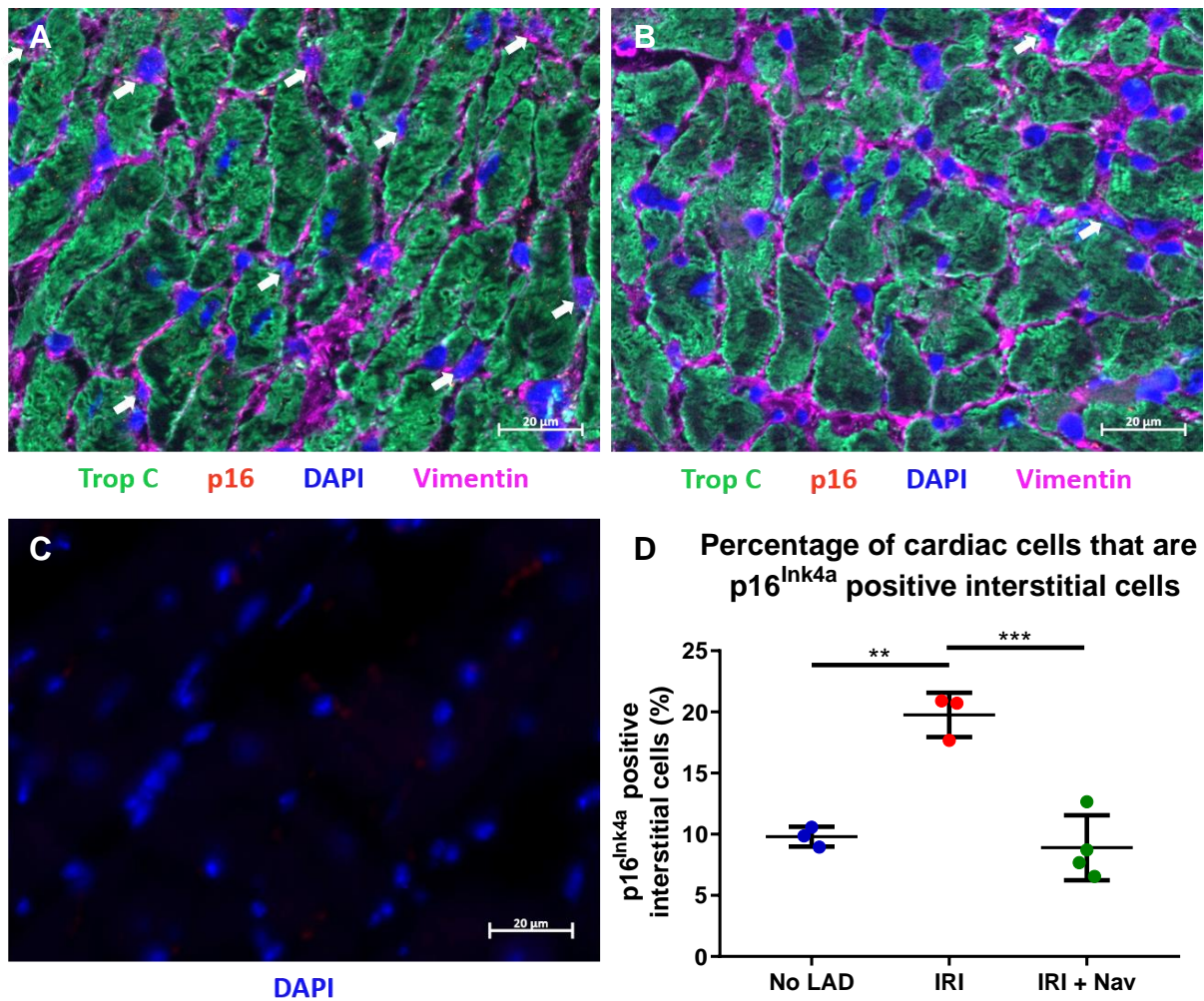


Figure 6.8 Navitoclax reduces the percentage of cardiac interstitial cells positive for p16^{Ink4a} after ischaemia-reperfusion injury to baseline levels.

A) Immunofluorescence staining in hearts post-IRI without navitoclax treatment.

Slides stained with CM marker troponin C (in green, wavelength 488nm), senescence marker p16^{Ink4a} (in red, wavelength 594nm), fibroblast and endothelial cell marker vimentin (in pink, wavelength 647nm) and nuclei (in blue with DAPI, wavelength 461nm). All images for this analysis were taken in the BZ. Interstitial cells positive for p16^{Ink4a} are highlighted with a white arrow.

B) Immunofluorescence staining in LAD ligated hearts with navitoclax treatment.

Slides stained with CM marker troponin C (in green, wavelength 488nm), senescence marker p16^{Ink4a} (in red, wavelength 594nm), fibroblast and endothelial marker vimentin (in pink, wavelength 647nm) and nuclei (in blue with DAPI, wavelength 461nm). All images for this analysis were taken in the BZ. Interstitial cells positive for p16^{Ink4a} are highlighted with a white arrow.

C) Negative control for both 1°Abs, slides were incubated in PBS instead.

D) Data show values of p16^{Ink4a} expression within interstitial cells as a percentage of total cardiac cells. It should be noted that one value (=9.37%) was omitted from the IRI cohort according to a ROUT outlier test.

N=3 and 4 for each experimental condition. NS≥0.05, *p<0.05, **p<0.01, ***p<0.001, ****p<0.0001 using One-way ANOVA.

Additionally, expression of p21^{Cip} in this population of vimentin expressing interstitial cells was significantly increased post-LAD ligation in the vehicle control mice (from 2.39% ± 1.23 to 15.87% ± 0.86, p<0.0001). Treatment with navitoclax (Figure 4.3) significantly reduced the levels of expression of this senescence marker in the interstitial cells to 8.65% ± 1.06 (p=0.0004, Figure 6.9).

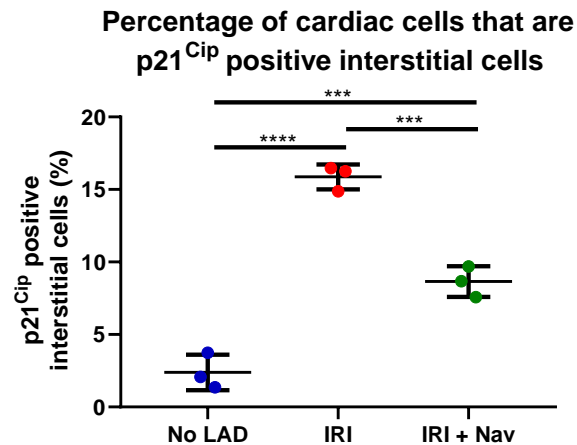


Figure 6.9 Navitoclax reduces the percentage of cardiac interstitial cells positive for p21^{Cip} post-ischaemia-reperfusion injury to baseline levels.

Data show values of p21^{Cip} expression within interstitial cells as a percentage of total cardiac cells.

N=3 for each experimental condition. NS≥0.05, *p<0.05, **p<0.01, ***p<0.001, ****p<0.0001 using One-way ANOVA.

6.5 Investigation of the short term effects of navitoclax post-ischaemia-reperfusion injury

The data above suggest that navitoclax reduces senescent fibroblast viability *in vitro* (Figure 6.2) and eliminates senescent cells expressing a fibroblast marker *in vivo* (Figure 6.8-Figure 6.9), together demonstrating that a fibroblast SASP negatively affects the biology of two cardiovascular cell lineages and a possible explanation as to why there was a lack of phenotype in the p16^{Ink4a} knockout mouse model in chapter 5.

Overall these data support the hypothesis that clearance of non-CMs, in particular the fibroblast population, may contribute to the beneficial effects of navitoclax. This may occur via two distinct mechanisms: 1) clearance of senescent cells from the infarct and interstitial regions may contribute to a reduction in fibrosis and the observed decrease in infarct size observed at 5 weeks post-IRI in the navitoclax treated mice; and 2)

clearance of senescent fibroblasts may reduce the expression of typical SASP proteins, which may contribute to a reduced progression of fibrosis and allow for better recovery by reducing the anti-proliferative/pro-senescent influence of the SASP. Therefore, I aimed to further investigate these possible mechanisms underlying the beneficial outcomes of navitoclax treatment.

One disadvantage of the longitudinal study in Chapter 4 that aimed to assess cardiac function following navitoclax treatment, was that any events occurring at the time of dosing that may contribute to beneficial effects could be completed by the point of tissue collection. As such, the navitoclax study was repeated with a smaller cohort and hearts collected after 4 days of navitoclax dosing, equivalent to the middle of the original dosing regimen (Figure 6.10). It was hypothesised that this experimental design would allow for the capture of biological and molecular changes elicited to the myocardium by navitoclax treatment.

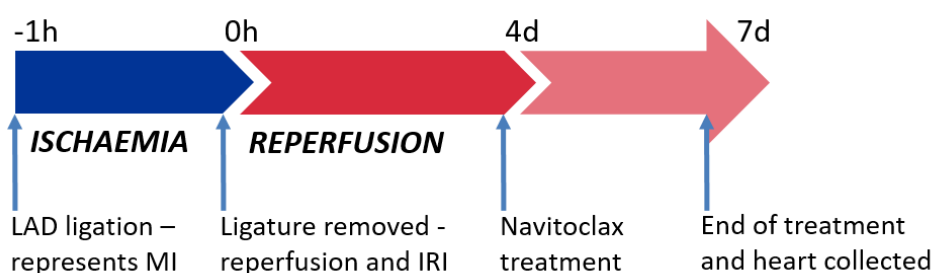


Figure 6.10 Experimental timeline.

Mice undergo LAD ligation surgery as outlined in Figure 3.2 and Figure 4.3. At day 4 post-surgery daily dosing with navitoclax (50mg/kg BW per day). On day 7 mid-treatment regime mice are sacrificed and hearts excised and other samples collected for analysis to determine cells directly cleared by navitoclax.

6.5.1 Total p21^{Cip} expression is significantly decreased following four days of navitoclax treatment

First, I ascertained whether this shorter navitoclax dosing regimen was able to significantly eliminate senescent cells. Therefore, I quantified the total percentage of p21^{Cip} expressing cells in the LV myocardium of vehicle and navitoclax treated mice at this 1 week post-LAD ligation time-point. After LAD ligation p21^{Cip} was significantly increased from 2.73% ± 1.39 to 9.73% ± 1.93 (p=0.0020). A significant reduction in p21^{Cip} expression was observed after 4 doses of navitoclax, which equated to a 2-fold reduction in p21^{Cip} expressing cells (4.77% ± 0.33, p=0.0111, Figure 6.11).

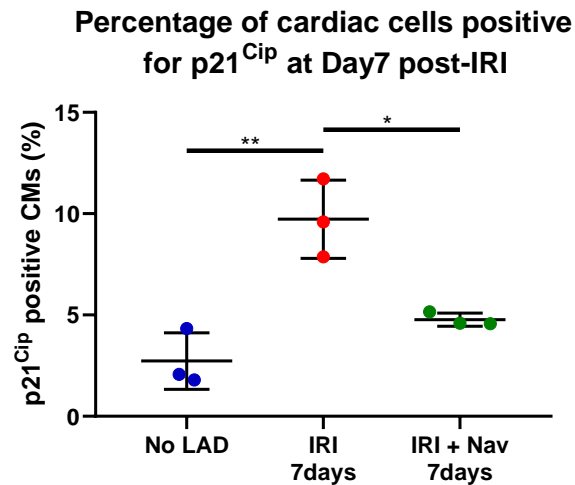


Figure 6.11 Expression of p21^{Cip} is significantly reduced following navitoclax after ischaemia-reperfusion injury.

Data demonstrate p21^{Cip} expression within cardiac cells is significantly reduced by day 7 after LAD ligation with navitoclax treatment.

N=3 for each experimental condition. NS \geq 0.05, * p <0.05, ** p <0.01, *** p <0.001, **** p <0.0001 using One-Way ANOVA.

6.5.2 TUNEL staining reveals navitoclax treatment increases apoptosis post-myocardial infarction, which primarily occurs in the interstitial cell population

The suggested mechanism of action of navitoclax is to trigger apoptosis in senescent cells that are primed for apoptosis (Zhu *et al.*, 2016). However, to date it has not been demonstrated in this cohort that the elimination of senescent cells in navitoclax treated hearts is associated with increased apoptosis. The TUNEL assay, which allows the detection of the DNA fragmentation that occurs during apoptosis (Kyrylkova *et al.*, 2012) was therefore performed to identify if at this time-point during navitoclax dosing whether apoptosis was increased.

Post-myocardial infarction, TUNEL positive cells were observed throughout the myocardium in the BZ of hearts from both vehicle and navitoclax treated mice. There was a higher percentage of TUNEL positive cells in the infarct BZ of LAD-ligated navitoclax treated mice (19.66% \pm 12.03), suggesting navitoclax does initiate apoptosis, compared to LAD-ligated vehicle treated control mice (8.12% \pm 3.82) but this was not significantly different (p =0.1882, Figure 6.12.A). Next I investigated which cell populations were undergoing the majority of apoptosis post-navitoclax by quantifying the proportion of TUNEL staining within the CM or interstitial cell

populations. Analysis revealed that after navitoclax 10.74% \pm 2.61 of the total TUNEL positive cells were troponin C expressing CMs and 89.26% \pm 2.61 were interstitial cells ($p < 0.0001$, Figure 6.12.B-C). This ratio of TUNEL positive CMs to interstitial cells was similar in the vehicle controls (11.20% \pm 4.63 vs 88.80% \pm 4.63, $p < 0.0001$, Figure 6.12.B). Therefore, after IRI the majority of cells that are undergoing apoptosis are interstitial cells, with only a tenth of all cells undergoing apoptosis being CMs (Figure 6.12.C).

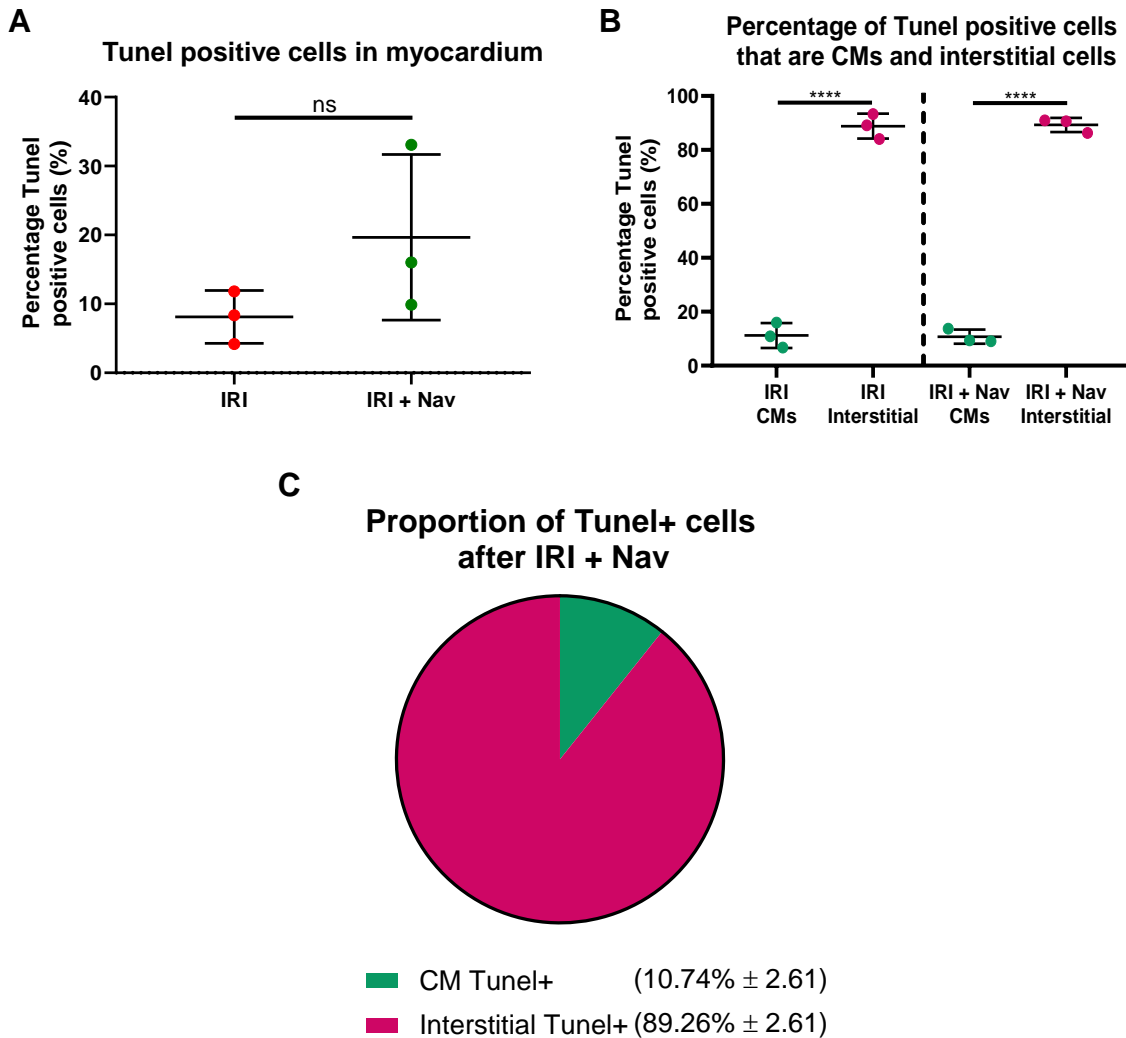


Figure 6.12 After ischaemia-reperfusion injury cells are TUNEL positive, with the majority of cells being interstitial cells.

- A)** Graph shows total percentage of cells in the myocardium positive for TUNEL and undergoing apoptosis. The average total TUNEL percentage is increased 2.4-fold after navitoclax but is not significant.
- B)** Graph shows the proportion of TUNEL positive cells that are CMs and interstitial cells following IRI and navitoclax. Treatment has no effect on the proportion of cells undergoing apoptosis after IRI.
- C)** Chart shows that 89.26% of cells positive for TUNEL staining are interstitial cells, with the remaining 10.74% of cells being CMs.

N=3 for each experimental condition. NS \geq 0.05, * p <0.05, ** p <0.01, *** p <0.001, **** p <0.0001 using Two-Tailed T-Test.

6.5.3 Cytokine array demonstrates effects on a variety of cytokines within the protein samples from left ventricle but minimal effects observed on cytokines circulating in the serum

At 5 weeks post-LAD ligation navitoclax treatment reduces the levels of myocardial senescence, which is associated with smaller infarct size and improved cardiac recovery (chapter 4). Quantifications of p21^{Cip} expression and TUNEL staining suggest that at 1 week post-LAD (4 days into the dosing regimen) navitoclax had actively eliminated senescent cells via inhibition of the anti-apoptotic proteins allowing apoptosis to proceed. Furthermore, apoptosis occurred primarily in the non-CM population. Therefore, I investigated if the beneficial effects of navitoclax involved a reduction of a typical SASP.

Hearts from vehicle control and navitoclax treated mice were again collected at the 1 week time-point (Figure 6.10), then the affected LV posterior to the suture was dissected from the heart and the total protein isolated from this region of LV. Serum was also isolated from the blood collected via cardiac puncture from the same animals.

A study has demonstrated that senescent CMs do not express a typical SASP (Anderson et al., 2019), therefore to focus these investigations onto the clearance of the interstitial population I used cytokine array technology to quantify changes in typical SASP proteins (Freund et al., 2010). Protein and serum samples were sent for analysis by Eve Technologies and run on their Discovery Assays ®: the Mouse Cytokine Array/Chemokine Array 44-Plex (MD44); and the TGF- β Cytokine Array (TGFB1-3). All samples were run on a Millipore assay kit and quantified using a lyophilised standard for each target recombinant target analyte of known concentrations. A standard curve was produced for each individual analyte and the concentration of the samples interpolated using those curves and a heatmap was created with data presented using an Average Linkage Clustering method with Pearson Distance Measurement (protein samples in Figure 6.13).

Adding further evidence that senescence and increased SASP are characteristics of IRI, from the MD44 array of protein samples 14 cytokines or chemokines demonstrated a significant increase ($p < 0.05$) or strong trend towards an increase in expression post-LAD (vehicle treated hearts). Demonstrating that senescent cells were at least in part responsible for the expression of these cytokines and showing that elimination of senescent cells by navitoclax attenuated the SASP, these 14 cytokines and

chemokines also displayed a significant decrease ($p < 0.05$) or strong trend in reduction after navitoclax treatment (Figure 6.14). Although some of the individual changes in expression are non-significant I hypothesise that taken together these data provide a strong indication that multiple SASP proteins are attenuated following senescence clearance. As such, I have included the data from the 14 selected individual SASP proteins that demonstrated changes between the experimental groups, which had the smallest p values, in Figure 6.14 and discussed these changes in more detail below. A full list of protein changes and statistical data can be found in appendix A.

Levels of Il-16 expression trended towards an increase following IRI ($p = 0.0589$). This was from $251.1 \text{ pg/ml} \pm 71.11$ in uninjured hearts to $382.7 \text{ pg/ml} \pm 53.75$ in the vehicle control ($p = 0.587$). Levels were significantly reduced, following navitoclax to $216.3 \text{ pg/ml} \pm 32.86$ ($p = 0.0231$, Figure 6.14.A).

In this cohort, baseline levels of fractalkine before injury were $71.21 \text{ pg/ml} \pm 2.53$. After IRI, expression was significantly increased ($p = 0.0022$) to $90.27 \text{ pg/ml} \pm 4.56$ and treatment significantly reduced ($p = 0.0014$) fractalkine levels to $67.98 \text{ pg/ml} \pm 4.49$ (Figure 6.14.B). Il-11 showed the same trends as fractalkine with levels significantly upregulated ($p = 0.0485$) due to IRI and diminished significantly ($p = 0.0279$) after treatment ($0.83 \text{ pg/ml} \pm 0.97$ to $2.76 \text{ pg/ml} \pm 0.76$ and down to $0.55 \text{ pg/ml} \pm 0.48$, Figure 6.14.C).

Post-myocardial infarction, Ip-10 levels were significantly increased ($p = 0.0404$) from $5.31 \text{ pg/ml} \pm 0.69$ to $48.28 \text{ pg/ml} \pm 28.02$. Levels were reduced ($p = 0.0559$) subsequent to navitoclax treatment to $8.80 \text{ pg/ml} \pm 2.15$ (Figure 6.14.D). Tissue inhibitor of metalloproteinases (Timp) -1, thymus and activation-regulated chemokine (Tarc) and Il-6 showed the same trends. Timp-1 had a significant 40-fold increase ($p = 0.0164$) associated with IRI from $31.68 \text{ pg/ml} \pm 0.707$ to $1298 \text{ pg/ml} \pm 443.6$ and trend toward a significant ($p = 0.0547$) reduction to $476.2 \text{ pg/ml} \pm 234.1$ in the navitoclax treated group (Figure 6.14.E). Tarc levels were altered significantly ($p = 0.0163$) from $0.72 \text{ pg/ml} \pm 0.39$ to $4.88 \text{ pg/ml} \pm 1.90$ and after navitoclax expression was decreased, but not statistically significantly ($p = 0.1474$) by approx. 2-fold to $2.60 \text{ pg/ml} \pm 1.01$, (Figure 6.14.F). Levels of Il-6 were also significantly higher ($p = 0.0347$) post-IRI at $2.73 \text{ pg/ml} \pm 0.64$ than before IRI at $1.21 \text{ pg/ml} \pm 0.04$. Navitoclax lowered expression, but not significantly ($p = 0.0841$), to $1.53 \text{ pg/ml} \pm 0.71$ (Figure 6.14.G).

Levels of the inflammatory marker Mip-3 β were 31.22pg/ml \pm 12.74 in healthy mice, and IRI significantly raised (p=0.0005) these levels to 134.2pg/ml \pm 16.86. Expression was significantly reduced (p=0.0119) with navitoclax to 79.63pg/ml \pm 16.55, however, these levels remained significantly higher (p=0.0204) than in the healthy baseline cohort (Figure 6.14.H). The dynamics of macrophage-derived chemokine (Mdc, also known as Ccl22) showed the same trends as Mip-3 β : levels significantly increased (p=<0.0001) from 0.99pg/ml \pm 0.23 before LAD to 5.03pg/ml \pm 0.49 post-LAD and significantly lessened (p=0.0014) to 2.86pg/ml \pm 0.44 in the navitoclax treated group (Figure 6.14.I). After IRI in this study, eotaxin levels were also significantly increased (p=0.0270). In healthy controls expression was 6.74pg/ml \pm 2.67 and coronary ischaemia from LAD ligation increased levels significantly to 16.10pg/ml \pm 4.28. Navitoclax lowered (p=0.0728) expression to 8.87pg/ml \pm 2.29 (Figure 6.14.J).

In contrast to these cytokine expression patterns, interferon- β 1 (Ifn- β 1) was not increased following LAD ligation (p=0.9130), but treatment with navitoclax significantly lowered expression (60.25pg/ml \pm 2.88) in comparison to both the healthy controls (66.52 pg/ml \pm 1.96, p=0.0243) and IRI groups (67.22pg/ml \pm 1.05, p=0.0153, Figure 6.14.K).

The data from the TGFB1-3 array demonstrated that all three Tgf- β protein isoforms expression increased significantly as a result of IRI (Figure 6.14.L-N). The expression of Tgf- β 1 was highly variable amongst the healthy group and as such wasn't significantly changed post-IRI, from 62.12pg/ml \pm 60.71 to 87.47pg/ml \pm 10.29 (p=0.6765). Navitoclax treatment significantly reduced expression of Tgf- β 1 to 16.47pg/ml \pm 4.25 (p=0.0004, Figure 6.14.L). In comparison, both Tgf- β 2 and 3 were significantly upregulated post-IRI: Tgf- β 2 increased from 8.89pg/ml \pm 3.76 in healthy mice to 65.62pg/ml \pm 28.09 (p=0.0214, Figure 6.14.M); and Tgf- β 3 expression was even more dramatically increased from 1.88pg/ml \pm 0.43 to 19.13pg/ml \pm 5.97 (p=0.0046, Figure 6.14.N). Following navitoclax treatment, levels of both were reduced, to 26.01pg/ml \pm 14.47 for Tgf- β 2 and 6.37pg/ml \pm 3.56 for Tgf- β 3, but this was only significant for Tgf- β 3 (p=0.0854 for Tgf- β 2, p=0.0190 for Tgf- β 3, Figure 6.14.M-N).

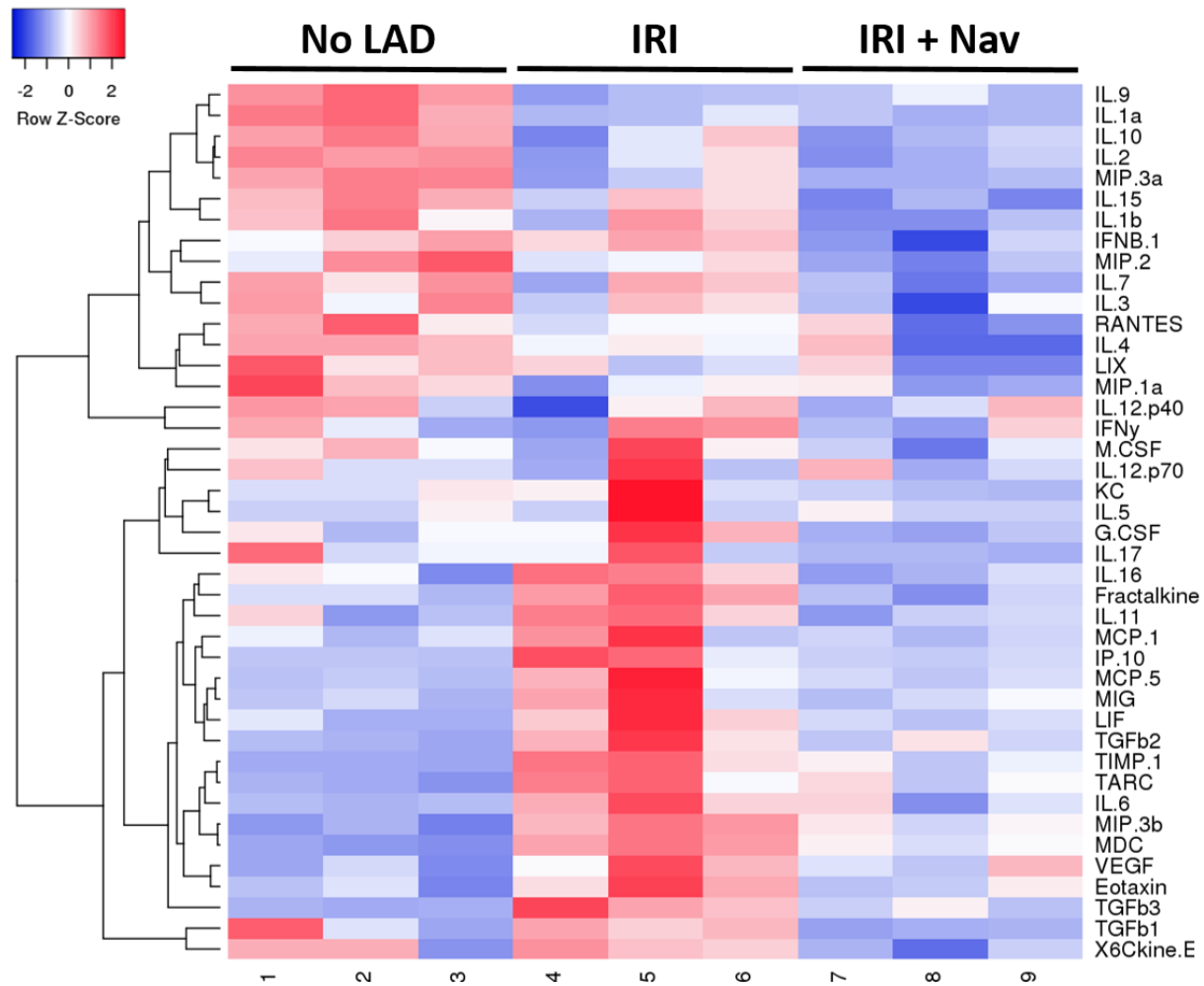
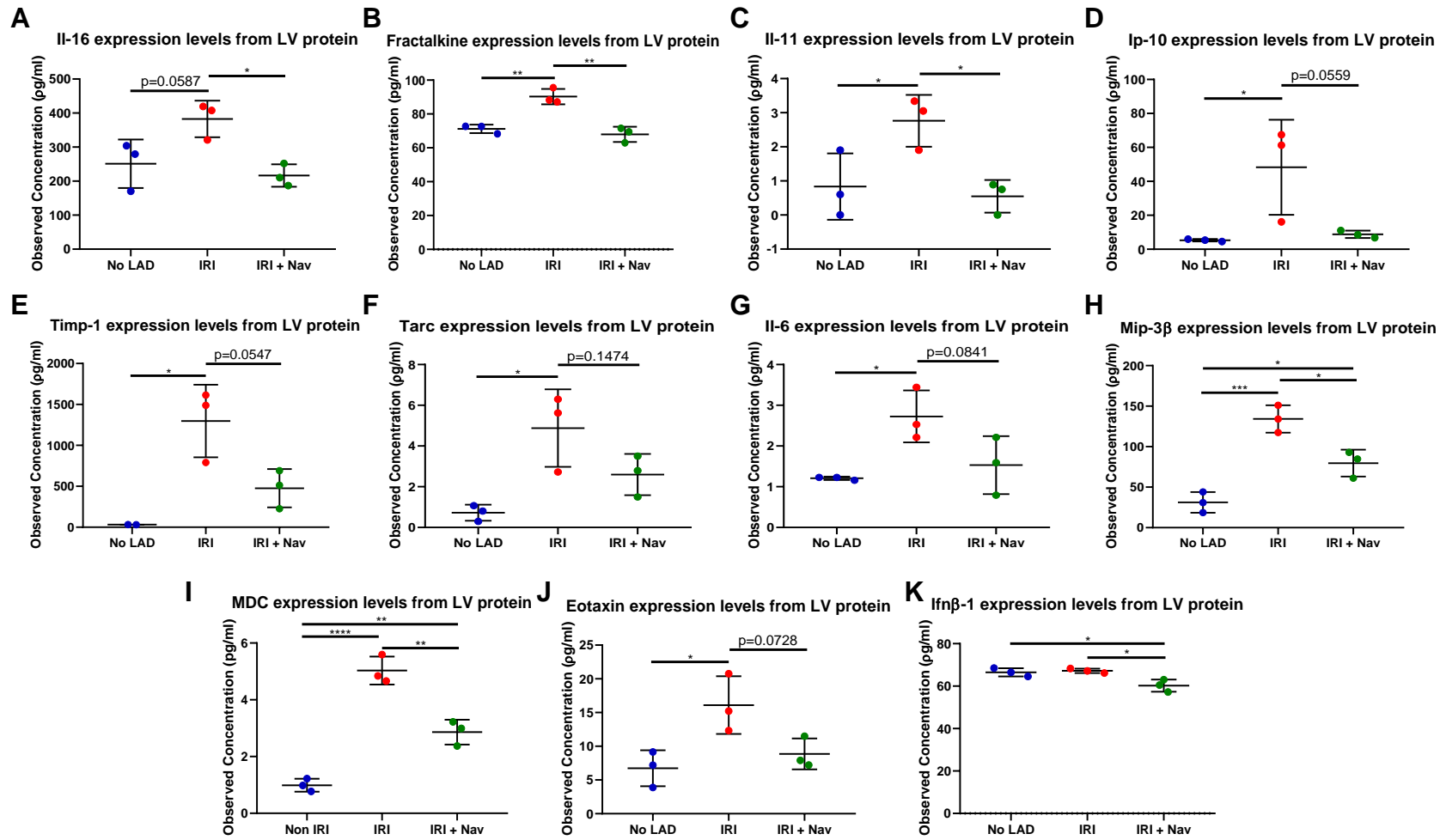


Figure 6.13 Heat map showing changes in expression of cytokines and chemokines from left ventricle protein samples run on the MD44 and TGFB1-3 arrays.

Cytokines and chemokines show varying responses within groups and between treatments. Those with significant changes in expression can be found in Figure 6.14.



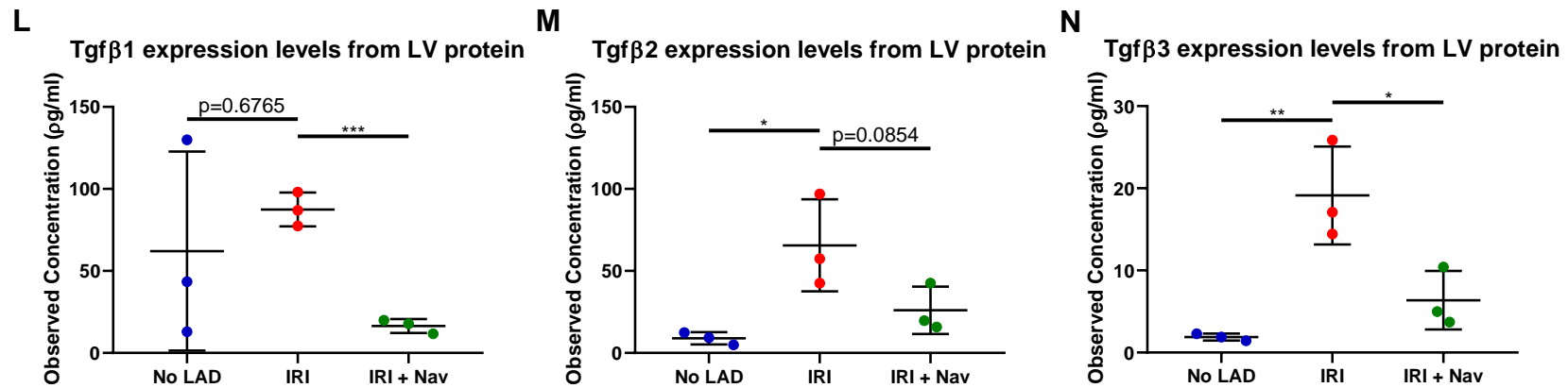


Figure 6.14 Graphs showing trends in the expression of left ventricle protein cytokines and chemokines relating to fibrosis and cardiovascular disease following ischaemia-reperfusion injury with and without navitoclax treatment.

- A)** Il-16: Levels increase post-IRI but not significantly ($p=0.0587$), and are significantly decreased following navitoclax treatment.
- B)** Fractalkine: Levels significantly increase post-IRI and are significantly decreased following navitoclax treatment.
- C)** Il-11: Levels significantly increase post-IRI and are significantly decreased following navitoclax treatment.
- D)** Ip-10: Levels significantly increase post-IRI and decrease following navitoclax treatment but not significantly.
- E)** Timp-1: Levels significantly increase post-IRI and decrease following navitoclax treatment but not significantly.
- F)** Tarc: Levels significantly increase post-IRI and decrease following navitoclax treatment but not significantly.
- G)** Il-6: Levels significantly increase post-IRI and decrease following navitoclax treatment but not significantly.
- H)** Mip-3b: Levels significantly increase post-IRI and are significantly decreased following navitoclax treatment, but are still significantly higher than no LAD controls.
- I)** Macrophage-Derived Cytokine (MDC): Levels significantly increase post-IRI and are significantly decreased following navitoclax treatment, but are still significantly higher than no LAD controls.
- J)** Eotaxin: Levels significantly increase post-IRI and decrease following navitoclax treatment but not significantly.
- K)** Ifn-β1: Levels do not change following IRI, however, are significantly decreased following navitoclax.
- L)** Tgfβ1: Levels do not change following IRI, however, are significantly decreased following navitoclax.
- M)** Tgfβ2: Levels significantly increase post-IRI and decrease following navitoclax treatment but not significantly.
- N)** Tgfβ3: Levels significantly increase post-IRI and are significantly decreased following navitoclax treatment.

N=3 for each experimental condition. NS \geq 0.05, * p <0.05, ** p <0.01, *** p <0.001, **** p <0.0001 using One-Way ANOVA/Kruskal-Wallis Test.

In order to see if IRI post-MI induced systemic changes to inflammation and SASP expression, the cytokine array was also used to test levels of cytokine and chemokines in serum samples isolated from the systemic circulation. In contrast to the array data for the protein samples, fewer trends were observed for the serum array (Figure 6.15). Variations within each group was much greater with only a few cytokines showing similar expression levels. Those cytokines that had detectable, substantial trends are outlined in Figure 6.16. Of the 47 cytokines tested, only 5 showed significant changes in expression, including Tarc, Il-6, eotaxin, Tgf- β 1 and Tgf- β 2.

The pattern of circulating Tarc expression in the serum differed greatly to the protein data in Figure 6.14.F. In the serum, levels in the healthy group were 95.77pg/ml \pm 6.72, and was unchanged following IRI (111.1pg/ml \pm 5.77, p=0.1328). However, navitoclax significantly lowered Tarc levels in comparison to both the uninjured and injured groups to 62.91pg/ml \pm 11.10 (p=0.0009, Figure 6.16.A). For Il-6, the changes in expression in serum samples reflected the observations from LV protein samples (Figure 6.14.G). At baseline Il-6 was 2.48pg/ml \pm 0.84 and this significantly increased (p=0.0424) to 48.19pg/ml \pm 24.41 post-IRI. The reduction in Il-6 levels due to navitoclax dosing was marginal (p=0.9811), to 45.53pg/ml \pm 17.89 (Figure 6.16.B). Compared to the results of eotaxin expression in Figure 6.14.J, where expression was significantly increased post-IRI and non-significantly reduced in the navitoclax cohort, from the serum data in Figure 6.16.C eotaxin was slightly but insignificantly raised (p=0.4040) from 497.0pg/ml \pm 63.90 to 558.2pg/ml \pm 46.24 post-LAD ligation. However, levels were significantly downregulated to 418.3 pg/ml \pm 50.05 as a result of treatment with navitoclax (p=0.0438, Figure 6.16.C).

In the serum samples only Tgf- β 1 and 2 demonstrated any changes in circulating levels. Circulating Tgf- β 1 levels were very high at baseline at 50838 pg/ml \pm 7732, and were slightly elevated due to IRI at 64029pg/ml \pm 7389. Although IRI had a non-significant effect on Tgf- β 1 (p=0.1203), navitoclax significantly lowered levels to 32737pg/ml \pm 4989 (p=0.0033). Similar trends were detected for Tgf- β 2. Before IRI, expression was 1844pg/ml \pm 143.9 which was slightly but insignificantly higher post-IRI at 2165pg/ml \pm 152.7 (p=0.0767). Again levels were significantly reduced to 1220pg/ml \pm 135.7 after navitoclax dosing (p=0.0005, Figure 6.16.D-E).

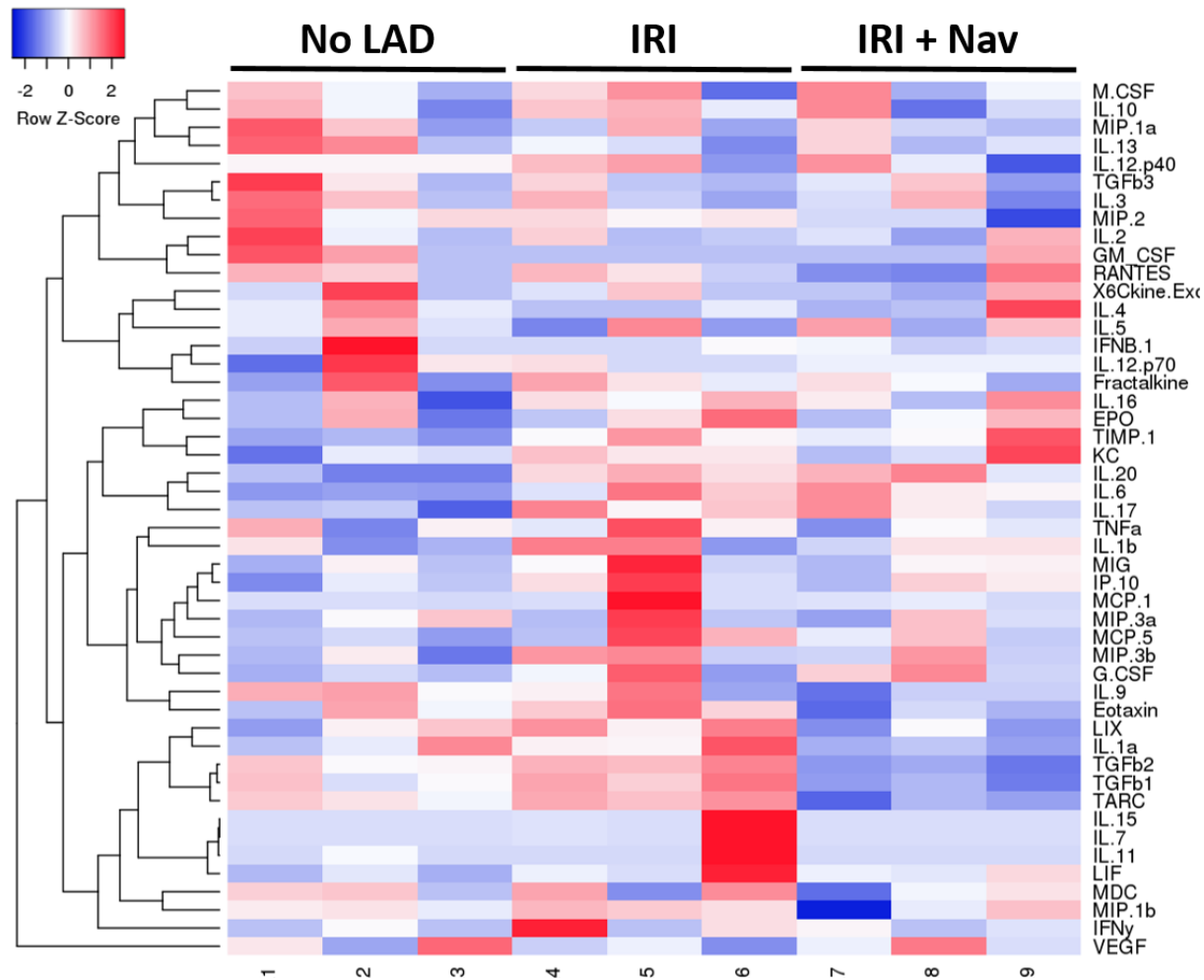


Figure 6.15 Heat map showing changes in expression of cytokines and chemokines from serum samples run on the MD44 and TGFB1-3 arrays.

Cytokines and chemokines show varying responses within groups and between treatments. Those with significant changes in expression can be found in Figure 6.16.

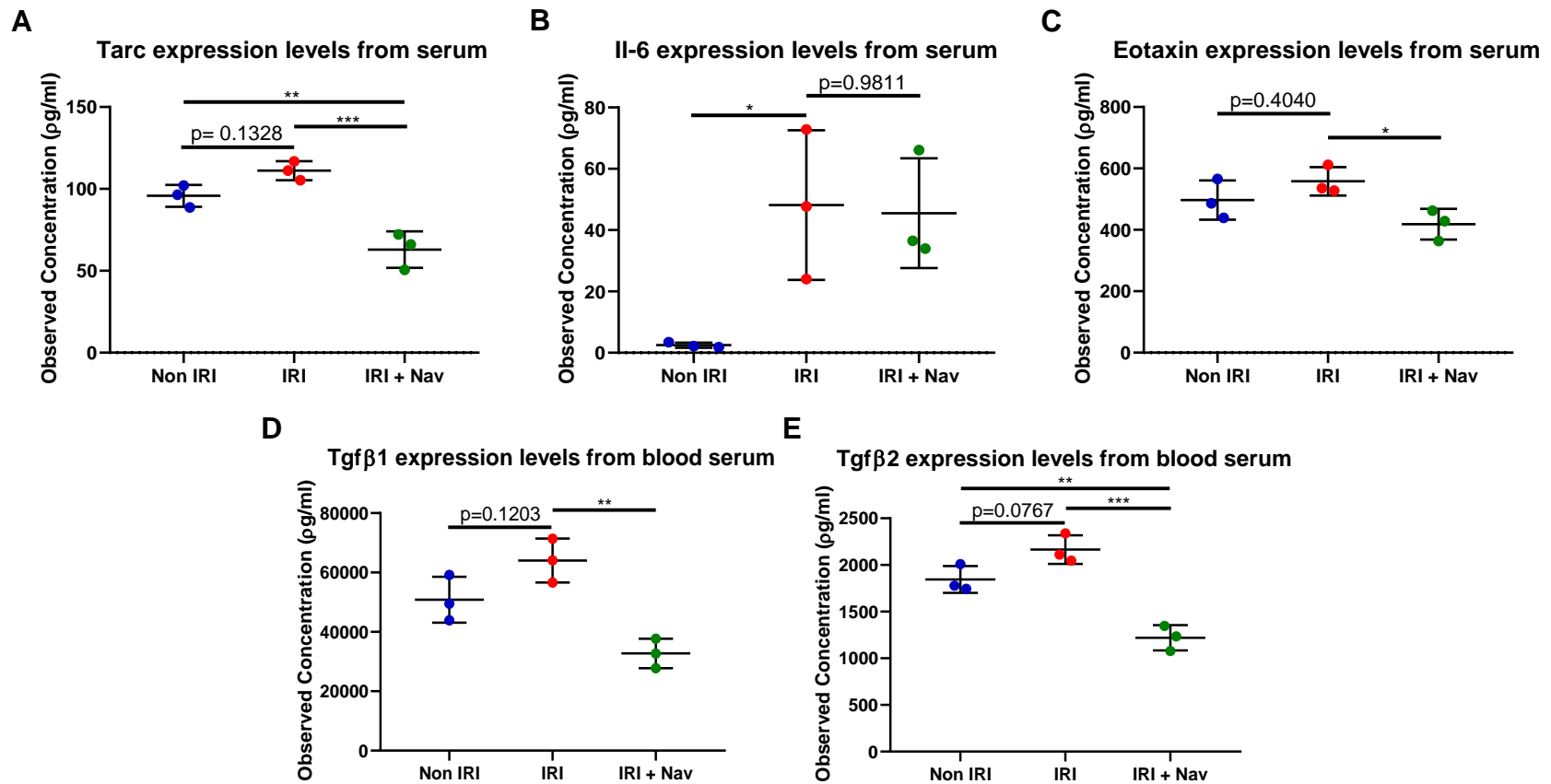


Figure 6.16 Circulating serum cytokines relating to fibrosis and cardiovascular disease following ischaemia-reperfusion injury with and without navitoclax.

A) Tarc: Levels do not change following IRI, however, are significantly decreased following navitoclax.

B) Il-6: Levels significantly increase post-IRI and not affected following navitoclax.

C) Eotaxin: Levels do not change following IRI, however, are significantly decreased following navitoclax.

D) Tgf-β1: Levels do not change following IRI, however, are significantly decreased following navitoclax.

E) Tgf-β2: Levels do not change following IRI, however, are significantly decreased following navitoclax.

N=3 for each experimental condition. NS≥0.05, *p<0.05, **p<0.01, ***p<0.001, ****p<0.0001 using One-Way ANOVA/Kruskal-Wallis Test.

6.5.4 Proliferation of cardiomyocytes is not upregulated following navitoclax therapy, but total proliferation and proliferation in the endothelial cell population is increased

The above data demonstrate that a SASP is anti-proliferative to CMs and endothelial cells *in vitro* (Figure 6.3-Figure 6.7). As such I next aimed to test the hypothesis that subsequent to MI with IRI an increased SASP inhibits proliferation *in vivo* and thereby improved CM regeneration and angiogenesis, as well as reduced infarct size, contributing to the improved functional recovery in the navitoclax treated animals.

As previously, mice were subjected to 60 minutes LAD ligation followed by reperfusion; 4 days post-reperfusion mice were treated with either drug vehicle only or navitoclax (50 mg/kg BW per day) and also EdU (100mg/kg BW per day) for 7 consecutive days (Figure 4.3) and hearts were again collected at 5 weeks post-LAD ligation. Providing EdU allowed a retrospective analysis of cell proliferation during the treatment period.

It has been reported that CM regeneration is triggered in response to MI (Hsieh *et al.*, 2007; Ellison *et al.*, 2013; Malliaras *et al.*, 2013) and that the heart's capacity for regeneration declines with age (Bergmann *et al.*, 2015) as a result of cardiac stem cell dysfunction (Lewis-McDougall *et al.*, 2019) and impaired CM proliferation (Oldershaw *et al.*, 2019). To investigate de novo CM regeneration following navitoclax treatment I quantified EdU-positive cells in combination with CM markers troponin C and cell membrane marker WGA. Navitoclax did not impact on EdU incorporation in the CM population specifically (Figure 6.17.A). After IRI the mean EdU incorporation in CMs was 0.72cells/FOV \pm 0.14 which was unchanged ($p=0.2896$) in the navitoclax cohort at 0.91cells/FOV \pm 0.30. These EdU data suggest that CM regeneration is not the mechanism driving the improved cardiac function after IRI with navitoclax observed in 4.5.

When the total proliferation in this region was evaluated, there was a significantly higher number of the total cell population which had incorporated EdU in the navitoclax treated cohort ($p=0.0235$). The number of total cells positive for EdU was 23.30 cells/FOV \pm 5.97 after IRI and this increased to 33.10 cells/FOV \pm 4.26 if treated with navitoclax (Figure 6.17.B). The number of endothelial cells only accounted for roughly 23% of the total EdU positive cells indicating that the majority of proliferative cardiac cells in the BZ are not relating to angiogenesis. A study that mapped out proliferative

cardiac cells after MI with reperfusion showed that there was a very low, non-significant level of CM regeneration and that the majority of proliferative cells were endothelial, haematopoietic or fibroblast cells (Kretzschmar *et al.*, 2018). Therefore, the remaining proliferative cells observed in this cohort after IRI both with and without navitoclax are postulated to be composed of haematopoietic cells and fibroblasts.

Expression of EdU in cells expressing CD31, a widely utilised marker for endothelial cells and also the process of angiogenesis (Liu and Shi, 2012), was performed to investigate this hypothesis. Analysis revealed that there were significantly more ($p=0.0113$) EdU positive CD31 expressing cells in the animals treated with navitoclax compared to IRI with vehicle. After IRI, 4.11cells/FOV \pm 1.34 were positive for both CD31 and EdU, but after navitoclax this was elevated to 7.62cells/FOV \pm 1.67 (Figure 6.17.C) demonstrating an approximately 2-fold increase (1.85-fold) in endothelial cell proliferation. These data indicate that following MI and IRI in young animals, senescent cell clearance is accompanied by a significant increase in angiogenesis but not CM proliferation.

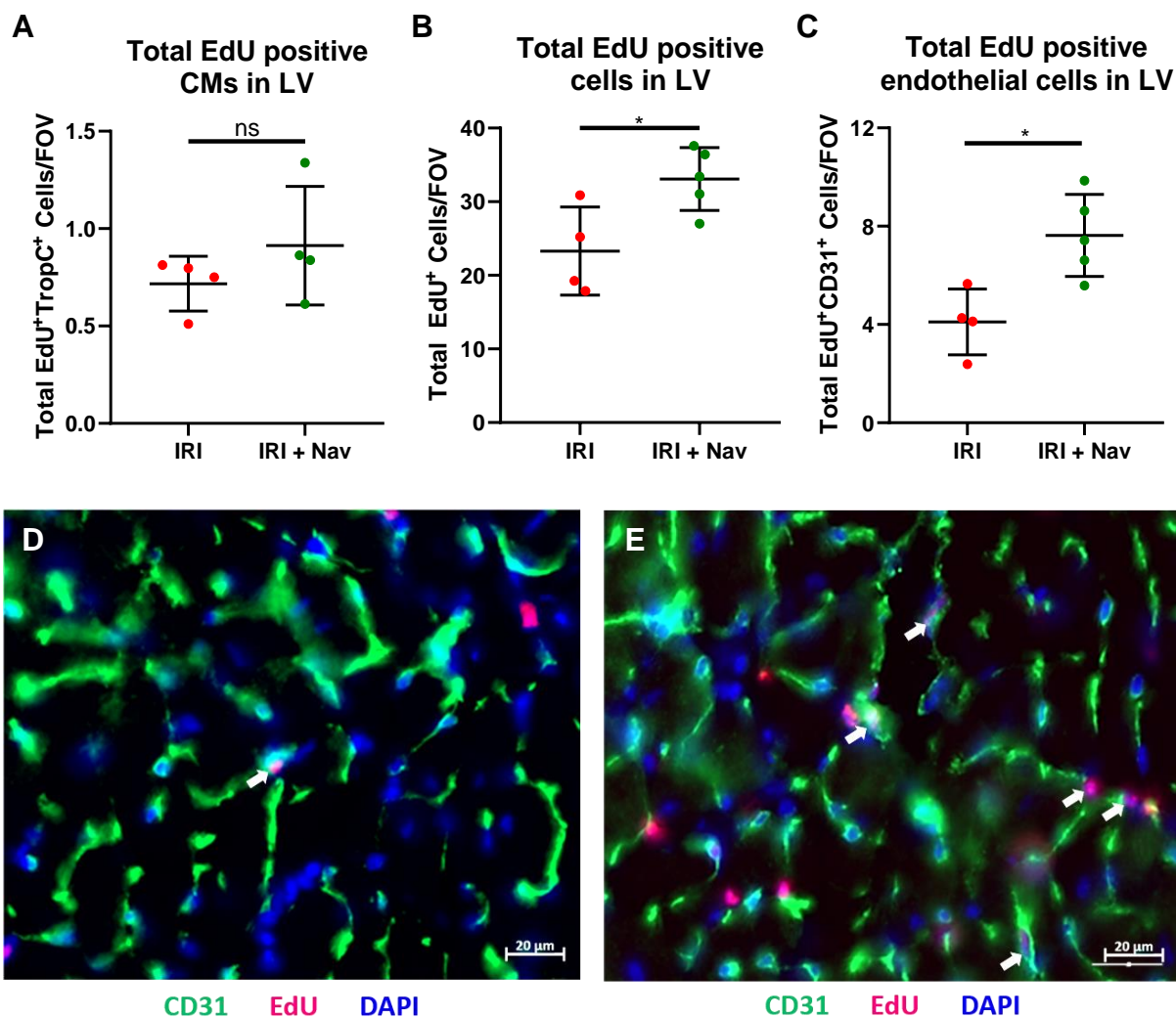
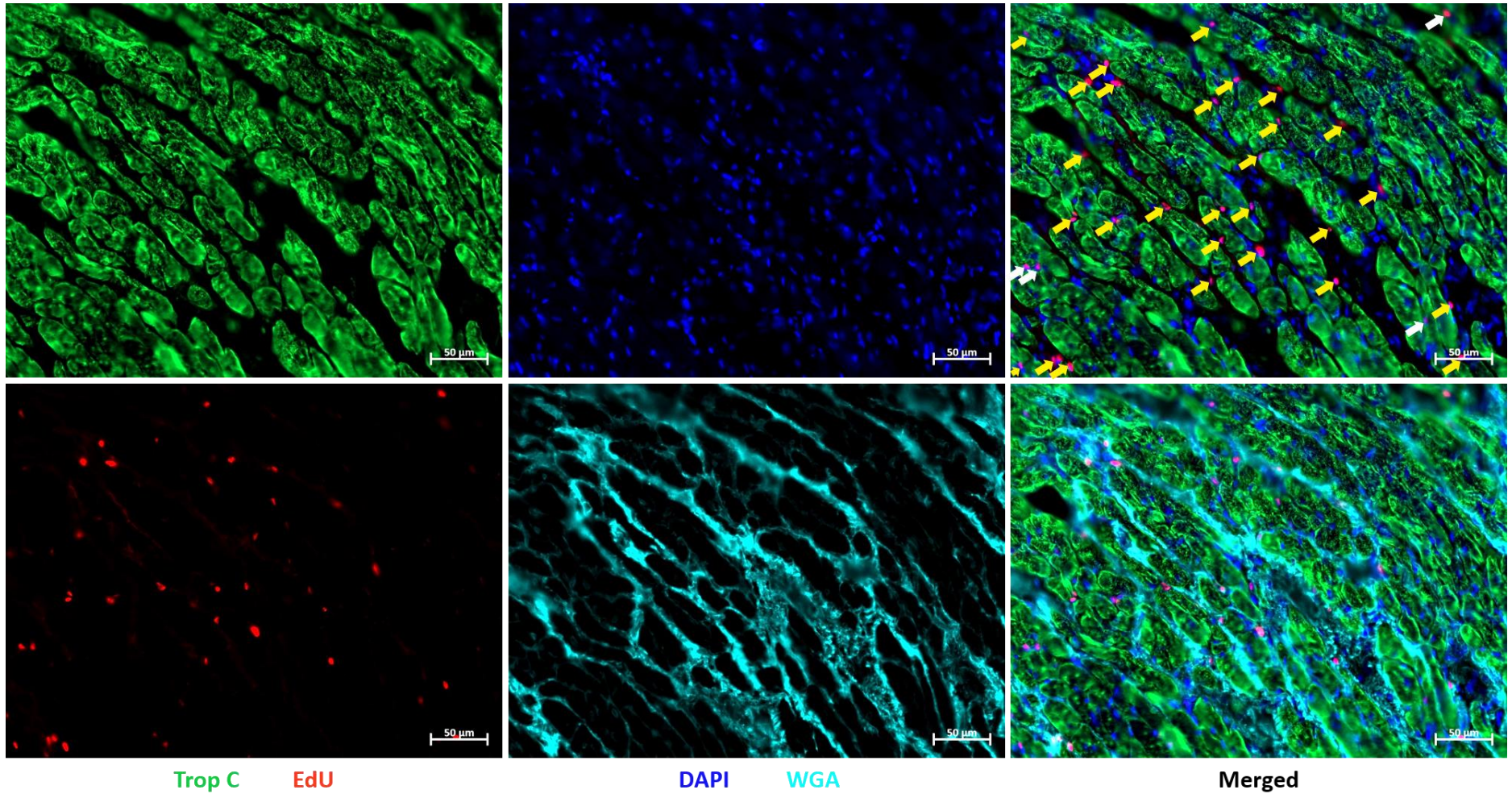


Figure 6.17 Navitoclax treatment increased proliferation of endothelial cells but not cardiomyocytes after ischaemia-reperfusion injury.

- A)** Percentage of EdU positive CMs in the LV are not significantly different between IRI and IRI treated with navitoclax cohorts.
- B)** Percentage of EdU positive total cardiac cells in the LV are significantly different between IRI and IRI treated with navitoclax cohorts.
- C)** Percentage of EdU positive endothelial cells in the LV are significantly different between IRI and IRI treated with navitoclax cohorts.
- D)** EdU (red, 594nm) co-staining with endothelial marker CD31 (green, 488nm) and nuclear marker DAPI (blue, 461nm) after IRI. Arrows indicate CD31 and EdU positive cells.
- E)** EdU (red, 594nm) co-staining with endothelial marker CD31 (green, 488nm) and nuclear marker DAPI (blue, 461nm) after IRI and navitoclax.
- F)** Tiles of immunofluorescence staining for EdU post-LAD ligation proximal to the infarct. Slides stained for CM marker troponin C (green 488nm), proliferation marker EdU (red, 594nm), nuclear marker DAPI (blue, 461nm) and membrane marker WGA (turquoise, 647nm). White arrows indicate troponin C EdU positive cells and yellow arrows WGA EdU positive cells. [next page]

N=4-5 for each experimental condition. NS≥0.05, *p<0.05, **p<0.01, ***p<0.001, ****p<0.0001 using One-Way ANOVA.

F



6.6 Discussion

The heart is made up of a heterogeneous population of cells. Although the CMs are the contractile functional unit of the heart, other cardiac cell lineages exert effects to influence the overall function of the heart (Roth *et al.*, 2014). In the interstitium, fibroblasts are essential for secretion of ECM factors during repair after injury to maintain structural integrity, however, can lead to pathological remodelling if the fibrosis interferes with conduction of contractile signals or stiffens the ventricles reducing heart function (Furtado *et al.*, 2016). Senescence has been demonstrated to be vital to recruit fibroblasts to the site of injury, differentiation into myofibroblasts, deposition of ECM to close the wound and also to regulate the extent of fibrosis (Meyer *et al.*, 2016). Despite the acute beneficial effects of fibroblast senescence, in organs such as the lungs, liver and kidneys if these senescent cells are not cleared efficiently then these can be detrimental to tissue function by creating an unfavourable environment via the SASP. This SASP can promote cellular dysfunction in other cell types and in fact contribute to progressive fibrosis as a result of the pro-fibrotic effects of many SASP proteins (Braun *et al.*, 2012; Ogrodnik *et al.*, 2017; Schafer *et al.*, 2017). Although in the heart preventing fibroblast senescence resulted in elevated fibrosis (Meyer *et al.*, 2016), the chronic effects of persistent fibroblast senescence on fibrosis and function are still unclear, but targeting senescent fibroblasts has been suggested to be potentially beneficial (Schafer *et al.*, 2018).

Short-term navitoclax treatment showed preferential induction of apoptosis in the interstitial population compared to CMs suggesting that elimination of senescence in this population may contribute to the reduction in scar formation and the rescue in cardiac function observed in the navitoclax treated mice. These observations and data suggesting that CM $p16^{Ink4a}$ knockout have no effect on outcome led me to investigate if a SASP from interstitial cell populations could have a negative impact on other cardiac cell types. Given that fibroblasts make up a major component of the interstitial cells and contribute to scar formation (Frangogiannis, 2016), for these proof of principle experiments I chose to investigate the fibroblast SASP. While there may be differences in fibroblast populations between various tissue sources, I performed these experiments on the established human embryonic lung fibroblast cell line, MRC5, as well as fibroblasts isolated from adult murine hearts. There were difficulties using adult cardiac fibroblasts including: only being able to isolate and expand limited numbers of these cells; and I also observed that these cells very quickly changed morphology to

take on a more myofibroblast phenotype in culture making these experiments difficult to control. The data from these experiments suggest a common feature of fibroblast senescence is the production of a SASP as the conditioned media from both cardiac fibroblasts and MRC5s was able to reduce proliferation in healthy primary embryonic CMs. Furthermore, the media from MRC5s promoted senescence and reduced proliferation of cardiac endothelial cells. These data suggest that clearance of senescent interstitial cells possibly including senescent fibroblasts may improve recovery in part by attenuating a detrimental SASP. By reducing a fibrotic SASP, it may promote proliferation and limit senescence activation in surrounding cells, potentially altering several processes required for effective recovery post-MI, such as angiogenesis and CM regeneration. Regeneration may involve CM proliferation and functional stem cells, both of which may be attenuated in a senescent heart (Anderson *et al.*, 2019; Lewis-McDougall *et al.*, 2019). Therefore, the impact of fibroblast senescence and SASP should be considered in future studies and more thoroughly investigated as a potential target to alleviate disease. Traditionally fibroblasts have been believed to account for the largest proportion of non-myocyte cardiac cells (Camelliti *et al.*, 2005; Porter and Turner, 2009; Nagalingam *et al.*, 2016), however, recent profiling studies reported that the fibroblast population is smaller than the endothelial cell population (Pinto *et al.*, 2016; Kretzschmar *et al.*, 2018). So therefore other interstitial cell populations should also be considered in this disease pathology, with further analysis determining the specific contributions of each cell type.

Having demonstrated *in vitro* that the SASP may be detrimental to processes considered as reparative post-IRI, I next aimed to ascertain if elimination of senescent cells correlated with a diminished SASP. Components of the SASP were quantified using a cytokine array. While my data does not indicate which senescence cell populations are responsible for the SASP, it does indicate that many factors that have been previously associated with the SASP were significantly altered after IRI. Many of these proteins decreased in line with senescence elimination as a result of navitoclax treatment. These data also provided evidence that these proteins were directly associated with cellular senescence and not simply a result of general inflammation from LAD ligation surgery. Based on the current literature, these proteins could contribute to remodelling in a number of ways.

Interleukin-16 (IL-16) is linked to many inflammatory diseases and has been reported to directly drive inflammation within the myocardium of a model of hypertension induced heart failure. This resulted in increased cardiac fibrosis contributing to the pathophysiology of heart failure (Tamaki *et al.*, 2013).

Fractalkine, also referred to as CX3CL1, is a unique chemokine in that it can present either in a soluble or membrane-bound form depending on the role required; the soluble form is a chemoattractant whereas the bound form is an adhesion molecule (Umehara *et al.*, 2004). This chemokine is known to play a role in CVDs including atherosclerosis and cardiac injury due to MI, and its expression correlates with poorer functional outcome and increased mortality in MI patients that undergo PPCI and have IRI (Boag *et al.*, 2015). In mice, neutralisation of fractalkine improved survival and cardiac functions after MI (Gu *et al.*, 2015).

Another interleukin, IL-11, is also specific to fibroblasts (Schafer *et al.*, 2017; Ng *et al.*, 2019). It acts in a pro-fibrotic fashion inducing differentiation of fibroblasts to myofibroblasts, increasing contractility, stimulation mobility and invasion towards sites of inflammation in a mouse model of MI. Additionally, administering recombinant IL-11 protein induced fibroblast activation and a further worsened cardiac function (Schafer *et al.*, 2017).

Interferon γ -induced protein-10 (IP-10), also known as CXCL10, is released upon stimulation by IFN- γ to stimulate the migration of a range of immune cells to sites of inflammation. In CVDs, IP-10 can directly and indirectly drive and manipulate the progression of CVDs including atherosclerotic plaque destabilisation (Safa *et al.*, 2016).

Remodelling of the LV involves production and removal of the cardiac ECM, which is dependent on a balanced expression of MMPs and their inhibitors, TIMPs. The cytokine TIMP-1 has been linked to increased risk of CVDs including atherosclerosis and also to cardiac structural and functional parameters associated with adverse remodelling such as increased LV thickness, end systolic diameter and end diastolic diameter (Sundström *et al.*, 2004).

Two additional cytokines that were considerably upregulated following LAD ligation were Tarc, also known as CC chemokine ligand 17 (Ccl17), and Il-6. Like TIMP-1, TARC expression is associated with atherosclerosis via the increased recruitment of T

cells resulting in the promotion of inflammation (Weber *et al.*, 2011). Interleukin-6 is a known secreted factor from senescent cardiac fibroblasts in response to MI, and is directly regulated by the activation of the p53 pathway (Zhu *et al.*, 2013). Therefore, the result in Figure 6.14.G suggests that in this cohort the SASP factors upregulated may relate to cardiac fibroblasts and induction of senescence.

Macrophage inflammatory protein-3 β , or CCL19, is a cytokine that has been linked to atherosclerosis and detected in the ruptured plaques in MI patients (Damas *et al.*, 2007; Erbel *et al.*, 2007; Akhavanpoor *et al.*, 2014; Halvorsen *et al.*, 2014). As such, it has been suggested as a potential therapeutic target to modulate the immune response and reducing levels may prevent plaque rupture by stabilising these lesions (Akhavanpoor *et al.*, 2014).

Like IP-10, MDC also drives inflammation in ischaemic heart disease (IHD) patients with a history of MI, impacts the progression of atherosclerosis and may be a reliable risk biomarker for IHD (Safa *et al.*, 2016). In support of these data my results show that levels of MDC are increased post-ischaemia, and reduced expression of MDC is associated with improved outcome which is observed in this navitoclax cohort that had attenuated remodelling and rescued cardiac function.

There is conflicting data as to whether eotaxin, or CCL11 levels are related to atherosclerosis or other cardiac diseases like coronary artery disease (CAD). Eotaxin expression was first shown to correlate with CAD and IHD in a study which showed levels were raised in CAD patients compared to asymptomatic controls (Economou *et al.*, 2001). However, more recently Mosedale, D. *et al.* observed no such correlation for eotaxin expression and atherosclerosis or MI in a cohort of 446 patients (Mosedale *et al.*, 2005). These discrepancies have been postulated to result from studies being underpowered and fundamental differences between study designs. Further studies have been conducted to provide clarification, and it has since been suggested that eotaxin may have alternative roles other than an eosinophil chemoattractant. In atherosclerosis, eotaxin was demonstrated to upregulate vascular inflammation via vascular smooth muscles cells in plaques secreting eotaxin and driving endothelial cell migration (Emanuele *et al.*, 2006; Niccoli *et al.*, 2010). Eotaxin expression has also been shown to be substantially higher after ischaemia, with ischaemic stroke patients having elevated eotaxin levels correlating to poorer outcomes both acutely and

chronically (Roy-O'Reilly *et al.*, 2017). After IRI in this study, eotaxin levels were also considerably increased.

Interferon- β 1 has been demonstrated to induce the expression of p21^{CIP}, and is described as having roles in both stimulating and prohibiting proliferation (Limborg *et al.*, 2007). Expression of IFN- β 1 has also been investigated in patients with rheumatoid arthritis. Due to reports that IFN- β 1 has anti-inflammatory properties, a group postulated that increased expression may reflect activation of anti-inflammatory mechanisms, but these were insufficient to prevent rheumatoid arthritis development (van Holten *et al.*, 2005). However, this study also suggested that lfn- β 1 may act to sustain inflammation, as previously it was demonstrated that this cytokine can prevent T cell apoptosis (Pilling *et al.*, 1999). Other studies showed that IFN- β 1 acted in an anti-inflammatory manner and therefore elevated levels may be of benefit to limit inflammation (Triantaphyllopoulos *et al.*, 1999; Tak, 2004; van Holten *et al.*, 2005).

Very few studies have evaluated the roles of type 1 IFNs, including IFN- β 1, in IHD and MI. A murine study of permanent MI demonstrated that MI resulted in elevated levels of lfn- β 1 and Cxcl10 (Ip-10) mRNA and increased protein levels of Cxcl10 and interferon stimulated genes, but protein levels of lfn- β 1 itself were not reported. When mice were allowed to reperfuse post-MI, the data suggested that ischaemic cardiac cells released DNA to activate phagocytes to induce a cGas and lfn response. Taken together, the influence of lfn- β 1 and other type 1 lfn are important after MI to activate cardiac macrophages to reduce inflammation and improve function to increase survival (King *et al.*, 2017). Although lfn- β has also been reported to be predominantly secreted by fibroblasts (Hoyer and Nahrendorf, 2019). In this study, however, I did not observe an increase in lfn- β 1 after MI, so investigations into other type 1 lfn would be of interest. This observation that lfn- β 1 isn't up-regulated to exert an anti-inflammatory effect post-IRI can only be validated with further studies. But considerations should be made that the systemic clearance of senescent cells and the SASP for therapeutic benefit may be detrimental if removing cytokines known to exert protective effects after injury or disease. Therefore, more targeted approaches could result in more effective therapeutic outcomes.

The data from the TGFB1-3 array demonstrated that all three Tgf- β protein isoforms were increased as a result of IRI. In CVD, the TGF- β family play multiple roles in regulating differentiation, migration, ECM production, tissue homeostasis as well as

other events. In the cardiovascular system, TGF- β 1 is a highly important member of the TGF- β family, contributing to the progression of numerous CVDs including atherosclerosis, hypertrophy and heart failure, and can act in both a deleterious and beneficial way (Ruiz-Ortega *et al.*, 2007). Following MI TGF- β 1 has been described as having paradoxical roles (Frangogiannis, 2017). In atherosclerosis it acts as both an anti-inflammatory and anti-fibrotic and as such is beneficial to stabilise the plaque and stimulate tissue repair (Grainger, 2004; Redondo *et al.*, 2012). However, as the disease progresses and expression of different TGF- β receptor composition changes, TGF- β 1 switches to exerting detrimental effects via ECM formation, destabilising plaques and leading to excessive remodelling (Ruiz-Ortega *et al.*, 2007; Redondo *et al.*, 2012). In terms of cardiac fibrosis, TGF- β 1 is a vital regulator of stimulating fibroblasts to secrete collagen and other ECM components. Due to the importance of fibrosis post-MI, targeting TGF- β 1 has shown great promise in trials to limit fibrosis (Khan and Sheppard, 2006; Yue *et al.*, 2017). From this study, navitoclax considerably reduced Tgf- β 1, which may be one mechanism that navitoclax acts via to reduced overall infarct size that was observed in the longer-term, original navitoclax study (chapter 4).

In summary, clearance of senescent cells with navitoclax reduced the expression of several cytokines and chemokines with known associations with senescence cells. These other studies discussed above have demonstrated these factors have roles in driving processes that would be detrimental to recovery post-IRI including inhibiting proliferation, promoting myocardial remodelling and reducing cardiac function. My data therefore supported the hypothesis that mechanistically, navitoclax reduces the SASP and this may attenuate some of the detrimental processes associated with the SASP proteins.

From the serum array, there were some changes in circulating SASP protein levels, suggesting that these cytokines are indeed secreted and circulated systemically. Therefore, they may affect the heart as a whole or even stimulate systemic effects including inflammation. After an MI, patients with additional health conditions at the time of their MI are at a greater risk of a significantly reduced life span according to the severity of their multi-morbidities (Hall *et al.*, 2018). Predicting disease progression raises another clinical application for the data included in this thesis, as levels of SASP proteins may provide circulating biomarkers to predict those patients that have higher

levels of senescence, and thereby experiencing more remodelling and potentially poorer outcome post-MI. This is useful to stratify senescence-targeting therapies to those patients with the greatest potential for benefit and subsequently monitor whether the therapies worked to predict patient long-term outcomes and disease progression.

Tarc, eotaxin, Tgf- β 1 and Tgf- β 2 are markers associated with inflammation in a cardiac disease setting (Emanuele *et al.*, 2006; Niccoli *et al.*, 2010; Weber *et al.*, 2011; Frangogiannis, 2017), and the substantial reduction in their levels after navitoclax potentially signifies that treatment has reduced systemic inflammation signalling. Therefore, the beneficial effects from navitoclax dosing may not result from effects locally in the heart but rather from clearing dysfunctional immune cells contributing to immunosenescence. Immunosenescence is defined as the loss of immune system function with age (Aw *et al.*, 2007) and accumulation of pro-inflammatory cytokines has been linked to both ageing and the pathogenesis of inflammatory age-related diseases (De Martinis *et al.*, 2005; Licastro *et al.*, 2005). However, from my data none of these cytokines were considerably increased following IRI from the serum array, questioning whether they are suitable biomarkers clinically if increases in their levels can only be detected locally to the injury. Conversely Il-6, another SASP factor associated with inflammation (Zhu *et al.*, 2013), was greatly upregulated after IRI but not affected with navitoclax treatment. Although, unlike Tarc, Eotaxin and Tgf- β 2, the pattern of Il-6 expression was the same from the serum sample and LV protein sample, making it a potentially more useful biomarker as serum levels reflects what is occurring locally at the site of injury.

Currently the Heart Failure Association affiliated with the European Society of Cardiology guidelines outline many biomarkers that may be useful clinically to diagnose and monitor patients with heart failure (Heart Failure Association, 2010). Natriuretic peptides, including B-type natriuretic peptide, have been comprehensively studied and shown that their levels correlated to heart failure severity (Di Angelantonio *et al.*, 2009; Lin *et al.*, 2014; Nadar and Shaikh, 2019). Although used to diagnose heart failure, it has been suggested to use this biomarker in conjunction with additional biomarkers and there are additional cardiac and non-cardiac causes that can result in elevated natriuretic peptides (Kim and Januzzi, 2011). The interleukin ST2 (Rehman *et al.*, 2008), galectin-3 (Amin *et al.*, 2017) and pro-adrenomedullin (Nishikimi and Nakagawa, 2018) are other biomarkers reported to increase with heart failure,

however, are also associated with other disorders making them not specific for heart failure (Nadar and Shaikh, 2019). These biomarkers are also used to track the prognosis of heart failure, and although useful, issues regarding disease specificity, reproducibility across studies and some biomarkers having short half-lives (Nadar and Shaikh, 2019) result in studies recommending using a panel of biomarkers (Gaggin *et al.*, 2017) and the European Society of Cardiology reporting but not recommending the use of any one biomarker in a clinical setting (Ponikowski *et al.*, 2016).

Overall, identifying SASP factors that correlate with the pathogenesis of IRI post-MI may be very useful to diagnose and monitor patients for associated co-morbidities or assign therapies to patients in a personalised fashion. From my data, however, information regarding SASP components relating to IRI, clearance of senescence and improvements in cardiac function is limited by many factors. Firstly, this study was performed in a very small sample size. Secondly, while these data do not provide any novel biomarkers of cardiac function the lack of differences in the circulating SASP supports the idea that it is local clearance of senescence and reduced inflammation that improves cardiac function and not a systemic reduction in inflammation or changes to the immune system that is important. Additional none targeted approaches, such as proteomic analysis, could identify novel SASP proteins that may be more useful as prognostic biomarkers or even identify new therapeutic targets to block the SASP and its effects.

My *in vitro* studies demonstrated that conditioned media from senescent fibroblasts directly reduced the proliferation of cardiac endothelial cells and CMs via paracrine signalling, likely via SASP factors. Having observed changes in many SASP factors *in vivo*, assessment of the proliferation of endothelial cells and CMs was then investigated to determine whether the observations *in vitro* were occurring in the heart post-IRI. Quantification of EdU incorporation into CMs 4 weeks after navitoclax dosing showed that treatment had no major effect on inducing CM proliferation, although levels were raised. From this analysis, the majority of EdU positive cells throughout the LV proximal to the infarct were interstitial cells, and navitoclax was observed to significantly increase the number of proliferating endothelial cells, identified by the endothelial marker CD31 (Liu and Shi, 2012). However, despite being widely considered as an endothelial cell marker, CD31 has also been demonstrated to be expressed by all leukocytes, including T and B lymphocytes, dendritic cells, natural

killer cells, macrophages, granulocytes as well as platelets. As such, expression of CD31 may also indicate activation of the immune system (Marelli-Berg *et al.*, 2013). Nevertheless, my data align with those previously published which demonstrated that a cardiac fibrotic SASP reduced endothelial cell proliferation (Hernandez-Lopez *et al.*, 2017). In venous thrombosis disease, premature senescence induction via OS greatly reduced endothelial proliferation, which in turn predisposed the patient to endothelial dysfunction and detrimentally contributed to the pathogenesis of disease (Hernandez-Lopez *et al.*, 2017). This may well be the case in terms of MI with IRI, with an accumulative effect from OS and a fibrotic SASP leading to endothelial dysfunction and attenuated angiogenesis.

Overall, after IRI cardiac interstitial cells become senescent. Treatment with navitoclax reduced levels of senescence markers, both during treatment and 4 weeks after, by preferential clearance of interstitial cells via apoptosis. Proof of principal studies confirmed that senescent fibroblasts exerted paracrine effects on non-fibroblast cardiac cells, and that after IRI there are elevated levels of cytokines that have previously been associated with the SASP. Additionally, *in vivo* removal of senescent cells, both CMs and interstitial populations, resulted in a reduction in several SASP proteins and was associated with a substantial increase in endothelial cell proliferation, which is indicative of improved angiogenesis (Cochain *et al.*, 2013).

Chapter 7. Discussion

Cardiovascular diseases account for the largest proportion of morbidity and mortality events globally (Hausenloy and Yellon, 2013; World Health Organisation, 2014), but thanks to advances in interventional procedures, survival rates after MI have considerably improved since the introduction of PPCI (Lønborg, 2015; Doost Hosseiny *et al.*, 2016). However, IRI and adverse remodelling post-MI accelerating patient's progression to heart failure is a serious clinical issue (Hausenloy and Yellon, 2013; Muhlestein, 2014; Lønborg, 2015). Unfortunately, to date, most efforts to target MI with IRI to repair the myocardium or rescue cardiac function have failed to successfully translate into the clinic (Baehr *et al.*, 2019).

Cellular senescence has been linked to or demonstrated to have a direct role in the progression of ageing and multiple age-related disorders (McHugh and Gil, 2018). These disorders include diseases associated with the respiratory, digestive, nervous, muscular, renal as well as cardiovascular system (Passos *et al.*, 2010; Jurk *et al.*, 2014; Birch *et al.*, 2015; Ogrodnik *et al.*, 2017; Anderson *et al.*, 2019). Pre-clinical trials have provided positive results relating to the modulation or clearance of senescent cells (Baker *et al.*, 2011; Baker *et al.*, 2016) and a new class of drugs called senolytics have attracted a lot of attention. These drugs specifically target senescent cells systemically to alleviate adverse symptoms (Zhu *et al.*, 2015; Kirkland and Tchkonja, 2017; Short *et al.*, 2019). In the ageing heart, senescence has been associated with a decline in cardiac function. Treatment with the senolytic navitoclax reduced CM senescence in aged mice which correlated with improved function and response to permanent MI (Walaszczyk *et al.*, 2019). Additionally, research has identified senescence within the cardiac stem and progenitor cell population as a potential mechanism obstructing efficient CM differentiation during repair. The adverse environment generated from senescence and the SASP may in part explain why regeneration therapies, both stimulating endogenous regeneration and transplantation approaches, have failed to efficiently translate from the lab to the clinic (Lewis-McDougall *et al.*, 2019; Oldershaw *et al.*, 2019).

The data presented from this study provide further evidence that the heart, including both CMs and interstitial cells, can become senescent when exposed to stressors such

as OS. This further challenges the traditional view that as the majority of CMs are post-mitotic and do not experiencing telomere attrition during DNA replication they are unable to senesce (Vicencio *et al.*, 2008). Regions in the LV proximal to the infarct after LAD ligation surgery showed an elevated intensity of the OS marker 4-HNE. Within this region CMs contained increased numbers of TAF and were positive for a range of senescence markers including SA- β -Gal, p21^{Cip} and p16^{Ink4a}. From the SA- β -Gal staining the interstitial cells, particularly in the infarct zone, were observed to be positive for this senescence marker from 72 hours post-ligation, whereas CMs were only identified after 1 week. Analysis of TAF in the CMs was very high at 1 week and was reduced by 4 weeks, suggesting that CMs containing high levels of genomic damage were cleared. The proportion of CMs containing TAF at 4 weeks post-ligation correlated to the percentage of CMs positive for both p21^{Cip} and p16^{Ink4a}. Markers of senescence weren't investigated after this time-point as senescence is reported to be permanent once established as cells have an upregulation of anti-apoptotic proteins to evade clearance. However, confirmation that these levels are persistent at time-points past 4 weeks would be of interest to fully understand the progression of senescence after IRI and whether levels increase via propagation of senescence to accelerate injury and adverse remodelling. If so, tracking senescence biomarkers may be useful to diagnose and predict patients most at risk of heart failure or stratify regeneration therapies to patients with the lowest senescence levels and are therefore most likely to have successful results (Althubiti *et al.*, 2014).

As well as this, after LAD ligation mice had extensive scars in their LV. To ensure that all mice had been reperfused properly, the morphology of their infarcts were checked. Any mice with transmural scars were assumed to have been insufficiently reperfused, and therefore had a permanent MI and not IRI so were excluded from further analyses. After treatment with navitoclax, the percentage of the LV composed of scar had substantially decreased. This reduction of the scar indicated that clearance of senescent cells reduced adverse remodelling in terms of structural changes including fibrosis. However, structural improvements are only beneficial if they can positively affect cardiac function.

From the cardiac function data, higher levels of senescence markers were associated with a reduction in functional variables that are currently used to diagnose heart failure in patients (Bolognese *et al.*, 2002; Ponikowski *et al.*, 2016; Redgrave *et al.*, 2016;

Borzage *et al.*, 2017; Bulluck *et al.*, 2017; Rodriguez-Palomares *et al.*, 2019). As MRI analysis is performed manually, incorrect inferences of the MRI variables can occur due to potential operator biases since the position of each measurement can be very subjective. To minimise errors and to improve the accuracy of the analysis, MRI analysis was performed by three individuals including myself and all analysis was performed in a blinded manner. Before un-blinding, any scans with a $\geq 5\%$ difference in EF were reanalysed (by a fourth individual when possible). Additionally, all measurements were only included if the LV mass measurements taken at end diastole and end systole was within $\pm 4\%$ as LV mass would be unchanged during contraction. From my data, navitoclax treatment also attenuated remodelling as functional variables were considerably improved. Most importantly EF was either maintained or improved reversing the trend for a progressive loss in cardiac function post-MI with IRI considering the importance senescence plays in wound repair to stimulate and self-limit fibrosis (Jun and Lau, 2010a). Navitoclax dosing was selected to begin 96 hours after surgery as there were concerns that prior to this time-point elimination of senescence within the infarct may result in incomplete wound healing and cardiac rupture. At the 72 hour time-point senescence, indicated by SA- β -Gal, was observed within the infarct region that was predicted to include myofibroblasts, and consequently dosing commenced after this time-point. Therefore, navitoclax dosing began after interstitial cell senescence initiation, implying wound repair mechanisms had begun, but prior to senescence becoming chronically expressed at 7 days. It was important to carefully monitor animals during and after treatment for any adverse outcomes, however, no mice displayed any harmful symptoms. In particular, no mice died after surgery and treatment as a result of cardiac rupture, so the timing of navitoclax dosing allowed for sufficient fibrosis to repair and strengthen the injured myocardium, but also minimised fibrosis to result in a smaller infarct, more elastic LV and overall improved cardiac function. It may be of interest to see if earlier treatment could improve outcomes even more, however, given that the outcomes from this study were highly favourable I would suggest that these studies should be performed on a small cohort of mice as improvements may be unlikely. It is also possible that the effects of navitoclax are beneficial in the short term but have consequences later in life. Again, this is something I am very aware of and studies should be performed to see what the long-term effects of navitoclax are, particularly as I have demonstrated treatment leads

to CM apoptosis, which may not have the same regenerative reserve as some other cell populations.

These beneficial outcomes following navitoclax treatment are encouraging and warrant further studies. However, there are concerns that senolytics may in fact be detrimental post-IRI as they exert their effects systemically (Ponikowski *et al.*, 2016; Kirkland and Tchkonja, 2017). An associated adverse side effect of navitoclax is thrombocytopenia, as the drug can act on the BCL-2 homologs including BCL-X_L. This protein along with other BCL-2 pro-survival proteins are expressed by platelets, and inhibition by senolytics including navitoclax can trigger apoptosis and a reduced platelet population. However, in several studies that reported thrombocytopenia, no clinically relevant bleeding events were described, thrombocytopenia was fully reversed upon cessation of drug use and no markers indicating platelet aggregation were detected (Zhang *et al.*, 2007; Rudin *et al.*, 2012). Additionally, many of the patients in these clinical trials were either relapsed or refractory cancer patients, and their bone marrow platelet population may already be compromised if tumour cells are present and proliferating in the bone marrow. In this case, progressing injury models using navitoclax should continue with these toxicities being regularly monitored (Kaefer *et al.*, 2014), although thrombocytopenia was not confirmed in the cohort of mice I used in this study.

To circumvent thrombocytopenia and avoid having to reduce navitoclax drug levels which may lessen its efficacy, a novel BCL-2 inhibitor was generated to be selective for BCL-2 and not bind BCL-X_L. To achieve this selectivity for BCL-2 navitoclax was re-designed to target a co-crystal structure only identified on BCL-2 molecules. Navitoclax and pro-apoptotic proteins bind to BCL-2 within the BH3 domain via two interfaces. By altering these two regions it was discovered that removal of a thiophenyl ring subunit caused a structural alteration to one binding point and together with the addition of an azaindole to strengthen the second binding point, this new compound bound strongly and specifically to BCL-2 (Figure 7.1). The new drug was called ABT199, also known as venetoclax, and in a small study on chronic lymphocytic leukaemia patients demonstrated a retained efficacy for clearing cells over-expressing BCL-2 whilst minimally affecting the platelet population. The ability of venetoclax to bind to BCL-X_L was over 3-fold lower compared to navitoclax, yet could still evoke a rapid apoptotic response after a single dose that was stronger than a corresponding dose of navitoclax (Souers *et al.*, 2013).

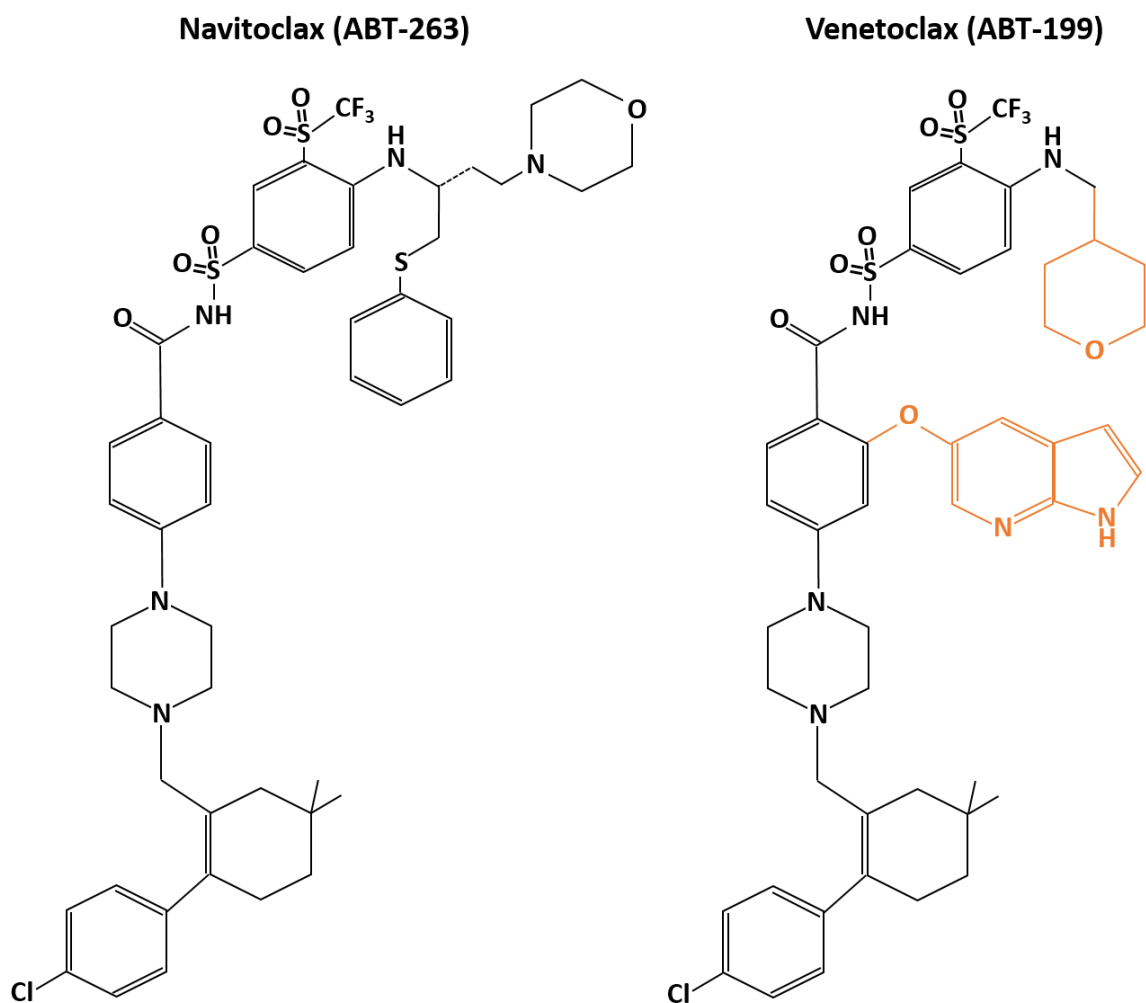


Figure 7.1 Chemical structure of navitoclax and venetoclax.

Navitoclax was modified with the addition of the thiophenyl ring and azaindole to produce venetoclax. Venetoclax in comparison has an improved efficacy for BCL-2 and reduced binding to BCL-X_L so addresses the issues surrounding toxicity of navitoclax. Adapted from (Souers *et al.*, 2013).

As aforementioned, navitoclax acts systemically (Short *et al.*, 2019). Although concerns regarding off-target events having detrimental outcomes in terms of repair mechanisms, another issue with analysing navitoclax treatment is dissecting the direct and indirect effects. To try and discern whether navitoclax was improving the cardiac function directly and not just improving the overall health of the mice, possibly by reducing inflammation systemically or improving vascular health, I performed two additional studies. The first was generating a novel CM-specific *p16^{Ink4a}* knockout mouse. This model provided evidence whether it was the CM population or interstitial cells that predominantly contributed to functional outcome. The second study was

repeating navitoclax treatment to investigate the events occurring during dosing, mainly to ensure the drug was activating apoptosis in the heart. However, this study did not confirm whether apoptosis was also occurring in additional organs.

From the knockout model, there was a considerable reduction in senescence markers $p16^{Ink4a}$ and $p21^{Cip}$. To initiate recombination via Cre, 4-OHT was administered instead of tamoxifen, as tamoxifen needs to be metabolised in the liver into the active 4-OHT, which takes time and also may not be the most efficient process (Felker *et al.*, 2016). Although $p16^{Ink4a}$ expression within the CMs was lower, there was a residual level of $p16^{Ink4a}$. This expression was attributed to the inducible Cre line utilised not being 100% efficient at floxing exon 1 α as previously reported (Sohal *et al.*, 2001), and so $p16^{Ink4a}$ could be transcribed and translated. One way to counteract this inefficient floxing would be to use a non-inducible conditional Cre line to excise $p16^{Ink4a}$. However, preventing $p16^{Ink4a}$ expression in the CMs from embryogenesis may interfere with development, as senescence is also an important regulatory mechanism during development and preventing senescence pathways may result in defects (Muñoz-Espín *et al.*, 2013; Storer *et al.*, 2013). Another way to increase excision by the inducible Cre used would be to optimise dosing concentrations and regimes. Also, as well as $p16^{Ink4a}$ expression not being completely inhibited, this model didn't target $p21^{Cip}$ dependent senescence. Both the $p16^{Ink4a}$ and $p53/p21^{Cip}$ pathways have been demonstrated to feedback on each other (Leong *et al.*, 2009), however, in the knockout model generated for this study, $p21^{Cip}$ was not upregulated in a compensatory manner. Reductions in $p21^{Cip}$ suggests that this pathway is affected by $p16^{Ink4a}$, however, knocking out $p21^{Cip}$ as well as $p16^{Ink4a}$ would generate a better model of inhibiting CM senescence.

Regardless, even though senescence wasn't prevented completely, levels were comparable to those observed in young, healthy, wild type mice CMs after navitoclax treatment. Results from this experiment suggest that reducing CM senescence is not the primary mechanism by which navitoclax attenuated remodelling to improve cardiac function. Therefore, future interventions should be focused on the interstitial cells as opposed to the CMs. Although fibrinolytic drugs have been trialled and shown to be unsuccessful in patients (National Clinical Guideline Centre (UK). 2013), targeting the chronically senescent myofibroblasts could possibly result in a successful anti-fibrotic treatment. Conversely, if treatments only target a specific cell lineage within an organ

and there are senescent cells elsewhere within the organ or in alternative tissues, via paracrine signalling from the SASP may lead to newly formed senescent cells in new areas. Overall, it could be debated that systemic treatments targeting all senescent cell types are more beneficial to increase treatment efficiency and improve total health (Kirkland and Tchkonja, 2017).

A limitation of the knockout mouse study is that the model was not fully characterised at baseline in terms of p16^{-/-} cardiac structure and function prior to LAD ligation. Although there were no unusual observations in both the p16^{fl/fl} and p16^{-/-} mice regarding their histology and function post-IRI, this information would confirm that the mouse resembled a wild type mouse and did not have a phenotype exacerbating their outcome to LAD ligation. As well as the baseline measurements, including a Cre control would also strengthen this analysis. By crossing the *αMHC-MerCreMer* onto a wild type, non-floxed line would also confirm whether the Cre itself had any effect on cardiac remodelling. These controls were lacking from this study due to issues with breeding sufficient numbers for experimentation and technical issues with the MRI. For future publications, these controls are being collected.

The short-term navitoclax *in vivo* study was also performed to identify the cell populations being cleared from the treatment. From the TUNEL assay, approximately 90% of the cells undergoing apoptosis were interstitial cells, with CMs making up the remaining 10%. Additionally, the proliferation of CMs was not increased, and therefore, unlike in the aged mice (Anderson *et al.*, 2019; Lewis-McDougall *et al.*, 2019), clearance of senescent CMs and other cells did not stimulate a regenerative response in the CMs. These data may also provide further evidence that CMs are not the most important senescent cell type to target for therapies to improve remodelling and function post-IRI. Additionally, the cytokine array demonstrated a range of known factors previously associated with the SASP increase after LAD ligation and are reduced following navitoclax treatment. Although these cytokines cannot be directly linked to a specific cell type from this analysis, many have been associated with inflammation and fibrosis, but attributing the expression of these factors to fibroblasts is purely speculative and requires thorough investigation and characterisation.

Regardless, the array shows that some components of the SASP are upregulated in response to MI and IRI, and navitoclax reverses these trends. This array provides additional data demonstrating that senescence occurs in this model of MI with IRI and

treatment with a senolytic reduces senescence and can be correlated to beneficial functional outcomes.

As MI mostly occurs in individuals at 65 years or older (Boyer *et al.*, 2012; Roger *et al.*, 2012) it would be beneficial to repeat this study using aged mice. Young mice were utilised as we have previously demonstrated that senescence accumulates in the heart with age (Anderson *et al.*, 2019; Walaszczyk *et al.*, 2019). Therefore, distinguishing the contribution of IRI from ageing in terms of senescence induction could be problematic. Nevertheless, an aged mouse IRI model would be more clinically relevant, and interesting to see if the positive outcomes in the young mice were reproduced. One concern may be that with age there is a higher residual level of senescence, and so after IRI navitoclax may induce apoptosis in a larger proportion of cells. Taking this factor into account along with the fact that regeneration of CMs declines with age both from stem cell dysfunction (Lewis-McDougall *et al.*, 2019) and limited CM proliferation (Richardson *et al.*, 2015a), if too many cardiac cells are cleared and not replaced cardiac function may deteriorate further causing a worsening outcome. However, when aged mice (24 months) were treated with navitoclax and had a permanent LAD ligation (MI without IRI), survival rates were dramatically improved to that of a younger mouse accompanied with better cardiac function and remodelling (Walaszczyk *et al.*, 2019), suggesting that elimination of senescent CMs and cardiac cells is a potentially very beneficial therapeutic strategy that should be investigated for MI with IRI.

The preliminary *in vitro* studies aimed to validate whether senescent fibroblasts could affect the proliferation and senescence status of other cardiac cell lineages via a SASP. Fibroblasts were selected as the interstitial cells positive for senescence markers were identified using the fibroblast marker vimentin. However, this marker is not exclusive to fibroblasts and can include other mesenchymal cell types (Goodpaster *et al.*, 2008). Including an additional marker for CFs, such as discoidin domain receptor 2 (DDR2) (Souders *et al.*, 2009), would considerably strengthen this analysis.

After culture in the conditioned media from proliferative and senescent fibroblasts, both endothelial cells and CMs demonstrated attenuated proliferation and induction of senescence markers. Initially, the MRC5 fibroblast cell line was utilised based on the literature reporting that they express a SASP (Passos *et al.*, 2010; Hewitt *et al.*, 2012; Menicacci *et al.*, 2017), however, repeating these experiments on the MMVEC-Cs using CFs would be required to verify that a CF SASP yielded the same results. This

verification is required due of the complex nature of the SASP and variations between factors expressed depending on the cell type and tissue of origin (Coppé *et al.*, 2010). Because of this, time was spent optimising the isolation of primary adult CFs. Experiments using these primary fibroblasts were comparable to the MRC5 media, however, the primary fibroblasts require further characterisation to identify CF SASP factors. The CFs were stained with vimentin to check they were positive for this marker (Figure 7.2). As discussed above, verifying the cell identity with additional and more specific CF markers would strengthen this analysis that the observations *in vitro* could be occurring in the heart.

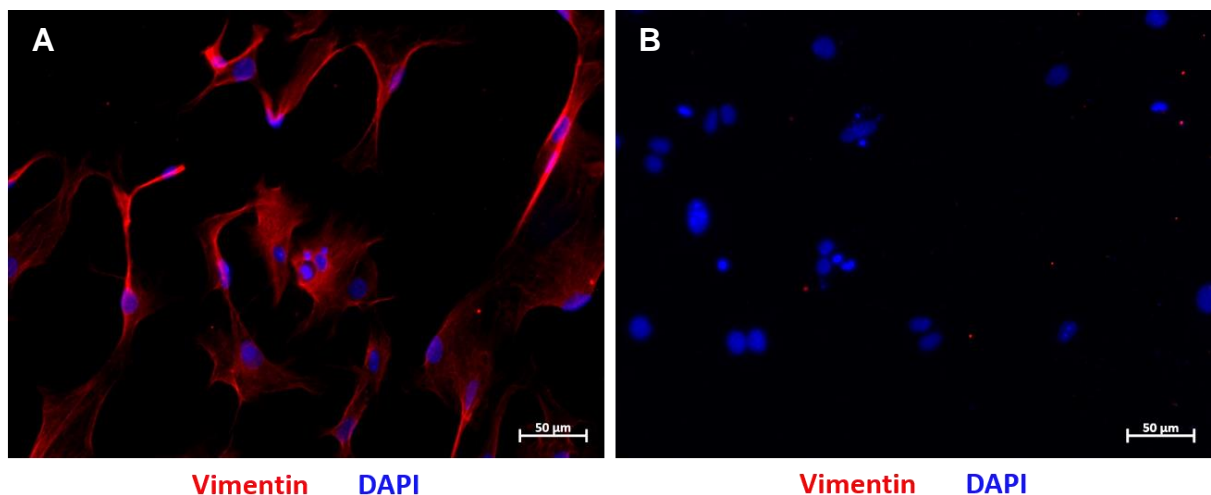


Figure 7.2 Isolated primary adult mouse cardiac fibroblasts are positive for the fibroblast marker vimentin.

A) Immunofluorescence staining of isolated cells for vimentin (red, wavelength 594nm) and DAPI (blue, wavelength 461nm).

B) Negative control for vimentin 1°Ab, slide was incubated in PBS instead.

Experiments to validate whether the fibroblasts are the senescent interstitial cells responsible for the results obtained from this study could include fibroblast knockout mouse lines. It would be preferable to generate supplementary conditional $p16^{Ink4a}$ models that used *Cre*-driven knockouts in specific interstitial cell types and repeat these studies. However, the navitoclax treatment did not inhibit senescence but rather removed senescent cells, which may explain the difference between my navitoclax studies and a previous study that used conditional knockout models for senescence genes in CFs. This study demonstrated that these conditional knockouts resulted in larger infarcts and poorer response to injury (Zhu *et al.*, 2013). The CM knockout model generated for this project could be retested and include an experimental group that

received subsequent treatment targeted towards fibroblasts. For example, p16^{-/-} mice could receive navitoclax treatment to see whether it would replicate the favourable phenotype from the initial navitoclax study. Or mice could be treated with anti-fibrotics, however, fibrinolytics as discussed previously have not been successful in clinics (National Clinical Guideline Centre (UK). 2013). Trials testing therapies that have been beneficial in pre-clinical trials but not in clinical trials could be tested in combination with a low dose or short-term regime of senolytics. These failed therapies may be more successful if combined with a senolytic to diminish the adverse environment from the SASP (Kirkland and Tchkonina, 2017).

In conclusion, MI and IRI in a young mouse surgical model induced senescence in both CM and non-CM cell lineages throughout the heart and were verified using a combination of different senescence markers (Figure 7.3, top row). A short-term treatment regime with the senolytic drug navitoclax reduced levels of senescence in multiple cell types and attenuated remodelling as demonstrated by the reduction in infarct size, elevated proliferation of endothelial cells and rescue of cardiac function (Figure 7.3, bottom row). However, not all components of remodelling were reversed with navitoclax, as proliferation of CMs was unchanged and hypertrophy of CMs was also unaffected.

Overall, the improvements from navitoclax warrant further testing and similar investigations into the SASP and senescence in the heart post-IRI should be tested in human samples. Identifying novel markers of cardiac senescence to correlate to function would be valuable to improve patient diagnosis and prognosis post-MI. If senolytics or other therapies targeting senescence were successfully translated into humans, this would have considerable ramifications globally to reduce the incidence of heart failure and associated morbidities to improve patient's recovery after MI and ultimately give them an extended, improved quality of life.

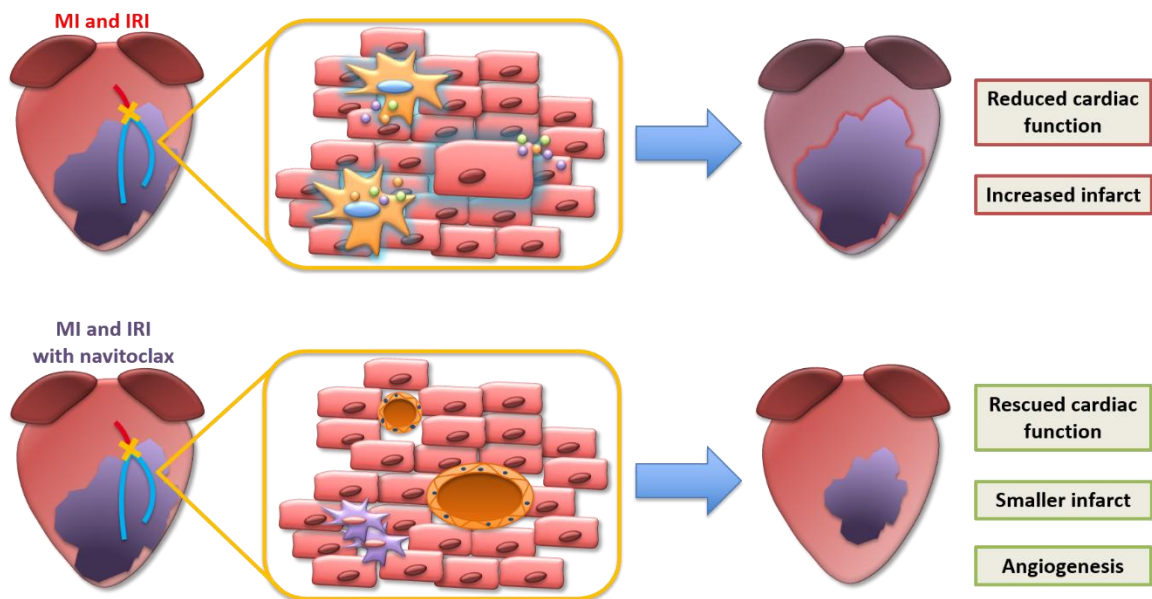


Figure 7.3 Graphical summary.

Myocardial infarction followed by IRI induces a state of OS that is associated with induction of senescence in multiple cardiac cell types including CMs and fibroblasts. Adverse remodelling events result in a larger infarct and severely reduced cardiac function (top row). However, treatment with navitoclax after MI with IRI was associated with reduced senescence and attenuated remodelling. A smaller infarct and endothelial cell regeneration, suggesting stimulation of angiogenesis, ultimately resulted in improved cardiac function (bottom row). Retaining or rescuing as much cardiac function as possible after an MI is essential to prevent or delay the onset of heart failure.

Appendix A

Raw values from MD-44 and TGFB1-3 Arrays from Eve Technologies

Table A.1 Values from MD-44 and TGFB1-3 for protein samples.

Cytokine	Concentration (pg/ml ± SD)			p Value		
	No LAD	IRI + Veh	IRI + Nav	No LAD vs IRI + Veh	No LAD vs IRI + Nav	IRI + Veh vs IRI + Nav
Eotaxin	6.74 ± 2.67	16.10 ± 4.28	8.87 ± 2.29	0.0270 (*)	0.7081	0.0728
EPO	-	-	-	-	-	-
Fractalkine	71.21 ± 2.53	90.27 ± 4.56	67.98 ± 4.49	0.0022 (**)	0.3579	0.0014 (**)
G-CSF	0.78 ± 0.17	1.17 ± 0.38	0.56 ± 0.07	0.1981	0.5537	0.0499 (*)
GM-CSF	-	-	-	-	-	-
IFNB-1	66.52 ± 1.94	67.22 ± 1.05	60.25 ± 2.88	0.9130	0.0243 (*)	0.0153 (*)
IFN γ	0.95 ± 0.79	2.09 ± 0.13	0.62 ± 0.72	0.2532	0.8323	0.1373
IL-1a	51.00 ± 6.92	17.17 ± 5.02	14.14 ± 2.21	0.0005 (***)	0.0003 (***)	0.7571
IL-1b	7.20 ± 0.77	6.65 ± 1.10	5.28 ± 0.36	0.6952	0.0560	0.1619
IL-2	25.73 ± 0.52	19.78 ± 2.93	17.75 ± 1.41	0.0200 (*)	0.0051 (**)	0.4403
IL-3	0.94 ± 0.12	0.84 ± 0.10	0.67 ± 0.16	0.6607	0.0969	0.3003
IL-4	0.19 ± 0.01	0.15 ± 0.01	0.12 ± 0.05	0.2437	0.1013	>0.9999
IL-5	0.01 ± 0.00	0.05 ± 0.00	0.01 ± 0.00	-	-	-
IL-6	1.21 ± 0.04	2.73 ± 0.64	1.53 ± 0.72	0.0347 (*)	0.7631	0.0841
IL-7	3.57 ± 0.46	2.93 ± 1.02	1.74 ± 0.42	0.5349	0.0403 (*)	0.1659
IL-9	229.7 ± 6.34	185.2 ± 5.28	191.8 ± 6.98	0.0003 (***)	0.0007 (***)	0.4525
IL-10	12.72 ± 0.60	9.56 ± 2.14	8.57 ± 0.80	0.0669	0.0229 (*)	0.6663
IL-11	0.83 ± 0.97	2.76 ± 0.76	0.55 ± 0.48	0.0422 (*)	0.6621	0.0357 (*)
IL-12/p40	4.94 ± 1.17	3.77 ± 1.87	4.04 ± 1.11	0.6013	0.7295	0.9722
IL-12/p70	3.34 ± 0.59	3.54 ± 1.84	3.16 ± 0.98	0.9798	0.9831	0.9286

IL-13	-	-	-	-	-	-
IL-15	33.18 ± 2.24	27.81 ± 4.00	19.19 ± 2.23	0.1437	0.0027 (**)	0.0268 (*)
IL-16	251.1 ± 71.11	382.7 ± 53.75	216.3 ± 32.86	0.0587	0.7297	0.0231 (*)
IL-17	0.13 ± 0.10	0.14 ± 0.12	0.03 ± 0.01	0.9989	0.3746	0.3554
IL-20	-	-	-	-	-	-
IP-10	5.31 ± 0.69	48.28 ± 28.02	8.80 ± 2.15	0.0404 (*)	0.9626	0.0559
KC	7.32 ± 2.72	13.73 ± 10.69	3.94 ± 1.01	0.4756	0.7970	0.2207
LIF	0.66 ± 0.18	1.58 ± 0.54	0.77 ± 0.09	0.0760	>0.9999	0.2209
LIX	268.7 ± 27.41	229.2 ± 19.23	208.8 ± 36.03	0.6097	0.1840	>0.9999
MCP-1	3.81 ± 0.86	11.39 ± 9.57	1.49 ± 1.14	0.4260	0.9107	0.2105
MCP-5	23.72 ± 7.91	224.4 ± 148.2	48.53 ± 16.07	0.0655	0.9345	0.1022
M-CSF	0.84 ± 0.20	0.85 ± 0.69	0.52 ± 0.10	0.9996	0.7363	0.7230
MDC	0.99 ± 0.23	5.03 ± 0.49	2.86 ± 0.44	<0.0001 (****)	0.0031 (**)	0.0014 (**)
MIG	36.13 ± 15.11	155.8 ± 100.7	52.99 ± 25.51	0.1134	0.9387	0.1751
MIP-1a	52.55 ± 9.31	36.41 ± 7.62	34.19 ± 7.56	0.1219	0.0800	0.9421
MIP-1b	-	-	-	-	-	-
MIP-2	273.1 ± 31.23	244.4 ± 10.57	214.0 ± 11.89	0.2675	0.0272 (*)	0.2366
MIP-3a	1.47 ± 0.06	1.05 ± 0.19	0.95 ± 0.02	0.0089 (**)	0.0030 (**)	0.5380
MIP-3b	31.22 ± 12.74	134.2 ± 16.86	79.63 ± 16.55	0.0005 (***)	0.0204 (*)	0.0119 (*)
RANTES	2.41 ± 0.48	1.73 ± 0.12	1.34 ± 0.66	0.2614	0.0743	0.6069
TARC	0.72 ± 0.39	4.88 ± 1.90	2.60 ± 1.01	0.0163 (*)	0.2433	0.1474
TIMP-1	31.68 ± 0.71	1298 ± 443.6	476.2 ± 234.1	0.0164 (*)	0.3527	0.0547
TNF α	-	-	-	-	-	-
VEGF	6.04 ± 1.69	12.49 ± 3.63	9.09 ± 2.62	0.0648	0.4203	0.3528
6Ckin/Exodus	850.3 ± 210.8	955.1 ± 64.56	642.0 ± 101.7	>0.9999	0.5391	0.2209
TGF- β 1	62.12 ± 60.71	87.47 ± 10.29	16.47 ± 4.25	0.6765	0.3278	0.0004 (***)
TGF- β 2	8.89 ± 3.76	65.62 ± 28.09	26.01 ± 14.47	0.0214 (*)	0.5262	0.0854
TGF- β 3	1.88 ± 0.43	19.13 ± 5.97	6.37 ± 3.56	0.0046 (**)	0.4130	0.0190 (*)

Table A.2 Values from MD-44 and TGFB1-3 for serum samples.

Cytokine	Concentration ($\mu\text{g/ml} \pm \text{SD}$)			p Value		
	No LAD	IRI + Veh	IRI + Nav	No LAD vs IRI + Veh	No LAD vs IRI + Nav	IRI + Veh vs IRI + Nav
Eotaxin	497.0 \pm 63.90	558.2 \pm 46.24	418.3 \pm 50.05	0.4040	0.2513	0.0438 (*)
EPO	74.87 \pm 57.14	116.9 \pm 53.29	96.09 \pm 35.14	0.5805	0.8621	0.8667
Fractalkine	172.2 \pm 51.72	187.5 \pm 17.04	170.5 \pm 18.94	0.8437	0.9977	0.8108
G-CSF	197.9 \pm 30.21	308.3 \pm 185.2	342.2 \pm 109.7	0.5606	0.3951	0.9422
GM-CSF	6.52 \pm 1.83	-	4.77 \pm 0.00	-	-	-
IFNB-1	186.0 \pm 157.6	112.0 \pm 22.27	107.5 \pm 17.30	0.6146	0.5817	0.9981
IFN γ	0.51 \pm 0.00	1.52 \pm 1.12	0.42 \pm 0.18	0.5901	>0.9999	0.3415
IL-1a	112.3 \pm 80.94	154.8 \pm 80.65	32.84 \pm 17.70	0.7280	0.3732	0.1426
IL-1b	0.34 \pm 0.26	0.60 \pm 0.50	0.44 \pm 0.14	>0.9999	>0.9999	>0.9999
IL-2	1.90 \pm 0.72	1.57 \pm 0.32	1.62 \pm 0.44	0.7339	0.7984	0.9924
IL-3	1.32 \pm 0.46	1.01 \pm 0.37	0.99 \pm 0.43	0.6618	0.6235	0.9975
IL-4	0.31 \pm 0.06	0.26 \pm 0.02	0.31 \pm 0.11	0.6511	0.8403	>0.9999
IL-5	7.77 \pm 1.93	6.23 \pm 4.18	8.07 \pm 2.98	0.8278	0.9926	0.7662
IL-6	2.48 \pm 0.84	48.19 \pm 24.41	45.53 \pm 17.89	0.0424 (*)	0.0533	0.9811
IL-7	2.90 \pm 0.12	143.3 \pm 241.7	2.74 \pm 0.37	>0.9999	>0.9999	0.6991
IL-9	43.62 \pm 8.89	36.99 \pm 20.24	19.48 \pm 9.75	0.8344	0.1659	0.3403
IL-10	9.08 \pm 3.01	10.80 \pm 1.44	9.09 \pm 3.97	0.7692	>0.9999	0.7707
IL-11	30.62 \pm 0.00	265.2 \pm 0.00	-	-	-	-
IL-12/p40	8.26 \pm 0.00	8.60 \pm 3.46	7.16 \pm 4.51	0.9910	0.9131	0.8564
IL-12/p70	11.90 \pm 6.95	10.43 \pm 1.59	10.42 \pm 0.00	>0.9999	>0.9999	>0.9999
IL-13	75.58 \pm 32.48	40.92 \pm 16.69	50.16 \pm 15.28	0.2308	0.4158	0.8763
IL-15	33.38 \pm 13.81	3496 \pm 5940	21.80 \pm 6.26	0.6097	0.8841	0.0610
IL-16	736.0 \pm 399.8	1029 \pm 122.6	982.0 \pm 289.9	0.4852	0.2892	0.9795
IL-17	0.22 \pm 0.12	0.51 \pm 0.11	0.45 \pm 0.15	0.0668	0.1408	0.8322
IL-20	80.55 \pm 0.00	205.0 \pm 30.61	213.8 \pm 85.29	0.3171	0.2800	0.9845

IP-10	60.88 ± 16.87	103.5 ± 38.65	81.26 ± 19.86	0.2079	0.6444	0.5960
KC	112.5 ± 37.32	165.4 ± 11.71	162.5 ± 72.46	0.4152	0.4502	0.9970
LIF	0.67 ± 0.13	1.19 ± 0.64	0.92 ± 0.14	0.2895	0.7081	0.6841
LIX	1818 ± 610.1	2553 ± 482.9	1353 ± 487.9	0.2812	0.5623	0.0724
MCP-1	1.86 ± 0.41	24.24 ± 37.55	3.17 ± 2.40	0.3032	0.8902	>0.9999
MCP-5	28.16 ± 13.29	84.78 ± 53.03	55.36 ± 23.82	0.1896	0.6218	0.5776
M-CSF	3.20 ± 1.47	3.36 ± 2.79	3.61 ± 2.11	0.9954	0.9720	0.9899
MDC	116.4 ± 22.44	122.4 ± 43.09	97.45 ± 31.98	0.9736	0.7781	0.6542
MIG	42.59 ± 29.85	105.4 ± 85.67	57.94 ± 28.99	0.3995	0.9383	0.5723
MIP-1a	49.17 ± 31.80	34.70 ± 21.03	34.25 ± 13.17	0.7386	0.7252	0.9997
MIP-1b	50.47 ± 4.86	59.63 ± 4.14	53.18 ± 11.37	0.2834	0.8934	0.5601
MIP-2	43.95 ± 15.07	36.86 ± 2.62	17.73 ± 15.03	0.7716	0.0906	0.2210
MIP-3a	31.05 ± 13.34	36.89 ± 30.92	27.00 ± 16.04	>0.9999	>0.9999	>0.9999
MIP-3b	36.89 ± 27.45	81.00 ± 33.14	62.05 ± 30.67	0.2569	0.5980	0.7387
RANTES	21.81 ± 4.48	21.64 ± 3.64	18.41 ± 9.05	0.9994	0.7878	0.8050
TARC	95.77 ± 6.72	111.1 ± 5.77	62.91 ± 11.10	0.1328	0.0064 (**)	0.0009 (***)
TIMP-1	984.1 ± 339.1	3160 ± 976.6	3442 ± 1758	0.1381	0.0950	0.9541
TNFα	2.96 ± 1.92	4.19 ± 1.96	2.32 ± 1.15	0.6756	0.8914	0.4292
VEGF	0.83 ± 0.47	0.51 ± 0.19	0.83 ± 0.35	0.5285	>0.9999	0.5285
6Ckin/Exodus	2343 ± 1435	1929 ± 581.1	1820 ± 891.6	0.8778	0.8140	0.9907
TGF-β1	50838 ± 7732	64029 ± 7389	32737 ± 4984	0.1203	0.0398 (*)	0.0033 (**)
TGF-β2	1844 ± 143.9	2165 ± 152.7	1220 ± 135.7	0.0767	0.0044 (**)	0.0005 (***)
TGF-β3	81.14 ± 40.87	57.44 ± 17.94	59.02 ± 23.70	0.6064	0.6437	0.9976

Appendix B

Conferences and travel awards:

10th Annual Alliance for Healthy Aging Conference ***Oct 2019***

Selected for poster presentation

Awarded "Outstanding Abstract"

Slaley Hall, Hexham, Northumberland, UK

Senescence Symposium ***May 2019***

Selected for oral presentation

MRC Institute of Genetics and Molecular Medicine, University of Edinburgh, Edinburgh, UK

9th Annual Alliance for Healthy Aging Conference ***Oct 2018***

Selected for oral and poster presentation

Awarded travel grant (£2,500) by conference sponsors Kogod Center of Aging

Mayo Clinic, Rochester, MN, USA

CVRC Trainees Meeting ***June 2018***

Selected for oral and poster presentation

Newcastle University, Newcastle-upon-Tyne, UK

BAS/BSCR 2018 Spring Meeting ***June 2018***

Selected for poster presentation

Manchester Central, Manchester, UK

Weinstein 2018 ***May 2018***

Selected for poster presentation

Awarded travel grants (£2,000) from The Genetics Society (2.1 Junior Scientist Conference Grant), Newcastle University (Postgraduate Travel Fund), and NUIA (Student Travel Bursary)

IRAKA, Nara, Japan

26th Northern Cardiovascular Research Group Meeting ***April 2018***

Selected for poster presentation

Discovery Museum, Newcastle-upon-Tyne, UK

Selected for poster presentation

Baltic Centre, Newcastle-upon-Tyne, UK

Publications:

Walaszczyk A, **Dookun E**, Redgrave R, Tual-Chalot S, Victorelli S, Spyridopoulos I, Owens WA, Arthur HM, Passos JF, Richardson GD. Pharmacological clearance of senescent cells improves survival and recovery in aged mice following acute myocardial infarction. *Aging Cell*, 2019 doi:10.1111/ace.12945. (Impact factor 7.6).

Anderson R, Lagnado A, Maggiorani D, Walaszczyk A, **Dookun E**, Chapman J, Birch J, Salmonowicz H, Ogronik M, Jurk D, Proctor C, Correia-Melo C, Victorelli S, Fielder E, Berlinguer-Palmini R, Owens WA, Greaves L, Kolsky K, Parini A, Douin-Echinard V, LeBrasseur N, Arthur H, Tual-Chalot S, Schafer M, Roos C, Miller J, Robertson N, Mann N, Adams P, Tchkonja T, Kirkland J, Mialet-Perez J, Richardson GD, Passos J. Length-independent telomere damage drives cardiomyocyte senescence. *EMBO J*, Jan 2019, doi:10.15252/embj.2018100492 (Impact factor 10.6).

Jones R, Krishnan A, Zeybel GL, **Dookun E**, Pearson JP, Simpson, J, Griffin SM, Ward C, Forrest IA. Reflux in idiopathic pulmonary fibrosis: treatment informed by an integrated approach. *ERJ Open Res*, Oct 2018, doi:10.1183/23120541.00051-2018 (Impact factor 12.2).

Dookun E, Walaszczyk A, Redgrave R, Tual-Chalot S, Yausep O, Spyridopoulos I, Owens A, Arthur H, Passos J, Richardson GD. Accumulation of cardiomyocyte senescence following ischaemia-reperfusion injury (IRI); a potential therapeutic target? *Heart* 104 (Suppl 6), A103-A103, 2018. (Impact factor 5.420). [Conference abstract].

Walaszczyk A, **Dookun E**, Redgrave R, Tual-Chalot S, Anderson R, Spyridopoulos I, Owens A, Arthur H, Passos J, Richardson GD. Senescence as a therapeutic target for myocardial ageing. *Heart* 104 (Suppl 6), A84-A84, 2018. (Impact factor 5.420). [Conference abstract].

Richardson G, Sage A, Bennaceur K, Al Zhrany N, Coelho-Lima J, **Dookun E**, Draganova L, Saretzki G, Breault DT, Mallat Z, Spyridopoulos I. Telomerase Mediates Lymphocyte Proliferation but Not the Atherosclerosis-Suppressive Potential of Regulatory T-Cells. *Arterioscler Thromb Vasc Biol*. 2018 Mar 29. pii: ATVBAHA.117.309940. (Impact factor 6.607).

Bibliography

- Acosta, J.C., Banito, A., Wuestefeld, T., Georgilis, A., Janich, P., Morton, J.P., Athineos, D., Kang, T.-W., Lasitschka, F., Andrulis, M., Pascual, G., Morris, K.J., Khan, S., Jin, H., Dharmalingam, G., Snijders, A.P., Carroll, T., Capper, D., Pritchard, C., Inman, G.J., Longerich, T., Sansom, O.J., Benitah, S.A., Zender, L. and Gil, J. (2013) 'A complex secretory program orchestrated by the inflammasome controls paracrine senescence', *Nature Cell Biology*, 15, p. 978.
- Acosta, J.C., O'Loughlen, A., Banito, A., Guijarro, M.V., Augert, A., Raguz, S., Fumagalli, M., Da Costa, M., Brown, C., Popov, N., Takatsu, Y., Melamed, J., d'Adda di Fagagna, F., Bernard, D., Hernando, E. and Gil, J. (2008) 'Chemokine Signaling via the CXCR2 Receptor Reinforces Senescence', *Cell*, 133(6), pp. 1006-1018.
- Adams, P.D. (2007) 'Remodeling chromatin for senescence', *Aging Cell*, 6(4), pp. 425-427.
- Adlam, V.J., Harrison, J.C., Porteous, C.M., James, A.M., Smith, R.A., Murphy, M.P. and Sammut, I.A. (2005) 'Targeting an antioxidant to mitochondria decreases cardiac ischaemia-reperfusion injury.', *FASEB J.*, 19(9), pp. 1088-95.
- Aguayo-Mazzucato, C., Andle, J., Lee, T.B., Midha, A., Talemal, L., Chipashvili, V., Hollister-Lock, J., van Deursen, J., Weir, G. and Bonner-Weir, S. (2019) 'Acceleration of β Cell Aging Determines Diabetes and Senolysis Improves Disease Outcomes', *Cell Metabolism*, 30(1), pp. 129-142.e4.
- Akhavanpoor, M., Gleissner, C.A., Gorbatsch, S., Doesch, A.O., Akhavanpoor, H., Wangler, S., Jahn, F., Lasitschka, F., Katus, H.A. and Erbel, C. (2014) 'CCL19 and CCL21 modulate the inflammatory milieu in atherosclerotic lesions', *Drug Design, Development and Therapy*, 8, pp. 2359-2371.
- Alam, P., Haile, B., Arif, M., Pandey, R., Rokvic, M., Nieman, M., Maliken, B.D., Paul, A., Wang, Y.G., Sadayappan, S., Ahmed, R.P.H. and Kanisicak, O. (2019a) 'Inhibition of Senescence-Associated Genes Rb1 and Meis2 in Adult Cardiomyocytes Results in Cell Cycle Reentry and Cardiac Repair Post-Myocardial Infarction', *Journal of the American Heart Association*, 8(15), p. e012089.
- Alam, P., Haile, B., Arif, M., Pandey, R., Rokvic, M., Nieman, M., Maliken, B.D., Paul, A., Wang, Y.G., Sadayappan, S., Ahmed, R.P.H. and Kanisicak, O. (2019b) 'Inhibition of Senescence-Associated Genes Rb1 and Meis2 in Adult Cardiomyocytes Results in Cell Cycle Reentry and Cardiac Repair Post-Myocardial Infarction', *Journal of the American Heart Association*, 8(15), p. e012089.
- Aldous, S.J. (2013) 'Cardiac biomarkers in acute myocardial infarction', *Int J Cardiol*, 164(3), pp. 282-94.
- Althubiti, M., Lezina, L., Carrera, S., Jukes-Jones, R., Giblett, S.M., Antonov, A., Barlev, N., Saldanha, G.S., Pritchard, C.A., Cain, K. and Macip, S. (2014) 'Characterization of novel markers of senescence and their prognostic potential in cancer', *Cell Death & Disease*, 5(11), pp. e1528-e1528.
- Amin, H.Z., Amin, L.Z. and Wijaya, I.P. (2017) 'Galectin-3: a novel biomarker for the prognosis of heart failure', *Clujul Medical*, 90(2), pp. 129-132.
- Anderson, R. (2016) *The Role of Telomere Damage in Cardiomyocyte Ageing*. Newcastle University.
- Anderson, R., Lagnado, A., Maggiorani, D., Walaszczyk, A., Dookun, E., Chapman, J., Birch, J., Salmonowicz, H., Ogrodnik, M., Jurk, D., Proctor, C., Correia-Melo, C., Victorelli, S., Fielder, E., Berlinguer-Palmini, R., Owens, A., Greaves, L.C., Kolsky, K.L., Parini, A., Douin-Echinard, V., LeBrasseur, N.K., Arthur, H.M., Tual-Chalot, S.,

Schafer, M.J., Roos, C.M., Miller, J.D., Robertson, N., Mann, J., Adams, P.D., Tchkonja, T., Kirkland, J.L., Miale-Perez, J., Richardson, G.D. and Passos, J.F. (2019) 'Length-independent telomere damage drives post-mitotic cardiomyocyte senescence', *The EMBO Journal*, p. e100492.

Anderson, R., Richardson, G.D. and Passos, J.F. (2018) 'Mechanisms driving the ageing heart', *Experimental Gerontology*, 109, pp. 5-15.

Artandi, S.E., Chang, S., Lee, S.-L., Alson, S., Gottlieb, G.J., Chin, L. and DePinho, R.A. (2000) 'Telomere dysfunction promotes non-reciprocal translocations and epithelial cancers in mice', *Nature*, 406(6796), pp. 641-645.

Assmus, B., Honold, J., Schächinger, V., Britten, M.B., Fischer-Rasokat, U., Lehmann, R., Teupe, C., Pistorius, K., Martin, H., Abolmaali, N.D., Tonn, T., Dimmeler, S. and Zeiher, A.M. (2006) 'Transcoronary Transplantation of Progenitor Cells after Myocardial Infarction', *New England Journal of Medicine*, 355(12), pp. 1222-1232.

Aw, D., Silva, A.B. and Palmer, D.B. (2007) 'Immunosenescence: emerging challenges for an ageing population', *Immunology*, 120(4), pp. 435-446.

Azevedo, P.S., Polegato, B.F., Minicucci, M.F., Paiva, S.A. and Zornoff, L.A. (2016) 'Cardiac Remodeling: Concepts, Clinical Impact, Pathophysiological Mechanisms and Pharmacologic Treatment', *Arq Bras Cardiol*, 106(1), pp. 62-9.

Baar, M.P., Brandt, R.M.C., Putavet, D.A., Klein, J.D.D., Derks, K.W.J., Bourgeois, B.R.M., Stryeck, S., Rijksen, Y., van Willigenburg, H., Feijtel, D.A., van der Pluijm, I., Essers, J., van Cappellen, W.A., van Ijcken, W.F., Houtsmuller, A.B., Pothof, J., de Bruin, R.W.F., Madl, T., Hoeijmakers, J.H.J., Campisi, J. and de Keizer, P.L.J. (2017) 'Targeted Apoptosis of Senescent Cells Restores Tissue Homeostasis in Response to Chemotoxicity and Aging', *Cell*, 169(1), pp. 132-147.e16.

Baehr, A., Klymiuk, N. and Kupatt, C. (2019) 'Evaluating Novel Targets of Ischemia Reperfusion Injury in Pig Models', *International journal of molecular sciences*, 20(19), p. 4749.

Baker, D.J., Childs, B.G., Durik, M., Wijers, M.E., Sieben, C.J., Zhong, J., Saltness, R., Jeganathan, K.B., Versoza, G.C., Pezeshki, A.-M., Khazaie, K., Miller, J.D. and van Deursen, J.M. (2016) 'Naturally occurring p16(Ink4a)-positive cells shorten healthy lifespan', *Nature*, 530(7589), pp. 184-189.

Baker, D.J., Jeganathan, K.B., Cameron, J.D., Thompson, M., Juneja, S., Kopecka, A., Kumar, R., Jenkins, R.B., de Groen, P.C., Roche, P. and van Deursen, J.M. (2004) 'BubR1 insufficiency causes early onset of aging-associated phenotypes and infertility in mice', *Nature Genetics*, 36(7), pp. 744-9.

Baker, D.J., Weaver, R.L. and van Deursen, J.M. (2013) 'p21 both attenuates and drives senescence and aging in BubR1 progeroid mice', *Cell Reports*, 3(4), pp. 1164-1174.

Baker, D.J., Wijshake, T., Tchkonja, T., LeBrasseur, N.K., Childs, B.G., van de Sluis, B., Kirkland, J.L. and van Deursen, J.M. (2011) 'Clearance of p16Ink4a-positive senescent cells delays ageing-associated disorders', *Nature*, 479(7372), pp. 232-236.

Balakumar, P., Maung-U, K. and Jagadeesh, G. (2016) 'Prevalence and prevention of cardiovascular disease and diabetes mellitus', *Pharmacological Research*, 113, pp. 600-609.

Bansilal, S., Castellano, J.M. and Fuster, V. (2015) 'Global burden of CVD: focus on secondary prevention of cardiovascular disease', *International Journal of Cardiology*, 201, pp. S1-S7.

Barta, E., Pechán, I., Cornák, V., Luknárová, O., Rendeková, V. and Verchovodko, P. (1991) 'Protective effect of alpha-tocopherol and L-ascorbic acid against the

ischemic-reperfusion injury in patients during open-heart surgery', *Bratislavské lekárské listy*, 92(3-4), pp. 174-183.

Bartis, D., Mise, N., Mahida, R.Y., Eickelberg, O. and Thickett, D.R. (2014) 'Epithelial–mesenchymal transition in lung development and disease: does it exist and is it important?', *Thorax*, 69(8), pp. 760-765.

Basisty, N., Kale, A., Jeon, O.H., Kuehnemann, C., Payne, T., Rao, C., Holtz, A., Shah, S., Sharma, V., Ferrucci, L., Campisi, J. and Schilling, B. (2020) 'A proteomic atlas of senescence-associated secretomes for aging biomarker development', *PLOS Biology*, 18(1), p. e3000599.

Baum, J. and Duffy, H.S. (2011) 'Fibroblasts and myofibroblasts: what are we talking about?', *Journal of cardiovascular pharmacology*, 57(4), pp. 376-379.

Beltrami, A.P., Barlucchi, L., Torella, D., Baker, M., Limana, F., Chimenti, S., Kasahara, H., Rota, M., Musso, E., Urbanek, K., Leri, A., Kajstura, J., Nadal-Ginard, B. and Anversa, P. (2003) 'Adult cardiac stem cells are multipotent and support myocardial regeneration', *Cell*, 114(6), pp. 763-76.

Beltrami, A.P., Urbanek, K., Kajstura, J., Yan, S.-M., Finato, N., Bussani, R., Nadal-Ginard, B., Silvestri, F., Leri, A., Beltrami, C.A. and Anversa, P. (2001) 'Evidence That Human Cardiac Myocytes Divide after Myocardial Infarction', *New England Journal of Medicine*, 344(23), pp. 1750-1757.

Bergmann, O., Bhardwaj, R.D., Bernard, S., Zdunek, S., Barnabé-Heider, F., Walsh, S., Zupicich, J., Alkass, K., Buchholz, B.A., Druid, H., Jovinge, S. and Frisén, J. (2009) 'Evidence for cardiomyocyte renewal in humans', *Science (New York, N.Y.)*, 324(5923), pp. 98-102.

Bergmann, O., Zdunek, S., Felker, A., Salehpour, M., Alkass, K., Bernard, S., Sjöström, S.L., Szewczykowska, M., Jackowska, T., Dos Remedios, C., Malm, T., Andra, M., Jashari, R., Nyengaard, J.R., Possnert, G., Jovinge, S., Druid, H. and Frisen, J. (2015) 'Dynamics of Cell Generation and Turnover in the Human Heart', *Cell*, 161(7), pp. 1566-75.

Bhatnagar, P., Wickramasinghe, K., Williams, J., Rayner, M. and Townsend, N. (2015) 'The epidemiology of cardiovascular disease in the UK 2014', *Heart*, 101(15), pp. 1182-1189.

Bhayadia, R., Schmidt, B.M.W., Melk, A. and Hömme, M. (2015) 'Senescence-Induced Oxidative Stress Causes Endothelial Dysfunction', *The Journals of Gerontology: Series A*, 71(2), pp. 161-169.

Bingham, V., McIlreavey, L., Greene, C., O'Doherty, E., Clarke, R., Craig, S., Salto-Tellez, M., McQuaid, S., Lewis, C. and James, J. (2017) 'RNAscope in situ hybridization confirms mRNA integrity in formalin-fixed, paraffin-embedded cancer tissue samples', *Oncotarget*, 8(55).

Biran, A., Zada, L., Abou Karam, P., Vadai, E., Roitman, L., Ovadya, Y., Porat, Z. and Krizhanovsky, V. (2017) 'Quantitative identification of senescent cells in aging and disease', *Aging Cell*, 16(4), pp. 661-671.

Birch, J., Anderson, R.K., Correia-Melo, C., Jurk, D., Hewitt, G., Marques, F.M., Green, N.J., Moisey, E., Birrell, M.A., Belvisi, M.G., Black, F., Taylor, J.J., Fisher, A.J., De Soyza, A. and Passos, J.F. (2015) 'DNA damage response at telomeres contributes to lung aging and chronic obstructive pulmonary disease', *American Journal of Physiology. Lung Cellular and Molecular Physiology*, 309(10), pp. L1124-L1137.

Birch, J., Barnes, P.J. and Passos, J.F. (2018) 'Mitochondria, telomeres and cell senescence: Implications for lung ageing and disease', *Pharmacology & therapeutics*, 183, pp. 34-49.

- Birling, M.C., Gofflot, F. and Warot, X. (2009) 'Site-specific recombinases for manipulation of the mouse genome', *Methods in Molecular Biology*, 561, pp. 245-63.
- Blankesteyn, W.M., Creemers, E., Lutgens, E., Cleutjens, J.P.M., Daemen, M.J.A.P. and Smits, J.F.M. (2001) 'Dynamics of cardiac wound healing following myocardial infarction: observations in genetically altered mice', *Acta Physiologica Scandinavica*, 173(1), pp. 75-82.
- Blasco, M.A., Lee, H.-W., Hande, M.P., Samper, E., Lansdorp, P.M., DePinho, R.A. and Greider, C.W. (1997) 'Telomere Shortening and Tumor Formation by Mouse Cells Lacking Telomerase RNA', *Cell*, 91(1), pp. 25-34.
- Boag, S.E., Das, R., Shmeleva, E.V., Bagnall, A., Egred, M., Howard, N., Bennaceur, K., Zaman, A., Keavney, B. and Spyridopoulos, I. (2015) 'T lymphocytes and fractalkine contribute to myocardial ischemia/reperfusion injury in patients', *The Journal of Clinical Investigation*, 125(8), pp. 3063-3076.
- Boateng, S. and Sanborn, T. (2013) 'Acute myocardial infarction', *Dis Mon*, 59(3), pp. 83-96.
- Boersma, E. and Primary Coronary Angioplasty vs. Thrombolysis, G. (2006) 'Does time matter? A pooled analysis of randomized clinical trials comparing primary percutaneous coronary intervention and in-hospital fibrinolysis in acute myocardial infarction patients', *Eur Heart J*, 27(7), pp. 779-88.
- Bogatryov, Y., Tomanek, R.J. and Dedkov, E.I. (2013) 'Structural Composition of Myocardial Infarction Scar in Middle-aged Male and Female Rats: Does Sex Matter?', *Journal of Histochemistry and Cytochemistry*, 61(11), pp. 833-848.
- Bolognese, L., Neskovic, A.N., Parodi, G., Cerisano, G., Buonamici, P., Santoro, G.M. and Antoniucci, D. (2002) 'Left Ventricular Remodeling After Primary Coronary Angioplasty', *Circulation*, 106(18), pp. 2351-2357.
- Borzage, M., Heidari, K., Chavez, T., Seri, I., Wood, J.C. and Bluml, S. (2017) 'Measuring Stroke Volume: Impedance Cardiography vs Phase-Contrast Magnetic Resonance Imaging', *American Journal of Critical Care*, 26(5), pp. 408-415.
- Boyer, N.M., Laskey, W.K., Cox, M., Hernandez, A.F., Peterson, E.D., Bhatt, D.L., Cannon, C.P. and Fonarow, G.C. (2012) 'Trends in Clinical, Demographic, and Biochemical Characteristics of Patients With Acute Myocardial Infarction From 2003 to 2008: A Report From the American Heart Association Get With The Guidelines Coronary Artery Disease Program', *Journal of the American Heart Association*, 1(4), p. e001206.
- Branco, A.F., Pereira, S.P., Gonzalez, S., Gusev, O., Rizvanov, A.A. and Oliveira, P.J. (2015) 'Gene Expression Profiling of H9c2 Myoblast Differentiation towards a Cardiac-Like Phenotype', *PLOS ONE*, 10(6), p. e0129303.
- Braut, V., Besson, V., Magnol, L., Duchon, A. and Herault, Y. (2007) 'Cre/loxP-mediated chromosome engineering of the mouse genome', *Handbook of Experimental Pharmacology*, (178), pp. 29-48.
- Braun, H., Schmidt, B.M.W., Raiss, M., Baisantry, A., Mircea-Constantin, D., Wang, S., Gross, M.-L., Serrano, M., Schmitt, R. and Melk, A. (2012) 'Cellular Senescence Limits Regenerative Capacity and Allograft Survival', *Journal of the American Society of Nephrology*, 23(9), pp. 1467-1473.
- Brophy, J.M., Levesque, L.E. and Zhang, B. (2007) 'The coronary risk of cyclo-oxygenase-2 inhibitors in patients with a previous myocardial infarction', *Heart*, 93(2), pp. 189-94.
- Broughton, K.M., Wang, B.J., Firouzi, F., Khalafalla, F., Dimmeler, S., Fernandez-Aviles, F. and Sussman, M.A. (2018) 'Mechanisms of Cardiac Repair and Regeneration', *Circulation Research*, 122(8), pp. 1151-1163.

- Buja, L.M. (2005) 'Myocardial ischemia and reperfusion injury', *Cardiovasc Pathol*, 14(4), pp. 170-5.
- Bujak, M., Kweon, H.J., Chatila, K., Li, N., Taffet, G. and Frangogiannis, N.G. (2008) 'Aging-Related Defects Are Associated With Adverse Cardiac Remodeling in a Mouse Model of Reperfused Myocardial Infarction', *Journal of the American College of Cardiology*, 51(14), pp. 1384-1392.
- Bulluck, H., Go, Y.Y., Crimi, G., Ludman, A.J., Rosmini, S., Abdel-Gadir, A., Bhuva, A.N., Treibel, T.A., Fontana, M., Pica, S., Raineri, C., Sirker, A., Herrey, A.S., Manisty, C., Groves, A., Moon, J.C. and Hausenloy, D.J. (2017) 'Defining left ventricular remodeling following acute ST-segment elevation myocardial infarction using cardiovascular magnetic resonance', *Journal of Cardiovascular Magnetic Resonance*, 19(1), p. 26.
- Bulluck, H., Yellon, D.M. and Hausenloy, D.J. (2016) 'Reducing myocardial infarct size: challenges and future opportunities', *Heart*, 102(5), pp. 341-348.
- Bune, L.T., Larsen, J.R., Thaning, P., Bune, N.E.T., Rasmussen, P. and Rosenmeier, J.B. (2013) 'Adenosine diphosphate reduces infarct size and improves porcine heart function after myocardial infarct', *Physiological Reports*, 1(1).
- Burd, C.E., Gill, M.S., Niedernhofer, L.J., Robbins, P.D., Austad, S.N., Barzilai, N. and Kirkland, J.L. (2016) 'Barriers to the Preclinical Development of Therapeutics that Target Aging Mechanisms', *The Journals of Gerontology: Series A*, 71(11), pp. 1388-1394.
- Burnett, M. (1975) 'Intrinsic mutagenesis: A genetic approach to ageing', *Annals of Internal Medicine*, 82(5), pp. 728-728.
- Burton, D.G.A. (2009) 'Cellular senescence, ageing and disease', *Age (Dordrecht, Netherlands)*, 31(1), pp. 1-9.
- Bush, C.A., Renner, W. and Boudoulas, H. (1980) 'Corticosteroids in Acute Myocardial Infarction', *Angiology*, 31(10), pp. 710-714.
- Bussian, T.J., Aziz, A., Meyer, C.F., Swenson, B.L., van Deursen, J.M. and Baker, D.J. (2018) 'Clearance of senescent glial cells prevents tau-dependent pathology and cognitive decline', *Nature*, 562(7728), pp. 578-582.
- Cai, B., Zhu, S., Li, J., Chen, N., Liu, Y. and Lu, Y. (2012) 'Bone marrow-derived mesenchymal stem cells protected rat cardiomyocytes from premature senescence', *International Journal of Cardiology*, 154(2), pp. 180-182.
- Cai, C.-L., Martin, J.C., Sun, Y., Cui, L., Wang, L., Ouyang, K., Yang, L., Bu, L., Liang, X., Zhang, X., Stallcup, W.B., Denton, C.P., McCulloch, A., Chen, J. and Evans, S.M. (2008) 'A myocardial lineage derives from Tbx18 epicardial cells', *Nature*, 454(7200), pp. 104-108.
- Calado, R.T. and Dumitriu, B. (2013) 'Telomere Dynamics in Mice and Humans', *Seminars in Hematology*, 50(2), pp. 165-174.
- Camelliti, P., Borg, T.K. and Kohl, P. (2005) 'Structural and functional characterisation of cardiac fibroblasts', *Cardiovasc Res*, 65(1), pp. 40-51.
- Cameron, A.C., Lang, N.N. and Touyz, R.M. (2016) 'Chapter 10 - Cardiovascular Complications from Cancer Therapy: Hypertension—Focus on Vascular Endothelial Growth Factor Inhibitors', in Herrmann, J. (ed.) *Clinical Cardio-Oncology*. Elsevier, pp. 185-211.
- Campisi, J. (2013) 'Aging, Cellular Senescence, and Cancer', *Annual review of physiology*, 75, pp. 685-705.
- Campisi, J. and d'Adda di Fagagna, F. (2007) 'Cellular senescence: when bad things happen to good cells', *Nat Rev Mol Cell Biol*, 8(9), pp. 729-740.
- Capparelli, C., Chiavarina, B., Whitaker-Menezes, D., Pestell, T.G., Pestell, R.G., Hult, J., Andò, S., Howell, A., Martinez-Outschoorn, U.E., Sotgia, F. and Lisanti, M.P.

(2012) 'CDK inhibitors (p16/p19/p21) induce senescence and autophagy in cancer-associated fibroblasts, "fueling" tumor growth via paracrine interactions, without an increase in neo-angiogenesis', *Cell Cycle*, 11(19), pp. 3599-3610.

Carnero, A. (2013) 'Markers of Cellular Senescence', in Galluzzi, L., Vitale, I., Kepp, O. and Kroemer, G. (eds.) *Cell Senescence: Methods and Protocols*. Totowa, NJ: Humana Press, pp. 63-81.

Carvalho, A.B. and de Carvalho, A.C.C. (2010) 'Heart regeneration: Past, present and future', *World Journal of Cardiology*, 2(5), pp. 107-111.

Cavasin, M.A., Tao, Z., Menon, S. and Yang, X.-P. (2004) 'Gender differences in cardiac function during early remodeling after acute myocardial infarction in mice', *Life Sciences*, 75(18), pp. 2181-2192.

Cell Signaling Technology (2016) *Senescence β -Galactosidase Staining Kit*. Available at: <http://media.cellsignal.com/pdf/9860.pdf> (Accessed: 14/03).

Cesna, S., Eicken, A., Juenger, H. and Hess, J. (2013) 'Successful Treatment of a Newborn With Acute Myocardial Infarction on the First Day of Life', *Pediatric Cardiology*, 34(8), pp. 1868-1870.

Chakravarty, T., Makkar, R.R., Ascheim, D.D., Traverse, J.H., Schatz, R., DeMaria, A., Francis, G.S., Povsic, T.J., Smith, R.R., Lima, J.A., Pogoda, J.M., Marbán, L. and Henry, T.D. (2017) 'ALLogeneic Heart STem Cells to Achieve Myocardial Regeneration (ALLSTAR) Trial: Rationale and Design', *Cell transplantation*, 26(2), pp. 205-214.

Chan, S., Filézac de L'Etang, A., Rangell, L., Caplazi, P., Lowe, J.B. and Romeo, V. (2018) 'A method for manual and automated multiplex RNAscope in situ hybridization and immunocytochemistry on cytopsin samples', *PLOS ONE*, 13(11), p. e0207619.

Chang, J., Wang, Y., Shao, L., Laberge, R.M., Demaria, M., Campisi, J., Janakiraman, K., Sharpless, N.E., Ding, S., Feng, W., Luo, Y., Wang, X., Aykin-Burns, N., Krager, K., Ponnappan, U., Hauer-Jensen, M., Meng, A. and Zhou, D. (2016) 'Clearance of senescent cells by ABT263 rejuvenates aged hematopoietic stem cells in mice', *Nat Med*, 22(1), pp. 78-83.

Chawla, L.S. and Kimmel, P.L. (2012) 'Acute kidney injury and chronic kidney disease: an integrated clinical syndrome', *Kidney International*, 82(5), pp. 516-24.

Chen, C.-H., Sereti, K.-I., Wu, B.M. and Ardehali, R. (2015) 'Translational aspects of cardiac cell therapy', *Journal of Cellular and Molecular Medicine*, 19(8), pp. 1757-1772.

Chen, W. and Frangogiannis, N.G. (2013) 'Fibroblasts in post-infarction inflammation and cardiac repair', *Biochimica et Biophysica Acta (BBA) - Molecular Cell Research*, 1833(4), pp. 945-953.

Childs, B.G., Baker, D.J., Kirkland, J.L., Campisi, J. and van Deursen, J.M. (2014) 'Senescence and apoptosis: dueling or complementary cell fates?', *EMBO reports*, 15(11), pp. 1139-1153.

Childs, B.G., Durik, M., Baker, D.J. and van Deursen, J.M. (2015) 'Cellular senescence in aging and age-related disease: from mechanisms to therapy', *Nat Med*, 21(12), pp. 1424-1435.

Childs, B.G., Li, H. and van Deursen, J.M. (2018) 'Senescent cells: a therapeutic target for cardiovascular disease', *The Journal of clinical investigation*, 128(4), pp. 1217-1228.

Cho, S.K., Ryu, M.Y., Shah, P., Poulsen, C.P. and Yang, S.W. (2016) 'Post-Translational Regulation of miRNA Pathway Components, AGO1 and HYL1, in Plants', *Molecules and Cells*, 39(8), pp. 581-586.

Chorvat, D., Kirchnerova, J., Cagalinec, M., Smolka, J., Mateasik, A. and Chorvatova, A. (2005) 'Spectral Unmixing of Flavin Autofluorescence Components in Cardiac Myocytes', *Biophysical Journal*, 89(6), pp. L55-L57.

Cleland, J.G.F., Daubert, J.-C., Erdmann, E., Freemantle, N., Gras, D., Kappenberger, L. and Tavazzi, L. (2005) 'The Effect of Cardiac Resynchronization on Morbidity and Mortality in Heart Failure', *New England Journal of Medicine*, 352(15), pp. 1539-1549.

Cochain, C., Channon, K.M. and Silvestre, J.-S. (2013) 'Angiogenesis in the infarcted myocardium', *Antioxidants & Redox Signaling*, 18(9), pp. 1100-1113.

Cohn, J.N., Ferrari, R. and Sharpe, N. (2000) 'Cardiac remodeling--concepts and clinical implications: a consensus paper from an international forum on cardiac remodeling. Behalf of an International Forum on Cardiac Remodeling', *Journal of the American College of Cardiology*, 35(3), pp. 569-82.

Conrad, N., Judge, A., Tran, J., Mohseni, H., Hedgecote, D., Crespillo, A.P., Allison, M., Hemingway, H., Cleland, J.G., McMurray, J.J.V. and Rahimi, K. (2018) 'Temporal trends and patterns in heart failure incidence: a population-based study of 4 million individuals', *The Lancet*, 391(10120), pp. 572-580.

Coppé, J.-P., Desprez, P.-Y., Krtolica, A. and Campisi, J. (2010) 'The Senescence-Associated Secretory Phenotype: The Dark Side of Tumor Suppression', *Annual review of pathology*, 5, pp. 99-118.

Coppé, J.-P., Patil, C.K., Rodier, F., Sun, Y., Muñoz, D.P., Goldstein, J., Nelson, P.S., Desprez, P.-Y. and Campisi, J. (2008) 'Senescence-Associated Secretory Phenotypes Reveal Cell-Nonautonomous Functions of Oncogenic RAS and the p53 Tumor Suppressor', *PLoS Biology*, 6(12), p. e301.

Correia-Melo, C., Hewitt, G. and Passos, J.F. (2014) 'Telomeres, oxidative stress and inflammatory factors: partners in cellular senescence?', *Longevity & Healthspan*, 3, pp. 1-1.

Courtois-Cox, S., Jones, S.L. and Cichowski, K. (2008) 'Many roads lead to oncogene-induced senescence', *Oncogene*, 27(20), pp. 2801-2809.

Cui, S., Xue, L., Yang, F., Dai, S., Han, Z., Liu, K., Liu, B., Yuan, Q., Cui, Z., Zhang, Y., Xu, F. and Chen, Y. (2018) 'Postinfarction Hearts Are Protected by Premature Senescent Cardiomyocytes Via GATA4-Dependent Ccn1 Secretion', *Journal of the American Heart Association*, 7(18), p. e009111.

Cung, T.T., Morel, O., Cayla, G., Rioufol, G., Garcia-Dorado, D., Angoulvant, D., Bonnefoy-Cudraz, E., Guerin, P., Elbaz, M., Delarche, N., Coste, P., Vanzetto, G., Metge, M., Aupetit, J.F., Jouve, B., Motreff, P., Tron, C., Labeque, J.N., Steg, P.G., Cottin, Y., Range, G., Clerc, J., Claeys, M.J., Coussement, P., Prunier, F., Moulin, F., Roth, O., Belle, L., Dubois, P., Barragan, P., Gilard, M., Piot, C., Colin, P., De Poli, F., Morice, M.C., Ider, O., Dubois-Rande, J.L., Untersee, T., Le Breton, H., Beard, T., Blanchard, D., Grollier, G., Malquarti, V., Staat, P., Sudre, A., Elmer, E., Hansson, M.J., Bergerot, C., Boussaha, I., Jossan, C., Derumeaux, G., Mewton, N. and Ovize, M. (2015) 'Cyclosporine before PCI in Patients with Acute Myocardial Infarction', *New England Journal of Medicine*, 373(11), pp. 1021-31.

Czubryt, M.P. (2012) 'Common threads in cardiac fibrosis, infarct scar formation, and wound healing', *Fibrogenesis & Tissue Repair*, 5(1), pp. 19-19.

d'Adda di Fagagna, F. (2008) 'Living on a break: cellular senescence as a DNA-damage response', *Nature Reviews Cancer*, 8(7), pp. 512-522.

Da Silva-Álvarez, S., Picallos-Rabina, P., Antelo-Iglesias, L., Triana-Martínez, F., Barreiro-Iglesias, A., Sánchez, L. and Collado, M. (2019) 'The development of cell senescence', *Experimental Gerontology*, 128, p. 110742.

- Damas, J.K., Smith, C., Oie, E., Fevang, B., Halvorsen, B., Waehre, T., Boullier, A., Breland, U., Yndestad, A., Ovchinnikova, O., Robertson, A.K., Sandberg, W.J., Kjekshus, J., Tasken, K., Froland, S.S., Gullestad, L., Hansson, G.K., Quehenberger, O. and Aukrust, P. (2007) 'Enhanced expression of the homeostatic chemokines CCL19 and CCL21 in clinical and experimental atherosclerosis: possible pathogenic role in plaque destabilization', *Arteriosclerosis, Thrombosis, and Vascular Biology*, 27(3), pp. 614-20.
- Darby, I.A., Laverdet, B., Bonté, F. and Desmoulière, A. (2014) 'Fibroblasts and myofibroblasts in wound healing', *Clinical, Cosmetic and Investigational Dermatology*, 7, pp. 301-311.
- Davis, A.J. and Chen, D.J. (2013) 'DNA double strand break repair via non-homologous end-joining', *Translational cancer research*, 2(3), pp. 130-143.
- Davis, A.S., Richter, A., Becker, S., Moyer, J.E., Sandouk, A., Skinner, J. and Taubenberger, J.K. (2014) 'Characterizing and Diminishing Autofluorescence in Formalin-fixed Paraffin-embedded Human Respiratory Tissue', *Journal of Histochemistry and Cytochemistry*, 62(6), pp. 405-423.
- Davis, J. and Molkenin, J.D. (2014) 'Myofibroblasts: trust your heart and let fate decide', *Journal of Molecular and Cellular Cardiology*, 70, pp. 9-18.
- Davison, B.J. (2014) *The Importance of Endoglin for Cardiac Structure and Function*. Newcastle University.
- de Groot, H. and Rauen, U. (2007) 'Ischemia-reperfusion injury: processes in pathogenetic networks: a review', *Transplant Proc*, 39(2), pp. 481-4.
- de Magalhães, J.P. and Passos, J.F. (2018) 'Stress, cell senescence and organismal ageing', *Mechanisms of Ageing and Development*, 170, pp. 2-9.
- De Martinis, M., Franceschi, C., Monti, D. and Ginaldi, L. (2005) 'Inflamm-ageing and lifelong antigenic load as major determinants of ageing rate and longevity', *FEBS Letters*, 579(10), pp. 2035-9.
- Deckers, J.W. (2013) 'Classification of myocardial infarction and unstable angina: a re-assessment', *Int J Cardiol*, 167(6), pp. 2387-90.
- Demaria, M., Desprez, P.Y., Campisi, J. and Velarde, M.C. (2015) 'Cell Autonomous and Non-autonomous Effects of Senescent Cells in the Skin', *The Journal of investigative dermatology*, 135(7), pp. 1722-1726.
- Demaria, M., Ohtani, N., Youssef, S.A., Rodier, F., Toussaint, W., Mitchell, J.R., Laberge, R.-M., Vijg, J., Van Steeg, H., Dollé, M.E.T., Hoeijmakers, J.H.J., de Bruin, A., Hara, E. and Campisi, J. (2014) 'An essential role for senescent cells in optimal wound healing through secretion of PDGF-AA', *Developmental cell*, 31(6), pp. 722-733.
- Demirag, K., Askar, F.Z., Uyar, M., Cevik, A., Ozmen, D., Mutaf, I. and Bayindir, O. (2001) 'The protective effects of high dose ascorbic acid and diltiazem on myocardial ischaemia-reperfusion injury', *Middle East Journal of Anesthesiology*, 16(1), pp. 67-79.
- Deng, Y., Chan, S. and Chang, S. (2008) 'Telomere dysfunction and Tumor Suppression-the Senescence Connection', *Nature reviews. Cancer*, 8(6), pp. 450-458.
- Dhingra, R. and Vasan, R.S. (2012) 'Age as a Cardiovascular risk factor', *The Medical clinics of North America*, 96(1), pp. 87-91.
- Di Angelantonio, E., Chowdhury, R., Sarwar, N., Ray, K.K., Gobin, R., Saleheen, D., Thompson, A., Gudnason, V., Sattar, N. and Danesh, J. (2009) 'B-type natriuretic peptides and cardiovascular risk: systematic review and meta-analysis of 40 prospective studies', *Circulation*, 120(22), pp. 2177-87.

- Diagnostics, A.C. (2018) *RNAscope® Multiplex Fluorescent Reagent Kit v2 User Manual*. Available at: <https://acdbio.com/technical-support/user-manuals> (Accessed: 29th November).
- Dimri, G.P., Lee, X., Basile, G., Acosta, M., Scott, G., Roskelley, C., Medrano, E.E., Linskens, M., Rubelj, I. and Pereira-Smith, O. (1995) 'A biomarker that identifies senescent human cells in culture and in aging skin in vivo', *Proceedings of the National Academy of Sciences of the United States of America*, 92(20), pp. 9363-9367.
- DiPietro, L. (2016) 'Angiogenesis and wound repair: When enough is enough', *Journal of Leukocyte Biology*, 100.
- Donato, A., Machin, D. and Lesniewski, L. (2018) 'Mechanisms of Dysfunction in the Aging Vasculature and Role in Age-Related Disease', *Circulation Research*, 123(7), pp. 825-848.
- Doost Hosseiny, A., Moloi, S., Chandrasekhar, J. and Farshid, A. (2016) 'Mortality pattern and cause of death in a long-term follow-up of patients with STEMI treated with primary PCI', *Open Heart*, 3(1), p. e000405.
- Dumont, P., Burton, M., Chen, Q.M., Gonos, E.S., Frippiat, C., Mazarati, J.-B., Eliaers, F., Remacle, J. and Toussaint, O. (2000) 'Induction of replicative senescence biomarkers by sublethal oxidative stresses in normal human fibroblast', *Free Radical Biology and Medicine*, 28(3), pp. 361-373.
- Dunlay, S.M. and Roger, V.L. (2012) 'Gender Differences in the Pathophysiology, Clinical Presentation, and Outcomes of Ischemic Heart Failure', *Current Heart Failure Reports*, 9(4), pp. 267-276.
- Dunnill, C., Patton, T., Brennan, J., Barrett, J., Dryden, M., Cooke, J., Leaper, D. and Georgopoulos, N.T. (2017) 'Reactive oxygen species (ROS) and wound healing: the functional role of ROS and emerging ROS-modulating technologies for augmentation of the healing process', *International Wound Journal*, 14(1), pp. 89-96.
- Economou, E., Tousoulis, D., Katinioti, A., Stefanadis, C., Trikas, A., Pitsavos, C., Tentolouris, C., Toutouza, M.G. and Toutouzas, P. (2001) 'Chemokines in patients with ischaemic heart disease and the effect of coronary angioplasty', *International Journal of Cardiology*, 80(1), pp. 55-60.
- Edlich, F. (2018) 'BCL-2 proteins and apoptosis: Recent insights and unknowns', *Biochemical and Biophysical Research Communications*, 500(1), pp. 26-34.
- Ellison-Hughes, G.M. and Lewis, F.C. (2017) 'Progenitor Cells from the Adult Heart', in Ieda, M. and Zimmermann, W.-H. (eds.) *Cardiac Regeneration*. Cham: Springer International Publishing, pp. 19-39.
- Ellison, G.M., Vicinanza, C., Smith, A.J., Aquila, I., Leone, A., Waring, C.D., Henning, B.J., Stirparo, G.G., Papait, R., Scarfò, M., Agosti, V., Viglietto, G., Condorelli, G., Indolfi, C., Ottolenghi, S., Torella, D. and Nadal-Ginard, B. (2013) 'Adult c-kit^{pos} Cardiac Stem Cells Are Necessary and Sufficient for Functional Cardiac Regeneration and Repair', *Cell*, 154(4), pp. 827-842.
- Emanuele, E., Falcone, C., D'Angelo, A., Minoretta, P., Buzzi, M.P., Bertona, M. and Geroldi, D. (2006) 'Association of plasma eotaxin levels with the presence and extent of angiographic coronary artery disease', *Atherosclerosis*, 186(1), pp. 140-145.
- Erbel, C., Sato, K., Meyer, F.B., Kopecky, S.L., Frye, R.L., Goronzy, J.J. and Weyand, C.M. (2007) 'Functional profile of activated dendritic cells in unstable atherosclerotic plaque', *Basic Research in Cardiology*, 102(2), pp. 123-32.
- Erusalimsky, J.D. (2009) 'Vascular endothelial senescence: from mechanisms to pathophysiology', *Journal of Applied Physiology*, 106(1), pp. 326-332.
- Erusalimsky, J.D. and Kurz, D.J. (2005) 'Cellular senescence in vivo: its relevance in ageing and cardiovascular disease', *Exp Gerontol*, 40(8-9), pp. 634-42.

- Fang, L., Gao, X.-M., Moore, X.-L., Kiriazis, H., Su, Y., Ming, Z., Lim, Y.L., Dart, A.M. and Du, X.-J. (2007) 'Differences in inflammation, MMP activation and collagen damage account for gender difference in murine cardiac rupture following myocardial infarction', *Journal of Molecular and Cellular Cardiology*, 43(5), pp. 535-544.
- Farah, I.O., Lewis, V.L., Ayensu, W.K. and Cameron, J.A. (2013) 'Assessing the survival of MRC5 and a549 cell lines upon exposure to pyruvic Acid, sodium citrate and sodium bicarbonate - biomed 2013', *Biomedical Sciences Instrumentation*, 49, pp. 109-16.
- Farooqi, K.M., Sutton, N., Weinstein, S., Menegus, M., Spindola-Franco, H. and Pass, R.H. (2012) 'Neonatal Myocardial Infarction: Case Report and Review of the Literature', *Congenital Heart Disease*, 7(6), pp. E97-E102.
- Farr, J.N., Xu, M., Weivoda, M.M., Monroe, D.G., Fraser, D.G., Onken, J.L., Negley, B.A., Sfeir, J.G., Ogrodnik, M.B., Hachfeld, C.M., LeBrasseur, N.K., Drake, M.T., Pignolo, R.J., Pirtskhalava, T., Tchkonja, T., Oursler, M.J., Kirkland, J.L. and Khosla, S. (2017) 'Targeting cellular senescence prevents age-related bone loss in mice', *Nature Medicine*, 23(9), pp. 1072-1079.
- Feil, S., Valtcheva, N. and Feil, R. (2009) 'Inducible Cre Mice', in Wurst, W. and Kühn, R. (eds.) *Gene Knockout Protocols: Second Edition*. Totowa, NJ: Humana Press, pp. 343-363.
- Féléto, M. and Vanhoutte, P.M. (2006) 'Endothelial dysfunction: a multifaceted disorder (The Wiggers Award Lecture)', *American Journal of Physiology-Heart and Circulatory Physiology*, 291(3), pp. H985-H1002.
- Felker, A., Nieuwenhuize, S., Dolbois, A., Blazkova, K., Hess, C., Low, L.W.L., Burger, S., Samson, N., Carney, T.J., Bartunek, P., Nevado, C. and Mosimann, C. (2016) 'In Vivo Performance and Properties of Tamoxifen Metabolites for CreERT2 Control', *PLOS ONE*, 11(4), pp. e0152989-e0152989.
- Fernandes, D.C., Goncalves, R.C. and Laurindo, F.R. (2017) 'Measurement of Superoxide Production and NADPH Oxidase Activity by HPLC Analysis of Dihydroethidium Oxidation', *Methods in Molecular Biology*, 1527, pp. 233-249.
- Feygin, J., Hu, Q., Swingen, C. and Zhang, J. (2008) 'Relationships between regional myocardial wall stress and bioenergetics in hearts with left ventricular hypertrophy', *American Journal of Physiology. Heart and Circulatory Physiology*, 294(5), pp. H2313-H2321.
- Figuroa, M.S. and Peters, J.I. (2006) 'Congestive Heart Failure: Diagnosis, Pathophysiology, Therapy, and Implications for Respiratory Care', *Respiratory Care*, 51(4), pp. 403-412.
- Foglia, M.J. and Poss, K.D. (2016) 'Building and re-building the heart by cardiomyocyte proliferation', *Development (Cambridge, England)*, 143(5), pp. 729-740.
- Frangogiannis, N.G. (2016) 'Fibroblast-Extracellular Matrix Interactions in Tissue Fibrosis', *Current Pathobiology Reports*, 4(1), pp. 11-18.
- Frangogiannis, N.G. (2017) 'The role of transforming growth factor (TGF)- β in the infarcted myocardium', *Journal of Thoracic Disease*, 9(Suppl 1), pp. S52-S63.
- Freund, A., Orjalo, A.V., Desprez, P.Y. and Campisi, J. (2010) 'Inflammatory networks during cellular senescence: causes and consequences', *Trends in Molecular Medicine*, 16(5), pp. 238-46.
- Friedman, H.M. and Koropchak, C. (1978) 'Comparison of WI-38, MRC-5, and IMR-90 cell strains for isolation of viruses from clinical specimens', *Journal of clinical microbiology*, 7(4), pp. 368-371.

Fröhlich, G.M., Meier, P., White, S.K., Yellon, D.M. and Hausenloy, D.J. (2013) 'Myocardial reperfusion injury: looking beyond primary PCI', *European Heart Journal*, 34(23), pp. 1714-1722.

Fuhrmann-Stroissnigg, H., Ling, Y.Y., Zhao, J., McGowan, S.J., Zhu, Y., Brooks, R.W., Grassi, D., Gregg, S.Q., Stripay, J.L., Dorronsoro, A., Corbo, L., Tang, P., Bukata, C., Ring, N., Giacca, M., Li, X., Tchkonja, T., Kirkland, J.L., Niedernhofer, L.J. and Robbins, P.D. (2017) 'Identification of HSP90 inhibitors as a novel class of senolytics', *Nature Communications*, 8(1), p. 422.

Fumagalli, M., Rossiello, F., Clerici, M., Barozzi, S., Cittaro, D., Kaplunov, J.M., Bucci, G., Dobрева, M., Matti, V., Beausejour, C.M., Herbig, U., Longhese, M.P. and d'Adda di Fagagna, F. (2012) 'Telomeric DNA damage is irreparable and causes persistent DNA-damage-response activation', *Nature Cell Biology*, 14(4), pp. 355-365.

Furtado, M.B., Nim, H.T., Boyd, S.E. and Rosenthal, N.A. (2016) 'View from the heart: cardiac fibroblasts in development, scarring and regeneration', *Development*, 143(3), pp. 387-397.

Gaggin, H.K., Truong, Q.A., Gandhi, P.U., Motiwala, S.R., Belcher, A.M., Weiner, R.B., Baggish, A.L. and Januzzi, J.L., Jr. (2017) 'Systematic Evaluation of Endothelin 1 Measurement Relative to Traditional and Modern Biomarkers for Clinical Assessment and Prognosis in Patients With Chronic Systolic Heart Failure: Serial Measurement and Multimarker Testing', *American Journal of Clinical Pathology*, 147(5), pp. 461-472.

Gao, X.-M., Xu, Q., Kiriazis, H., Dart, A.M. and Du, X.-J. (2005) 'Mouse model of post-infarct ventricular rupture: time course, strain- and gender-dependency, tensile strength, and histopathology', *Cardiovascular Research*, 65(2), pp. 469-477.

Gaspar, D., Peixoto, R., De Pieri, A., Striegl, B., Zeugolis, D.I. and Raghunath, M. (2019) 'Local pharmacological induction of angiogenesis: Drugs for cells and cells as drugs', *Advanced Drug Delivery Reviews*.

Gendron, T.F. and Petrucelli, L. (2009) 'The role of tau in neurodegeneration', *Molecular neurodegeneration*, 4, pp. 13-13.

Gil, J. and Peters, G. (2006) 'Regulation of the INK4b–ARF–INK4a tumour suppressor locus: all for one or one for all', *Nature Reviews Molecular Cell Biology*, 7(9), pp. 667-677.

Gilbertson, L. (2003) 'Cre-lox recombination: Cre-ative tools for plant biotechnology', *Trends in Biotechnology*, 21(12), pp. 550-5.

Giordano, F.J. (2005) 'Oxygen, oxidative stress, hypoxia, and heart failure', *Journal of Clinical Investigation*, 115(3), pp. 500-508.

Gislason, G.H., Jacobsen, S., Rasmussen, J.N., Rasmussen, S., Buch, P., Friberg, J., Schramm, T.K., Abildstrom, S.Z., Kober, L., Madsen, M. and Torp-Pedersen, C. (2006) 'Risk of death or reinfarction associated with the use of selective cyclooxygenase-2 inhibitors and nonselective nonsteroidal antiinflammatory drugs after acute myocardial infarction', *Circulation*, 113(25), pp. 2906-13.

Go, J., Park, T.S., Han, G.H., Park, H.Y., Ryu, Y.K., Kim, Y.H., Hwang, J.H., Choi, D.H., Noh, J.R., Hwang, D.Y., Kim, S., Oh, W.K., Lee, C.H. and Kim, K.S. (2018) 'Piperlongumine decreases cognitive impairment and improves hippocampal function in aged mice', *International Journal of Molecular Medicine*, 42(4), pp. 1875-1884.

Gogiraju, R., Xu, X., Bochenek, M.L., Steinbrecher, J.H., Lehnart, S.E., Wenzel, P., Kessel, M., Zeisberg, E.M., Dobbstein, M. and Schäfer, K. (2015) 'Endothelial p53 deletion improves angiogenesis and prevents cardiac fibrosis and heart failure induced by pressure overload in mice', *Journal of the American Heart Association*, 4(2), p. e001770.

Gonzalez-Perez, O. and Quiñones-Hinojosa, A. (2012) 'Astrocytes as neural stem cells in the adult brain', *Journal of Stem Cells*, 7(3), pp. 181-188.

Gonzalez-Valdes, I., Hidalgo, I., Bujarrabal, A., Lara-Pezzi, E., Padron-Barthe, L., Garcia-Pavia, P., Gomez, P., Redondo, J.M., Ruiz-Cabello, J.M., Jimenez-Borreguero, L.J., Enriquez, J.A., de la Pompa, J.L., Hidalgo, A. and Gonzalez, S. (2015) 'Bmi1 limits dilated cardiomyopathy and heart failure by inhibiting cardiac senescence', *Nature Communications*, 6, p. 6473.

Goodpaster, T., Legesse-Miller, A., Hameed, M.R., Aisner, S.C., Randolph-Habecker, J. and Collier, H.A. (2008) 'An immunohistochemical method for identifying fibroblasts in formalin-fixed, paraffin-embedded tissue', *The Journal of Histochemistry and Cytochemistry*, 56(4), pp. 347-358.

Gough, N.R. (2015) 'Senescent Cells Promote Tissue Repair', *Science Signaling*, 8(358), pp. ec3-ec3.

Grainger, D.J. (2004) 'Transforming growth factor beta and atherosclerosis: so far, so good for the protective cytokine hypothesis', *Arteriosclerosis, Thrombosis, and Vascular Biology*, 24(3), pp. 399-404.

Grossman, W. and Paulus, W.J. (2013) 'Myocardial stress and hypertrophy: a complex interface between biophysics and cardiac remodeling', *The Journal of Clinical Investigation*, 123(9), pp. 3701-3703.

Grüntzig, A.R., Senning, Å. and Siegenthaler, W.E. (1979) 'Nonoperative Dilatation of Coronary-Artery Stenosis', *New England Journal of Medicine*, 301(2), pp. 61-68.

Gu, X., Xu, J., Yang, X.P., Peterson, E. and Harding, P. (2015) 'Fractalkine neutralization improves cardiac function after myocardial infarction', *Experimental Physiology*, 100(7), pp. 805-17.

Hahn, J.-Y., Song, Y.B., Kim, E.K., Yu, C.W., Bae, J.-W., Chung, W.-Y., Choi, S.-H., Choi, J.-H., Bae, J.-H., An, K.J., Park, J.-S., Oh, J.H., Kim, S.-W., Hwang, J.-Y., Ryu, J.K., Park, H.S., Lim, D.-S. and Gwon, H.-C. (2013) 'Ischemic Postconditioning During Primary Percutaneous Coronary Intervention', *Circulation*, 128(17), pp. 1889-1896.

Hall, M., Dondo, T.B., Yan, A.T., Mamas, M.A., Timmis, A.D., Deanfield, J.E., Jernberg, T., Hemingway, H., Fox, K.A.A. and Gale, C.P. (2018) 'Multimorbidity and survival for patients with acute myocardial infarction in England and Wales: Latent class analysis of a nationwide population-based cohort', *PLOS Medicine*, 15(3), pp. e1002501-e1002501.

Halladin, N. (2015) 'Oxidative and inflammatory biomarkers of ischemia and reperfusion injuries', *Danish Medical Journal*, 62(4), p. B5054.

Halvorsen, B., Dahl, T.B., Smedbakken, L.M., Singh, A., Michelsen, A.E., Skjelland, M., Krohg-Sorensen, K., Russell, D., Hopken, U.E., Lipp, M., Damas, J.K., Holm, S., Yndestad, A., Biessen, E.A. and Aukrust, P. (2014) 'Increased levels of CCR7 ligands in carotid atherosclerosis: different effects in macrophages and smooth muscle cells', *Cardiovascular Research*, 102(1), pp. 148-56.

Hanada, M., Aime-Sempe, C., Sato, T. and Reed, J.C. (1995) 'Structure-function analysis of Bcl-2 protein. Identification of conserved domains important for homodimerization with Bcl-2 and heterodimerization with Bax', *The Journal of Biological Chemistry*, 270(20), pp. 11962-9.

Hanawalt, P.C. (2015) 'Historical Perspective on the DNA Damage Response', *DNA repair*, 36, pp. 2-7.

Hasdan, G., Benchetrit, S., Rashid, G., Green, J., Bernheim, J. and Rathaus, M. (2002) 'Endothelial dysfunction and hypertension in 5/6 nephrectomized rats are mediated by vascular superoxide', *Kidney International*, 61(2), pp. 586-590.

Hassell, M.E., Vlastra, W., Robbers, L., Hirsch, A., Nijveldt, R., Tijssen, J.G., van Rossum, A.C., Zijlstra, F., Piek, J.J. and Delewi, R. (2017) 'Long-term left ventricular remodelling after revascularisation for ST-segment elevation myocardial infarction as assessed by cardiac magnetic resonance imaging', *Open Heart*, 4(1), p. e000569.

Haubner, B.J., Schneider, J., Schweigmann, U., Schuetz, T., Dichtl, W., Velik-Salchner, C., Stein, J.-I. and Penninger, J.M. (2016) 'Functional Recovery of a Human Neonatal Heart After Severe Myocardial Infarction: Novelty and Significance', *Circulation Research*, 118(2), pp. 216-221.

Hausenloy, D.J., Barrabes, J.A., Bøtker, H.E., Davidson, S.M., Di Lisa, F., Downey, J., Engstrom, T., Ferdinandy, P., Carbrera-Fuentes, H.A., Heusch, G., Ibanez, B., Iliodromitis, E.K., Inzerle, J., Jennings, R., Kalia, N., Kharbanda, R., Lecour, S., Marber, M., Miura, T., Ovize, M., Perez-Pinzon, M.A., Piper, H.M., Przyklenk, K., Schmidt, M.R., Redington, A., Ruiz-Meana, M., Vilahur, G., Vinten-Johansen, J., Yellon, D.M. and Garcia-Dorado, D. (2016) 'Ischaemic conditioning and targeting reperfusion injury: a 30 year voyage of discovery', *Basic Research in Cardiology*, 111(6), p. 70.

Hausenloy, D.J. and Yellon, D.M. (2013) 'Myocardial ischemia-reperfusion injury: a neglected therapeutic target', *J Clin Invest*, 123(1), pp. 92-100.

Hayashi, S., Lewis, P., Pevny, L. and McMahon, A.P. (2002) 'Efficient gene modulation in mouse epiblast using a Sox2Cre transgenic mouse strain', *Mechanisms of Development*, 119, pp. S97-S101.

Hayflick, L. and Moorhead, P.S. (1961) 'The serial cultivation of human diploid cell strains', *Experimental Cell Research*, 25(3), pp. 585-621.

He, L., Huang, X., Kanisicak, O., Li, Y., Wang, Y., Li, Y., Pu, W., Liu, Q., Zhang, H., Tian, X., Zhao, H., Liu, X., Zhang, S., Nie, Y., Hu, S., Miao, X., Wang, Q.-D., Wang, F., Chen, T., Xu, Q., Lui, K.O., Molkentin, J.D. and Zhou, B. (2017) 'Preexisting endothelial cells mediate cardiac neovascularization after injury', *The Journal of Clinical Investigation*, 127(8), pp. 2968-2981.

Health, N.I.o. (2017) *Navitoclax studies*. Available at: <https://www.clinicaltrials.gov/ct2/results?term=Navitoclax&Search=Search> (Accessed: 28/04).

Heart Failure Association (2010) *Biomarkers in Heart Failure*. Available at: <https://www.escardio.org/Guidelines/Recommended-Reading/Heart-Failure/Biomarkers-in-Heart-Failure> (Accessed: 02/11).

Heffner, C.S., Herbert Pratt, C., Babiuk, R.P., Sharma, Y., Rockwood, S.F., Donahue, L.R., Eppig, J.T. and Murray, S.A. (2012) 'Supporting conditional mouse mutagenesis with a comprehensive cre characterization resource', *Nature Communications*, 3, pp. 1218-1218.

Hernandez-Lopez, R., Chavez-Gonzalez, A., Torres-Barrera, P., Moreno-Lorenzana, D., Lopez-Diazguerrero, N., Santiago-Germán, D., Isordia-Salas, I., Smadja, D., Yoder, M., Majluf-Cruz, A. and Alvarado-Moreno, J. (2017) 'Reduced proliferation of endothelial colony-forming cells in unprovoked venous thromboembolic disease as a consequence of endothelial dysfunction', *PLOS ONE*, 12, p. e0183827.

Hewitt, G., Jurk, D., Marques, F.D., Correia-Melo, C., Hardy, T., Gackowska, A., Anderson, R., Taschuk, M., Mann, J. and Passos, J.F. (2012) 'Telomeres are favoured targets of a persistent DNA damage response in ageing and stress-induced senescence', *Nat Commun*, 3, p. 708.

Hong, S.-B., Furihata, M., Baba, M., Zbar, B. and Schmidt, L.S. (2006) 'Vascular defects and liver damage by the acute inactivation of the VHL gene during mouse embryogenesis', *Laboratory Investigation*, 86(7), pp. 664-675.

Honnegowda, T.M., Kumar, P., Udupa, E.G., Kumar, S., Kumar, U. and Rao, P. (2015) 'Role of angiogenesis and angiogenic factors in acute and chronic wound healing', *Plastic and Aesthetic Research*, 2, pp. 239-42.

Hoyer, F.F. and Nahrendorf, M. (2019) 'Interferon- γ regulates cardiac myeloid cells in myocardial infarction', *Cardiovascular Research*.

Hsieh, P.C.H., Segers, V.F.M., Davis, M.E., MacGillivray, C., Gannon, J., Molkentin, J.D., Robbins, J. and Lee, R.T. (2007) 'Evidence from a genetic fate-mapping study that stem cells refresh adult mammalian cardiomyocytes after injury', *Nature Medicine*, 13(8), pp. 970-974.

Huang, S. and Frangogiannis, N.G. (2018) 'Anti-inflammatory therapies in myocardial infarction: failures, hopes and challenges', *British Journal of Pharmacology*, 175(9), pp. 1377-1400.

Hybertson, B.M., Gao, B., Bose, S.K. and McCord, J.M. (2011) 'Oxidative stress in health and disease: The therapeutic potential of Nrf2 activation', *Molecular Aspects of Medicine*, 32(4), pp. 234-246.

Iannello, R.C., Mar, J.H. and Ordahl, C.P. (1991) 'Characterization of a promoter element required for transcription in myocardial cells', *The Journal of Biological Chemistry*, 266(5), pp. 3309-16.

Ibarrola, J., Matilla, L., Martínez-Martínez, E., Gueret, A., Fernández-Celis, A., Henry, J.-P., Nicol, L., Jaisser, F., Mulder, P., Ouvrard-Pascaud, A. and López-Andrés, N. (2019) 'Myocardial Injury After Ischemia/Reperfusion Is Attenuated By Pharmacological Galectin-3 Inhibition', *Scientific Reports*, 9(1), p. 9607.

Incalza, M.A., D'Oria, R., Natalicchio, A., Perrini, S., Laviola, L. and Giorgino, F. (2018) 'Oxidative stress and reactive oxygen species in endothelial dysfunction associated with cardiovascular and metabolic diseases', *Vascular Pharmacology*, 100, pp. 1-19.

Invitrogen (2011) *Click-iT® EdU Imaging Kits mp10338*. Available at: <https://www.thermofisher.com/order/catalog/product/C10339> (Accessed: 18/07).

Itahana, K., Itahana, Y. and Dimri, G.P. (2013) 'Colorimetric detection of senescence-associated beta galactosidase', *Methods Mol Biol*, 965, pp. 143-56.

Jacobs, J.P., Jones, C.M. and Baille, J.P. (1970) 'Characteristics of a Human Diploid Cell Designated MRC-5', *Nature*, 227(5254), pp. 168-170.

Jain, C.C. and Borlaug, B.A. (2019) 'Hemodynamic assessment in heart failure', *Catheterization and Cardiovascular Interventions*, 0(0).

Janssen, B., Debets, J., Leenders, P. and Smits, J. (2002) 'Chronic measurement of cardiac output in conscious mice', *American Journal of Physiology-Regulatory, Integrative and Comparative Physiology*, 282(3), pp. R928-R935.

Jhaveri, K., Taldone, T., Modi, S. and Chiosis, G. (2012) 'Advances in the clinical development of heat shock protein 90 (Hsp90) inhibitors in cancers', *Biochimica et Biophysica Acta (BBA) - Molecular Cell Research*, 1823(3), pp. 742-755.

Jiang, H., Shen, J. and Ran, Z. (2017) 'Epithelial–mesenchymal transition in Crohn's disease', *Mucosal Immunology*, 11, p. 294.

Jinde, K., Nikolic-Paterson, D.J., Huang, X.R., Sakai, H., Kurokawa, K., Atkins, R.C. and Lan, H.Y. (2001) 'Tubular phenotypic change in progressive tubulointerstitial fibrosis in human glomerulonephritis', *American Journal of Kidney Disease*, 38(4), pp. 761-9.

Jones, N.R., Roalfe, A.K., Adoki, I., Hobbs, F.D.R. and Taylor, C.J. (2019) 'Survival of patients with chronic heart failure in the community: a systematic review and meta-analysis', *European Journal of Heart Failure*, 0(0).

Joost, P.H.S., Nathalie, M.M.B., Niels, P.R., Arie, P.J.v.D., Louise, B., Maria, T.E.H., Cable, N.T. and Dick, H.J.T. (2016) 'Heart failure is associated with exaggerated

endothelial ischaemia–reperfusion injury and attenuated effect of ischaemic preconditioning', *European Journal of Preventive Cardiology*, 23(1), pp. 33-40.

Jordan, J.E., Zhao, Z.Q. and Vinten-Johansen, J. (1999) 'The role of neutrophils in myocardial ischemia-reperfusion injury', *Cardiovascular Research*, 43(4), pp. 860-78.

Jordan, M. and Caesar, J. (2016) 'Improving door-to-needle times for patients presenting with ST-elevation myocardial infarction at a rural district general hospital', *BMJ Qual Improv Rep*, 5(1).

Jun, J.-I. and Lau, L.F. (2010a) 'Cellular senescence controls fibrosis in wound healing', *Aging (Albany NY)*, 2(9), pp. 627-631.

Jun, J.I. and Lau, L.F. (2010b) 'The matricellular protein CCN1 induces fibroblast senescence and restricts fibrosis in cutaneous wound healing', *Nature Cell Biology*, 12(7), pp. 676-85.

Juríková, M., Danihel, L., Polák, Š. and Varga, I. (2016) 'Ki67, PCNA, and MCM proteins: Markers of proliferation in the diagnosis of breast cancer', *Acta Histochemica*, 118(5), pp. 544-552.

Jurk, D., Wilson, C., Passos, J.F., Oakley, F., Correia-Melo, C., Greaves, L., Saretzki, G., Fox, C., Lawless, C., Anderson, R., Hewitt, G., Pender, S.L.F., Fullard, N., Nelson, G., Mann, J., van de Sluis, B., Mann, D.A. and von Zglinicki, T. (2014) 'Chronic inflammation induces telomere dysfunction and accelerates ageing in mice', *Nature Communications*, 2, p. 4172.

Justice, J., Miller, J.D., Newman, J.C., Hashmi, S.K., Halter, J., Austad, S.N., Barzilai, N. and Kirkland, J.L. (2016) 'Frameworks for Proof-of-Concept Clinical Trials of Interventions That Target Fundamental Aging Processes', *The Journals of Gerontology: Series A*, 71(11), pp. 1415-1423.

Justice, J.N., Nambiar, A.M., Tchkonja, T., LeBrasseur, N.K., Pascual, R., Hashmi, S.K., Prata, L., Masternak, M.M., Kritchevsky, S.B., Musi, N. and Kirkland, J.L. (2019) 'Senolytics in idiopathic pulmonary fibrosis: Results from a first-in-human, open-label, pilot study', *EBioMedicine*, 40, pp. 554-563.

Kaefer, A., Yang, J., Noertersheuser, P., Mensing, S., Humerickhouse, R., Awni, W. and Xiong, H. (2014) 'Mechanism-based pharmacokinetic/pharmacodynamic meta-analysis of navitoclax (ABT-263) induced thrombocytopenia', *Cancer Chemotherapy and Pharmacology*, 74(3), pp. 593-602.

Kalogeris, T., Baines, C.P., Krenz, M. and Korthuis, R.J. (2012) 'Cell biology of ischemia/reperfusion injury', *Int Rev Cell Mol Biol*, 298, pp. 229-317.

Kam, M.K., Lee, K.Y., Tam, P.K. and Lui, V.C. (2012) 'Generation of NSE-MerCreMer transgenic mice with tamoxifen inducible Cre activity in neurons', *PLoS One*, 7(5), p. e35799.

Kaneko, M., Singal, P.K. and Dhalla, N.S. (1990) 'Alterations in heart sarcolemmal Ca²⁺-ATPase and Ca²⁺-binding activities due to oxygen free radicals', *Basic Research in Cardiology*, 85(1), pp. 45-54.

Kapelios, C.J., Nanas, J.N. and Malliaras, K. (2016) 'Allogeneic cardiosphere-derived cells for myocardial regeneration: current progress and recent results', *Future Cardiology*, 12(1), pp. 87-100.

Kastrup, J., Jorgensen, E., Ruck, A., Tagil, K., Glogar, D., Ruzyllo, W., Botker, H.E., Dudek, D., Drvota, V., Hesse, B., Thuesen, L., Blomberg, P., Gyongyosi, M. and Sylven, C. (2005) 'Direct intramyocardial plasmid vascular endothelial growth factor-A165 gene therapy in patients with stable severe angina pectoris A randomized double-blind placebo-controlled study: the Euroinject One trial', *Journal of the American College of Cardiology*, 45(7), pp. 982-8.

Keeley, E.C., Boura, J.A. and Grines, C.L. (2003) 'Primary angioplasty versus intravenous thrombolytic therapy for acute myocardial infarction: a quantitative review of 23 randomised trials', *The Lancet*, 361(9351), pp. 13-20.

Kehat, I. and Molkenstein, J.D. (2010) 'Molecular pathways underlying cardiac remodeling during pathophysiological stimulation', *Circulation*, 122(25), pp. 2727-2735.

Kelekar, A. and Thompson, C.B. (1998) 'Bcl-2-family proteins: the role of the BH3 domain in apoptosis', *Trends in Cell Biology*, 8(8), pp. 324-330.

Khan, R. and Sheppard, R. (2006) 'Fibrosis in heart disease: understanding the role of transforming growth factor-beta in cardiomyopathy, valvular disease and arrhythmia', *Immunology*, 118(1), pp. 10-24.

Khan, S.Y., Awad, E.M., Oszwald, A., Mayr, M., Yin, X., Waltenberger, B., Stuppner, H., Lipovac, M., Uhrin, P. and Breuss, J.M. (2017) 'Premature senescence of endothelial cells upon chronic exposure to TNF α can be prevented by N-acetyl cysteine and plumericin', *Scientific Reports*, 7, p. 39501.

Kidambi, A., Mather, A.N., Motwani, M., Swoboda, P., Uddin, A., Greenwood, J.P. and Plein, S. (2013) 'The effect of microvascular obstruction and intramyocardial hemorrhage on contractile recovery in reperfused myocardial infarction: insights from cardiovascular magnetic resonance', *J Cardiovasc Magn Reson*, 15(1), p. 58.

Kikuchi, K. and Poss, K.D. (2012) 'Cardiac regenerative capacity and mechanisms', *Annual Review of Cell and Developmental Biology*, 28, pp. 719-741.

Kilbey, A., Terry, A., Cameron, E.R. and Neil, J.C. (2008) 'Oncogene-induced senescence: an essential role for Runx', *Cell cycle (Georgetown, Tex.)*, 7(15), pp. 2333-2340.

Kim, E.-C. and Kim, J.-R. (2019) 'Senotherapeutics: emerging strategy for healthy aging and age-related disease', *BMB reports*, 52(1), pp. 47-55.

Kim, H.-N. and Januzzi, J.L. (2011) 'Natriuretic Peptide Testing in Heart Failure', *Circulation*, 123(18), pp. 2015-2019.

Kimes, B.W. and Brandt, B.L. (1976) 'Properties of a clonal muscle cell line from rat heart', *Experimental Cell Research*, 98(2), pp. 367-381.

King, K.R., Aguirre, A.D., Ye, Y.-X., Sun, Y., Roh, J.D., Ng, R.P., Jr., Kohler, R.H., Arlauckas, S.P., Iwamoto, Y., Savol, A., Sadreyev, R.I., Kelly, M., Fitzgibbons, T.P., Fitzgerald, K.A., Mitchison, T., Libby, P., Nahrendorf, M. and Weissleder, R. (2017) 'IRF3 and type I interferons fuel a fatal response to myocardial infarction', *Nature Medicine*, 23(12), pp. 1481-1487.

Kipps, T.J., Eradat, H., Grosicki, S., Catalano, J., Cosolo, W., Dyagil, I.S., Yalamanchili, S., Chai, A., Sahasranaman, S., Punnoose, E., Hurst, D. and Pylypenko, H. (2015) 'A phase 2 study of the BH3 mimetic BCL2 inhibitor navitoclax (ABT-263) with or without rituximab, in previously untreated B-cell chronic lymphocytic leukemia', *Leukemia & Lymphoma*, 56(10), pp. 2826-2833.

Kirkland, J.L. and Tchkonja, T. (2017) 'Cellular Senescence: A Translational Perspective', *EBioMedicine*, 21, pp. 21-28.

Kirkland, J.L., Tchkonja, T., Zhu, Y., Niedernhofer, L.J. and Robbins, P.D. (2017) 'The Clinical Potential of Senolytic Drugs', *J Am Geriatr Soc*, 65(10), pp. 2297-2301.

Kleinbongard, P., Schulz, R. and Heusch, G. (2011) 'TNF α in myocardial ischemia/reperfusion, remodeling and heart failure', *Heart Failure Reviews*, 16(1), pp. 49-69.

Klopsch, C., Gaebel, R., Lemcke, H., Beyer, M., Vasudevan, P., Fang, H.Y., Quante, M., Vollmar, B., Skorska, A., David, R. and Steinhoff, G. (2018) 'Vimentin-Induced Cardiac Mesenchymal Stem Cells Proliferate in the Acute Ischemic Myocardium', *Cells Tissues Organs*, 206(1-2), pp. 35-45.

Knoppert, S.N., Valentijn, F.A., Nguyen, T.Q., Goldschmeding, R. and Falke, L.L. (2019) 'Cellular Senescence and the Kidney: Potential Therapeutic Targets and Tools', *Frontiers in Pharmacology*, 10(770).

Konstam, M.A., Kramer, D.G., Patel, A.R., Maron, M.S. and Udelson, J.E. (2011) 'Left Ventricular Remodeling in Heart Failure: Current Concepts in Clinical Significance and Assessment', *JACC: Cardiovascular Imaging*, 4(1), pp. 98-108.

Kos, C.H. (2004) 'Cre/loxP system for generating tissue-specific knockout mouse models', *Nutrition Reviews*, 62(6 Pt 1), pp. 243-6.

Kosaraju, A. and Makaryus, A.N. (2019) 'Left Ventricular Ejection Fraction', in *StatPearls*. Treasure Island (FL): StatPearls Publishing LLC.

Kretzschmar, K., Post, Y., Bannier-Hélaouët, M., Mattiotti, A., Drost, J., Basak, O., Li, V.S.W., van den Born, M., Gunst, Q.D., Versteeg, D., Kooijman, L., van der Elst, S., van Es, J.H., van Rooij, E., van den Hoff, M.J.B. and Clevers, H. (2018) 'Profiling proliferative cells and their progeny in damaged murine hearts', *Proceedings of the National Academy of Sciences*, 115(52), pp. E12245-E12254.

Krijnen, P.A.J., Nijmeijer, R., Meijer, C.J.L.M., Visser, C.A., Hack, C.E. and Niessen, H.W.M. (2002) 'Apoptosis in myocardial ischaemia and infarction', *Journal of Clinical Pathology*, 55(11), pp. 801-811.

Krizhanovsky, V., Yon, M., Dickins, R.A., Hearn, S., Simon, J., Miething, C., Yee, H., Zender, L. and Lowe, S.W. (2008) 'Senescence of activated stellate cells limits liver fibrosis', *Cell*, 134(4), pp. 657-67.

Krug, A., Du Mesnil de Rochement, R. and Korb, G. (1966) 'Blood supply of the myocardium after temporary coronary occlusion.', *Circ Res* 19, pp. 57-62.

Kuilman, T., Michaloglou, C., Vredeveld, L.C.W., Douma, S., van Doorn, R., Desmet, C.J., Aarden, L.A., Mooi, W.J. and Peeper, D.S. (2008) 'Oncogene-Induced Senescence Relayed by an Interleukin-Dependent Inflammatory Network', *Cell*, 133(6), pp. 1019-1031.

Kurian, G.A., Rajagopal, R., Vedantham, S. and Rajesh, M. (2016) 'The Role of Oxidative Stress in Myocardial Ischemia and Reperfusion Injury and Remodeling: Revisited', *Oxidative Medicine and Cellular Longevity*, 2016, pp. 1656450-1656450.

Kuznetsov, A.V., Javadov, S., Sickinger, S., Frotschnig, S. and Grimm, M. (2015) 'H9c2 and HL-1 cells demonstrate distinct features of energy metabolism, mitochondrial function and sensitivity to hypoxia-reoxygenation', *Biochimica et Biophysica Acta (BBA) - Molecular Cell Research*, 1853(2), pp. 276-284.

Kyrylkova, K., Kyryachenko, S., Leid, M. and Kioussi, C. (2012) 'Detection of apoptosis by TUNEL assay', *Methods in Molecular Biology*, 887, pp. 41-7.

Laberge, R.-M., Awad, P., Campisi, J. and Desprez, P.-Y. (2012) 'Epithelial-mesenchymal transition induced by senescent fibroblasts', *Cancer Microenvironment*, 5(1), pp. 39-44.

Laboratory, T.J. (2017) *Mouse Strain Datasheet - 024240*. Available at: <https://www.jax.org/strain/024240> (Accessed: 27/04).

Lairez, O., Calise, D., Bianchi, P., Ordener, C., Spreux-Varoquaux, O., Guilbeau-Frugier, C., Escourrou, G., Seif, I., Roncalli, J., Pizzinat, N., Galinier, M., Parini, A. and Mialet-Perez, J. (2009) 'Genetic deletion of MAO-A promotes serotonin-dependent ventricular hypertrophy by pressure overload', *Journal of Molecular and Cellular Cardiology*, 46(4), pp. 587-595.

Lalit, P.A., Hei, D.J., Raval, A.N. and Kamp, T.J. (2014) 'Induced Pluripotent Stem Cells for Post-Myocardial Infarction Repair', *Circulation Research*, 114(8), pp. 1328-1345.

Lanza, A.M., Dyess, T.J. and Alper, H.S. (2012) 'Using the Cre/lox system for targeted integration into the human genome: loxFAS-loxP pairing and delayed

introduction of Cre DNA improve gene swapping efficiency', *Biotechnology Journal*, 7(7), pp. 898-908.

LaPak, K.M. and Burd, C.E. (2014) 'The molecular balancing act of p16(INK4a) in cancer and aging', *Molecular Cancer Research*, 12(2), pp. 167-83.

Leask, A. (2015) 'Getting to the Heart of the Matter', *Circulation Research*, 116(7), pp. 1269-1276.

Lee, B.Y., Han, J.A., Im, J.S., Morrone, A., Johung, K., Goodwin, E.C., Kleijer, W.J., DiMaio, D. and Hwang, E.S. (2006) 'Senescence-associated β -galactosidase is lysosomal β -galactosidase', *Aging Cell*, 5(2), pp. 187-195.

Lei, L., Guo, S.R., Chen, W.L., Rong, H.J. and Lu, F. (2011) 'Stents as a platform for drug delivery', *Expert Opin Drug Deliv*, 8(6), pp. 813-31.

Lemcke, H., Voronina, N., Steinhoff, G. and David, R. (2018) 'Recent Progress in Stem Cell Modification for Cardiac Regeneration', *Stem Cells International*, 2018, pp. 1-22.

Leong, W.F., Chau, J.F.L. and Li, B. (2009) 'p53 Deficiency Leads to Compensatory Up-Regulation of p16INK4a', *Molecular Cancer Research*, 7(3), pp. 354-360.

Leri, A., Franco, S., Zacheo, A., Barlucchi, L., Chimenti, S., Limana, F., Nadal-Ginard, B., Kajstura, J., Anversa, P. and Blasco, M.A. (2003) 'Ablation of telomerase and telomere loss leads to cardiac dilatation and heart failure associated with p53 upregulation', *EMBO J*, 22(1), pp. 131-9.

Lewis-McDougall, F.C., Ruchaya, P.J., Domenjo-Vila, E., Shin Teoh, T., Prata, L., Cottle, B.J., Clark, J.E., Punjabi, P.P., Awad, W., Torella, D., Tchkonja, T., Kirkland, J.L. and Ellison-Hughes, G.M. (2019) 'Aged-senescent cells contribute to impaired heart regeneration', *Aging Cell*, 18(3), p. e12931.

Li, L.T., Jiang, G., Chen, Q. and Zheng, J.N. (2015) 'Ki67 is a promising molecular target in the diagnosis of cancer (review)', *Molecular Medicine Reports*, 11(3), pp. 1566-72.

Li, M.X. and Hwang, P.M. (2015) 'Structure and Function of Cardiac Troponin C (TNNC1): Implications for Heart Failure, Cardiomyopathies, and Troponin Modulating Drugs', *Gene*, 571(2), pp. 153-166.

Li, Q., Cheng, L., Shen, K., Jin, H., Li, H., Cheng, Y. and Ma, X. (2019) 'Efficacy and Safety of Bcl-2 Inhibitor Venetoclax in Hematological Malignancy: A Systematic Review and Meta-Analysis of Clinical Trials', *Frontiers in pharmacology*, 10, pp. 697-697.

Licastro, F., Candore, G., Lio, D., Porcellini, E., Colonna-Romano, G., Franceschi, C. and Caruso, C. (2005) 'Innate immunity and inflammation in ageing: a key for understanding age-related diseases', *Immunity & Ageing*, 2, p. 8.

Lieber, M.R. (2010) 'The mechanism of double-strand DNA break repair by the nonhomologous DNA end-joining pathway', *Annual Review of Biochemistry*, 79, pp. 181-211.

Lieberman, H.B., Panigrahi, S.K., Hopkins, K.M., Wang, L. and Broustas, C.G. (2017) 'p53 and RAD9, the DNA Damage Response, and Regulation of Transcription Networks', *Radiation Research*, 187(4), pp. 424-432.

Limborg, S.W., Krakauer, M., Hedegaard, C.J., Nielsen, C.H., Sørensen, P.S. and Sellebjerg, F. (2007) 'Anti-proliferative effects of interferon beta associated with increased expression of p21', *Multiple Sclerosis*, 13(2 suppl.), pp. s64-s64.

Lin, C.-C., Pan, C.-S., Wang, C.-Y., Liu, S.-W., Hsiao, L.-D. and Yang, C.-M. (2015) 'Tumor necrosis factor-alpha induces VCAM-1-mediated inflammation via c-Src-dependent transactivation of EGF receptors in human cardiac fibroblasts', *Journal of Biomedical Science*, 22(1), pp. 53-53.

Lin, D.C., Diamandis, E.P., Januzzi, J.L., Jr., Maisel, A., Jaffe, A.S. and Clerico, A. (2014) 'Natriuretic peptides in heart failure', *Clinical Chemistry*, 60(8), pp. 1040-6.

Liu, J.-Y., Souroullas, G.P., Diekman, B.O., Krishnamurthy, J., Hall, B.M., Sorrentino, J.A., Parker, J.S., Sessions, G.A., Gudkov, A.V. and Sharpless, N.E. (2019) 'Cells exhibiting strong p16INK4a promoter activation in vivo display features of senescence', *Proceedings of the National Academy of Sciences*, 116(7), pp. 2603-2611.

Liu, L. and Shi, G.-P. (2012) 'CD31: Beyond a marker for endothelial cells', *Cardiovascular Research*, 94, pp. 3-5.

Liu, Y., Johnson, S.M., Fedoriw, Y., Rogers, A.B., Yuan, H., Krishnamurthy, J. and Sharpless, N.E. (2011) 'Expression of p16(INK4a) prevents cancer and promotes aging in lymphocytes', *Blood*, 117(12), pp. 3257-3267.

Liu, Z., Wild, C., Ding, Y., Ye, N., Chen, H., Wold, E.A. and Zhou, J. (2016) 'BH4 domain of Bcl-2 as a novel target for cancer therapy', *Drug Discovery Today*, 21(6), pp. 989-996.

Loffredo, F.S., Steinhauser, M.L., Gannon, J. and Lee, R.T. (2011) 'Bone marrow-derived cell therapy stimulates endogenous cardiomyocyte progenitors and promotes cardiac repair', *Cell Stem Cell*, 8(4), pp. 389-98.

Lønborg, J., Kelbæk, H., Vejlsstrup, N., Bøtker, H.E., Kim, W.Y., Holmvang, L., Jørgensen, E., Helqvist, S., Saunamäki, K., Terkelsen, C.J., Schoos, M.M., Køber, L., Clemmensen, P., Treiman, M. and Engstrøm, T. (2012) 'Exenatide Reduces Final Infarct Size in Patients With ST-Segment-Elevation Myocardial Infarction and Short-Duration of Ischemia', *Circulation: Cardiovascular Interventions*, 5(2), pp. 288-295.

Lønborg, J.T. (2015) 'Targeting reperfusion injury in the era of primary percutaneous coronary intervention: hope or hype?', *Heart*, 101(20), pp. 1612-8.

Losordo, D.W., Vale, P.R. and Isner, J.M. (1999) 'Gene therapy for myocardial angiogenesis', *American Heart Journal*, 138(2, Supplement), pp. S132-S141.

Lowe, D., Horvath, S. and Raj, K. (2016) 'Epigenetic clock analyses of cellular senescence and ageing', *Oncotarget*, 7(8), pp. 8524-8531.

Lunde, K., Solheim, S., Aakhus, S., Arnesen, H., Abdelnoor, M., Egeland, T., Endresen, K., Ilebakk, A., Mangschau, A., Fjeld, J.G., Smith, H.J., Taraldsrud, E., Grøgaard, H.K., Bjørnerheim, R., Brekke, M., Müller, C., Hopp, E., Ragnarsson, A., Brinchmann, J.E. and Forfang, K. (2006) 'Intracoronary Injection of Mononuclear Bone Marrow Cells in Acute Myocardial Infarction', *New England Journal of Medicine*, 355(12), pp. 1199-1209.

Maejima, Y., Adachi, S., Ito, H., Hirao, K. and Isobe, M. (2008) 'Induction of premature senescence in cardiomyocytes by doxorubicin as a novel mechanism of myocardial damage', *Aging Cell*, 7(2), pp. 125-136.

Maekawa, Y., Anzai, T., Yoshikawa, T., Sugano, Y., Mahara, K., Kohno, T., Takahashi, T. and Ogawa, S. (2004) 'Effect of granulocyte-macrophage colony-stimulating factor inducer on left ventricular remodeling after acute myocardial infarction', *Journal of the American College of Cardiology*, 44(7), pp. 1510-1520.

Maher, P. (2015) 'How fisetin reduces the impact of age and disease on CNS function', *Frontiers in bioscience (Scholar edition)*, 7, pp. 58-82.

Makkar, R.R., Smith, R.R., Cheng, K., Malliaras, K., Thomson, L.E., Berman, D., Czer, L.S., Marbán, L., Mendizabal, A., Johnston, P.V., Russell, S.D., Schuleri, K.H., Lardo, A.C., Gerstenblith, G. and Marbán, E. (2012) 'Intracoronary cardiosphere-derived cells for heart regeneration after myocardial infarction (CADUCEUS): a prospective, randomised phase 1 trial', *Lancet (London, England)*, 379(9819), pp. 895-904.

Malliaras, K., Zhang, Y., Seinfeld, J., Galang, G., Tseliou, E., Cheng, K., Sun, B., Aminzadeh, M. and Marbán, E. (2013) 'Cardiomyocyte proliferation and progenitor cell recruitment underlie therapeutic regeneration after myocardial infarction in the adult mouse heart', *EMBO Molecular Medicine*, 5(2), pp. 191-209.

Mao, P., Liu, J., Zhang, Z., Zhang, H., Liu, H., Gao, S., Rong, Y.S. and Zhao, Y. (2016) 'Homologous recombination-dependent repair of telomeric DSBs in proliferating human cells', *Nature Communications*, 7, pp. 12154-12154.

Marbán, E. (2014) 'Breakthroughs in cell therapy for heart disease: focus on cardiosphere-derived cells', *Mayo Clinic proceedings*, 89(6), pp. 850-858.

Marczin, N., El-Habashi, N., Hoare, G.S., Bundy, R.E. and Yacoub, M. (2003) 'Antioxidants in myocardial ischemia–reperfusion injury: therapeutic potential and basic mechanisms', *Archives of Biochemistry and Biophysics*, 420(2), pp. 222-236.

Marelli-Berg, F.M., Clement, M., Mauro, C. and Caligiuri, G. (2013) 'An immunologist's guide to CD31 function in T-cells', *Journal of Cell Science*, 126(11), pp. 2343-2352.

Martínez, P. and Blasco, M.A. (2015) 'Replicating through telomeres: a means to an end', *Trends in Biochemical Sciences*, 40(9), pp. 504-515.

Matsusaka, H., Ide, T., Matsushima, S., Ikeuchi, M., Kubota, T., Sunagawa, K., Kinugawa, S. and Tsutsui, H. (2006) 'Targeted deletion of p53 prevents cardiac rupture after myocardial infarction in mice', *Cardiovascular Research*, 70, pp. 457-65.

May, D., Gilon, D., Djonov, V., Itin, A., Lazarus, A., Gordon, O., Rosenberger, C. and Keshet, E. (2008) 'Transgenic system for conditional induction and rescue of chronic myocardial hibernation provides insights into genomic programs of hibernation', *Proceedings of the National Academy of Sciences*, 105(1), pp. 282-287.

McAlindon, E., Bucciarelli-Ducci, C., Suleiman, M.S. and Baumbach, A. (2015) 'Infarct size reduction in acute myocardial infarction', *Heart*, 101(2), pp. 155-160.

McHugh, D. and Gil, J. (2018) 'Senescence and aging: Causes, consequences, and therapeutic avenues', *The Journal of Cell Biology*, 217(1), pp. 65-77.

McManus, D.D., Shah, S.J., Fabi, M.R., Rosen, A., Whooley, M.A. and Schiller, N.B. (2009) 'Prognostic value of left ventricular end-systolic volume index as a predictor of heart failure hospitalization in stable coronary artery disease: data from the Heart and Soul Study', *Journal of the American Society of Echocardiography : official publication of the American Society of Echocardiography*, 22(2), pp. 190-197.

McSharry, B.P., Jones, C.J., Skinner, J.W., Kipling, D. and Wilkinson, G.W.G. (2001) 'Human telomerase reverse transcriptase-immortalized MRC-5 and HCA2 human fibroblasts are fully permissive for human cytomegalovirus', *Journal of General Virology*, 82(Pt 4), pp. 855-863.

Meng, X., Wang, H., Song, X., Clifton, A.C. and Xiao, J. (2019) 'The potential role of senescence in limiting fibrosis caused by aging', *Journal of Cellular Physiology*.

Menicacci, B., Laurenzana, A., Chillà, A., Margheri, F., Peppicelli, S., Tanganelli, E., Fibbi, G., Giovannelli, L., Del Rosso, M. and Mocali, A. (2017) 'Chronic Resveratrol Treatment Inhibits MRC5 Fibroblast SASP-Related Protumoral Effects on Melanoma Cells', *The Journals of Gerontology: Series A*, 72(9), pp. 1187-1195.

Meyer, K., Hodwin, B., Ramanujam, D., Engelhardt, S. and Sarikas, A. (2016) 'Essential Role for Premature Senescence of Myofibroblasts in Myocardial Fibrosis', *Journal of the American College of Cardiology*, 67(17), pp. 2018-2028.

Midwood, K.S., Williams, L.V. and Schwarzbauer, J.E. (2004) 'Tissue repair and the dynamics of the extracellular matrix', *The International Journal of Biochemistry & Cell Biology*, 36(6), pp. 1031-1037.

- Min, J.-Y., Yang, Y., Converso, K.L., Liu, L., Huang, Q., Morgan, J.P. and Xiao, Y.-F. (2002) 'Transplantation of embryonic stem cells improves cardiac function in postinfarcted rats', *Journal of Applied Physiology*, 92(1), pp. 288-296.
- Minamino, T., Orimo, M., Shimizu, I., Kunieda, T., Yokoyama, M., Ito, T., Nojima, A., Nabetani, A., Oike, Y., Matsubara, H., Ishikawa, F. and Komuro, I. (2009) 'A crucial role for adipose tissue p53 in the regulation of insulin resistance', *Nat Med*, 15(9), pp. 1082-1087.
- Minicucci, M.F., Azevedo, P.S., Polegato, B.F., Paiva, S.A.R. and Zornoff, L.A.M. (2011) 'Heart Failure After Myocardial Infarction: Clinical Implications and Treatment', *Clinical Cardiology*, 34(7), pp. 410-414.
- Mirzayans, R., Andrais, B., Hansen, G. and Murray, D. (2012) 'Role of p16(INK4A) in Replicative Senescence and DNA Damage-Induced Premature Senescence in p53-Deficient Human Cells', *Biochemistry Research International*, 2012, pp. 951574-951574.
- Moens, A.L., Claeys, M.J., Timmermans, J.P. and Vrints, C.J. (2005) 'Myocardial ischemia/reperfusion-injury, a clinical view on a complex pathophysiological process', *Int J Cardiol*, 100(2), pp. 179-90.
- Monahan, K.B., Rozenberg, G.I., Krishnamurthy, J., Johnson, S.M., Liu, W., Bradford, M.K., Horner, J., Depinho, R.A. and Sharpless, N.E. (2010) 'Somatic p16(INK4a) loss accelerates melanomagenesis', *Oncogene*, 29(43), pp. 5809-5817.
- Moncsek, A., Al-Suraih, M.S., Trussoni, C.E., O'Hara, S.P., Splinter, P.L., Zuber, C., Patsenker, E., Valli, P.V., Fingas, C.D., Weber, A., Zhu, Y., Tchkonja, T., Kirkland, J.L., Gores, G.J., Müllhaupt, B., LaRusso, N.F. and Mertens, J.C. (2018) 'Targeting senescent cholangiocytes and activated fibroblasts with B-cell lymphoma-extra large inhibitors ameliorates fibrosis in multidrug resistance 2 gene knockout (Mdr2(-/-)) mice', *Hepatology (Baltimore, Md.)*, 67(1), pp. 247-259.
- Montecucco, F., Carbone, F. and Schindler, T.H. (2016) 'Pathophysiology of ST-segment elevation myocardial infarction: novel mechanisms and treatments', *Eur Heart J*, 37(16), pp. 1268-83.
- Montero, J. and Letai, A. (2018) 'Why do BCL-2 inhibitors work and where should we use them in the clinic?', *Cell Death & Differentiation*, 25(1), pp. 56-64.
- Mosedale, D.E., Smith, D.J., Aitken, S., Schofield, P.M., Clarke, S.C., McNab, D., Goddard, H., Gale, C.R., Martyn, C.N. and Bethell, H.W. (2005) 'Circulating levels of MCP-1 and eotaxin are not associated with presence of atherosclerosis or previous myocardial infarction', *Atherosclerosis*, 183(2), pp. 268-274.
- Moses, K.A., DeMayo, F., Braun, R.M., Reecy, J.L. and Schwartz, R.J. (2001) 'Embryonic expression of an Nkx2-5/Cre gene using ROSA26 reporter mice', *Genesis*, 31(4), pp. 176-180.
- Muchmore, S.W., Sattler, M., Liang, H., Meadows, R.P., Harlan, J.E., Yoon, H.S., Nettesheim, D., Chang, B.S., Thompson, C.B., Wong, S.-L., Ng, S.-C. and Fesik, S.W. (1996) 'X-ray and NMR structure of human Bcl-xL, an inhibitor of programmed cell death', *Nature*, 381(6580), pp. 335-341.
- Muhlestein, J.B. (2014) 'Adverse left ventricular remodelling after acute myocardial infarction: is there a simple treatment that really works?', *European Heart Journal*, 35(3), pp. 144-146.
- Muñoz-Espín, D., Cañamero, M., Maraver, A., Gómez-López, G., Contreras, J., Murillo-Cuesta, S., Rodríguez-Baeza, A., Varela-Nieto, I., Ruberte, J., Collado, M. and Serrano, M. (2013) 'Programmed Cell Senescence during Mammalian Embryonic Development', *Cell*, 155(5), pp. 1104-1118.
- Munoz-Espin, D. and Serrano, M. (2014) 'Cellular senescence: from physiology to pathology', *Nat Rev Mol Cell Biol*, 15(7), pp. 482-496.

- Murphy, E. and Steenbergen, C. (2007) 'Preconditioning: The Mitochondrial Connection', *Annual Review of Physiology*, 69(1), pp. 51-67.
- Murry, C.E., Jennings, R.B. and Reimer, K.A. (1986) 'Preconditioning with ischemia: a delay of lethal cell injury in ischemic myocardium', *Circulation*, 74(5), pp. 1124-1136.
- Murugan, S.J., Gnanapragasam, J. and Vettukattil, J. (2009) 'Acute myocardial infarction in the neonatal period', *Cardiology in the Young*, 12(04), p. 411.
- Nabel, E.G. and Braunwald, E. (2012) 'A Tale of Coronary Artery Disease and Myocardial Infarction', *New England Journal of Medicine*, 366(1), pp. 54-63.
- Nadar, S.K. and Shaikh, M.M. (2019) 'Biomarkers in Routine Heart Failure Clinical Care', *Cardiac Failure Review*, 5(1), pp. 50-56.
- Nagalingam, R.S., Safi, H.A. and Czubryt, M.P. (2016) 'Gaining myocytes or losing fibroblasts: Challenges in cardiac fibroblast reprogramming for infarct repair', *Journal of Molecular and Cellular Cardiology*, 93, pp. 108-114.
- Nah, D.-Y. and Rhee, M.-Y. (2009) 'The inflammatory response and cardiac repair after myocardial infarction', *Korean Circulation Journal*, 39(10), pp. 393-398.
- Nakada, Y., Canseco, D.C., Thet, S., Abdisalaam, S., Asaithamby, A., Santos, C.X., Shah, A.M., Zhang, H., Faber, J.E., Kinter, M.T., Szweda, L.I., Xing, C., Hu, Z., Deberardinis, R.J., Schiattarella, G., Hill, J.A., Oz, O., Lu, Z., Zhang, C.C., Kimura, W. and Sadek, H.A. (2017) 'Hypoxia induces heart regeneration in adult mice', *Nature*, 541(7636), pp. 222-227.
- National Clinical Guideline Centre (UK). (2013) 'Myocardial Infarction with ST-Segment Elevation: The Acute Management of Myocardial Infarction with ST-Segment Elevation [Internet].', (*NICE Clinical Guidelines, No. 167.*), [Online]. Available at: https://www.ncbi.nlm.nih.gov/pubmedhealth/PMH0068969/pdf/PubMedHealth_PMH0068969.pdf (Accessed: 09/04/2017).
- National Institute for Health and Care Excellence (NICE) (2007) *MI: Secondary prevention*. Available at: <https://www.nice.org.uk/donotdo/patients-should-be-advised-not-to-take-supplements-containing-betacarotene-and-should-not-be-advised-to-take-antioxidant-supplements-vitamin-e-and-or-c-or-folic-acid-to-reduce-cardiovascular-risk> (Accessed: 18/10).
- Naylor, R.M., Baker, D.J. and van Deursen, J.M. (2013) 'Senescent Cells: A Novel Therapeutic Target for Aging and Age-Related Diseases', *Clinical pharmacology and therapeutics*, 93(1), pp. 105-116.
- Nazir, S., Jamal, N., Mahmoud, I., Greenwood, J., Blackman, D., Kunadian, V., Been, M., Abrams, K., Wilcox, R., Adgey, A., McCann, G. and Gershlick, A. (2016) 'The REFLO-STEMI (REperfusion Facilitated by LOcal adjunctive therapy in ST-Elevation Myocardial Infarction) trial: a randomised controlled trial comparing intracoronary administration of adenosine or sodium nitroprusside with control for attenuation of microvascular obstruction during primary percutaneous coronary intervention', *Efficacy and Mechanism Evaluation*, 3(9).
- Nelson, G., Wordsworth, J., Wang, C., Jurk, D., Lawless, C., Martin-Ruiz, C. and von Zglinicki, T. (2012) 'A senescent cell bystander effect: senescence-induced senescence', *Aging Cell*, 11(2), pp. 345-9.
- Neri, M., Fineschi, V., Di Paolo, M., Pomara, C., Riezzo, I., Turillazzi, E. and Cerretani, D. (2015) 'Cardiac Oxidative Stress and Inflammatory Cytokines Response after Myocardial Infarction', *Current Vascular Pharmacology*, 13(1), pp. 26-36.
- Neri, M., Riezzo, I., Pascale, N., Pomara, C. and Turillazzi, E. (2017) 'Ischemia/Reperfusion Injury following Acute Myocardial Infarction: A Critical Issue for Clinicians and Forensic Pathologists', *Mediators Inflamm*, 2017, p. 7018393.

Ng, B., Dong, J., D'Agostino, G., Viswanathan, S., Widjaja, A.A., Lim, W.-W., Ko, N.S.J., Tan, J., Chothani, S.P., Huang, B., Xie, C., Pua, C.J., Chacko, A.-M., Guimarães-Camboa, N., Evans, S.M., Byrne, A.J., Maher, T.M., Liang, J., Jiang, D., Noble, P.W., Schafer, S. and Cook, S.A. (2019) 'Interleukin-11 is a therapeutic target in idiopathic pulmonary fibrosis', *Science Translational Medicine*, 11(511), p. 1237.

Niccoli, G., Ferrante, G., Cosentino, N., Conte, M., Belloni, F., Marino, M., Bacà, M., Montone, R.A., Sabato, V., Schiavino, D., Patriarca, G. and Crea, F. (2010) 'Eosinophil cationic protein: A new biomarker of coronary atherosclerosis', *Atherosclerosis*, 211(2), pp. 606-611.

Niccoli, T. and Partridge, L. (2012) 'Ageing as a Risk Factor for Disease', *Current Biology*, 22(17), pp. R741-R752.

NIH U.S National Library of Medicine (2019) *Effect of Remote Ischaemic Conditioning on Clinical Outcomes in STEMI Patients Undergoing PPCI (CONDI2/ERIC-PPCI)*. Available at: <https://clinicaltrials.gov/ct2/show/NCT02342522> (Accessed: 13/09).

Nishikimi, T. and Nakagawa, Y. (2018) 'Adrenomedullin as a Biomarker of Heart Failure', *Heart Failure Clinics*, 14(1), pp. 49-55.

Ogrodnik, M., Miwa, S., Tchkonja, T., Tiniakos, D., Wilson, C.L., Lahat, A., Day, C.P., Burt, A., Palmer, A., Anstee, Q.M., Grellescheid, S.N., Hoeijmakers, J.H.J., Barnhoorn, S., Mann, D.A., Bird, T.G., Vermeij, W.P., Kirkland, J.L., Passos, J.F., von Zglinicki, T. and Jurk, D. (2017) 'Cellular senescence drives age-dependent hepatic steatosis', *Nature Communications*, 8, p. 15691.

Ogrodnik, M., Salmonowicz, H. and Gladyshev, V.N. (2019a) 'Integrating cellular senescence with the concept of damage accumulation in aging: Relevance for clearance of senescent cells', *Aging cell*, 18(1), pp. e12841-e12841.

Ogrodnik, M., Zhu, Y., Langhi, L.G.P., Tchkonja, T., Kruger, P., Fielder, E., Victorelli, S., Ruswhandi, R.A., Giorgadze, N., Pirtskhalava, T., Podgorni, O., Enikolopov, G., Johnson, K.O., Xu, M., Inman, C., Palmer, A.K., Schafer, M., Weigl, M., Ikeno, Y., Burns, T.C., Passos, J.F., von Zglinicki, T., Kirkland, J.L. and Jurk, D. (2019b) 'Obesity-Induced Cellular Senescence Drives Anxiety and Impairs Neurogenesis', *Cell Metabolism*, 29(5), pp. 1061-1077.e8.

Oldershaw, R., Owens, W.A., Sutherland, R., Linney, M., Liddle, R., Magana, L., Lash, G.E., Gill, J.H., Richardson, G. and Meeson, A. (2019) 'Human Cardiac-Mesenchymal Stem Cell-Like Cells, a Novel Cell Population with Therapeutic Potential', *Stem Cells and Development*, 28(9), pp. 593-607.

Orn, S., Manhenke, C., Anand, I.S., Squire, I., Nagel, E., Edvardsen, T. and Dickstein, K. (2007) 'Effect of left ventricular scar size, location, and transmural extent on left ventricular remodeling with healed myocardial infarction', *Am J Cardiol*, 99(8), pp. 1109-14.

Papneja, K., Chan, A.K., Mondal, T.K. and Paes, B. (2017) 'Myocardial Infarction in Neonates: A Review of an Entity with Significant Morbidity and Mortality', *Pediatric Cardiology*, 38(3), pp. 427-441.

Paradies, V., Chan, M.H.H. and Hausenloy, D.J. (2018) 'Strategies for Reducing Myocardial Infarct Size Following STEMI', in Watson, T.J., Ong, P.J.L. and Tcheng, J.E. (eds.) *Primary Angioplasty: A Practical Guide*. Singapore: Springer Singapore, pp. 307-322.

Paradis, A.N., Gay, M.S. and Zhang, L. (2014) 'Binucleation of cardiomyocytes: the transition from a proliferative to a terminally differentiated state', *Drug Discovery Today*, 19(5), pp. 602-609.

Parrinello, S., Coppe, J.-P., Krtolica, A. and Campisi, J. (2005) 'Stromal-epithelial interactions in aging and cancer: senescent fibroblasts alter epithelial cell differentiation', *Journal of Cell Science*, 118(Pt 3), pp. 485-496.

Passos, J.F., Nelson, G., Wang, C., Richter, T., Simillion, C., Proctor, C.J., Miwa, S., Olijslagers, S., Hallinan, J., Wipat, A., Saretzki, G., Rudolph, K.L., Kirkwood, T.B.L. and von Zglinicki, T. (2010) 'Feedback between p21 and reactive oxygen production is necessary for cell senescence', *Molecular Systems Biology*, 6, pp. 347-347.

Passos, J.F., Saretzki, G., Ahmed, S., Nelson, G., Richter, T., Peters, H., Wappler, I., Birket, M.J., Harold, G., Schaeuble, K., Birch-Machin, M.A., Kirkwood, T.B.L. and von Zglinicki, T. (2007) 'Mitochondrial Dysfunction Accounts for the Stochastic Heterogeneity in Telomere-Dependent Senescence', *PLOS Biology*, 5(5), p. e110.

Passos, J.F., Simillion, C., Hallinan, J., Wipat, A. and von Zglinicki, T. (2009) 'Cellular senescence: unravelling complexity', *Age (Dordr)*, 31(4), pp. 353-63.

Penna, C., Mancardi, D., Rastaldo, R. and Pagliaro, P. (2009) 'Cardioprotection: A radical view: Free radicals in pre and postconditioning', *Biochimica et Biophysica Acta (BBA) - Bioenergetics*, 1787(7), pp. 781-793.

Pérez, L., Muñoz-Durango, N., Riedel, C.A., Echeverría, C., Kalergis, A.M., Cabello-Verrugio, C. and Simon, F. (2017) 'Endothelial-to-mesenchymal transition: Cytokine-mediated pathways that determine endothelial fibrosis under inflammatory conditions', *Cytokine & Growth Factor Reviews*, 33, pp. 41-54.

Peshavariya, H.M., Dusting, G.J. and Selemidis, S. (2007) 'Analysis of dihydroethidium fluorescence for the detection of intracellular and extracellular superoxide produced by NADPH oxidase', *Free Radical Research*, 41(6), pp. 699-712.

Peters, R.W., Norman, A., Parmley, W.W., Emilson, B.B., Scheinman, M.M. and Cheitlin, M. (1978) 'Effect of therapy with methylprednisolone on the size of myocardial infarcts in man', *Chest*, 73(4), pp. 483-8.

Phillips, H.M., Stothard, C.A., Shaikh Qureshi, W.M., Kousa, A.I., Briones-Leon, J.A., Khasawneh, R.R., O'Loughlin, C., Sanders, R., Mazzotta, S., Dodds, R., Seidel, K., Bates, T., Nakatomi, M., Cockell, S.J., Schneider, J.E., Mohun, T.J., Maehr, R., Kist, R., Peters, H. and Bamforth, S.D. (2019) 'Pax9 is required for cardiovascular development and interacts with Tbx1 in the pharyngeal endoderm to control 4th pharyngeal arch artery morphogenesis', *Development (Cambridge, England)*, 146(18), p. dev177618.

Piegari, E., De Angelis, A., Cappetta, D., Russo, R., Esposito, G., Costantino, S., Graiani, G., Frati, C., Prezioso, L., Berrino, L., Urbanek, K., Quaini, F. and Rossi, F. (2013) 'Doxorubicin induces senescence and impairs function of human cardiac progenitor cells', *Basic Research in Cardiology*, 108(2), p. 334.

Piera-Velazquez, S., Li, Z. and Jimenez, S.A. (2011) 'Role of endothelial-mesenchymal transition (EndoMT) in the pathogenesis of fibrotic disorders', *The American Journal of Pathology*, 179(3), pp. 1074-1080.

Pilling, D., Akbar, A.N., Girdlestone, J., Orteu, C.H., Borthwick, N.J., Amft, N., Scheel-Toellner, D., Buckley, C.D. and Salmon, M. (1999) 'Interferon-beta mediates stromal cell rescue of T cells from apoptosis', *European Journal of Immunology*, 29(3), pp. 1041-50.

Pinto, A.R., Ilinykh, A., Ivey, M.J., Kuwabara, J.T., D'Antoni, M.L., Debuque, R., Chandran, A., Wang, L., Arora, K., Rosenthal, N.A. and Tallquist, M.D. (2016) 'Revisiting Cardiac Cellular Composition', *Circulation Research*, 118(3), pp. 400-409.

Pinto, D., Gibson, C. and Wykrzkowska, J. (2017) 'Ischemic reperfusion injury of the heart. In: UpToDate', in Post, T.W. (ed.) UpToDate, Waltham, MA.

Piot, C., Croisille, P., Staat, P., Thibault, H., Rioufol, G., Mewton, N., Elbelghiti, R., Cung, T.T., Bonnefoy, E., Angoulvant, D., Macia, C., Raczka, F., Sportouch, C., Gahide, G., Finet, G., Andre-Fouet, X., Revel, D., Kirkorian, G., Monassier, J.P., Derumeaux, G. and Ovize, M. (2008) 'Effect of cyclosporine on reperfusion injury in acute myocardial infarction', *The New England Journal of Medicine*, 359(5), pp. 473-81.

Pleil, J.D. (2016) 'QQ-plots for assessing distributions of biomarker measurements and generating defensible summary statistics', *J Breath Res*, 10(3), p. 035001.

Ponikowski, P., Voors, A.A., Anker, S.D., Bueno, H., Cleland, J.G.F., Coats, A.J.S., Falk, V., González-Juanatey, J.R., Harjola, V.-P., Jankowska, E.A., Jessup, M., Linde, C., Nihoyannopoulos, P., Parissis, J.T., Pieske, B., Riley, J.P., Rosano, G.M.C., Ruilope, L.M., Ruschitzka, F., Rutten, F.H., van der Meer, P., Members, A.T.F. and Reviewers, D. (2016) '2016 ESC Guidelines for the diagnosis and treatment of acute and chronic heart failure', *European Journal of Heart Failure*, 18(8), pp. 891-975.

Porter, K.E. and Turner, N.A. (2009) 'Cardiac fibroblasts: At the heart of myocardial remodeling', *Pharmacology & Therapeutics*, 123(2), pp. 255-278.

Pradeep, A.R., Agarwal, E., Bajaj, P. and Rao, N.S. (2013) '4-Hydroxy-2-nonenal, an oxidative stress marker in crevicular fluid and serum in type 2 diabetes with chronic periodontitis', *Contemporary Clinical Dentistry*, 4(3), pp. 281-285.

Prata, L.G.P.L., Ovsyannikova, I.G., Tchkonja, T. and Kirkland, J.L. (2019) 'Senescent cell clearance by the immune system: Emerging therapeutic opportunities', *Seminars in Immunology*, p. 101275.

Prieur, A., Besnard, E., Babled, A. and Lemaître, J.-M. (2011) 'p53 and p16INK4A independent induction of senescence by chromatin-dependent alteration of S-phase progression', *Nature Communications*, 2(1), p. 473.

Qiagen (2012) *RNeasy® Mini Handbook*. Available at: <file:///campus/home/home46/b0022917/Downloads/1072935-hb-rneasy-mini-0612.pdf> (Accessed: 26th July).

Rahmayani, F., Paryono and Setyopranoto, I. (2018) 'The Role of Ejection Fraction to Clinical Outcome of Acute Ischemic Stroke Patients', *Journal of Neurosciences in Rural Practice*, 9(2), pp. 197-202.

Ranjbarvaziri, S., Park, S., Nguyen, N.B., Gilmore, W.B., Zhao, P. and Ardehali, R. (2017) 'Generation of Nkx2-5/CreER transgenic mice for inducible Cre expression in developing hearts', *Genesis*, 55(8), p. 10.1002/dvg.23041.

Rayess, H., Wang, M.B. and Srivatsan, E.S. (2012) 'Cellular senescence and tumor suppressor gene p16', *International Journal of Cancer*, 130(8), pp. 1715-1725.

Redgrave, R.E., Tual-Chalot, S., Davison, B.J., Grealley, E., Santibanez-Koref, M., Schneider, J.E., Blamire, A.M. and Arthur, H.M. (2016) 'Using MRI to predict future adverse cardiac remodelling in a male mouse model of myocardial infarction.', *Int J Cardiol Heart Vasc*, 11, pp. 29-34.

Redondo, S., Navarro-Dorado, J., Ramajo, M., Medina, Ú. and Tejerina, T. (2012) 'The complex regulation of TGF- β in cardiovascular disease', *Vascular Health and Risk Management*, 8, pp. 533-539.

Rehman, S.U., Mueller, T. and Januzzi, J.L., Jr. (2008) 'Characteristics of the novel interleukin family biomarker ST2 in patients with acute heart failure', *Journal of the American College of Cardiology*, 52(18), pp. 1458-65.

Rhinn, M., Ritschka, B. and Keyes, W.M. (2019) 'Cellular senescence in development, regeneration and disease', *Development*, 146(20), p. dev151837.

- Richardson, G.D., Laval, S. and Owens, W.A. (2015a) 'Cardiomyocyte Regeneration in the mdx Mouse Model of Nonischemic Cardiomyopathy', *Stem Cells Dev*, 24(14), pp. 1672-9.
- Richardson, W.J., Clarke, S.A., Quinn, T.A. and Holmes, J.W. (2015b) 'Physiological Implications of Myocardial Scar Structure', *Comprehensive Physiology*, 5(4), pp. 1877-1909.
- Riezebos, R.K. and Verheugt, F.W. (2013) 'Timing of angiography in non-ST elevation myocardial infarction', *Heart*, 99(24), pp. 1867-73.
- Rikhtegar, R., Pezeshkian, M., Dolati, S., Safaie, N., Afrasiabi Rad, A., Mahdipour, M., Nouri, M., Jodati, A.R. and Yousefi, M. (2019) 'Stem cells as therapy for heart disease: iPSCs, ESCs, CSCs, and skeletal myoblasts', *Biomedicine & Pharmacotherapy*, 109, pp. 304-313.
- Ritschka, B., Storer, M., Mas, A., Heinzmann, F., Ortells, M.C., Morton, J.P., Sansom, O.J., Zender, L. and Keyes, W.M. (2017) 'The senescence-associated secretory phenotype induces cellular plasticity and tissue regeneration', *Genes & Development*, 31(2), pp. 172-183.
- Roberts, R., DeMello, V. and Sobel, B.E. (1976) 'Deleterious effects of methylprednisolone in patients with myocardial infarction', *Circulation*, 53(3 Suppl), pp. I204-6.
- Robinson-Bennett, B. and Han, A. (2006) '30 - Role of Immunohistochemistry in Elucidating Lung Cancer Metastatic to the Ovary from Primary Ovarian Carcinoma', in Hayat, M.A. (ed.) *Handbook of Immunohistochemistry and in Situ Hybridization of Human Carcinomas*. Academic Press, pp. 537-545.
- Rockman, H.A., Ross, R.S., Harris, A.N., Knowlton, K.U., Steinhilber, M.E., Field, L.J., Ross, J., Jr. and Chien, K.R. (1991) 'Segregation of atrial-specific and inducible expression of an atrial natriuretic factor transgene in an in vivo murine model of cardiac hypertrophy', *Proceedings of the National Academy of Sciences of the United States of America*, 88(18), pp. 8277-8281.
- Rodier, F. and Campisi, J. (2011) 'Four faces of cellular senescence', *The Journal of Cell Biology*, 192(4), pp. 547-556.
- Rodríguez-Palomares, J.F., Gavara, J., Ferreira-González, I., Valente, F., Rios, C., Rodríguez-García, J., Bonanad, C., García del Blanco, B., Miñana, G., Mutuberria, M., Nuñez, J., Barrabés, J., Evangelista, A., Bodí, V. and García-Dorado, D. (2019) 'Prognostic Value of Initial Left Ventricular Remodeling in Patients With Reperused STEMI', *JACC: Cardiovascular Imaging*, p. 3023.
- Roger, V.L. (2007) 'Epidemiology of myocardial infarction', *The Medical clinics of North America*, 91(4), pp. 537-ix.
- Roger, V.L., Go, A.S., Lloyd-Jones, D.M., Benjamin, E.J., Berry, J.D., Borden, W.B., Bravata, D.M., Dai, S., Ford, E.S., Fox, C.S., Fullerton, H.J., Gillespie, C., Hailpern, S.M., Heit, J.A., Howard, V.J., Kissela, B.M., Kittner, S.J., Lackland, D.T., Lichtman, J.H., Lisabeth, L.D., Makuc, D.M., Marcus, G.M., Marelli, A., Matchar, D.B., Moy, C.S., Mozaffarian, D., Mussolino, M.E., Nichol, G., Paynter, N.P., Soliman, E.Z., Sorlie, P.D., Sotoodehnia, N., Turan, T.N., Virani, S.S., Wong, N.D., Woo, D. and Turner, M.B. (2012) 'Heart Disease and Stroke Statistics - 2012 Update', *Circulation*, 125(1), pp. e2-e220.
- Roleder, T., Smolka, G., Pysz, P., Kozyra, A. and Ochala, A. (2015) 'Non-ST elevation myocardial infarction related to total coronary artery occlusion - prevalence and patient characteristics', *Postępy Kardiologii Interwencyjnej*, 11(1), pp. 9-13.
- Romson, J.L., Hook, B.G., Kunkel, S.L., Abrams, G.D., Schork, M.A. and Lucchesi, B.R. (1983) 'Reduction of the extent of ischemic myocardial injury by neutrophil depletion in the dog', *Circulation*, 67(5), pp. 1016-23.

- Roos, C.M., Zhang, B., Palmer, A.K., Ogrodnik, M.B., Pirtskhalava, T., Thalji, N.M., Hagler, M., Jurk, D., Smith, L.A., Casaclang-Verzosa, G., Zhu, Y., Schafer, M.J., Tchkonja, T., Kirkland, J.L. and Miller, J.D. (2016a) 'Chronic senolytic treatment alleviates established vasomotor dysfunction in aged or atherosclerotic mice', *Aging Cell*, 15(5), pp. 973-7.
- Roos, S.T., Timmers, L., Biesbroek, P.S., Nijveldt, R., Kamp, O., van Rossum, A.C., van Hout, G.P.J., Stella, P.R., Doevendans, P.A., Knaapen, P., Velthuis, B.K., van Royen, N., Voskuil, M., Nap, A. and Appelman, Y. (2016b) 'No benefit of additional treatment with exenatide in patients with an acute myocardial infarction', *International Journal of Cardiology*, 220, pp. 809-814.
- Rosell, R., Bivona, T.G. and Karachaliou, N. (2013) 'Genetics and biomarkers in personalisation of lung cancer treatment', *The Lancet*, 382(9893), pp. 720-731.
- Rosenmann, H., Blum, D., Kaye, R. and Ittner, L.M. (2012) 'Tau protein: function and pathology', *International journal of Alzheimer's disease*, 2012, pp. 707482-707482.
- Roth, G.M., Bader, D.M. and Pfaltzgraff, E.R. (2014) 'Isolation and physiological analysis of mouse cardiomyocytes', *Journal of Visualized Experiments : JoVE*, (91), p. e51109.
- Rouillard, A.D. and Holmes, J.W. (2012) 'Mechanical regulation of fibroblast migration and collagen remodelling in healing myocardial infarcts', *The Journal of physiology*, 590(18), pp. 4585-4602.
- Roy-O'Reilly, M., Ritzel, R.M., Conway, S.E., Staff, I., Fortunato, G. and McCullough, L.D. (2017) 'CCL11 (Eotaxin-1) Levels Predict Long-Term Functional Outcomes in Patients Following Ischemic Stroke', *Translational Stroke Research*, 8(6), pp. 578-584.
- Rudin, C.M., Hann, C.L., Garon, E.B., Ribeiro de Oliveira, M., Bonomi, P.D., Camidge, D.R., Chu, Q., Giaccone, G., Khaira, D., Ramalingam, S.S., Ranson, M.R., Dive, C., McKeegan, E.M., Chyla, B.J., Dowell, B.L., Chakravarty, A., Nolan, C.E., Rudersdorf, N., Busman, T.A., Mabry, M.H., Krivoshik, A.P., Humerickhouse, R.A., Shapiro, G.I. and Gandhi, L. (2012) 'Phase II study of single-agent navitoclax (ABT-263) and biomarker correlates in patients with relapsed small cell lung cancer', *Clinical cancer research : an official journal of the American Association for Cancer Research*, 18(11), pp. 3163-3169.
- Ruiz-Ortega, M., Rodríguez-Vita, J., Sanchez-Lopez, E., Carvajal, G. and Egido, J. (2007) 'TGF- β signaling in vascular fibrosis', *Cardiovascular Research*, 74(2), pp. 196-206.
- Safa, A., Rashidinejad, H.R., Khalili, M., Dabiri, S., Nemati, M., Mohammadi, M.M. and Jafarzadeh, A. (2016) 'Higher circulating levels of chemokines CXCL10, CCL20 and CCL22 in patients with ischemic heart disease', *Cytokine*, 83, pp. 147-157.
- Sahin, E. and Depinho, R.A. (2010) 'Linking functional decline of telomeres, mitochondria and stem cells during ageing', *Nature*, 464(7288), pp. 520-8.
- Salto-Tellez, M., Yung Lim, S., El Oakley, R.M., Tang, T.P.L., Almsheerqi, Z.A.M. and Lim, S.-K. (2004) 'Myocardial infarction in the C57BL/6J mouse: A quantifiable and highly reproducible experimental model', *Cardiovascular Pathology*, 13(2), pp. 91-97.
- Sanchis-Gomar, F., Perez-Quilis, C., Leischik, R. and Lucia, A. (2016) 'Epidemiology of coronary heart disease and acute coronary syndrome', *Ann Transl Med*, 4(13), p. 256.
- Sano, M., Minamino, T., Toko, H., Miyauchi, H., Orimo, M., Qin, Y., Akazawa, H., Tateno, K., Kayama, Y., Harada, M., Shimizu, I., Asahara, T., Hamada, H., Tomita, S., Molkenstein, J.D., Zou, Y. and Komuro, I. (2007) 'p53-induced inhibition of Hif-1

causes cardiac dysfunction during pressure overload', *Nature*, 446(7134), pp. 444-448.

Sanz, A., Pamplona, R. and Barja, G. (2006) 'Is the Mitochondrial Free Radical Theory of Aging Intact?', *Antioxidants & Redox Signaling*, 8, pp. 582-99.

Sapieha, P. and Mallette, F.A. (2018) 'Cellular Senescence in Postmitotic Cells: Beyond Growth Arrest', *Trends in Cell Biology*, 28(8), pp. 595-607.

Sauer, B. (2002) 'Cre/lox: one more step in the taming of the genome', *Endocrine*, 19(3), pp. 221-8.

Schächinger, V., Erbs, S., Elsässer, A., Haberbosch, W., Hambrecht, R., Hölschermann, H., Yu, J., Corti, R., Mathey, D.G., Hamm, C.W., Süselbeck, T., Assmus, B., Tonn, T., Dimmeler, S. and Zeiher, A.M. (2006) 'Intracoronary Bone Marrow-Derived Progenitor Cells in Acute Myocardial Infarction', *New England Journal of Medicine*, 355(12), pp. 1210-1221.

Schafer, M.J., Haak, A.J., Tschumperlin, D.J. and LeBrasseur, N.K. (2018) 'Targeting Senescent Cells in Fibrosis: Pathology, Paradox, and Practical Considerations', *Current Rheumatology Reports*, 20(1), p. 3.

Schafer, M.J., White, T.A., Iijima, K., Haak, A.J., Ligresti, G., Atkinson, E.J., Oberg, A.L., Birch, J., Salmonowicz, H., Zhu, Y., Mazula, D.L., Brooks, R.W., Fuhrmann-Stroissnigg, H., Pirtskhalava, T., Prakash, Y.S., Tchkonja, T., Robbins, P.D., Aubry, M.C., Passos, J.F., Kirkland, J.L., Tschumperlin, D.J., Kita, H. and LeBrasseur, N.K. (2017) 'Cellular senescence mediates fibrotic pulmonary disease', *Nat Commun*, 8, p. 14532.

Schiattarella, G.G., Altamirano, F., Tong, D., French, K.M., Villalobos, E., Kim, S.Y., Luo, X., Jiang, N., May, H.I., Wang, Z.V., Hill, T.M., Mammen, P.P.A., Huang, J., Lee, D.I., Hahn, V.S., Sharma, K., Kass, D.A., Lavandro, S., Gillette, T.G. and Hill, J.A. (2019) 'Nitrosative stress drives heart failure with preserved ejection fraction', *Nature*, 568(7752), pp. 351-356.

Schneider, J.E., Wiesmann, F., Lygate, C.A. and Neubauer, S. (2006) 'How to Perform an Accurate Assessment of Cardiac Function in Mice using High-Resolution Magnetic Resonance Imaging', *Journal of Cardiovascular Magnetic Resonance*, 8(5), pp. 693-701.

Schumacher, B., Pecher, P., Specht, B.U.v. and Stegmann, T. (1998) 'Induction of Neoangiogenesis in Ischemic Myocardium by Human Growth Factors', *Circulation*, 97(7), pp. 645-650.

Scialò, F., Sriram, A., Fernández-Ayala, D., Gubina, N., Löhmus, M., Nelson, G., Logan, A., Cooper, Helen M., Navas, P., Enríquez, Jose A., Murphy, Michael P. and Sanz, A. (2016) 'Mitochondrial ROS Produced via Reverse Electron Transport Extend Animal Lifespan', *Cell Metabolism*, 23(4), pp. 725-734.

Sedelnikova, O.A., Horikawa, I., Zimonjic, D.B., Popescu, N.C., Bonner, W.M. and Barrett, J.C. (2004) 'Senescing human cells and ageing mice accumulate DNA lesions with unrepairable double-strand breaks', *Nat Cell Biol*, 6(2), pp. 168-170.

Senyo, S.E., Steinhauser, M.L., Pizzimenti, C.L., Yang, V.K., Cai, L., Wang, M., Wu, T.D., Guerquin-Kern, J.L., Lechene, C.P. and Lee, R.T. (2013) 'Mammalian heart renewal by pre-existing cardiomyocytes', *Nature*, 493(7432), pp. 433-6.

Serrano, A.L. and Andrés, V. (2004a) 'Telomeres and Cardiovascular Disease', *Does Size Matter?*, 94(5), pp. 575-584.

Serrano, A.L. and Andrés, V. (2004b) 'Telomeres and Cardiovascular Disease: Does Size Matter?', *Circulation Research*, 94(5), pp. 575-584.

Shamas-Din, A., Brahmabhatt, H., Leber, B. and Andrews, D.W. (2011) 'BH3-only proteins: Orchestrators of apoptosis', *Biochimica et Biophysica Acta (BBA) - Molecular Cell Research*, 1813(4), pp. 508-520.

- Sharpless, N.E., Alson, S., Chan, S., Silver, D.P., Castrillon, D.H. and DePinho, R.A. (2002) 'p16INK4a and p53 Deficiency Cooperate in Tumorigenesis', *Cancer Research*, 62(10), pp. 2761-2765.
- Shay, J.W. and Wright, W.E. (2000) 'Hayflick, his limit, and cellular ageing', *Nat Rev Mol Cell Biol*, 1(1), pp. 72-76.
- Sheng, C.C., Zhou, L. and Hao, J. (2013) 'Current stem cell delivery methods for myocardial repair', *BioMed Research International*, 2013, pp. 547902-547902.
- Shimizu, I. and Minamino, T. (2016) 'Physiological and pathological cardiac hypertrophy', *Journal of Molecular and Cellular Cardiology*, 97, pp. 245-262.
- Shimizu, I. and Minamino, T. (2019) 'Cellular senescence in cardiac diseases', *Journal of Cardiology*, 74(4), pp. 313-319.
- Shiojima, I., Sato, K., Izumiya, Y., Schiekofer, S., Ito, M., Liao, R., Colucci, W.S. and Walsh, K. (2005) 'Disruption of coordinated cardiac hypertrophy and angiogenesis contributes to the transition to heart failure', *The Journal of Clinical Investigation*, 115(8), pp. 2108-2118.
- Shioura, K.M., Geenen, D.L. and Goldspink, P.H. (2008) 'Sex-related changes in cardiac function following myocardial infarction in mice', *American Journal of Physiology. Regulatory, Integrative and Comparative Physiology*, 295(2), pp. R528-R534.
- Short, S., Fielder, E., Miwa, S. and von Zglinicki, T. (2019) 'Senolytics and senostatics as adjuvant tumour therapy', *EBioMedicine*, 41, pp. 683-692.
- Sigma Aldrich (2019) *Dihydroethidium Product Information D7008*. Available at: <https://www.sigmaaldrich.com/catalog/product/sial/d7008?lang=en®ion=GB> (Accessed: 11/09).
- Silva, F.M., Pesaro, A.E., Franken, M. and Wajngarten, M. (2015) 'Acute management of unstable angina and non-ST segment elevation myocardial infarction', *Einstein (Sao Paulo)*, 13(3), pp. 454-61.
- Silvestre, J.-S. (2012) 'Pro-angiogenic cell-based therapy for the treatment of ischemic cardiovascular diseases', *Thrombosis Research*, 130, pp. S90-S94.
- Simons, M., Annex, B.H., Laham, R.J., Kleiman, N., Henry, T., Dauerman, H., Udelson, J.E., Gervino, E.V., Pike, M., Whitehouse, M.J., Moon, T. and Chronos, N.A. (2002) 'Pharmacological Treatment of Coronary Artery Disease With Recombinant Fibroblast Growth Factor-2', *Circulation*, 105(7), pp. 788-793.
- Smart, N., Bollini, S., Dubé, K.N., Vieira, J.M., Zhou, B., Davidson, S., Yellon, D., Riegler, J., Price, A.N., Lythgoe, M.F., Pu, W.T. and Riley, P.R. (2011) 'De novo cardiomyocytes from within the activated adult heart after injury', *Nature*, 474(7353), pp. 640-644.
- Sneddon, L.U., Halsey, L.G. and Bury, N.R. (2017) 'Considering aspects of the 3Rs principles within experimental animal biology', *The Journal of Experimental Biology*, 220(Pt 17), pp. 3007-3016.
- Sohal, D.S., Nghiem, M., Crackower, M.A., Witt, S.A., Kimball, T.R., Tymitz, K.M., Penninger, J.M. and Molkentin, J.D. (2001) 'Temporally Regulated and Tissue-Specific Gene Manipulations in the Adult and Embryonic Heart Using a Tamoxifen-Inducible Cre Protein', *Circulation Research*, 89(1), pp. 20-25.
- Sörensson, P., Saleh, N., Bouvier, F., Böhm, F., Settergren, M., Caidahl, K., Tornvall, P., Arheden, H., Rydén, L. and Pernow, J. (2010) 'Effect of postconditioning on infarct size in patients with ST elevation myocardial infarction', *Heart*, 96(21), pp. 1710-1715.
- Soto-Gamez, A. and Demaria, M. (2017) 'Therapeutic interventions for aging: the case of cellular senescence', *Drug Discovery Today*, 22(5), pp. 786-795.

Souders, C.A., Bowers, S.L.K. and Baudino, T.A. (2009) 'Cardiac fibroblast: the renaissance cell', *Circulation research*, 105(12), pp. 1164-1176.

Souers, A.J., Levenson, J.D., Boghaert, E.R., Ackler, S.L., Catron, N.D., Chen, J., Dayton, B.D., Ding, H., Enschede, S.H., Fairbrother, W.J., Huang, D.C., Hymowitz, S.G., Jin, S., Khaw, S.L., Kovar, P.J., Lam, L.T., Lee, J., Maecker, H.L., Marsh, K.C., Mason, K.D., Mitten, M.J., Nimmer, P.M., Oleksijew, A., Park, C.H., Park, C.M., Phillips, D.C., Roberts, A.W., Sampath, D., Seymour, J.F., Smith, M.L., Sullivan, G.M., Tahir, S.K., Tse, C., Wendt, M.D., Xiao, Y., Xue, J.C., Zhang, H., Humerickhouse, R.A., Rosenberg, S.H. and Elmore, S.W. (2013) 'ABT-199, a potent and selective BCL-2 inhibitor, achieves antitumor activity while sparing platelets', *Nature Medicine*, 19(2), pp. 202-8.

Spallarossa, P., Altieri, P., Aloï, C., Garibaldi, S., Barisione, C., Ghigliotti, G., Fugazza, G., Barsotti, A. and Brunelli, C. (2009) 'Doxorubicin induces senescence or apoptosis in rat neonatal cardiomyocytes by regulating the expression levels of the telomere binding factors 1 and 2', *American Journal of Physiology - Heart and Circulatory Physiology*, 297(6), pp. H2169-H2181.

Staat, P., Rioufol, G., Piot, C., Cottin, Y., Cung, T.T., L'Huillier, I., Aupetit, J.-F., Bonnefoy, E., Finet, G., André-Fouët, X. and Ovize, M. (2005) 'Postconditioning the Human Heart', *Circulation*, 112(14), pp. 2143-2148.

Stamelos, V.A., Redman, C.W. and Richardson, A. (2012) 'Understanding sensitivity to BH3 mimetics: ABT-737 as a case study to foresee the complexities of personalized medicine', *Journal of molecular signaling*, 7(1), pp. 12-12.

Stegger, L., Heijman, E., Schafers, K.P., Nicolay, K., Schafers, M.A. and Strijkers, G.J. (2009) 'Quantification of left ventricular volumes and ejection fraction in mice using PET, compared with MRI', *J Nucl Med*, 50(1), pp. 132-8.

Stenmark, K.R., Frid, M. and Perros, F. (2016) 'Endothelial-to-Mesenchymal Transition', *Circulation*, 133(18), pp. 1734-1737.

Stewart, D.J., Hilton, J.D., Arnold, J.M.O., Gregoire, J., Rivard, A., Archer, S.L., Charbonneau, F., Cohen, E., Curtis, M., Buller, C.E., Mendelsohn, F.O., Dib, N., Page, P., Ducas, J., Plante, S., Sullivan, J., Macko, J., Rasmussen, C., Kessler, P.D., Rasmussen, H.S. and on behalf of the, R.I. (2006) 'Angiogenic gene therapy in patients with nonrevascularizable ischemic heart disease: a phase 2 randomized, controlled trial of AdVEGF121 (AdVEGF121) versus maximum medical treatment', *Gene Therapy*, 13(21), pp. 1503-1511.

Stewart, D.J., Kutryk, M.J.B., Fitchett, D., Freeman, M., Camack, N., Su, Y., Della Siega, A., Bilodeau, L., Burton, J.R., Proulx, G., Radhakrishnan, S. and Investigators, N.T. (2009) 'VEGF gene therapy fails to improve perfusion of ischemic myocardium in patients with advanced coronary disease: results of the NORTHERN trial', *Molecular Therapy : the Journal of the American Society of Gene Therapy*, 17(6), pp. 1109-1115.

Storer, M., Mas, A., Robert-Moreno, A., Pecoraro, M., Ortells, M.C., Di Giacomo, V., Yosef, R., Pilpel, N., Krizhanovsky, V., Sharpe, J. and Keyes, William M. (2013) 'Senescence Is a Developmental Mechanism that Contributes to Embryonic Growth and Patterning', *Cell*, 155(5), pp. 1119-1130.

Streit, W.J. (2006) 'Microglial senescence: does the brain's immune system have an expiration date?', *Trends in Neurosciences*, 29(9), pp. 506-510.

Stub, D., Smith, K., Bernard, S., Bray, J.E., Stephenson, M., Cameron, P., Meredith, I. and Kaye, D.M. (2012) 'A randomized controlled trial of oxygen therapy in acute myocardial infarction Air Verses Oxygen In myocarDial infarction study (AVOID Study)', *American Heart Journal*, 163(3), pp. 339-345.e1.

Stub, D., Smith, K., Bernard, S., Nehme, Z., Stephenson, M., Bray, J.E., Cameron, P., Barger, B., Ellims, A.H., Taylor, A.J., Meredith, I.T. and Kaye, D.M. (2015) 'Air Versus Oxygen in ST-Segment Elevation Myocardial Infarction', *Circulation*.

Sturza, A., Leisegang, M.S., Babelova, A., Schröder, K., Benkhoff, S., Loot, A.E., Fleming, I., Schulz, R., Muntean, D.M. and Brandes, R.P. (2013) 'Monoamine Oxidases Are Mediators of Endothelial Dysfunction in the Mouse Aorta.', *Hypertension*, 62(1), pp. 140-146.

Sundström, J., Evans, J.C., Benjamin, E.J., Levy, D., Larson, M.G., Sawyer, D.B., Siwik, D.A., Colucci, W.S., Wilson, P.W.F. and Vasan, R.S. (2004) 'Relations of plasma total TIMP-1 levels to cardiovascular risk factors and echocardiographic measures: the Framingham heart study', *European Heart Journal*, 25(17), pp. 1509-1516.

Sutton, M.S.J., Pfeffer, M.A., Moye, L., Plappert, T., Rouleau, J.L., Lamas, G., Rouleau, J., Parker, J.O., Arnold, M.O., Sussex, B. and Braunwald, E. (1997) 'Cardiovascular Death and Left Ventricular Remodeling Two Years After Myocardial Infarction', *Circulation*, 96(10), pp. 3294-3299.

Suzuki, E., Takahashi, M., Oba, S. and Nishimatsu, H. (2013) 'Oncogene- and Oxidative Stress-Induced Cellular Senescence Shows Distinct Expression Patterns of Proinflammatory Cytokines in Vascular Endothelial Cells', *The Scientific World Journal*, 2013, p. 754735.

Tak, P.P. (2004) 'IFN-beta in rheumatoid arthritis', *Front Biosci*, 9, pp. 3242-7.

Takagawa, J., Zhang, Y., Wong, M.L., Sievers, R.E., Kapasi, N.K., Wang, Y., Yeghiazarians, Y., Lee, R.J., Grossman, W. and Springer, M.L. (2007) 'Myocardial infarct size measurement in the mouse chronic infarction model: comparison of area- and length-based approaches', *Journal of Applied Physiology*, 102(6), pp. 2104-2111.

Takahashi, A., Ohtani, N. and Hara, E. (2007) 'Irreversibility of cellular senescence: dual roles of p16INK4a/Rb-pathway in cell cycle control', *Cell Division*, 2(1), p. 10.

Takemura, G., Ohno, M., Hayakawa, Y., Misao, J., Kanoh, M., Ohno, A., Uno, Y., Minatoguchi, S., Fujiwara, T. and Fujiwara, H. (1998) 'Role of Apoptosis in the Disappearance of Infiltrated and Proliferated Interstitial Cells After Myocardial Infarction', *Circulation Research*, 82(11), pp. 1130-1138.

Tamaki, S., Mano, T., Sakata, Y., Ohtani, T., Takeda, Y., Kamimura, D., Omori, Y., Tsukamoto, Y., Ikeya, Y., Kawai, M., Kumanogoh, A., Hagihara, K., Ishii, R., Higashimori, M., Kaneko, M., Hasuwa, H., Miwa, T., Yamamoto, K. and Komuro, I. (2013) 'Interleukin-16 Promotes Cardiac Fibrosis and Myocardial Stiffening in Heart Failure with Preserved Ejection Fraction', *PLOS ONE*, 8(7), p. e68893.

Tan, X., Wang, D.B., Lu, X., Wei, H., Zhu, R., Zhu, S.S., Jiang, H. and Yang, Z.J. (2010) 'Doxorubicin induces apoptosis in H9c2 cardiomyocytes: role of overexpressed eukaryotic translation initiation factor 5A', *Biological and Pharmaceutical Bulletin*, 33(10), pp. 1666-72.

Tateishi-Yuyama, E., Matsubara, H., Murohara, T., Ikeda, U., Shintani, S., Masaki, H., Amano, K., Kishimoto, Y., Yoshimoto, K., Akashi, H., Shimada, K., Iwasaka, T. and Imaizumi, T. (2002) 'Therapeutic angiogenesis for patients with limb ischaemia by autologous transplantation of bone-marrow cells: a pilot study and a randomised controlled trial', *The Lancet*, 360(9331), pp. 427-435.

Terkelsen, C.J., Christiansen, E.H., Sorensen, J.T., Kristensen, S.D., Lassen, J.F., Thuesen, L., Andersen, H.R., Vach, W. and Nielsen, T.T. (2009) 'Primary PCI as the preferred reperfusion therapy in STEMI: it is a matter of time', *Heart*, 95(5), pp. 362-9.

Thermo Scientific (2019) *Pierce™ BCA Protein Assay Kit*. Available at: <https://assets.thermofisher.com/TFS->

Assets/LSG/manuals/MAN0011430 Pierce BCA Protein Assay UG.pdf (Accessed: 4th December).

Thygesen, K., Alpert, J.S., Jaffe, A.S., Simoons, M.L., Chaitman, B.R., White, H.D., Joint, E.S.C.A.A.H.A.W.H.F.T.F.f.U.D.o.M.I., Authors/Task Force Members, C., Thygesen, K., Alpert, J.S., White, H.D., Biomarker, S., Jaffe, A.S., Katus, H.A., Apple, F.S., Lindahl, B., Morrow, D.A., Subcommittee, E.C.G., Chaitman, B.R., Clemmensen, P.M., Johanson, P., Hod, H., Imaging, S., Underwood, R., Bax, J.J., Bonow, J.J., Pinto, F., Gibbons, R.J., Classification, S., Fox, K.A., Atar, D., Newby, L.K., Galvani, M., Hamm, C.W., Intervention, S., Uretsky, B.F., Steg, P.G., Wijns, W., Bassand, J.P., Menasche, P., Ravkilde, J., Trials, Registries, S., Ohman, E.M., Antman, E.M., Wallentin, L.C., Armstrong, P.W., Simoons, M.L., Trials, Registries, S., Januzzi, J.L., Nieminen, M.S., Gheorghiade, M., Filippatos, G., Trials, Registries, S., Luepker, R.V., Fortmann, S.P., Rosamond, W.D., Levy, D., Wood, D., Trials, Registries, S., Smith, S.C., Hu, D., Lopez-Sendon, J.L., Robertson, R.M., Weaver, D., Tendera, M., Bove, A.A., Parkhomenko, A.N., Vasilieva, E.J., Mendis, S., Guidelines, E.S.C.C.f.P., Bax, J.J., Baumgartner, H., Ceconi, C., Dean, V., Deaton, C., Fagard, R., Funck-Brentano, C., Hasdai, D., Hoes, A., Kirchhof, P., Knuuti, J., Kolh, P., McDonagh, T., Moulin, C., Popescu, B.A., Reiner, Z., Sechtem, U., Sirnes, P.A., Tendera, M., Torbicki, A., Vahanian, A., Windecker, S., Document, R., Morais, J., Aguiar, C., Almahmeed, W., et al. (2012) 'Third universal definition of myocardial infarction', *J Am Coll Cardiol*, 60(16), pp. 1581-98.

Tirziu, D., Chorianopoulos, E., Moodie, K.L., Palac, R.T., Zhuang, Z.W., Tjwa, M., Roncal, C., Eriksson, U., Fu, Q., Elfenbein, A., Hall, A.E., Carmeliet, P., Moons, L. and Simons, M. (2007) 'Myocardial hypertrophy in the absence of external stimuli is induced by angiogenesis in mice', *The Journal of Clinical Investigation*, 117(11), pp. 3188-3197.

Tong, C., Morrison, A., Mattison, S., Qian, S., Bryniarski, M., Rankin, B., Wang, J., Thomas, D.P. and Li, J. (2013) 'Impaired SIRT1 nucleocytoplasmic shuttling in the senescent heart during ischemic stress', *The FASEB Journal*, 27(11), pp. 4332-42.

Torabi, A., Cleland, J.G., Rigby, A.S. and Sherwi, N. (2014) 'Development and course of heart failure after a myocardial infarction in younger and older people', *Journal of Geriatric Cardiology : JGC*, 11(1), pp. 1-12.

Toussaint, O., Dumont, P., Remacle, J., Dierick, J.-F., Pascal, T., Fripiat, C., Magalhaes, J.P., Zdanov, S. and Chainiaux, F. (2002) 'Stress-Induced Premature Senescence or Stress-Induced Senescence-Like Phenotype: One In Vivo Reality, Two Possible Definitions?', *TheScientificWorldJOURNAL*, 2.

Triantaphyllopoulos, K.A., Williams, R.O., Taylor, H. and Chernajovsky, Y. (1999) 'Amelioration of collagen-induced arthritis and suppression of interferon-gamma, interleukin-12, and tumor necrosis factor alpha production by interferon-beta gene therapy', *Arthritis and Rheumatism*, 42(1), pp. 90-9.

Tse, C., Shoemaker, A.R., Adickes, J., Anderson, M.G., Chen, J., Jin, S., Johnson, E.F., Marsh, K.C., Mitten, M.J., Nimmer, P., Roberts, L., Tahir, S.K., Xiao, Y., Yang, X., Zhang, H., Fesik, S., Rosenberg, S.H. and Elmore, S.W. (2008) 'ABT-263: A Potent and Orally Bioavailable Bcl-2 Family Inhibitor', *Cancer Research*, 68(9), pp. 3421-3428.

Tyler, J.M., Kereiakes, D.J. and Henry, T.D. (2018) 'No Risk, No Reward', *Circulation Research*, 123(5), pp. 521-523.

UK Government (1986) *Animals (Scientific Procedures) Act 1986*. Available at: <https://www.gov.uk/government/publications/consolidated-version-of-asp-1986> (Accessed: 14/03).

- Ulrich, M.M.W., Janssen, A.M.H., Daemen, M.J.A.P., Rappaport, L., Samuel, J.-L., Contard, F., Smits, J.F.M. and Cleutjens, J.P.M. (1997) 'Increased Expression of Fibronectin Isoforms After Myocardial Infarction in Rats', *Journal of Molecular and Cellular Cardiology*, 29(9), pp. 2533-2543.
- Umehara, H., Bloom, E.T., Okazaki, T., Nagano, Y., Yoshie, O. and Imai, T. (2004) 'Fractalkine in vascular biology: from basic research to clinical disease', *Arteriosclerosis, Thrombosis, and Vascular Biology*, 24(1), pp. 34-40.
- Unger, E.F., Goncalves, L., Epstein, S.E., Chew, E.Y., Trapnell, C.B., Cannon, R.O., Quyyumi, A.A., Loscalzo, F. and Stiber, J.A. (2000) 'Effects of a single intracoronary injection of basic fibroblast growth factor in stable angina pectoris', *The American Journal of Cardiology*, 85(12), pp. 1414-1419.
- Valentijn, F.A., Falke, L.L., Nguyen, T.Q. and Goldschmeding, R. (2018) 'Cellular senescence in the aging and diseased kidney', *Journal of Cell Communication and Signaling*, 12(1), pp. 69-82.
- Valiente-Alandi, I., Albo-Castellanos, C., Herrero, D., Arza, E., Garcia-Gomez, M., Segovia, J.C., Capecchi, M. and Bernad, A. (2015) 'Cardiac Bmi1(+) cells contribute to myocardial renewal in the murine adult heart', *Stem Cell Research & Therapy*, 6, p. 16.
- van Berlo, J.H., Kanisicak, O., Maillet, M., Vagnozzi, R.J., Karch, J., Lin, S.C., Middleton, R.C., Marban, E. and Molkentin, J.D. (2014) 'c-kit+ cells minimally contribute cardiomyocytes to the heart', *Nature*, 509(7500), pp. 337-41.
- van der Laan, A.M., Nahrendorf, M. and Piek, J.J. (2012) 'Healing and adverse remodelling after acute myocardial infarction: role of the cellular immune response', *Heart*, 98(18), pp. 1384-1390.
- van Deursen, J.M. (2014) 'The role of senescent cells in ageing', *Nature*, 509(7501), pp. 439-446.
- van Deursen, J.M. (2019) 'Senolytic therapies for healthy longevity', *Science*, 364(6441), pp. 636-637.
- Van Duyne, G.D. (2015) 'Cre Recombinase', *Microbiology Spectrum*, 3(1).
- van Holten, J., Smeets, T.J.M., Blankert, P. and Tak, P.P. (2005) 'Expression of interferon β in synovial tissue from patients with rheumatoid arthritis: comparison with patients with osteoarthritis and reactive arthritis', *Annals of the Rheumatic Diseases*, 64(12), pp. 1780-1782.
- van Willigenburg, H., de Keizer, P.L.J. and de Bruin, R.W.F. (2018) 'Cellular senescence as a therapeutic target to improve renal transplantation outcome', *Pharmacological Research*, 130, pp. 322-330.
- Vanezis, A.P., Rodrigo, G.C., Squire, I.B. and Samani, N.J. (2016) 'Remote ischaemic conditioning and remodelling following myocardial infarction: current evidence and future perspectives', *Heart Fail Rev*, 21(5), pp. 635-43.
- Velarde, M.C. and Demaria, M. (2016) 'Targeting Senescent Cells: Possible Implications for Delaying Skin Aging: A Mini-Review', *Gerontology*, 62(5), pp. 513-518.
- Vicencio, J., Galluzzi, L., Tajeddine, N., Ortiz, C., Criollo, A., Tasmimir, E., Morselli, E., Ben Younes, A., Maiuri, M., Lavandro, S. and Kroemer, G. (2008) 'Senescence, Apoptosis or Autophagy?', *Gerontology*, 54, pp. 92-9.
- Vicente, R., Mausset-Bonnefont, A.-L., Jorgensen, C., Louis-Plence, P. and Brondello, J.-M. (2016) 'Cellular senescence impact on immune cell fate and function', *Ageing cell*, 15(3), pp. 400-406.
- Vicinanza, C., Aquila, I., Scalise, M., Cristiano, F., Marino, F., Cianflone, E., Mancuso, T., Marotta, P., Sacco, W., Lewis, F.C., Couch, L., Shone, V., Gritti, G., Torella, A., Smith, A.J., Terracciano, C.M., Britti, D., Veltri, P., Indolfi, C., Nadal-

Ginard, B., Ellison-Hughes, G.M. and Torella, D. (2017) 'Adult cardiac stem cells are multipotent and robustly myogenic: c-kit expression is necessary but not sufficient for their identification', *Cell death and differentiation*, 24(12), pp. 2101-2116.

Victorelli, S., Lagnado, A., Halim, J., Moore, W., Talbot, D., Barrett, K., Chapman, J., Birch, J., Ogrodnik, M., Meves, A., Pawlikowski, J.S., Jurk, D., Adams, P.D., van Heemst, D., Beekman, M., Slagboom, P.E., Gunn, D.A. and Passos, J.F. (2019) 'Senescent human melanocytes drive skin ageing via paracrine telomere dysfunction', *The EMBO Journal*, p. e101982.

Victorelli, S. and Passos, J.F. (2017) 'Telomeres and Cell Senescence - Size Matters Not', *EBioMedicine*.

Vikram, A. and Jena, G. (2010) 'S961, an insulin receptor antagonist causes hyperinsulinemia, insulin-resistance and depletion of energy stores in rats', *Biochemical and Biophysical Research Communications*, 398(2), pp. 260-265.

Villari, B., Vassalli, G., Schneider, J., Chiariello, M. and Hess, O.M. (1997) 'Age Dependency of Left Ventricular Diastolic Function in Pressure Overload Hypertrophy', *Journal of the American College of Cardiology*, 29(1), pp. 181-186.

Villeneuve, C., Guilbeau-Frugier, C., Sicard, P., Lairez, O., Ordener, C., Duparc, T., De Paulis, D., Couderc, B., Spreux-Varoquaux, O., Tortosa, F., Garnier, A., Knauf, C., Valet, P., Borch, E., Nediani, C., Gharib, A., Ovize, M., Delisle, M.-B., Parini, A. and Mialet-Perez, J. (2013) 'p53-PGC-1 α Pathway Mediates Oxidative Mitochondrial Damage and Cardiomyocyte Necrosis Induced by Monoamine Oxidase-A Upregulation: Role in Chronic Left Ventricular Dysfunction in Mice', *Antioxidants & Redox Signaling*, 18(1), pp. 5-18.

Vincent, S.D. and Robertson, E.J. (2003) 'Highly efficient transgene-independent recombination directed by a maternally derived SOX2CRE transgene', *Genesis*, 37(2), pp. 54-56.

Visser, C.A. (2003) 'Left ventricular remodelling after myocardial infarction: importance of residual myocardial viability and ischaemia', *Heart*, 89(10), pp. 1121-1122.

von Gise, A. and Pu, W.T. (2012) 'Endocardial and epicardial epithelial to mesenchymal transitions in heart development and disease', *Circulation Research*, 110(12), pp. 1628-1645.

von Zglinicki, T. (2002) 'Oxidative stress shortens telomeres', *Trends in Biochemical Sciences*, 27(7), pp. 339-44.

Walaszczyk, A., Dookun, E., Redgrave, R., Tual-Chalot, S., Victorelli, S., Spyridopoulos, I., Owens, A., Arthur, H.M., Passos, J.F. and Richardson, G.D. (2019) 'Pharmacological clearance of senescent cells improves survival and recovery in aged mice following acute myocardial infarction', *Aging Cell*, 18(3), p. e12945.

Wang, F., Keimig, T., He, Q., Ding, J., Zhang, Z., Pourabdollah-Nejad, S. and Yang, X.-P. (2007) 'Augmented Healing Process in Female Mice with Acute Myocardial Infarction', *Gender Medicine*, 4(3), pp. 230-247.

Wang, J., Hoshijima, M., Lam, J., Zhou, Z., Jokiel, A., Dalton, N.D., Hultenby, K., Ruiz-Lozano, P., Ross, J., Jr., Tryggvason, K. and Chien, K.R. (2006) 'Cardiomyopathy associated with microcirculation dysfunction in laminin alpha4 chain-deficient mice', *The Journal of Biological Chemistry*, 281(1), pp. 213-20.

Wang, Y., Chang, J., Liu, X., Zhang, X., Zhang, S., Zhang, X., Zhou, D. and Zheng, G. (2016) 'Discovery of piperlongumine as a potential novel lead for the development of senolytic agents', *Aging*, 8(11), pp. 2915-2926.

Wang, Y., Yau, Y.Y., Perkins-Balding, D. and Thomson, J.G. (2011) 'Recombinase technology: applications and possibilities', *Plant Cell Reports*, 30(3), pp. 267-85.

- Watanabe, S., Kawamoto, S., Ohtani, N. and Hara, E. (2017) 'Impact of senescence-associated secretory phenotype and its potential as a therapeutic target for senescence-associated diseases', *Cancer Science*, 108(4), pp. 563-569.
- Waters, D.W., Blokland, K.E.C., Pathinayake, P.S., Burgess, J.K., Mutsaers, S.E., Prele, C.M., Schuliga, M., Grainge, C.L. and Knight, D.A. (2018) 'Fibroblast senescence in the pathology of idiopathic pulmonary fibrosis', *American Journal of Physiology-Lung Cellular and Molecular Physiology*, 315(2), pp. L162-L172.
- Watkins, S.J., Borthwick, G.M. and Arthur, H.M. (2011) 'The H9C2 cell line and primary neonatal cardiomyocyte cells show similar hypertrophic responses in vitro', *In Vitro Cellular & Developmental Biology - Animal*, 47(2), pp. 125-31.
- Weber, C., Meiler, S., Döring, Y., Koch, M., Drechsler, M., Megens, R.T.A., Rowinska, Z., Bidzhekov, K., Fecher, C., Ribechini, E., van Zandvoort, M.A.M.J., Binder, C.J., Jelinek, I., Hristov, M., Boon, L., Jung, S., Korn, T., Lutz, M.B., Förster, I., Zenke, M., Hieronymus, T., Junt, T. and Zerneck, A. (2011) 'CCL17-expressing dendritic cells drive atherosclerosis by restraining regulatory T cell homeostasis in mice', *The Journal of Clinical Investigation*, 121(7), pp. 2898-2910.
- Werfel, S., Jungmann, A., Lehmann, L., Ksienzyk, J., Bekeredjian, R., Kaya, Z., Leuchs, B., Nordheim, A., Backs, J., Engelhardt, S., Katus, H.A. and Müller, O.J. (2014) 'Rapid and highly efficient inducible cardiac gene knockout in adult mice using AAV-mediated expression of Cre recombinase', *Cardiovascular Research*, 104(1), pp. 15-23.
- Westhuyzen, J., Cochrane, A.D., Tesar, P.J., Mau, T., Cross, D.B., Frenneaux, M.P., Khafagi, F.A. and Fleming, S.J. (1997) 'Effect of preoperative supplementation with α -tocopherol and ascorbic acid on myocardial injury in patients undergoing cardiac operations', *The Journal of Thoracic and Cardiovascular Surgery*, 113(5), pp. 942-948.
- Westman, P.C., Lipinski, M.J., Luger, D., Waksman, R., Bonow, R.O., Wu, E. and Epstein, S.E. (2016) 'Inflammation as a Driver of Adverse Left Ventricular Remodeling After Acute Myocardial Infarction', *Journal of the American College of Cardiology*, 67(17), pp. 2050-2060.
- White, H.D., Norris, R.M., Brown, M.A., Brandt, P.W., Whitlock, R.M. and Wild, C.J. (1987) 'Left ventricular end-systolic volume as the major determinant of survival after recovery from myocardial infarction', *Circulation*, 76(1), pp. 44-51.
- Whittaker, A., Rowell, L., Olatawura, O., Poliacikova, P., Glover, J., Brookes, C. and Bishop, A. (2013) 'Primary angioplasty for acute STEMI in secondary care: feasibility, outcomes and potential advantages', *The British Journal of Cardiology*, 20(1), pp. 32-37.
- Widgerow, A.D. (2014) 'Ischemia-reperfusion injury: influencing the microcirculatory and cellular environment', *Ann Plast Surg*, 72(2), pp. 253-60.
- Wilson, W.H., O'Connor, O.A., Czuczman, M.S., LaCasce, A.S., Gerecitano, J.F., Leonard, J.P., Tulpule, A., Dunleavy, K., Xiong, H., Chiu, Y.-L., Cui, Y., Busman, T., Elmore, S.W., Rosenberg, S.H., Krivoshik, A.P., Enschede, S.H. and Humerickhouse, R.A. (2010) 'Navitoclax, a targeted high-affinity inhibitor of BCL-2, in lymphoid malignancies: a phase 1 dose-escalation study of safety, pharmacokinetics, pharmacodynamics, and antitumour activity', *The Lancet. Oncology*, 11(12), pp. 1149-1159.
- Windecker, S., Kolh, P., Alfonso, F., Collet, J.-P., Cremer, J., Falk, V., Filippatos, G., Hamm, C., Head, S.J., Jüni, P., Kappetein, A.P., Kastrati, A., Knuuti, J., Landmesser, U., Laufer, G., Neumann, F.-J., Richter, D.J., Schauerte, P., Sousa Uva, M., Stefanini, G.G., Taggart, D.P., Torracca, L., Valgimigli, M., Wijns, W., Witkowski, A., Zamorano, J.L., Achenbach, S., Baumgartner, H., Bax, J.J., Bueno, H., Dean, V.,

Deaton, C., Erol, Ç., Fagard, R., Ferrari, R., Hasdai, D., Hoes, A.W., Kirchhof, P., Knuuti, J., Kolh, P., Lancellotti, P., Linhart, A., Nihoyannopoulos, P., Piepoli, M.F., Ponikowski, P., Sirnes, P.A., Tamargo, J.L., Tendera, M., Torbicki, A., Wijns, W., Windecker, S., Sousa Uva, M., Achenbach, S., Pepper, J., Anyanwu, A., Badimon, L., Bauersachs, J., Baumbach, A., Beygui, F., Bonaros, N., De Carlo, M., Deaton, C., Dobrev, D., Dunning, J., Eeckhout, E., Gielen, S., Hasdai, D., Kirchhof, P., Luckraz, H., Mahrholdt, H., Montalescot, G., Paparella, D., Rastan, A.J., Sanmartin, M., Sergeant, P., Silber, S., Tamargo, J., ten Berg, J., Thiele, H., van Geuns, R.-J., Wagner, H.-O., Wassmann, S., Wendler, O., Zamorano, J.L., Weidinger, F., Ibrahimov, F., Legrand, V., Terzić, I., Postadzhiyan, A., Skoric, B., Georgiou, G.M., Zelizko, M., Junker, A., Eha, J., Romppanen, H., Bonnet, J.-L., Aladashvili, A., Hambrecht, R., Becker, D., Gudnason, T., et al. (2014) '2014 ESC/EACTS Guidelines on myocardial revascularization The Task Force on Myocardial Revascularization of the European Society of Cardiology (ESC) and the European Association for Cardio-Thoracic Surgery (EACTS) Developed with the special contribution of the European Association of Percutaneous Cardiovascular Interventions (EAPCI)', *European Heart Journal*, 35(37), pp. 2541-2619.

Wirth, D., Gama-Norton, L., Riemer, P., Sandhu, U., Schucht, R. and Hauser, H. (2007) 'Road to precision: recombinase-based targeting technologies for genome engineering', *Current Opinion in Biotechnology*, 18(5), pp. 411-9.

Witek, P., Korga, A., Burdan, F., Ostrowska, M., Nosowska, B., Iwan, M. and Dudka, J. (2016) 'The effect of a number of H9C2 rat cardiomyocytes passage on repeatability of cytotoxicity study results', *Cytotechnology*, 68(6), pp. 2407-2415.

World Health Organisation (2014) '298', *Global Status Report on noncommunicable diseases*. Available at: http://apps.who.int/iris/bitstream/10665/148114/1/9789241564854_eng.pdf?ua=1 (Accessed: 10/01).

Wu, E., Ortiz, J.T., Tejedor, P., Lee, D.C., Bucciarelli-Ducci, C., Kansal, P., Carr, J.C., Holly, T.A., Lloyd-Jones, D., Klocke, F.J. and Bonow, R.O. (2008) 'Infarct size by contrast enhanced cardiac magnetic resonance is a stronger predictor of outcomes than left ventricular ejection fraction or end-systolic volume index: prospective cohort study', *Heart*, 94(6), pp. 730-736.

Xia, Z., Li, H. and Irwin, M.G. (2016) 'Myocardial ischaemia reperfusion injury: the challenge of translating ischaemic and anaesthetic protection from animal models to humans', *BJA: British Journal of Anaesthesia*, 117(suppl_2), pp. ii44-ii62.

Xu, M., Pirtskhalava, T., Farr, J.N., Weigand, B.M., Palmer, A.K., Weivoda, M.M., Inman, C.L., Ogradnik, M.B., Hachfeld, C.M., Fraser, D.G., Onken, J.L., Johnson, K.O., Verzosa, G.C., Langhi, L.G.P., Weigl, M., Giorgadze, N., LeBrasseur, N.K., Miller, J.D., Jurk, D., Singh, R.J., Allison, D.B., Ejima, K., Hubbard, G.B., Ikeno, Y., Cubro, H., Garovic, V.D., Hou, X., Weroha, S.J., Robbins, P.D., Niedernhofer, L.J., Khosla, S., Tchkonja, T. and Kirkland, J.L. (2018) 'Senolytics improve physical function and increase lifespan in old age', *Nature Medicine*, 24(8), pp. 1246-1256.

Yan, J., Zhang, L., Sultana, N., Park, D.S., Shekhar, A., Bu, L., Hu, J., Razzaque, S. and Cai, C.-L. (2015) 'A Murine Myh6MerCreMer Knock-In Allele Specifically Mediates Temporal Genetic Deletion in Cardiomyocytes after Tamoxifen Induction', *PLOS ONE*, 10(7), p. e0133472.

Yazdanyar, A. and Newman, A.B. (2009) 'The burden of cardiovascular disease in the elderly: morbidity, mortality, and costs', *Clinics in Geriatric Medicine*, 25(4), pp. 563-vii.

Yin, F.C., Spurgeon, H.A., Rakusan, K., Weisfeldt, M.L. and Lakatta, E.G. (1982) 'Use of tibial length to quantify cardiac hypertrophy: application in the aging rat', *The American Journal of Physiology*, 243(6), pp. H941-7.

Yosef, R., Pilpel, N., Tokarsky-Amiel, R., Biran, A., Ovadya, Y., Cohen, S., Vadai, E., Dassa, L., Shahar, E., Condiotti, R., Ben-Porath, I. and Krizhanovsky, V. (2016) 'Directed elimination of senescent cells by inhibition of BCL-W and BCL-XL', *Nature communications*, 7, pp. 11190-11190.

Yousefzadeh, M.J., Zhu, Y., McGowan, S.J., Angelini, L., Fuhrmann-Stroissnigg, H., Xu, M., Ling, Y.Y., Melos, K.I., Pirtskhalava, T., Inman, C.L., McGuckian, C., Wade, E.A., Kato, J.I., Grassi, D., Wentworth, M., Burd, C.E., Arriaga, E.A., Ladiges, W.L., Tchkonja, T., Kirkland, J.L., Robbins, P.D. and Niedernhofer, L.J. (2018) 'Fisetin is a senotherapeutic that extends health and lifespan', *EBioMedicine*, 36, pp. 18-28.

Yue, Y., Meng, K., Pu, Y. and Zhang, X. (2017) 'Transforming growth factor beta (TGF- β) mediates cardiac fibrosis and induces diabetic cardiomyopathy', *Diabetes Research and Clinical Practice*, 133, pp. 124-130.

Zeisberg, E.M., Tarnavski, O., Zeisberg, M., Dorfman, A.L., McMullen, J.R., Gustafsson, E., Chandraker, A., Yuan, X., Pu, W.T., Roberts, A.B., Neilson, E.G., Sayegh, M.H., Izumo, S. and Kalluri, R. (2007a) 'Endothelial-to-mesenchymal transition contributes to cardiac fibrosis', *Nature Medicine*, 13(8), pp. 952-61.

Zeisberg, M., Yang, C., Martino, M., Duncan, M.B., Rieder, F., Tanjore, H. and Kalluri, R. (2007b) 'Fibroblasts derive from hepatocytes in liver fibrosis via epithelial to mesenchymal transition', *The Journal of Biological Chemistry*, 282(32), pp. 23337-47.

Zhang, H., Nimmer, P.M., Tahir, S.K., Chen, J., Fryer, R.M., Hahn, K.R., Iciek, L.A., Morgan, S.J., Nasarre, M.C., Nelson, R., Preusser, L.C., Reinhart, G.A., Smith, M.L., Rosenberg, S.H., Elmore, S.W. and Tse, C. (2007) 'Bcl-2 family proteins are essential for platelet survival', *Cell Death And Differentiation*, 14, p. 943.

Zhao, H., Joseph, J., Fales, H.M., Sokoloski, E.A., Levine, R.L., Vasquez-Vivar, J. and Kalyanaraman, B. (2005) 'Detection and characterization of the product of hydroethidine and intracellular superoxide by HPLC and limitations of fluorescence', *Proceedings of the National Academy of Sciences of the United States of America*, 102(16), pp. 5727-5732.

Zhao, Z.-Q., Corvera, J.S., Halkos, M.E., Kerendi, F., Wang, N.-P., Guyton, R.A. and Vinten-Johansen, J. (2003) 'Inhibition of myocardial injury by ischemic postconditioning during reperfusion: comparison with ischemic preconditioning', *American Journal of Physiology-Heart and Circulatory Physiology*, 285(2), pp. H579-H588.

Zhong, J., Basu, R., Guo, D., Chow, F.L., Byrns, S., Schuster, M., Loibner, H., Wang, X.-h., Penninger, J.M., Kassiri, Z. and Oudit, G.Y. (2010) 'Angiotensin-Converting Enzyme 2 Suppresses Pathological Hypertrophy, Myocardial Fibrosis, and Cardiac Dysfunction', *Circulation*, 122(7), pp. 717-728.

Zhou, B., Ma, Q., Rajagopal, S., Wu, S.M., Domian, I., Rivera-Feliciano, J., Jiang, D., von Gise, A., Ikeda, S., Chien, K.R. and Pu, W.T. (2008) 'Epicardial progenitors contribute to the cardiomyocyte lineage in the developing heart', *Nature*, 454(7200), pp. 109-113.

Zhou, P., Zhang, Y., Ma, Q., Gu, F., Day, D.S., He, A., Zhou, B., Li, J., Stevens, S.M., Romo, D. and Pu, W.T. (2013) 'Interrogating translational efficiency and lineage-specific transcriptomes using ribosome affinity purification', *Proceedings of the National Academy of Sciences*, 110(38), pp. 15395-15400.

- Zhu, F., Li, Y., Zhang, J., Piao, C., Liu, T., Li, H.-H. and Du, J. (2013) 'Senescent Cardiac Fibroblast Is Critical for Cardiac Fibrosis after Myocardial Infarction', *PLOS ONE*, 8(9), p. e74535.
- Zhu, Y., Doornebal, E.J., Pirtskhalava, T., Giorgadze, N., Wentworth, M., Fuhrmann-Stroissnigg, H., Niedernhofer, L.J., Robbins, P.D., Tchkonina, T. and Kirkland, J.L. (2017) 'New agents that target senescent cells: the flavone, fisetin, and the BCL-X(L) inhibitors, A1331852 and A1155463', *Aging*, 9(3), pp. 955-963.
- Zhu, Y., Tchkonina, T., Fuhrmann-Stroissnigg, H., Dai, H.M., Ling, Y.Y., Stout, M.B., Pirtskhalava, T., Giorgadze, N., Johnson, K.O., Giles, C.B., Wren, J.D., Niedernhofer, L.J., Robbins, P.D. and Kirkland, J.L. (2016) 'Identification of a novel senolytic agent, navitoclax, targeting the Bcl-2 family of anti-apoptotic factors', *Aging Cell*, 15(3), pp. 428-435.
- Zhu, Y., Tchkonina, T., Pirtskhalava, T., Gower, A.C., Ding, H., Giorgadze, N., Palmer, A.K., Ikeno, Y., Hubbard, G.B., Lenburg, M., O'Hara, S.P., LaRusso, N.F., Miller, J.D., Roos, C.M., Verzosa, G.C., LeBrasseur, N.K., Wren, J.D., Farr, J.N., Khosla, S., Stout, M.B., McGowan, S.J., Fuhrmann-Stroissnigg, H., Gurkar, A.U., Zhao, J., Colangelo, D., Dorransoro, A., Ling, Y.Y., Barghouthy, A.S., Navarro, D.C., Sano, T., Robbins, P.D., Niedernhofer, L.J. and Kirkland, J.L. (2015) 'The Achilles' heel of senescent cells: from transcriptome to senolytic drugs', *Aging Cell*, 14(4), pp. 644-658.
- Zordoky, B.N.M. and El-Kadi, A.O.S. (2007) 'H9c2 cell line is a valuable in vitro model to study the drug metabolizing enzymes in the heart', *Journal of Pharmacological and Toxicological Methods*, 56(3), pp. 317-322.

